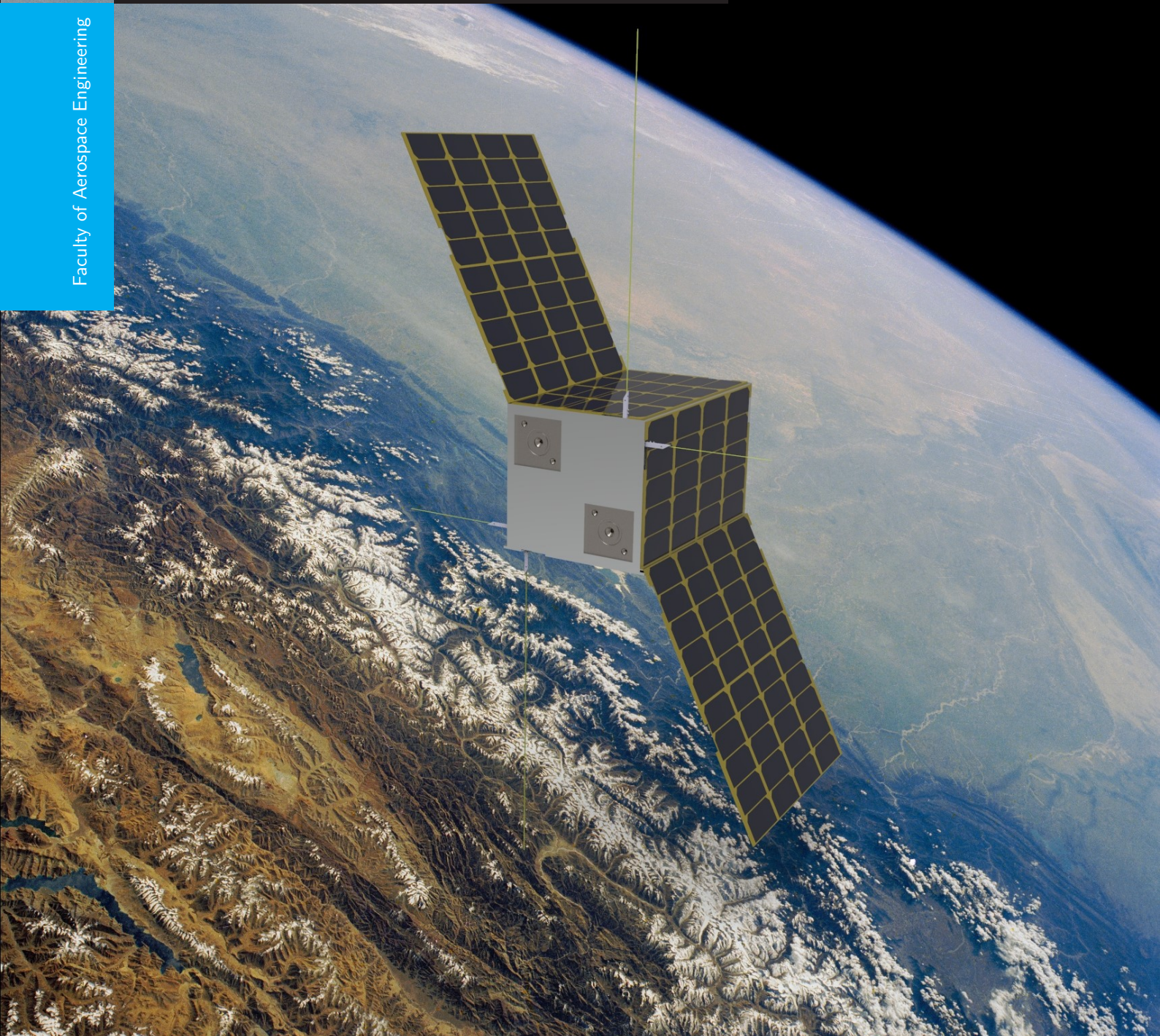


Sat-ELITE: a benchmark for Earth Observation in VLEO

Final Report

DSE Group 17

Faculty of Aerospace Engineering



This page is intentionally left blank.

DESIGN SYNTHESIS EXERCISE AE3200

FINAL REPORT

*submitted in partial fulfilment of
the requirements for the award of the degree of*

Bachelor of Sciences
in
Aerospace Engineering

Group 17:

Ali Alsudani - 4462769
Jesse Hummel - 4497554
Andrej Kluka - 4548019
Martins Kuzņecovs - 4560388
Tullio Nutta - 4564243
Dāvis Pazars - 4615727
Michael Plumaris - 4537629
Helvijs Sebris - 4550730
Niels Vanlaerhoven - 4557018

Tutor:

Dr.ir. Robert Fonod

Coaches:

ir. Gourav Mahapatra
ir. Federico Paredes-Valles

Customer:

Dr.ir. Hans Kuiper

July 2, 2019

Issue 1.0

Cover image consists of our own render and background picture from NASA ¹



¹https://www.nasa.gov/images/content/639784main_41g-120-0009_full.jpg [Date accessed: 22-05-2019]

Acknowledgements

We would like to express our gratitude towards our tutor Dr.ir Robert Fonod, together with the coaches ir. Gourav Mahapatra and ir. Federico Paredes-Valles, for the precious guidance, the copious amount of time spent listening to our challenges and constant supervision in the design of the Sat-ELITE.

We would also like to acknowledge Dr.ir. Hans Kuiper for his advice on the design of ADCS and payload subsystems, and for acting as a customer throughout the whole project. Our thanks and appreciations also go to all the professors and engineers from Delft University of Technology that had no obligation to help us, but still did spend their precious time to provide us with priceless advice. These include: ir. Jasper Bouwmeester, ir. Barry Zandbergen, Dr. Stefano Speretta, Dr ir. Q.P. Chu, Dr. Botchu Jyot, Dr.ir. Erwin Mooij and Günther March.

Finally, we appreciate the precious feedback of the DSE teaching assistants, without whom the project management and system engineering tools would not have been implemented as effectively.

Executive overview

The present project embodies the closing piece of the Aerospace Engineering curriculum at TU Delft, notably the Design Synthesis Exercise (DSE). By implementing and broadening the technical knowledge acquired in the Bachelor phase, students are guided by a tutor and coaches to experience the real-life design process with an eye of regard for project management and systems engineering.

Group 17 is commissioned to create a *CubeSat constellation for Earth observation in Very Low Earth Orbit*, an environment dominated by the presence of strong atmospheric disturbances. This presents several challenges to be overcome with ingenious and innovative design solutions at a price of 500 000 € per unit.

This Final Report encompasses the entirety of the design process: across ten weeks, the team has worked enthusiastically to arrive at a detailed description of the best possible configuration to perform a successful mission. Aside from the technical considerations inherent to spacecraft systems, the team's focus has been to examine the mission from a marketing framework, to design a platform relevant for today's needs allowing customers to enhance their business models through the use of satellite imagery.

Mission overview

Whilst there are many platforms offering sharp-resolution imagery, efforts are being made to push for higher temporal resolution, of great importance for many applications. CubeSats are a perfect candidate to approach this mission, due to their low-cost standardised structure hinting at the construction of a space constellation. Planet Corp, an American satellite company, has attempted this challenge in 2013 by launching over 130 CubeSats actively mapping the Earth at 4m resolution with a daily refresh rate. The goal of this project is to outperform this platform with regards to spatial and temporal resolution, using the strategy of flying in VLEO, incorporating an innovative propulsion system and applying super-resolution software to enhance image quality. The Mission Need Statement is now defined:

Develop a CubeSat that can compete with current Earth observation platforms using the strategy of flying in a Very Low Earth Orbit.

The strong aerodynamic forces in VLEO limit mission lifetime and introduce torque disturbances. This stresses the importance of a highly responsive Attitude Determination & Control system to provide adequate pointing accuracy for imaging. Technological developments, pushing for miniaturisation of propulsive components, bear great potential to improve performance in a confined size: for this reason, the design incorporates an electrostatic propulsion thruster. Leveraging on such innovative concepts, the Extended Lifetime Innovative TEchnology Satellite -or Sat-ELITE- is fully equipped to sustain the harsh VLEO environment for over five years, decreasing the costs of replenishment, manufacturing and launch. This leads to the Project Objective Statement, which include the team's objectives:

Design a Very Low Earth Orbit CubeSat for Earth observation with a spatial resolution of less than 4 m, a pointing accuracy of less than 0.25 deg and a lifetime of more than five years, with a particular focus on the Attitude Determination & Control and Micro-Propulsion subsystems, by nine students in ten weeks.

Despite the aerodynamic complications incurred at VLEO, one can benefit from this environment in several ways. First and foremost, improved spatial resolution is possible as the distance to the target is reduced. High particle drag also facilitates End-Of-Life manoeuvres, meaning no additional propellant is needed for de-orbit. The majority of satellites are concentrated at higher altitudes, which reduces the risk of collision with other satellites and space debris. Lastly, mechanics dictate shorter orbital periods, with enhanced temporal resolution as a result. By correctly harvesting such possibilities, Group 17 confidently believes their platform will become the most competitive on the market.

Requirement outline

High-level customer requirements serve as a starting point to the mission, as these are most demanding. The five driving requirements of this mission are summarised in [Table 1](#).

Table 1: Driving mission requirements

Identifier	Requirement
SYS-OBJ-ORB-1	The spacecraft shall orbit in the altitude range 230-380 km
SYS-OBJ-PL-2	The spacecraft shall provide images with a spatial resolution better than 4 m
SYS-OBJ-PL-3	The spacecraft shall provide images with a temporal resolution of at least 2 images a day
SYS-OBJ-COST-1	The unit price of the spacecraft (design, development, test model, and production) shall be less than 500,000 €
SYS-SC-ADCS-1	The spacecraft shall have a pointing stability along all 3-axis better than 0.22 deg/s (3σ)
SYS-SC-ADCS-3	The spacecraft shall have a Nadir pointing accuracy better than 0.25 deg (3σ)

Market analysis

To assess the project margins with respect to cost and performance, explore competitors and identify a product development direction, an extensive market analysis was performed.

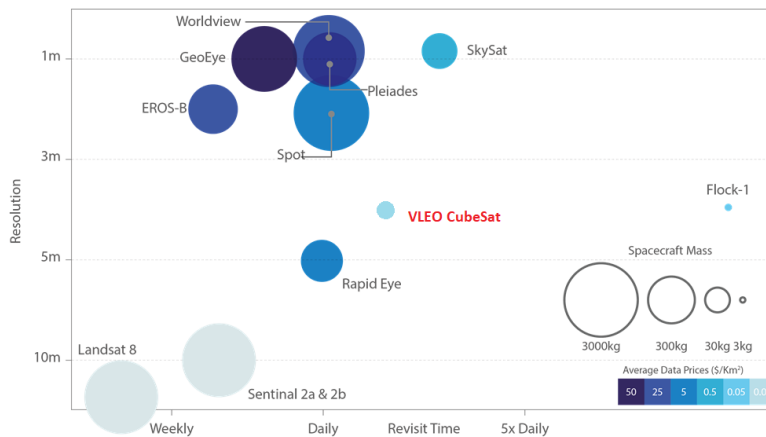
Currently, around a third of all operational satellites perform Earth Observation (EO) missions, with a data market share worth 1.7 b\$. This is bound to increase, with an annual predicted growth of 20% over the next ten years^[1].

Touching on size, CubeSats (below 10 kg) represent 39% of all EO satellites, whilst heavier (above 500 kg) amount to 30%, although this does not account for unlisted military satellites. This statistic reflects the two design philosophies of EO satellite design: large, high orbit systems offering sharp ground resolution and small, high orbital velocity systems yielding significant temporal resolutions. Optical miniaturisation advancements favour the CubeSat philosophy, packing powerful instruments in restricted size.

Applications range across commercial, financial, civil government and defence sectors. Specific examples are: crop monitoring for agriculture, traffic control, emergency response coordination, maritime tracking, asset surveillance, intelligence gathering, resource assessment for mining and climate prediction. After careful consideration, it is decided that the observable spectrum will range across the visible and near-infrared, which satisfies most applications: this near-infrared region is of particular importance for biological applications, namely for soil composition and moisture estimation.

With regards to spatial and temporal resolution, the project's goal is to outperform existing observation platforms, illustrated in Figure 1. The market gap is identified at a ground resolution of 4m, which coupled with a twice-daily revisit time and an affordable price per image is deemed to ensure commercial success of the platform. Offering two views of the same area under different lighting conditions is an unprecedented advantage of the platform. It should be noted that the temporal resolution of the Flock-1 constellation reported in Figure 1 seems inconsistent with Planet's own website which indicates that it is capable of daily revisits at most².

Figure 1: Spatial and temporal resolution of competing platforms. Courtesy of ESA³



Risk management

Functions and requirements serve as a guide to risk discovery. Designing a system with a certain degree of reliability requires an exhaustive risk assessment and mitigation strategy. This was approached by listing all

²<https://www.planet.com/products/monitoring/> [Date accessed: 20-05-2019]

possible circumstances of failures, which have been allocated into three main categories:

- *Subsystems risks* - inherent to the components inside the system. These are incorporated throughout each subsystem analysis
- *Environmental risks* - resulting from the interaction with the space environment (radiation, space debris, atomic oxygen corrosion)
- *Operational risks* - associated with the production and launch of the satellite

An identification code was allocated to each risk for referencing throughout the report. These are classified by multiplying their likelihood by their impact on the system. Five gradations in likelihood are introduced ranging from very likely to very unlikely, similarly four gradations regarding estimated impact to the system are introduced ranging from negligible to catastrophic; this allows assigning risks to a map. For each risk a possible mitigation scenario is proposed to reduce the likelihood and/or the impact. The two most common mitigation methods are adhering to flight-proven concepts and adding redundancy to circumvent single points of failure, which generally induces higher weights and cost. The most mission-threatening risk is identified as improper subsystem mounting, which would result in structural collapse during ground handling operations and launch loads. Connections between subsystems are yet to be considered, as the assembly phase is left as a post-DSE activity: the team will draw inspiration from flight-proven concepts and perform extensive testing to ensure structural integrity of the satellite.

Sustainable development

Environmental and social impacts of the mission are investigated to ensure compliance with the team's sustainability principles, stemming from the "United Nations sustainable Development goals". With the creation of CubeSats, the cost of constructing and operating satellites has decreased, allowing for the inclusion of lesser-privileged countries into space, such that they could benefit from the use of satellite imagery. Sat-ELITE promotes applications for tracking the development of these areas, and mitigating the effects of potential hazards (illegal environmental transformation, environmental disasters...). Attention is paid to inhibit the creation of space debris, seen as an example of "space pollution" threatening future missions. For this purpose, tracking of the satellite during de-orbit will be performed, a process facilitated by the low orbits, lasting half a year at most. To limit negative effects of satellite production, communication with manufacturers will ensure that only components manufactured in an environmentally-friendly way are purchased. The launch was identified as the main focus for high system level analysis, as it contributes to greenhouse gas emissions as well as black carbon in case of kerosene and alumina particles in case of solid propellant. These are deposited in the stratosphere for extended periods of time, contributing to ozone layer depletion. Therefore, it is concluded that the most important high-level parameter for sustainability is the total mass sent to orbit, as larger masses imply polluting launchers. Furthermore, green propellant is preferred over hydrazine for the launcher, which is extremely toxic and harmful to the environment. Furthermore, this technology is flight proven and outperforms hydrazine for small satellite applications in almost every way. Throughout the design process, choices are made which impact the environment in a way or another: the sustainable approach is therefore included in every decision across all subsystems.

Logistics and modes description

The special nature and high cost incurred in space missions entails a "Start-to-End" design, where every operation must be foreseen and optimised. This engineering must be tailored to the business model, which in the present mission comprises of a need for satellite images. The customer identifies the area of interest to be monitored. This information is passed on to the satellite in forms of commands, which are verified for correctness. Onboard, after the pictures are taken, they are then sent to a ground station, where image processing takes place. The data is then provided to the customer through an online platform.

To size the subsystems correctly, the modes undertaken by the spacecraft whilst orbiting are described. Immediately after leaving the canister, the satellite experiences angular rates in all directions which necessitates *detumbling mode* for stabilisation. *Nominal mode* requires accurate attitude control to generate the pictures, which are transmitted during the *communication mode* through two patch antennas, equally important to retrieve user commands. *Thrusting mode* activates the propulsion system for orbit maintenance, whilst *desaturation mode* discharges the momentum in the reaction wheels. In case of anomalies or excessive power drainage, the satellite enters *safe mode*, where all non-vital systems are shut off to safeguard power. To maximise the payload

outcome, daytime is reserved for power generation and image acquisition, and thrusting occasionally. When the communication window is reached (at the Poles), data is uplinked/downlined, whilst nighttime is allocated to maintenance operations (desaturation, data processing and thrusting).

Trade-off outcome and payload selection

The market analysis imposed the following criteria for an optical system: capturing visible and near-infrared portions of the spectrum, a ground resolution of 4m and a Field of View (FoV) wide enough to map Earth twice a day with a reasonable constellation size. The allocated time and monetary budget lead to an investigation of commercial cameras suitable for the mission, yielding the Ant-2A developed at TU Delft and the SEEING by Safran Reosc., available in sharp resolution or wide field of view. These cameras differ in a number of parameters, notably size, hence seven different configurations were devised which could house and operate them, as depicted in Figure 2.

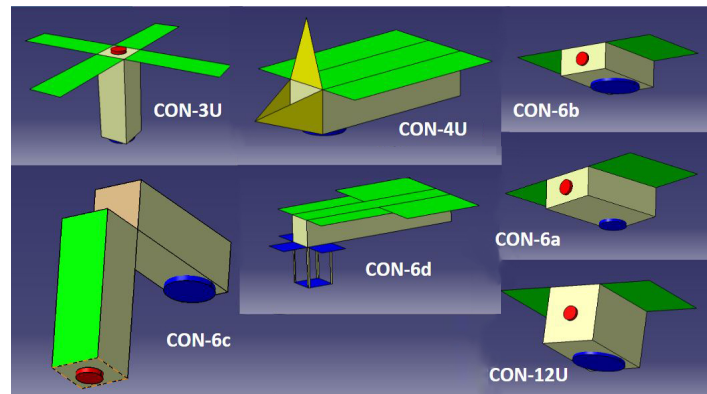


Figure 2: CAD models for the generated concepts. Green, red and blue represent solar panels, propulsion system and payload aperture, respectively.

Converging to the "best" design required an extensive trade-off, performed in two stages: first, a study was performed to discard impossible concepts and justify the feasibility of the three remaining ones, which were the **CON-6c(hinged)**, **CON-6c** for ANT-2A and **CON-12U-a(high res)** and **CON-12U-b(wide FoV)** for SEEING. The performance of each concept was assessed through an in-depth analysis based on utility functions, incorporating the following criteria: mission cost, spatial resolution, sustainability, reliability and innovation. A sensitivity analysis was conducted to test the robustness of this method, by modifying the criteria and observing at what point the winning concept is overtaken. Eventually, CON-12U-b emerged as the leading candidate to face the challenge, comprised of twelve 10x10 cm units arranged in a 2x2x3 configuration. The moderate FoV reduces the constellation size needed for Earth monitoring, whilst meeting the spatial resolution requirement at an altitude of 342km.

Orbits, maintenance and propulsion

The orbital altitude is single-handedly driving the mission, affecting every subsystem one way or another. Determining this is no easy task, as it quickly becomes a circular logic problem: altitude yields total drag, needed for propellant sizing to maintain the orbit for a number of years. This allocates a volume for the camera aperture, directly affecting the resolution, which again depends on the altitude. To tackle this problem, an upper bound was set according to the diffraction limit of the selected camera at 342 km.

An aerodynamic analysis was performed, aimed at quantifying the external forces acting on the satellite. First, the physical framework was laid out: this investigated the behaviour of the flow, establishing that free molecular flow is more suitable for analysis. A crude first estimate of the drag was based on Schamberg's equations, yielding promising results and equally important for verification of subsequent methods. Mission launch date (relevant for solar cycle activity), satellite position and altitude were used to run a numerical tool proving atmospheric molecular compositions, which are subsequently integrated in more refined simulation. The latter stands on the principles of Sentman's equations, describing interactions between molecules and satellite surfaces with a high degree of precision. A high degree of flexibility is incorporated through the use of

mesh ray tracing, allowing for the representation of complex geometries. External forces are thus obtained and decomposed into drag and disturbance torques (associated with attitude control). Additionally, experimentation with different frontal shaped was carried out, however this was not deemed cost-effective.

Different kinds of propulsion systems were investigated based on the required thrust for orbit maintenance: electrostatic IFM nano-thrusters were deemed most suitable, as their high specific impulse entails smaller volume storage for propellant. Two thrusters are selected allowing for shorter burn times and placed diagonally with regards to the centre of mass to minimise torque disturbances. Nonetheless, these will be present to a certain degree as a result of slight thruster misalignment; a Monte Carlo simulation was carried out to ensure attitude control will cope with this effect. Aerodynamic drag calculations, coupled with the total impulse required to meet a lifetime of five years, eventually lead to a lower altitude bound of 332 km.

A requirement dictating 99% Earth coverage acted as a starting point to determine the type of orbit. It was decided that a Heliosynchronous orbit is most desired: constant solar incidence angle and sunlight time maximise solar cell efficiency whilst offering favourable ground lighting conditions. A piggyback approach will be used to launch and validate the first satellite, then two dedicated launchers will distribute the constellation along two orbital planes arranged at $\pm 45^\circ$ Sun incidence angle. This compromise provides customers with pictures spaced sufficiently apart, whilst maximising solar power from the cells. Accounting for reliability estimates of SmallSats facing five-year missions, the total amount of satellites becomes 202, 101 per plane weighing 2233 kg. This led to the selection of the European VEGA launcher, a suitable candidate in terms of cost and propellant burned (relevant for sustainability). The total ΔV budget is comprised of: 489 m/s for orbit maintenance, 22 m/s for initial orbit correction and 8.5 m/s for orbit phasing (spreading across plane). No propellant is needed for End-Of-Life manoeuvres, simulated using ESA's DRAMA software package: accounting for worst-case scenarios of solar minimums, natural de-orbit will occur in less than two years, comfortably within the regulatory 25 year margin.

Attitude Determination and Control

For the acquisition of high-quality images, adequate stability and pointing requirements must be met, only possible through three-axis control and stabilisation. An extensive literature study identified state of the art hardware tailored for the mission and hinted at the formation of a primary and secondary system:

- Four reaction wheels, two star trackers and two Internal Measurement Units form the *primary* system active in nominal mode, effectively fulfilling mission needs
- Three magnetometers and magnetorquers constitute the *secondary* system, providing support to its primary counterpart through detumbling and desaturation procedures.

To better understand and model the most prominent disturbance sources, these have been categorised accordingly into aerodynamic, gravity, magnetic, solar and thruster induced torques. Summing these together yields the maximum torque and the momentum buildup over one orbit of the order of magnitude of 10^{-6} Nm and 10^{-3} Nms, respectively. Controllability over the full mission envelope is ensured by sizing the actuators based on the maximum experienced torque. The angular momentum buildup over the daytime is used to size the wheels, as these provide stability during the imaging phase. Magnetorquers take over during eclipse, dumping the acquired momentum as well as detumble the spacecraft from residual spin rates. Slew rates required during communications are met with comfortable margins, but verifying pointing accuracy and detumbling capabilities, required a numerical MATLAB simulation. This enabled the selection of an adequate control algorithm: Bdot was opted for detumbling due to its robustness, simple implementation and low computational expense, while a Proportional-Derivative controller was chosen for nominal operations. It must be underlined that the simulation is limited to rigid body representation, meaning the pointing stability requirement could not be verified. Validation procedures will commence once the prototype is delivered.

Data Handling, Telecommunication and Electronics

All on-board operations and data flows are managed by the Command and Data Handling subsystem, analogously to a nervous system in the human body. Software necessary to run the satellite was compiled in a list and combined with all on-board hardware in a block diagram for clear identification of data flows across subsystems. Two On-Board Computers from ISIS Delft are implemented to reduce risks of failure and enhance computational speed. The databus will mostly consist of I^2C , widely employed on CubeSats platforms due to its high reliability and minimal power consumption. As this protocol is limited to 400 kbps, a special SpaceWire

connection is established to handle the exceptionally high payload data rates of 1.18 Gbit/s. Accommodating the necessary 339 GB of data will require two flash drive units, preferred over SSD as these are non-volatile (power interruptions do not compromise data) and are capable of high writing and reading speeds. The cable harness mass is extrapolated from similar-sized Delfi-n3xt at 120 g.

These will enable the flow of housekeeping and payload data through the system, reaching a telecommunications unit for transmission. The mission will employ two ground stations from the Kongsberg Satellite Services network, located near each Arctic pole. A GPS receiver will accurately determine the orbital position, used to precisely schedule ground communication windows. Each orbit, roughly 7.9 min are available for downlink and uplink of data. Selecting communication bands and antenna types will depend on the available link budget and data volume, comprised mostly of payload imagery. Estimates of raw data indicate a colossal amount of 6445 Gbits per orbit; accounting for eclipse and communication periods, discarding cloud and ocean images, applying reasonable compression rates and spectral region splitting techniques, this is reduced to a feasible 40.6 Gbits, requiring an average transmission rate of 85.8 Mbit/s. A link budget is created, balancing transmitter power, antenna gain and compression rates to meet a telecommunication standard - 3dB signal to noise margin. It is concluded that X-Band is sufficiently powerful to transmit all imaging data using two patch antennas (for redundancy), without adding aerodynamic drag. An omni-directional UHF/VHF-Band transceiver downlinks telemetry data, uplinks commands and software updates, even during of detumbling.

At this stage in the design, all power-consuming units have been defined, meaning a supportive Electrical Power System can be drawn out. Sat-ELITE will feature two double-folding opposed solar panel configurations at $\pm 26.5^\circ$, maximising the solar influx for both orbital planes. These contain triple-junction Gallium-Arsenide cells at an efficiency of 30%. Two lithium-ion battery packs will store the power for eclipse conditions, managed by a simple but reliable power distribution and conditioning unit. To prove that sufficient power levels are maintained throughout orbit, a self-developed simulation is employed. This will monitor instantaneous power production and consumption, accounting for component efficiencies, actual losses and battery charge levels for the most challenging modes. If, due to unforeseen circumstances, power levels drop below a critical threshold, a signal will be redirected to a special module within the OBC, which will trigger safe mode. Finally, risks inherent to electrical components are assessed: these can result from human errors or excessive radiation dosages, and can be circumvented through forms of redundancy, judicious component selection, special coatings or testing procedures.

Structural and Environmental hazards

Careful material consideration is needed to ensure survivability in the hostile space environment with regards to atomic oxygen corrosion, particle radiation and space debris impact. Aluminium 7075-T6 was deemed most suitable based on its thermal expansion coefficient and specific stiffness. A SHIELDOSE-2 depth-dose analysis tool is implemented to determine the radiation dose striking the most radiation-sensitive component of the design, namely the optical imaging sensor, as a function of the aluminium shielding thickness. A statistical investigation foreseeing the possibility of perforation from space debris is undertaken using the NASA90 model. Ultimately, the 1.2 mm thickness is deemed sufficient to prevent both issues from occurring. Finally, material corrosion associated with presence of atomic oxygen is considered. Fortunately, aluminium is unaffected by this corrosion, hence the integrity of the structure will remain uncompromised.

The launch canister dictates the shape of the satellite, as well as the load introduction into the structure. The Canisterised Satellite Dispenser from Planetary Systems Corporation was deemed appropriate, due to the extensive documentation available and high reliability for deployment, with more than 30,00 successful flights. During the few minutes of launch, the spacecraft is subjected to significant longitudinal and lateral loads, which entails a static and vibrational load analysis. The VEGA launcher documentation provided static load envelope and vibrational mode frequency requirements. Critical buckling loads, determined based on structural mechanics, proved that the structure will withstand these loads. Modelling the subsystems as point masses and the structural connectors as springs, a spring-mass model was created to investigate the mode frequencies of the satellite. This concluded that launch vibrations would not pose a threat to the system's integrity. A brief inquiry of other launchers showed the design to be compatible with such platforms. The centroid and moments of inertia were determined analytically: these are well within the margin for proper load introduction in the structure and adequate attitude control.

The scarcity of atmospheric particles in space means electromagnetic radiation is the only mechanism for

heat regulation: the thermal control system must exploit this to ensure all components remain within their operational and survival temperatures. All constituents of the satellite have been evaluated with regards to their absorptivity, emissivity and heat capacity characteristics. These were implemented within a simulation framework to monitor the temperature variations throughout the mission, particularly with respect to extreme (hot and cold) scenarios. The results are as follows: fully passive thermal control is deemed sufficient, only the optical system will be insulated with a silica-aerogel blanket.

Design evaluation

Table 2: Sat-ELITE specifications

Length	362 mm	Average system power	55 W
Height	218.5 mm	Orbit type	SSO
Width	239 mm	Orbit altitude	332-342 km
Dry mass	20.55 kg	Orbit time	91 min
Earth's coverage	99%	Lifetime	5 years
Temporal res.	2x per day	Downlink rate	100 Mbit/s
Spatial res.	<4 m	Unit cost	390 k€

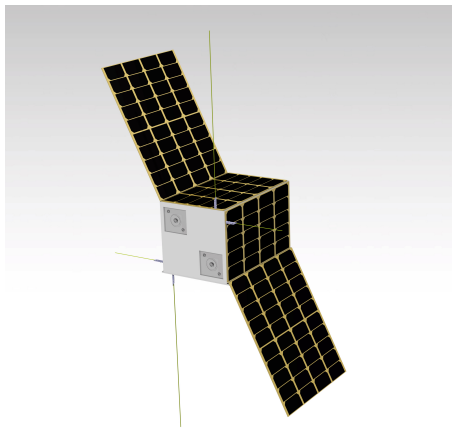


Figure 3: View from above

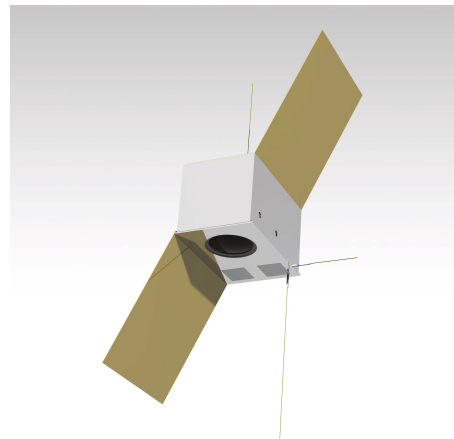


Figure 4: View from below

To reflect on the robustness of the design with respect to unforeseen changes in key system parameters, a sensitivity analysis is performed. It is deemed that a slight increase in required power will threaten the culmination of mission objectives with regards to pointing stability, as the additional solar panels might induce controllability issues.

Verification and Validation

V&V procedures are essential to ensure compliance with established requirements and that the right design was conceived for a successful mission. This is stressed throughout the analysis of each subsystem: requirement verification, and code verification plus validation are the only plausible approaches at this stage of the design. Future V&V procedures are planned to further enhance confidence in the product's proficiency.

Post DSE

Gantt chart, Project Design and Development Logic were compiled, outlining all activities needed in the near future until the start of the main manufacturing phase. Particular emphasis was placed in the creation of a Production and Testing Plan, as the prototype spacecraft will be extremely useful in establishing an integration and assembly procedure for the constellation production. Eight tests were identified, which are essential for the demonstration of the design's capabilities.

Contents

Executive summary	VIII
Abbreviations	XII
List of symbols	XV
Version management	XV
1 Introduction	1
2 Strategy analysis	2
2.1 Mission objectives and goals	2
2.2 Technical requirements	2
2.3 Market analysis	2
2.4 Risk management	10
2.5 Sustainable development strategy	11
3 Concept operations and selection	15
3.1 Functional diagrams	15
3.2 Operations and concepts logistics description	16
3.3 Coordinate systems	18
3.4 N ² chart	18
3.5 Trade-off	19
4 Orbit analysis and drag compensation	26
4.1 Orbit selection	26
4.2 Aerodynamic model	28
4.3 Propulsion system	35
4.4 Mission altitude	42
4.5 Constellation design	43
4.6 ΔV budget estimation	47
4.7 Recommendations	51
5 Payload design	52
5.1 Physics of electro-optical systems	52
5.2 Resolution compromise	54
5.3 Disturbances	55
5.4 The SEEING camera	57
5.5 Signal to noise ratio	58
5.6 Super-resolution imagery	58
5.7 Future recommendations	59
6 Attitude Determination & Control design	60
6.1 Requirements	60
6.2 Hardware setup	62
6.3 Risk assessment	63
6.4 Environmental disturbances	64
6.5 Momentum buildup	65
6.6 Sizing	66
6.7 Verification and Validation	66
6.8 Future framework	69

7	Data Handling, Telecommunication and Electronics	71
7.1	Command and data handling	71
7.2	Telecommunication	74
7.3	Electrical power	81
7.4	Possible failure modes	87
8	Structural and Environmental Hazards	88
8.1	Material selection	88
8.2	Structural design	89
8.3	Thermal control	96
8.4	Environmental protection	100
9	The Sat-ELITE	103
9.1	Description of operational modes	103
9.2	Sustainability assessment	104
9.3	Technical budgets	104
9.4	Cost	105
9.5	Performance and general characteristics	106
10	Design assessment	109
10.1	Sensitivity analysis	109
10.2	Verification and Validation procedures	111
10.3	Final risk assessment	112
11	Post-DSE developments	114
11.1	Project Design & Development Logic	114
11.2	Project Gantt chart	114
11.3	Production and testing plan	114
12	Conclusion & Recommendations	117
	Bibliography	118
	Appendix A Technical requirement compliance matrix	123
	Appendix B Functional flow diagram	127
	Appendix C Functional breakdown structure	128
	Appendix D List of technical risks	129
	Appendix E Technical drawings	130
	Appendix F Project design & development logic	131
	Appendix G Project Gantt chart	

Abbreviations

ADCS	Attitude Determination & Control Subsystem	1, 17, 18, 20, 38, 39, 41, 42, 49, 60–64, 66, 68, 91, 94, 95, 107, 110, 112
AI	Artificial Intelligence	7, 8
C&DH	Command & Data handling	17, 91, 107
CMG	Control Moment Gyro	62
CMOS	Complementary Metal Oxide Semiconductor	54
CoM	Center of Mass	39
COTS	Commercial off the Shelf	10, 14, 39, 75, 109, 114, 115, 125
CSD	Canisterised Satellite Dispenser	89, 90, 92, 94
CTE	Coefficient of Thermal Expansion	53
DEPEST	Demographic, Economic, Political, Ecological, Social, Technological	2, 6
DoD	Depth of Discharge	115, 125
DOF	Degree of freedom	91
DSE	Design Synthesis Exercise	1, 5, 81, 95, 105, 111, 114
ECI	Earth Centered Inertial	60, 61
EO	Earth Observation	1, 3, 4, 78
EOL	End-of-Life	8, 9, 50, 51, 83, 84, 86, 125
EPS	Electric Power Subsystem	1, 17, 36, 65, 71, 73, 81–85, 91, 97, 98, 110, 111, 125
ESA	European Space Agency	12, 13, 42, 59, 65, 70, 100, 112
EU	European Union	9
FBS	Functional Breakdown Structure	2, 16
FEA	Finite Element Analysis	112
FEPP	Field-emission electric propulsion	36–38
FFD	Functional Flow Diagram	15, 16
FoV	Field of View	V, 20, 23, 24, 44, 47, 52, 54, 56, 57
GaAs	Galium-Arsenide	83
GEO	Geostationary Earth Orbit	76
GHG	Greenhouse Gas	13, 14, 104
GPS	Global Positioning System	63, 76, 81
GSD	Ground Sampling Distance	20, 22
GSP	Ground Station Pointing	60
HPGP	High Performance Green Propellants	14
I/O	Input/Output	75
IEEE	Institute of Electrical and Electronics Engineers	75, 76
IFoV	Instantaneous Field of View	52, 57
IMU	Inertial Measurement Unit	62, 64, 67, 68
ISIS	Innovative Solutions in Space	80
ISS	International Space Station	26–28
KSAT	Kongsberg Satellite Services	76–78

LCA	Life Cycle Assessment	12, 13
LEO	Low Earth Orbit	8, 9, 27, 76, 97
MEMS	Microelectromechanical Systems	62, 68
MNS	Mission Need Statement	2, 112
MTF	Modulation Transfer Function	57
NASA	National Aeronautics and Space Administration	30, 33, 61, 62, 76, 114
NEO	Near-Earth Objects	6
NORAD	North American Aerospace Defense Command	76, 81
PD	Proportional Derivative	68
PDDL	Project Design & Development Logic	113, 114
PEET	Pointing Error Engineering Tool	70, 112
PID	Proportional Integral Derivative	68
POS	Project objective statement	2
RAAN	right ascension of the ascending node	45, 48
RGB	red, green, blue	55
RMS	Root Mean Square	61
SaaS	Software-as-a-Service	7
SAR	Synthetic Aperture Radar	7, 8
Sat-ELITE	Extended Lifetime Innovative TEchnology Satellite	1, 10, 15, 17, 38, 61, 62, 64–67, 70, 71, 85, 88–95, 97, 99, 103–105, 107, 110, 112–114, 117
SDGs	Sustainable Development Goals	11, 12
SMAD	Space Mission Analysis and Design	16, 17
SMOS	Soil Moisture and Ocean Salinity	2
SNR	Signal-to-Noise Ratio	54, 55, 58, 59, 79, 80
SPF	Single Point of Failure	64, 75, 84, 113
SSA	Space Situational Awareness	6
SSC	Swedish Space Corporation	77, 78
SSO	Sun-synchronous orbit	26–28, 43, 45–48, 83, 97, 107
STK	Systems Tool Kit	45, 47
SWOT	Strengths, Weaknesses, Opportunities, Threats	2, 5, 9
TCS	Thermal Control System	88, 96–98, 112, 125
TLE	Two Line Element	76, 81
TRL	Technology Readiness level	10, 14, 76, 89, 95
V&V	Verification & Validation	1, 111, 112
Vega	Vettore Europeo di Generazione Avanzata	46–48, 90, 91, 93
VLEO	Very Low Earth Orbit	1, 8–10, 12, 17, 27, 29, 30, 36, 50, 88, 104, 117

List of symbols

Sign	Description	Unit
A_a	aperture area	m^2
A	cross sectional area	m^2
BPC	bits per communication channel	Bits/channel
BPP	bits per pixel	bit/pix
B	Earth's magnetic field	T
C_D	drag coefficient	-
C_L	lift coefficient	-
C	effective length constant	-
D	residual magnetic dipole moment	Am^2
E	Young's modulus	Pa
F_t	thrust	N
GSD	Ground Sampling Distance	m
G	shear modulus	Pa
H	angular momentum	$kg \cdot m^2/s$
I_c	emitter current	A
I_{sp}	specific impulse	s
I_s	solar flux	W/m^2
I	area moment of Inertia	m^4
J_2	perturbation coefficient	-
Kn	Knudsen number	-
L_e	spectral radiance	$\frac{W}{sm^2 sr m}$
L	length	m
M	mass	kg
N_{CH}	number of communication channels	-
PIX	number of pixels	-
P_{cr}	critical load	N
P_{gen}	power generated	W
QE	quantum efficiency detector	-
Q	heatflow	W
R_{Earth}	radius of the Earth	m
R	individual gas constant	J/kg K
S_i	incoming signal	e^-
S_{eff}	effective slenderness ratio	-
S	speed ratio	W/m^2
T_o	orbital period	s
T_{sat}	thermodynamic temperature of spacecraft	K
T	thermodynamic temperature	K
U_x	utility of criterion x	-
U_{tot}	total utility	-
V_e	emitter potential	V
ΔV	delta V	m/s
Ω_s	solid ground angle	sr
α_{ac}	accommodation coefficient	-
α_{sun}	absorbivity for sun spectrum	-
α	thermal expansion coefficient	1/K
β	coefficient of reflection	-
\dot{B}	change	nT
$\dot{\Omega}$	change in longitude of ascending node	rad/s
$\dot{\omega}$	angular acceleration	deg/s
η_d	efficiency after a year	-

Sign	Description	Unit
η_{sc}	efficiency of solar cells	-
η	optical throughput	-
η	efficiency	-
γ	angle between the inward normal and the drag vector	rad
\hat{n}	outward panel normal	-
\hat{u}_D	unit vector in the drag direction	-
\hat{u}_L	unit vector in the lift direction	-
λ_t	thermal conductivity	W/K
λ_{fp}	mean free path	m
λ	wavelength	m
I	mass moment of Inertia matrix	kg m ²
K	stiffness matrix	N/m
M	mass matrix	kg
$\ddot{\mathbf{x}}$	acceleration vector	m/s ²
$\tilde{\mathbf{K}}$	mass-normalised stiffness matrix	N/m
\mathbf{x}	position vector	m
μ	Earth's gravitational parameter	m ³ /s ²
ω_n	natural frequency	rad/s
ω	angular velocity	deg/s
ρ	density	kg/m ³
σ_f	fatigue strength	Pa
σ_u	ultimate tensile strength	Pa
σ_y	tensile yield strength	Pa
σ	standard deviation	-
τ_u	shear strength	Pa
τ	torque	Nm
θ_i	incidence angle	rad
ν	Poisson's ratio	-
ϵ_{IR}	emissivity for infra-red spectrum	-
ζ	misalignment angle	degree
a	semi-major axis	m
c_{mp}	thermal velocity of the molecules	m/s
c_h	specific heat capacity	J/kg/K
c	speed of light	m/s
d_p	particle hard-shell diameter	m
e	eccentricity	-
f_b	beam spreading factor	-
f_{nat}	natural frequency	Hz
g_0	gravitational acceleration	m/s ²
h_p	Plank's constant	m ² kg/s
h	altitude	m
i	inclination	rad
j	number of orbits	-
k_d	derivative gain	-
k_p	proportional gain	-
k_x	weight of criterion x	-
k_B	Boltzmann constant	m ² kg/s ² K
k_{alb}	albedo	-
k_{lat}	lateral stiffness of a beam	N/m
k_{long}	longitudinal stiffness of a beam	N/m
k_{pixel}	image sharpness criterion	-
k	number of days	-
l_y	length of mission in years	years

Sign	Description	Unit
l	angle between the inward normal and the lift vector	rad
m	molecular mass	kg
n_{shot}	shot noise	e^-
p	total pressure	Pa
r_{CoM}	distance geometric centre to centre of mass	m
r_{cp}	distnce geometric centre to centre of pressure	m
r	distance between orbiting bodies	m
t_i	integration time	s
t_{day}	day time	s
v_{rem}	velocity re-emission ratio	-
v_r	aerodynamic velocity	m/s
v	velocity	m/s

Version management

Issue	Date	Pages affected	Brief description of change
0.1	11-06-2019	All	New document
0.2	24-06-2019	All	Final Draft
1.0	02-07-2019	All	Implementation feedback

1. Introduction

This is the final report of the Design Synthesis Exercise (DSE) topic "VLEO CubeSat Design for Earth observation" by group 17. Over the last ten weeks, the group has conceived the design of a satellite and will present the final result as well as the analysis leading up to it. It includes a detailed design of all subsystems and their integration, as well as operation and production descriptions.

Earth Observation (EO) is used to gather data about a broad range of phenomena on Earth, ranging from tracking deforestation in remote areas to pollution by industrial activities. In recent decades, humanity has found out what a dramatic impact pollution has on the planet and EO has been a key feature in understanding the extent of consequences and evaluating potential mitigation strategies. Traditionally, EO satellites were designed to be big with extremely sophisticated cameras. On the other hand, the CubeSat trend is emerging and it is growing in popularity. Since they consist of $10 \times 10 \times 10 \text{ cm}^3$ standardised units (U), development, production and launch costs can be dramatically reduced. This paved the way for building small satellite constellations where a large number of satellites can work together to achieve a common goal.

Current platforms that offer EO data gathered with CubeSats are flying around 500 km altitude. A potential strategy to compete with these platforms is to use less sophisticated, cheaper cameras and fly in lower orbits to achieve similar spatial resolutions. Therefore, to achieve a spatial resolution of less than 4 m, the CubeSat shall operate in Very Low Earth Orbit (VLEO) meaning that atmospheric drag poses a significant challenge for mission duration and for stability during payload operation. At this altitude range the mission duration of CubeSats without propulsion is up to 12 months [2]. This mission aspires to reach a lifetime of more than five years. The Extended Lifetime Innovative TEchnology Satellite (Sat-ELITE) will have to compensate for the constant drag that will be experienced in VLEO and correct for altitude changes. As drag varies heavily with the exact orbit altitude, finding the optimal orbital altitude requires a trade-off between mission lifetime and spatial resolution.

To obtain high-quality, sharp images, the spacecraft shall be stable during the exposure time. This drives the choice of Attitude Determination & Control Subsystem (ADCS), which will have to ensure that sufficient accuracy is provided for the payload. The accuracy concerns both the ability to point the spacecraft in the direction of interest and the pointing stability. From the aforementioned discussions the mission need statement can be set up:

Develop a CubeSat that can compete with current Earth Observation platforms using the strategy of flying in a Very Low Earth Orbit.

This is a long-term goal that can only be realised by going step-by-step and over time iterating through several designs. For this DSE project, the goal is to make the first step, therefore, the project objective statement becomes:

Design a Very Low Earth Orbit CubeSat for Earth observation with a spatial resolution of less than 4 m, a pointing accuracy of less than 0.25 deg and a lifetime of more than five years, with a particular focus on the Attitude Determination & Control and Micro-Propulsion subsystems, in ten weeks, with nine students.

The report starts with a strategy analysis in [Chapter 2](#), where mission objectives are derived from an extensive market analysis, as well as the approach throughout the whole design process with respect to risk and sustainability. [Chapter 3](#), gives the reader an extensive overview of both the operations and functions of the satellite and explains the trade-off made to arrive at the chosen concept. Since the satellite flies in VLEO, a lot of attention is given to orbit maintenance. This is discussed in [Chapter 4](#), where amongst other things, the final ΔV budget is presented. To effectively take pictures of Earth, a suitable payload needs to be selected and analysed. This is done in [Chapter 5](#). From payload requirements and aerodynamic disturbances, requirements were set up for the ADCS. How these requirements will be met is shown in [Chapter 6](#). The data from the payload as well as housekeeping data from the satellite need to be communicated to Earth. This has been grouped with command, data handling and the Electric Power Subsystem (EPS), and is discussed in [Chapter 7](#). To complete the design of the satellite the structural and thermal design needs to be addressed. This is discussed in [Chapter 8](#). To wrap up subsystem design, the spacecraft performance is summarised in [Chapter 9](#). The design assessment is done in [Chapter 10](#), where a sensitivity analysis, Verification & Validation (V&V) and a final risk assessment is shown. Finally, an effort is made to provide the reader with an idea on how the project could be further developed outside the scope of DSE in [Chapter 11](#). The report ends with a conclusion in [Chapter 12](#).

2. Strategy analysis

Any good design process starts off with defining the design strategy, since the entire design process will depend on this. First of all, the mission objectives and personal goals need to be defined, which is done in [Section 2.1](#). After this, the project objective statement needs to be decided on, which is more on a technical level and leads to a list of requirements which the design needs to adhere to, as shown in [Section 2.2](#). This project objective statement is based on the gaps in the market, as analysed in [Section 2.3](#). Lastly, there needs to be a framework set up for risk and sustainability management, which is done in [Section 2.4](#) and [Section 2.5](#) respectively.

2.1 Mission objectives and goals

The first thing to do for any project is defining the Mission Need Statement (MNS). This is a statement defining the long term goal of the team. It is more of a vision and should span beyond the scope of the project. After careful consideration, the MNS was defined as:

Develop a CubeSat that can compete with current Earth observation platforms using the strategy of flying in a Very Low Earth Orbit.

Once this has been done, the first technical step towards a successful project is defining the Project objective statement (POS). It is the highest level description of what the to-be-designed system should achieve and under what constraints. The initial statement was given by the project guide but after initial weeks the team iterated this statement to better suit personal & user requirements. The final version of the statement is as follows:

Design a Very Low Earth Orbit CubeSat for Earth observation with a spatial resolution of less than 4 m, a pointing accuracy of less than 0.25 deg and a lifetime of more than five years, with a particular focus on the Attitude Determination & Control and Micro-Propulsion subsystems, by nine students in ten weeks.

Besides a technical description of the project, it is also vital to identify all parties involved in the project and work towards meeting their goals. The team spotted 8 different parties and has summarised their needs in [Table 2.1](#).

2.2 Technical requirements

Once it is clear what the project direction is, the next step is to define technical requirements that help the project kick-off and serve as a guideline for meeting its goals. While several requirements were already defined in the project guide, it was the team's responsibility to not only complete the list but also validate that the initial requirements adhere to the VALID principle (Verifiable Achievable Logical Integral Definitive). This was done by generating a requirement discovery tree which helped identify various aspects of the mission. The Functional Breakdown Structure (FBS) described in [Section 3.1](#) was used extensively to generate requirements as it highlights the various aspects of the mission in low level detail. Furthermore, the Soil Moisture and Ocean Salinity (SMOS) mission requirements served as inspiration¹. During the generation process, both POS and MNS, as well as the user requirements were taken into account. The final list of system and subsystem requirements is given in [Appendix A](#). Moreover, the verification of each requirement is discussed throughout the report. The requirements in the report are referenced by their identifiers in bold.

2.3 Market analysis

Market analysis aims to identify the direction for product development. This is done in a number of steps: relevant market traits are investigated first, followed by a competitor analysis to determine offered services (customers and research) and hopefully a market gap to be exploited. Assessing future market is done using a Strength, Weaknesses, Opportunities and Threats (Strengths, Weaknesses, Opportunities, Threats (SWOT)) analysis, as outlined in the Delft Design Guide [3]. This SWOT analysis is composed of internal factors namely the strengths and weaknesses of the team, and the external factors targeting current trends with respect to Earth observation using CubeSats. The latter is performed according to Demographic, Economic, Political, Ecological, Social, Technological (DEPEST) aspects.

¹http://www.cesbio.ups-tlse.fr/data_all/pdf/SAG/SRD.pdf [Date accessed: 23-06-19]

Table 2.1: Stakeholders and their requirements

Project group	
SH-REQ-PG-1	The project shall help improve each individual's soft skills like presenting in front of an audience and working efficiently in a team.
SH-REQ-PG-2	The project shall positively contribute to each individual's technical ability related to the degree program.
SH-REQ-PG-3	The project shall result in the completion of the BSc Aerospace Engineering programme at TU Delft.
Supervisor/Coaches	
SH-REQ-SC-1	The project group shall successfully complete the project.
Customer	
SH-REQ-CUS-1	The final product shall meet the requirements as specified in the project guide.
TU Delft	
SH-REQ-TU-1	The project shall meet the study programme's learning outcomes.
SH-REQ-TU-2	The project shall help educate the future generation of capable engineers.
SH-REQ-TU-3	The project shall consider and incorporate a sustainable development strategy.
Engineering/Scientific community	
SH-REQ-ESC-1	The mission results and lessons learned shall help develop and improve future missions.
Society	
SH-REQ-SOC-1	The mission shall not increase the amount of space debris.
SH-REQ-SOC-2	The mission shall help to improve the quality of life on Earth.
Launch company	
SH-REQ-LCH-1	The spacecraft shall fit the rocket's interface.
SH-REQ-LCH-2	The mission shall not delay any operations that are not directly related to it.
SH-REQ-LCH-3	The customer shall adhere to the established contract's terms & conditions.
Ground station operator	
SH-REQ-GND-1	The mission shall not delay any operations that are not directly related to it.
SH-REQ-GND-2	The customer shall adhere to the established contract's terms & conditions.
International Telecommunications Union	
SH-REQ-ITU-1	The communication between the satellite and ground shall occur only in frequency ranges legally allocated to the mission.

2.3.1 Current market

Before competing in the market, it is essential to identify current trends and applications of Earth observation data; these are respectively outlined in the following sections.

Earth imaging

According to the Union of Concerned Scientists (UCS)² there were 1 957 satellites orbiting the Earth at the end of April 2018, active Earth Observation (EO) accounting for 658 of them. A significant amount is attributed to the presence of commercial-use CubeSats by US companies such as Planet and Spire (to a lesser extent); Planet alone accounts for roughly 140 active satellites capable of reaching global coverage. This sector is expected to grow, with 419 EO launches expected in the next decade [4]; as demand shifts to higher temporal resolution imaging, more satellite constellations will be present. As a result, stricter regulations will be necessary to ensure correct de-orbiting and minimising risk of collision.

Touching on size, CubeSats (below 10 kg) represent 39% of all EO satellites, whilst large (above 500 kg) amount to 30%, although this statistic does not account for unlisted military satellites³. These opposites of the spectrum encompass the two main approaches to EO satellite design: large, high orbit systems offering sharp ground resolution and small, high orbital velocity systems yielding significant temporal resolutions. Optical

²<https://www.ucsusa.org/nuclear-weapons/space-weapons/satellite-database> [Date accessed: 23-06-2019]

³<https://www.pixalytics.com/eo-satellites-in-space-2018/> [Date accessed: 23-06-2019]

miniaturisation advancements favour the CubeSat philosophy, packing powerful instruments into restricted sizes.

Optical sensors represent half of the payloads aboard EO satellites; other uses include Meteorology (12%) and Earth Science (9%), as reflected in Figure 2.2. This demonstrates the variety of applications possible with Earth imaging data, further elaborated in Figure 2.3.1.

According to [4] the commercial data market was valued at 1.7 billion USD in 2015 and is anticipated to total 3 billion in 2025. As seen in Figure 2.1, the defence sector is the number one consumer (61%) of data: this is no surprise, as governments constitute the top ten data users.

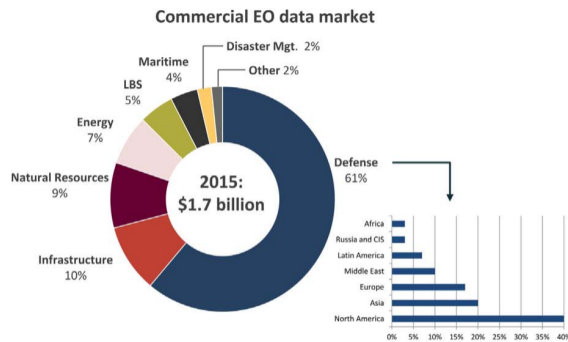


Figure 2.1: Commercial EO data market 2015. Courtesy of Euroconsult [4]

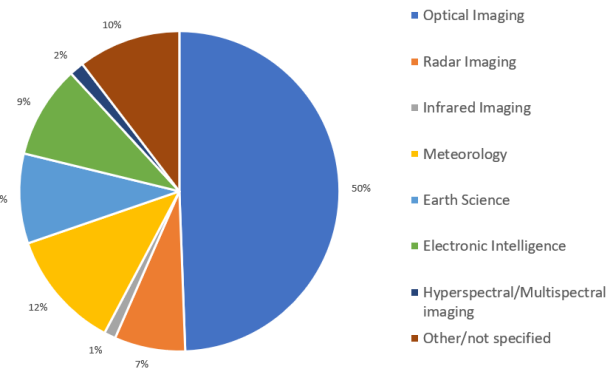


Figure 2.2: Classification of EO sensors. Data from ⁴

Earth observation applications

Earth imaging data is finding its place in a variety of applications. Depending on the sector, key performance parameters are: revisit time, speed of delivery to the customer, radiometric, spatial and spectral resolution, location accuracy and acquisition capacity.

Commercial applications are widely adopted by businesses as means to “peer over the fence” and obtain key information to boost productivity. Multispectral imaging has been successfully adopted in agricultural applications, enabling farmers to monitor crops, evaluate growth maturity and soil composition. EO data is slowly emerging in the finance sector notably in insurance claims verification and assets monitoring. Insurers could predict and evaluate the effect of hurricanes, earthquakes, fires and floods⁵. Synthetic aperture radar technology, suited for wide swath coverage and adverse weather conditions, is extensively employed to measure oil spills [5] and maritime vessel surveillance[6]: engine settings can then be optimised for performance and port waiting times reduced. The mining industry has also benefited from satellite imagery, facilitating the hunt for new resources and construction of new sites, especially in vast, mineral-rich countries like Australia⁶.

Civil government uses Earth observation for infrastructure development, emergency response planning and natural resource monitoring⁷. Landscape images allow for monitoring the effects of climate change and enforcing sustainability measures: Brazil’s government uses satellite data to monitor deforestation⁸. Ice melting and illegal dumping can easily be detected⁹.

Defence & intelligence is the most mature sector in Earth Observation, enabling foreign intelligence gathering. In recent news, satellite imaging enables the USA to track activity at North Korea’s rocket facilities and establish evidence for policy negotiation. With increasing resolution, the army will perform exercise monitoring and site monitoring for potential hazards¹⁰.

⁴<https://www.pixalytics.com/eo-satellites-in-space-2018/> [Date accessed: 23-06-2019]

⁵<https://cordis.europa.eu/news/rcn/9669/en> [Date accessed: 23-06-2019]

⁶https://www.geoimage.com.au/media/brochure_pdfs/GeoimageMiningBrochure_FEB%202015.pdf Date accessed: 23-06-2019]

⁷https://www.mdpi.com/journal/remotesensing/special_issues/urban_development [Date accessed: 23-06-2019]

⁸<https://www.dw.com/en/brazils-amazon-deforestation-documented-via-massive-satellite-imaging/a-46651844> [Date accessed: 23-06-2019]

⁹https://m.esa.int/Our_Activities/Observing_the_Earth/Space_for_our_climate/Monitoring_climate_change_from_space2 [Date accessed: 23-06-2019]

¹⁰[https://www.airbus.com/newsroom/press-releases/en/2018/12/Airbus-built-French-military-Earth-observation-satellite-\(CS0\)-launched-successfully.html](https://www.airbus.com/newsroom/press-releases/en/2018/12/Airbus-built-French-military-Earth-observation-satellite-(CS0)-launched-successfully.html) [Date accessed: 23-06-2019]

2.3.2 Competitor analysis

In Figure 2.3 an overview of competing platforms is shown. The reported temporal resolution of the Flock-1 constellation by Planet was adjusted in the original figure based on Planet's own information which indicates that it is capable of daily revisits at most¹¹. Two design philosophies can be distinguished when looking at the figure: large satellites for cheap, low-resolution imagery, and large satellites for expensive high-resolution. A new emerging design philosophy is using a constellation of smaller satellites with a medium resolution but a high revisit time.

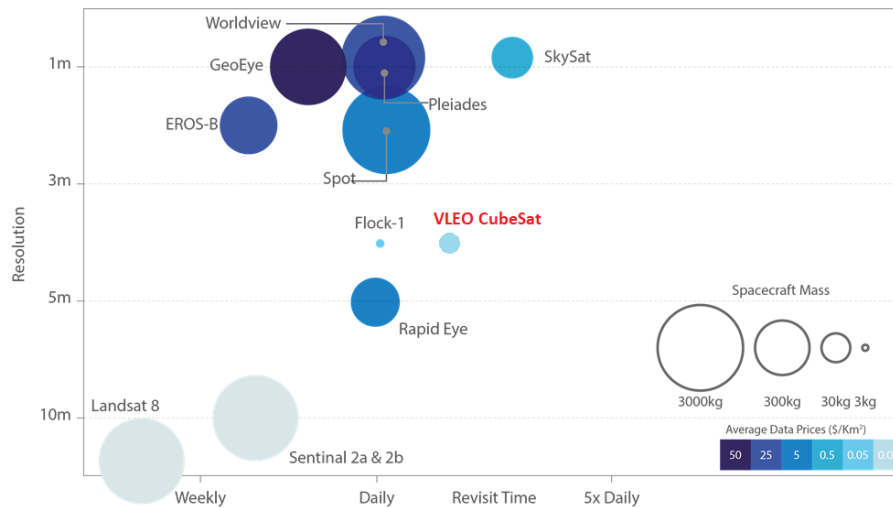


Figure 2.3: Competitor overview. Adapted from ¹²

2.3.3 SWOT analysis

The SWOT analysis consists of internal and external factors. Internal factors are the strengths and weaknesses of the organisation that is developing the product. External factors are the opportunities and threats that external parties pose. External parties consist of (potential) customers, competitors, suppliers and knowledge institutes [3].

It should be clear that the internal factors, the strengths and weaknesses, are about the organisation that is going to develop the product, not the product itself¹³. So, a piggy-back launching option for CubeSats to reduce the cost of launching is not a strength of the team, but an opportunity to reduce mission cost, and thus belongs to the external factors.

Internal factors

To come up with the internal factors, the strengths and weaknesses of the team, the condition and other boundary conditions of the project team were listed. From this, the following strengths and weaknesses were derived. This was done with the mindset that this DSE team is an early stage start-up in Delft.

Strengths

- Low stakes because the company is in an early development stage. Therefore, the team can take more risk in development.
- Good work atmosphere between recent graduates who are eager to prove themselves in the real world.
- Being located near TU Delft, where a lot of knowledgeable professors are located that can be asked for help because they are former professors of the team members. This environment has spawned some space start-ups such as ISIS, Hyperion, T-minus and Dawn aerospace.

Weaknesses

¹¹<https://www.planet.com/products/monitoring/> [Date accessed: 20-05-2019]

¹³<https://www.strategischmarketingplan.com/swot-analyse/> [Date accessed: 23-06-2019]

- Limited development time of 10 weeks
- The team members are recent graduates and thus have limited experience in the field
- The team consists of only aerospace engineers, so the team is not very multidisciplinary

External factors (trends)

External factors are the opportunities and threats that the current and future market possesses. Meaning, the external factors are about market trends. To structurally identify these market trends the external factors are grouped into fundamental opportunities & threats of CubeSats for Earth observation, and the six aspects of the DEPEST checklist.

Fundamental trends A key focal point of CubeSats is reducing mission cost, possible through their standardisation and size. Standardisation of components makes development times way shorter and thus cheaper. The smaller size reduces the launch cost because CubeSats can usually be launched as secondary payload, i.e. a piggy-back option.

Size limitations restrict the use of complex and sophisticated payloads; this can be offset by orbiting closer to the target, leveraging camera aperture dimensions as a result of higher spatial resolution. This entails reduced power requirements for telecommunication in spite of shorter distances to the ground station. Eventually, a smaller antenna is needed which alleviates the effects of atmospheric perturbations.

Another threat for missions using CubeSats is that the insertion orbit is often the same as the insertion orbit of the main payload because they are launched as secondary payloads. So the target orbit should be one which has frequent launches that could be piggy-backed.

Demographic trends More people are moving from the countryside to urban areas. This means that less farmers are in charge of providing the same, if not higher, amount of food for themselves and people living in urban areas. This means the farmers need to increase their efficiency to meet the needs of the market. Earth observation is already used in agriculture and, at a cheaper price, can serve a lot more farmers in the future to achieve their efficiency targets.

Economic/market trends The global CubeSat market is estimated to have a size of about 150 million USD and is expected to grow to about 375 million USD in 2023 [1], [7], [8]. This means a growth of about 20% annually. This growth will be the average of the following market segments: Earth observation & traffic monitoring, meteorology, space observation, communication, and science & technology and education. Of these sectors, the Earth observation & traffic monitoring is expected to experience the highest annual growth [1], [7], [8] of up to 49% [9]. Most of the growth of the whole market is expected in North America, because there the number of CubeSats launched every year is the highest and there is an increasing demand for satellite services from government agencies and commercial satellite operators [1], [7], [8]. If the market is segmented based on the number of units in a CubeSat, the 3U segment is estimated to have been the biggest in 2018 [8] and is expected to grow the most in the coming years [1]. The biggest threat to economic growth of the CubeSat market is the lack of launch vehicles [7].

CubeSat technology in Space Situational Awareness (Space Situational Awareness (SSA)) is expected to grow with about 20% annually in the next ten years [9]. Examples of this market are: Survey and tracking of objects in Earth orbit, monitoring of space weather and watching for Near-Earth Objects (NEOs)¹⁴. Most current SSA applications focus on government and military applications, but it is expected that the commercial sector will grow substantially in the next years [9]. CubeSats are expected to take a significant market share of this growth because of their benefits: a high temporal resolution, low latency and low cost of deployment. A limitation for CubeSats is their limited communication capability. But usually SSA applications only require small data packets, so CubeSats are actually very suitable for SSA applications¹⁵.

Customers want better images of their assets, and in order to attract new customers to unexplored applications, a higher spatial resolution is required. In Figure 2.4, the current trend can be seen. It is clear, that in the last forty years the spatial resolution has been steadily becoming better, with spatial resolutions of three meters

¹⁴https://m.esa.int/Our_Activities/Operations/Space_Situational_Awareness/About_SSA [Date accessed: 23-06-2019]

¹⁵<https://www.linkedin.com/pulse/situational-awareness-key-smallsat-target-carolyn-belle/> [Date accessed: 23-06-2019]

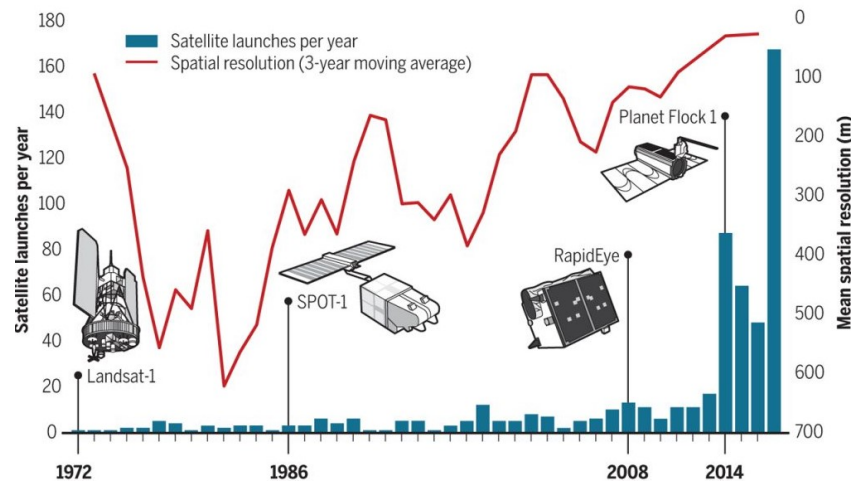


Figure 2.4: Market trends in spatial resolution¹⁶

on the CubeSat platform and sub-meter spatial resolutions now available on small satellites. It can also be seen that the amount of satellites launched each year has dramatically increased in the last five years.

Besides a better spatial resolution, the temporal resolution is also increasing [10]. "New Space" companies such as Planet have built constellations of satellite to have temporal resolutions of one day or less¹⁷.

Social trends Just like DIY-biotech, some people are afraid of the potential evil that can be performed with CubeSat technology¹⁸. Since it is relatively easy to develop a CubeSat, there is a possibility for evil amateurs to build their own CubeSats for applications that could be dangerous to the general public. However, it is important to mention that overall public view is positive, as CubeSats are used for education and make space cheaper and more accessible.

Some people also see it as space trash¹⁹. Space debris is a serious problem, of which the general public is aware. Some people see the deployment of CubeSat as an increase of space debris rather than the applications that they can actually fulfil.

Technological trends There are several technological trends in progress for CubeSats: mission design, small satellite launchers, high-resolution imaging, Synthetic Aperture Radar (SAR), communication, miniaturisation, propulsion systems and deorbit & space debris removal technologies.

Mission design: One of the trends in mission design is the introduction of Software-as-a-Service (SaaS). With this trend, satellite operators sell the ability to monitor a certain piece of land on the Earth directly to their customers instead of selling satellites with the capability to do so²⁰. In this case, a customer does not need to be involved in the satellite design at all and only needs to discuss with the satellite operator what their end-goal is. The satellite operator can then offer an (existing) software solution to achieve this end-goal. All design, production and operational aspects of the satellite are completely taken care of by satellite operator itself. This opens the market to new customers who are not familiar with satellite technology but see the potential of the service provided. An example of this is the company Planet²¹. More information about their capabilities will be outlined in Subsection 2.3.2.

With the continuous monitoring of Earth, an enormous amount of data becomes available every day. For this data to be useful, it needs to be processed. Lots of users don't have the capability to process this amount of data. Cloud computing services using Artificial Intelligence (AI) for automated change detection are on the

¹⁶<https://www.planet.com/products/monitoring/> [Date accessed: 23-06-2019]

¹⁷www.planet.com [Date accessed: 23-06-2019]

¹⁸<https://theconversation.com/the-future-of-personal-satellite-technology-is-here-are-we-ready-for-it-58478> [Date accessed: 23-06-2019]

¹⁹<https://www.space.com/36506-cubesats-space-junk-apocalypse.html> [Date accessed: 23-06-2019]

²⁰<https://www.pixalytics.com/4-eo-trends-2018/> [Date accessed: 23-06-2019]

²¹<https://www.planet.com/> [Date accessed: 23-06-2019]

rise²². In this case AI can automate the work of scanning through all the pictures while looking for items/events of interests.

Small satellite launchers: In recent years, the development of dedicated small satellite launchers has increased significantly. Encouraged by government programs such as the European Unions Horizon 2020. Currently, there are six small launch vehicles under operation, and 34 are under development [11]. These small satellite launchers are capable of carrying at most 1000 kg of payload to Low Earth Orbit (LEO). Higher availability of these launchers can make it possible for CubeSats to have their own dedicated launch and thus be inserted in their target orbit by the launcher. This is in contrast to piggy-back options where the CubeSat end up in the target orbit of the main payload.

High-resolution imaging: In the future the difference in resolution between small and large satellite imaging will diminish [9]. To increase the resolution capabilities on small satellites, they can be deployed at a lower altitude, have bigger apertures, use deployable lenses, employ post-processing software, develop aperture synthesis interferometry technologies, combine multiple low-res images, and use in-space manufacturing technologies to increase SmallSat size in space [9]. A lot of these technologies are being introduced on small satellites (<100 kg) but it is expected that CubeSats will eventually also reach higher resolutions. For this project, flying in a VLEO is one of the means for increasing resolution.

Synthetic aperture radar: During night or when there are clouds the monitoring capabilities of satellites with visual spectrum cameras are very limited. The introduction of SAR technology can change this as this technology can see through clouds and during the night. There are several organisations exploring the possibility of SAR technology on CubeSats and it is expected that this will be operational around 2030 [9].

Communication: Communication is a big limitation for CubeSats. Because of their limited size and power, they are usually equipped with an unidirectional antenna which has a limited bandwidth to send data back to Earth. On-board processing can reduce the required bandwidth by doing some of the image processing on board of the satellite, instead of at the ground station [9]. A way to increase the bandwidth is the use of optical communication. Optical communication could allow data rates from 100 Mbit/s up to 10 Gbit/s²³. TESAT, KSAT and Gomspace aim to demonstrate this technology later in 2019.

Miniaturisation: Miniaturisation of subsystems can lead to reduced power requirement, volume and mass. This can allow the payload to consume more power and/or be heavier and thus have higher specifications. A smaller size is especially interesting for a CubeSat mission in VLEO because of the reduced drag that comes with a smaller size.

Miniaturisation can be done by integrating the propulsion subsystem in the ADCS, so the ADCS control actuators become redundant and can be removed [9]. Another area of improvement is an increase in efficiency of solar panels and energy storage [9].

TU Delft is also working a lot on miniaturisation of space systems. One way to reduce the size of the camera is to remove the lens of it altogether and replace it using masks/coded apertures [12]. This breakthrough could potentially lead to higher resolution imaging from CubeSats as the limitation on camera size that can be fitted on a CubeSat includes the size of a lens.

Propulsion systems: Trends in propulsion systems are to develop micro-propulsion systems capable of providing a ΔV of 1000-2000 m/s [9]. These systems would be required to increase the lifetime of CubeSat operating in a lower orbit. So this development could be quite interesting for this project in order to expand the mission duration of CubeSats in VLEO.

Deorbit & space debris removal technologies: De-orbiting satellites at their End-of-Life (EOL) is now a requirement for satellites in LEO. If satellites are not equipped with active propulsion, new technologies like drag sails could help to create enough atmospheric drag to deorbit a satellite at the desired moment.

Ecological trends In the last years, the global impacts of climate change have become far more pronounced. There has been an increase in forest fires²⁴, and ice caps are melting at an increased speed²⁵. These problems entail adequate monitoring to facilitate policy enforcement. Hence it is expected that governments and non-profit organisations will develop and expand existing programs to gain insights on climate change mitigation.

²²<https://www.pixalytics.com/4-eo-trends-2018/> [Date accessed: 23-06-2019]

²³<https://www.kongsberg.com/ksat/news-and-media/news-archive/2019/nanosatellites-see-the-light-laser-communication/> [Date accessed: 23-06-2019]

²⁴<https://climateatlas.ca/forest-fires-and-climate-change> [Date accessed: 23-06-2019]

²⁵<https://www.sciencenewsforstudents.org/article/antarcticas-melting-speeds> [Date accessed: 23-06-2019]

Additionally, an inherent advantage of VLEO is the ease of EOL manoeuvres for de-orbit, enabling easier certification procedures.

Political trends The European Union (EU) has developed a Space Strategy for Europe in which they outline the strategy to address climate change, stimulate and help the economy, and provide immediate information when disaster strikes. Two points from their strategy, that are particularly interesting to this project, are their plan to promote investments in space-related start-ups and their support for the development of dedicated small satellite launchers.

Another policy point, that is becoming more important within the scope of CubeSats, are collisions in space. If the launching of CubeSats goes on like this, it could pose a threat to other space missions, because the amount of CubeSats can grow to an enormous amount²⁶. Because of this, it is not unimaginable that in the future, CubeSats are required to be equipped with a deorbiting technology that can ensure safe deorbiting at end of life [9]. The amount of objects in Low Earth Orbit (LEO) is already approaching 15 000, as can be seen in Figure 2.5.

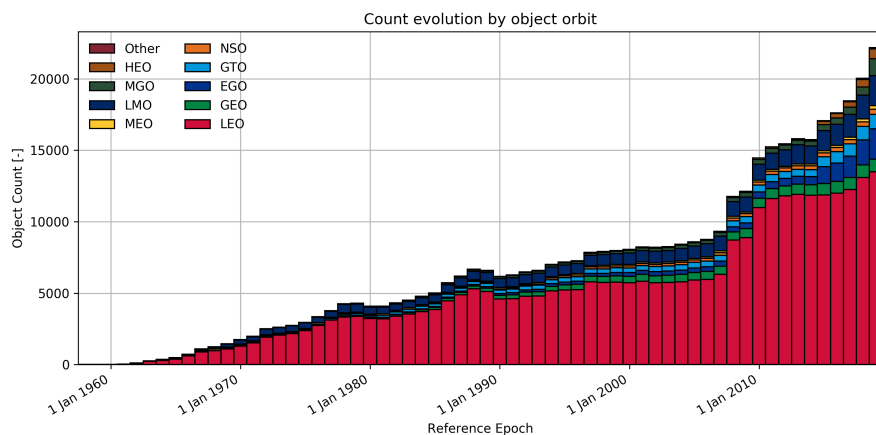


Figure 2.5: Space debris evolution in various orbits²⁷

SWOT-matrix

Using all information of the previous sections, a SWOT-matrix was created and is presented in Figure 2.6. The SWOT matrix, together with the competitor analysis will be used to conclude on the product approach to market.

2.3.4 Product approach to market

The customer wants Group 17 to develop an Earth observation CubeSat orbiting in VLEO. This allows for fitting cheaper and smaller cameras on a CubeSat whilst maintaining a spatial resolution of less than 4 m. Temporal resolution will be pushed to 12 hours, as this has not been done before with the CubeSat platform.

Without propulsion, the mission duration of CubeSats with an orbit between 230 and 380 km is between 6 and 12 months [2]. Proximity to the TU Delft, a leading player in micro-propulsion development, yields possibilities to include a propulsion system in the design, to compensate for drag. Being able to take more risks in the design, it has been decided to develop a CubeSat that has a longer lifetime than competitors in an attempt to drive down launch cost. The design lifetime of this CubeSat shall be 5 years.

Focus on mission duration will likely push the product development in the following directions:

- Micro-propulsion
- Aerodynamic design
- High accuracy attitude control

²⁶<https://www.newscientist.com/article/mg22329882-500-cubesat-craze-could-create-space-debris-catastrophe/> [Date accessed: 23-06-2019]

²⁷https://www.esa.int/Our_Activities/Space_Safety/Space_Debris/Analysis_and_prediction [Date accessed: 23-06-2019]



Figure 2.6: SWOT matrix

The latter is needed to allow for accurate payload pointing despite high aerodynamic torques experienced in VLEO. Additionally, a stringent stability requirement is compulsory during picture capture to avoid blurring.

2.4 Risk management

The risk management is an important aspect of the design process. When risks are not properly managed, they could have a catastrophic impact on the mission, resulting in a complete failure of the product. Risk management comes with trade-offs, on whether or not it is worth to mitigate certain risks, as the mitigation process costs money and other resources. The risks have been divided into different types. First of all, there are the subsystem based risks, those are technical risks which go into depth regarding subsystems. Secondly, there are the environmental risks, which come from the hazardous space environment the Sat-ELITE has to survive in. Lastly, there are the operational risks, which are risks regarding the production and launch process.

2.4.1 Assessment and mitigation

The risk management process started in the planning phase of the project. A big list of potential risks was set up by the risk manager, responsible for keeping an eye on these risks and making sure mitigation is incorporated throughout the design. As the project progressed, certain risks were expanded upon and new risks were found. Throughout this report, relevant subsystem based risks will be identified, and each risk gets its own unique identifier. These identifiers are mentioned in the relevant sections, and in [Appendix D](#) the complete list will be given for reference.

After a risk is identified, the severity of the risk should be accessed. A highly likely risk for example might not prove severe if its impact is negligible. If however, a risk does prove severe, there should be a thought on mitigation techniques. Common mitigation techniques include adding in redundancy, using Commercial off the Shelf (COTS) parts with a higher Technology Readiness level (TRL), or redesigning components to make them more robust to unexpected situations.

During important trade-offs, risks were taken into account, resulting in certain options being eliminated, since they would be too risky, and a safer approach was available. This, for example, resulted in an innovative hinged design to not be chosen for the detailed design phase, as its feasibility was questionable, resulting in its risk being too high. This is an example of a higher level trade-off, but also on a lower level, the feasibility, and thus to an extent the risks, have been taken into account.

2.4.2 Contingencies

A risk that should be mentioned in advance is the risk of a design oversight [TR-OP-6]. Design oversights appear very early in the project's lifetime, and their severity steadily increases as long as they stay undiscovered. This is why there are contingencies put into place. These contingencies build in a safety margin so that when a design oversight is discovered it is less likely for a subsystem, or the entire system for that matter, to exceed its allocated budgets. These contingencies are based on the design progress of each subsystem.

2.5 Sustainable development strategy

Any project or, for that matter, any economic, social or political activity shall adhere and contribute to the three pillars of sustainability: economic, social and environmental. One of the earliest major statements on sustainability is in the report named *The Limits to Growth* [13]. The report brings to public discourse various major trends of global concern such as growing industrialisation, depletion of environment and non-renewable resources, rapid population growth. The report has two major conclusions:

- If the present trends of growth continue, the limits of growth will be reached within the next century and most likely will end with an abrupt decline in world population and industrial capability;
- It is possible to alter the growth trends, to ensure a sustainable stability between economic and environmental factors for the far future. The state could be designed such that the basic needs are met for all of the Earth's inhabitants and that each person has an equal opportunity to maximise his own individual potential.

The surfacing of the term sustainable development is attributed to the report *Our Common Future* [14] or how it is often referred - the Brundtland Report, named after the chairman of the commission. This report presents a definition of sustainability that goes beyond economic and environmental spheres, to also include the social and inter-generational aspects. The most recent major report was published in 2015 by the UN called *Transforming our world: The 2030 agenda for sustainable development* [15]. The report defines 17 Sustainable Development Goals (SDGs), as seen in Figure 2.7, which must be achieved by year 2030.



Figure 2.7: 17 Sustainable Development goals as defined in the UN report from year 2015 ²⁸

CubeSats and other forms of small satellites can provide a lot of support for the SDGs [16]. The miniaturisation trend advances space to be a technological frontier that is much more socially and economically inclusive.

²⁸http://www.bitc.ie/wp-content/uploads/2016/08/Chart_of_UN_Sustainable_Development_Goals.png [Date accessed: 06/05/2019]

2.5.1 Contribution to sustainable development goals

The miniaturisation of space systems has allowed the space sector to become much more versatile and socially including. Especially, the inclusion of the Global South has never been more possible with the declining costs of designing and launching satellites [16], contributing to SDGs 4, 8, 9 and 10. With the demand rising for commercial production of CubeSat components, the efficiency of production and standardisation increases.

A satellite constellation dedicated to Earth observation can provide critical data to better understand the sustainable development on a global, as well as on a local scale. With a high temporal resolution, the change in the state of a system can be effectively monitored. With more creative approaches the data from the satellites can provide proxies for many hard-to-measure parameters. One such approach was to obtain data on economic livelihoods in the developing world, combining night and daytime satellite imagery and machine learning, to predict poverty [17], understanding the extent of it and contributing to the first SDGs.

The project could provide individually assessed, non-governmental organisations with data to monitor crisis areas, illegal environment transformation, such as logging in protected rain forests, monitor the movement of animal species, monitor violent weather, etc, enabling the project to contribute to goals 13 and 16. It follows that there is an immense spectrum of applications that could contribute positively to SDGs.

2.5.2 Issues related to CubeSats

In the space sector environmental issues have only recently come under closer scrutiny [18], especially the crowding of low Earth orbits with space debris and the radio frequency interference between space systems, high altitude platform systems, unmanned aerial vehicles and also ground based communication systems [16].

In the recent years the CubeSat market has grown immensely and is expected to continue growing at almost 20% yearly according to a global forecast till year 2023²⁹. Recent studies suggest that well above 90% of defunct small satellites, especially from large constellations, have to be safely deorbited to avoid the formation of new space debris. Therefore, it is crucial to design an extremely reliable deorbit mechanism for the CubeSats. An attractive feature of the requirement on the VLEO is that at such low heights the drag component is quite prominent, meaning that the satellite naturally deorbits at a rapid rate. Assessing the current and past CubeSat project launches³⁰ it is evident that for CubeSats without a propulsion system at circular orbits of approx. 390 km the re-entry is performed after 3-6 months after launch. Even so, all the satellites must be tracked over their orbital lifetime.

The need for less toxic manufacturing solutions shall also be communicated to the market. An increase in demand leads to an increase in supply and a reshaping of the market. The project, which encompasses hundreds of CubeSats, would definitely have an impact to the market and could even attract more investors by being the flagship of sustainability in space design.

2.5.3 Environmental assessment

To assess the environmental impacts of the satellite project the tool of choice is Life Cycle Assessment (LCA) [18]. One of the benefits of using LCA is that it is a standardised model based [19], which is already in use in different industries. This allows for structured environmental analysis throughout the whole project life 'from cradle to grave', avoiding the effect of burden shifting from one life cycle phase to another one. European Space Agency (ESA) has been showing a lot of interest in green approach and considers itself a pioneer in an eco-friendly approach to space activities³¹.

Figure 2.8 is an excellent example developed by ESA Clean Space. The relationship between the project and the environment is clearly seen. The arrows coming in represent resources used and the arrows departing - pollution to the environment.

For the next stages of the project it is advised to perform a partial and later a full scale LCA to evaluate the environmental impacts of the project using a thorough approach and tools developed by ESA.

²⁹<https://www.marketsandmarkets.com/Market-Reports/cubesat-market-58068326.html> [Date accessed: 21-05-2019]

³⁰<https://airtable.com/shrafcwXODMMKeRgU/tbldJoOBp5w1N0JQY> [Date accessed: 21-05-2019]

³¹https://www.esa.int/Our_Activities/Space_Safety/Clean_Space [Date accessed: 23-06-2019]

³²https://www.esa.int/Our_Activities/Space_Safety/Clean_Space/The_Challenge [Date accessed: 23/06/2019]

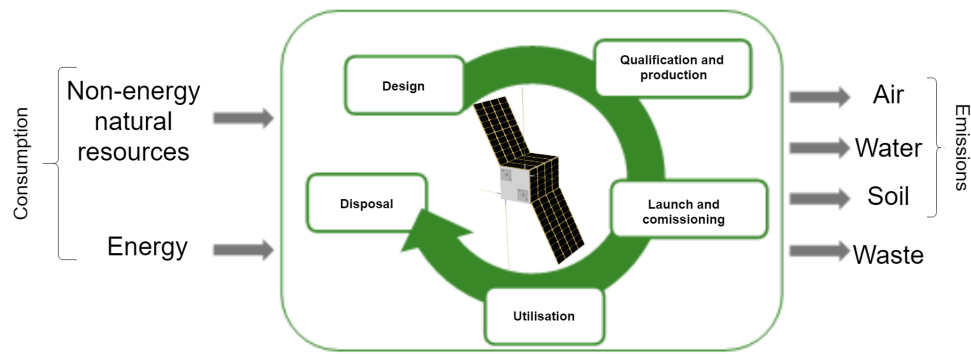


Figure 2.8: LCA model adapted from ESA Clean Space initiative ³²

The philosophy of lean practice shall be implemented on every level. This has implications for both organisational and technical parts of the project. Examples in the organisational sector are usage of cloud services to avoid printing, using reusable cups for coffee, averting the use of 400-500 single use cups. Active management of workload is also used to ensure effective use of man hours.

The engineers and managerial staff are encouraged to travel with bicycles to work for health benefits and reduced greenhouse gas emissions. To maximise productivity, short, but frequent breaks are taken as it has been shown that not taking breaks has a potentially detrimental effect on the productivity and focus [20].

2.5.4 High level approach

It is useful to define sustainability objectives, that can help to determine the aspects of sustainability as a design parameter. These are already largely represented in an organised way in Figure 2.8. The mission's sustainability objectives are - eliminate waste, prevent pollution, maximise recycling, minimise energy use, minimise greenhouse gas emissions.

To ensure that the design and project is adhering to sustainable development, sustainability is introduced as an additional and mandatory design parameter in all trade-offs. Furthermore, the sustainability engineer shall be present in the technical meetings where major design decisions are made to ensure that sustainability objectives are taken in account. The parameter shall estimate the use of energetic and non-energetic resources, emissions to the environment and waste throughout the manufacture of the CubeSat. The weighing of the environmental parameter shall be done according to the project's sustainability objectives.

The framework is to evaluate the effect on the environment and come up with possible sustainable alternatives, while keeping the impact on the overall system to a minimum. Important to take notice of is the fact that the design space narrows as the project advances. Therefore, it is crucial to pay special attention to sustainability in the very early stage of design [18].

2.5.5 Emission quantification

Launchers emit both Greenhouse Gas (GHG) emissions and other particulate contaminants during the ascent. On the global scale the GHG emissions do not constitute a large emission source, at least with the current launch rates. A single Falcon 9 launch emits $O(10^5)$ kg of CO_2 emissions, which is a tiny fraction of global CO_2 emissions that are in the order of $O(10^{13})$ kg³³. Although, it can be argued that the CO_2 emissions are not critical for the planet, the stratospheric deposition of black carbon from kerosene-fuelled engines and alumina particles from solid rocket motors [21] are potentially quite dangerous to the ozone layer, which already is not in prime health status. If the emissions needed for launch are compared to the positive impact that the data acquired by satellites can bring, the argument that the positive impact outweighs the negative impact of launch emissions stands on solid ground.

The deposited particles in stratosphere have a cooling effect on the Earth's surface and is similar to geo-engineering techniques, which increase the reflectivity of upper levels of atmosphere to decrease the flux that reaches the lower parts of atmosphere and Earth's surface. While this might seem beneficial, the deposited particles damage the ozone layer most commonly through two mechanisms. First, by increasing temperature of

³³<https://www.globalcarbonproject.org/carbonbudget/18/highlights.htm> [Date accessed: 21-05-2019]

the stratosphere the already existing chemical reactions are accelerated. Second, through reactions on the surface of the deposited alumina particles. Currently the net effect is not precisely understood, but it is estimated that global ozone depletion does not exceed 0.1% [21]. Furthermore, the stratosphere and troposphere mix extremely slowly, therefore the emissions remain there for long periods of time [22]. Accordingly, it is important to minimise the mass that has to be sent to space to minimise both the GHG emissions and the deposition of byproducts of the burning of rocket fuel.

Ground operation CO₂ emissions largely depend on the design of the facilities. Currently, it is not yet estimated how much GHGs are to be emitted in the atmosphere throughout the manufacturing process. The emissions and energy usage of a corporate building with floor area of 200 to 300 m² vary between 0-30 tonnes of CO₂ per year³⁴. It becomes apparent that over the mission time of more than 5 years, the operations also become an important player in the sustainability of the project. Thus, it is crucial to use a sustainably designed office space.

2.5.6 Green propellants

Currently, the most widely used propellant on satellites for attitude control and propulsion is hydrazine [23]. It allows for a simple, reliable and well-established design of the propulsion system. Hydrazine has a high vapour pressure, which is often favourable for propulsion systems as it's natural pressure can be used to deliver the fuel to the combustion chamber even further simplifying the design.

This comes at a high cost. Hydrazine is a highly reducing agent that poses serious threat to environment. Even more so, it is extremely destructive to living tissue and is a possible carcinogen [23]. It is listed as one of the most shock-sensitive chemicals. Due to the high vapour pressure it is extremely volatile and it's handling can be performed only in specially certified locations. All of these reasons call for strict regulation, which in turn make the process slow and expensive [23].

Research in High Performance Green Propellants (HPGP) is actively ongoing, with the micro-propulsion technology recently being flight proven. In 2014 NASA led the Green Propellant Infusion Mission that brought the TRL from 6 to 9 [24]. This HPGP has higher specific impulse, density, it is more stable and much less toxic. Some estimate that for the same propellant volume it can produce up to 50% higher performance [24]. Most importantly, it does not pose an environmental hazard and is not corrosive and carcinogenic. This could decrease the risk of serious environmental damage in the case of propellant mishandling during ground operations. Moreover, the costs are also greatly lowered in logistics and it allows for more responsive launch preparations as the regulations are much more lenient³⁵. It does have drawbacks as, for example, it is notoriously hard to ignite [23]. Consequently, large thruster systems are yet to even surpass conceptual design stages, but it might prove to be a viable alternative for launchers in the future.

2.5.7 Subsystem sustainability

This chapter has laid out a framework within which it is possible to evaluate the sustainability of the design as a whole as well as within each of the subsystems. One of the main challenges with respect to sustainability is that it covers a large range of aspects, which may sometimes mean that a reduction in one of the factors can lead to a worse situation in another one. Figure 2.8 serves as a good baseline for evaluating the impacts on sustainability as it includes multiple criteria that represent the problem zones, therefore, does not allow for shift of consequences between the criteria.

Unfortunately, not much information is present in the product data sheets that would provide an exact estimate for the sustainability of it. As a result, a decision to use mostly COTS components was made with the assumption that much less resources have to be spent on their design and manufacturing. Furthermore, the choice to use toxic materials and resources will be averted where possible. In further discussion with the part manufacturers data on their emissions, waste processing and manufacturing processes will be requested to evaluate the effects explicitly.

³⁴<https://fusiontables.google.com/DataSource?dsrclid=531109> [Date accessed: 23/06/2019]

³⁵<https://directory.eoportal.org/web/eoportal/satellite-missions/s/skysat> [Date accessed: 22-05-2019]

3. Concept operations and selection

With the strategy clearly defined, the top level operations need to be decided on. This is where system engineering comes into play. First of all, a functional flow diagram and functional breakdown structure are made, so that an idea is created of what the tasks of the Sat-ELITE will be. These diagrams can be found in [Section 3.1](#). These functional diagrams are then made into an operations and concepts logistics description, which will show the different modes that the Sat-ELITE will come across, as seen in [Section 3.2](#). To keep an overview of the system design, an N^2 chart was created found in [Section 3.4](#), so that each subsystem designer knew what values were expected from them. Finally, the conceptual trade-off is summarised in [Subsection 3.5.4](#).

3.1 Functional diagrams

Functional diagrams are an important, systems engineering tool to schematically represent all the functions that the system has to perform. All the logical connections between the functions are represented and analysed. The diagrams allow to keep a high level overview of the different functions of the satellite ensuring that no function is left untended. Moreover, the diagrams are useful for generating the requirements.

3.1.1 Functional Flow Diagram

The whole Functional Flow Diagram (FFD) is shown in [Figure B.1](#) found in [Appendix B](#). The FFD layout for the top level is inspired from a NASA example for a FFD¹ and can be seen in [Figure 3.1](#). Instead of having a simple sequential functional development, it is organised such that all the main functions of the spacecraft are connected according to their possible interactions. An example could be the following one: after receiving a command for changing attitude at block 8, the system passes through the *OR* gate before block 5 and 4 to check for contingencies. Then it passes through the hold block, passes the *OR* switch, arriving at *Manoeuvre the spacecraft* containing the required sub-function. The decision on which path to follow after an *OR* switch is made according to the specific situation or process ongoing. Block 10, namely, *Perform operational support functions*, is included to show all the background processes required during each function showed in the diagram and it interacts with all other blocks.

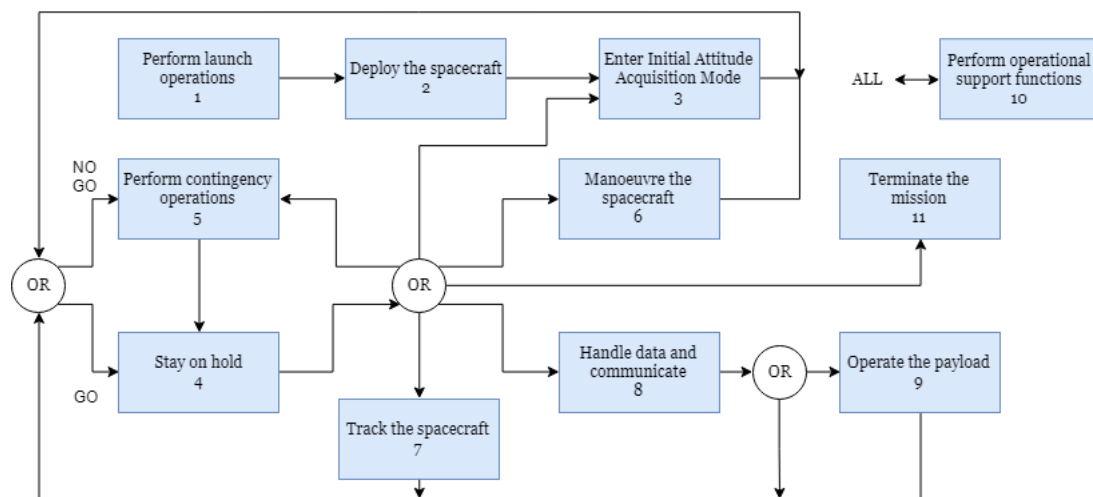


Figure 3.1: FFD top level structure

In the complete diagram present in [Appendix B](#) the structure is conserved, adding all the corresponding sub-functions. The principal functions are underlined colouring the blocks with the same shade of blue as the one used in [Figure 3.1](#). Blocks that are difficult to connect with arrows are repeated to avoid confusion; an example of that is block 3. Furthermore, each block has a unique identifier that can be seen just below the title.

¹https://upload.wikimedia.org/wikipedia/commons/7/79/Functional_Flow_Block_Diagram_for_Mission_Control.gif [Date accessed: 20/6/2019]

3.1.2 Functional Breakdown Structure

The FBS is presented in [Figure C.1](#) found in [Appendix C](#). It contains all the identified functions, starting from the higher level functions corresponding to the same blue blocks as seen in [Subsection 3.1.1](#).

The grouping of the criteria in chronological and logical order is kept similar to the FFD to keep the numbering logical and consistent. The additional lower level functions are derived from the subsystem levels. Only for block 8, *Handle data and communicate*, colour coding is added for lower level tasks and can be seen in [Figure 3.2](#). This is to distinguish between the functions related to the two different subsystem and show their interlinks. Blue colour is kept for high level tasks.

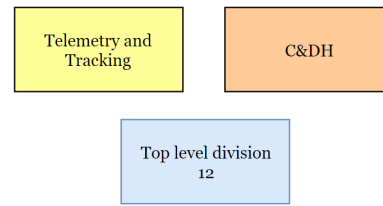


Figure 3.2: Colour legend for subsystem FBS

Block 11, *Terminate the mission* does not have any sub-functions as all the actions required to terminate the mission of the spacecraft are included elsewhere. For example, a deorbit burn does not have any particular difference from a normal manoeuvre burn.

3.2 Operations and concepts logistics description

During the mission, operations are performed on a cyclic basis. These operations can be visualised in the form of an operational flow diagram as can be seen in [Figure 3.3](#). This diagram is based on the mission operations presented in Space Mission Analysis and Design (SMAD) [25].

The mission is driven by the market. Customers either want a single picture (e.g. making a road map), temporary monitoring (e.g. measuring oil spills) or continuous monitoring (e.g. agriculture). These different customer needs are an input for mission planning, which decides how the constellation of satellites will be able to comply with the needs. From mission planning commands are generated and sent to the spacecraft. However, before being sent the commands will run through a simulation, which checks if they result in the desired outcome or if more iterations are needed in the calculations of the command. Finally, the spacecraft can then receive the command sent by the ground station. After taking pictures, the spacecraft sends down the obtained data together with orbit and spacecraft functional data, to the ground where it will be saved, analysed and post-processed. The pictures will be processed and sent to the customer while the other data will be used to resolve any anomalies concerning spacecraft functioning and/or orbit control.

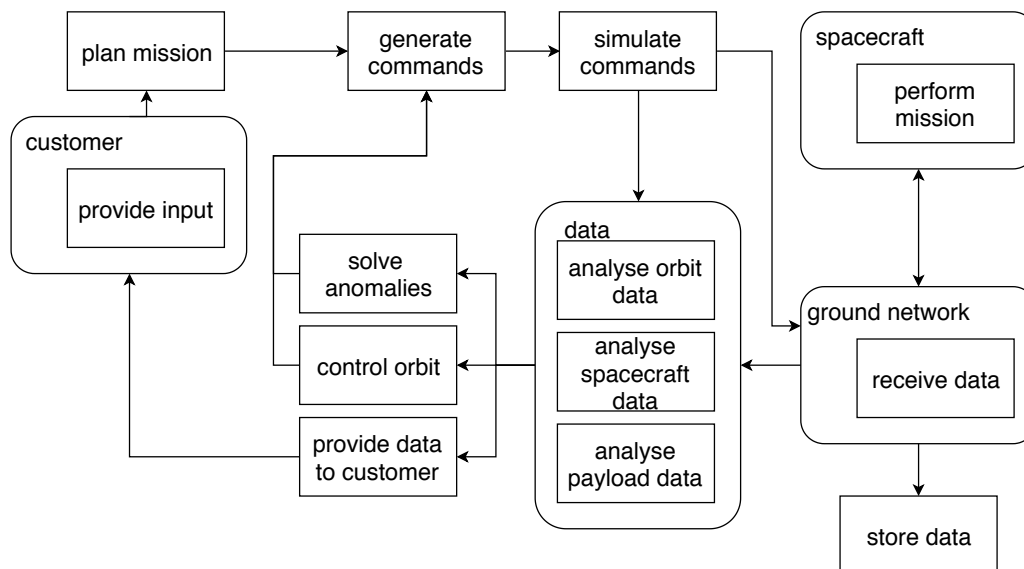


Figure 3.3: Mission operations diagram

3.2.1 Initial operations

Before the nominal operations can be started, the spacecraft needs to be initialised. This starts when the launcher deploys the satellite and ends when the spacecraft is ready to start nominal operations. An overview is given in [Figure 3.4](#). It can be seen that detumbling and liquifying of propellants can be done in parallel. Going from the initial to the final orbit will be the last operation before nominal operation and will be elaborated on in [Section 4.6](#).

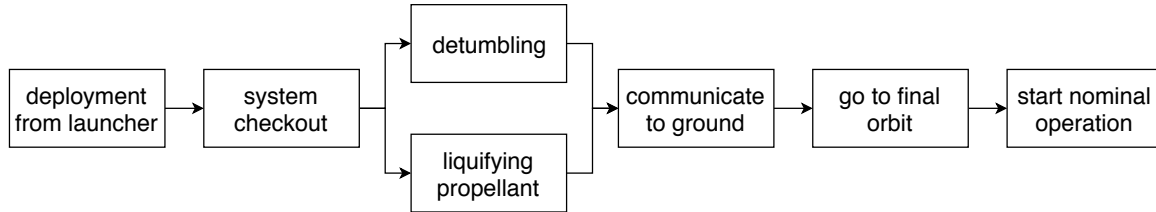


Figure 3.4: Initial operations

3.2.2 Operational modes

Discrimination between operational modes is typically based on the function (e.g. ensuring operation of payload), control and attitude requirements, as well as the power consumption. Identification of these modes aids preliminary design of certain subsystems, such as ADCS and EPS, as well as Command & Data handling (C&DH) subsystem. The operation modes presented in reference missions are used as the building basis for the modes required for Sat-ELITE [26, 27] in addition to SMAD [28]. The modes used for operations of the Sat-ELITE are nominal, communication, thrusting, desaturation, detumbling and safe mode. In [Section 9.1](#) a more technical overview of the modes is given with allocated time during each orbit and power consumption for each mode.

Nominal mode The goal of the mission is accomplished employing nominal mode because pictures are taken during this mode. It follows that the time of this mode during operations should be maximised. In order to make pictures of the right place on Earth the spacecraft shall be able to align its payload with nadir with a pointing accuracy better than 0.25 deg. Furthermore, to maintain the ability to take sharp images, the CubeSat shall maintain attitude stability of 0.22 deg/s around all 3 rotational axes. The source of this requirement is discussed in [Subsection 6.1.3](#).

Communication mode While orbiting the Earth, the spacecraft will accumulate data as it is taking pictures. For this data to be useful, it needs to be downlinked to Earth. During communication mode, the spacecraft will first point its antenna towards the ground station and then it needs to slew such that the antenna is continuously pointing towards the ground station.

In addition to downlinking data, the communication mode also allows for data to be sent to the spacecraft. Useful data for the spacecraft are new commands to redirect the mission.

Thrusting mode Because the satellite is flying in VLEO, it will lose energy during orbiting due to aerodynamic drag. That is why for certain moments over the orbit the propulsion system will be activated to raise the orbit to stay within operational limits.

Desaturation mode The ADCS reaction wheels will build up momentum during operation and at one point will not be able to spin any faster to counteract external torques. To prevent this, the reaction wheels need to be desaturated, which will happen during this mode.

Detumbling mode After initial deployment from the canister, the satellite will likely have some angular rates in all directions. So it is typically the starting mode of the spacecraft after booting [27]. This control mode aims to reduce this tumbling of the satellite so it can operate normally. In addition, this mode can also potentially be initiated if during any point in the mission the spacecraft is experiencing tumbling.

Safe mode In case of a substantial anomaly within the operation of the spacecraft for which the spacecraft cannot correct on board, safe mode is activated. During this mode, only vital life systems are operational to save power until the anomaly can be resolved. If power is low, the spacecraft shall assume an attitude state that ensures maximum power generation. When there is enough power left in the batteries, the spacecraft shall align itself in minimum drag configuration, so it does not lose too much altitude while being in safe mode. The spacecraft can only exit this mode after the anomaly has been assessed and safe further operations can be guaranteed.

3.3 Coordinate systems

Overall, four right-handed coordinate systems (CS) are setup (Earth, Orbit, Velocity and Body CS) so that sun vector can be transformed to incidence angles on different satellite faces. These are presented in Figure 3.5. Orbit CS is defined by angle ascension node with respect to sun (b) and inclination (i) moving from E. Velocity CS is then defined by some fixed rotations and orbital angle (t). Body CS is defined by angles roll (r), pitch (p) and yaw (y) with respect to Velocity CS. Body axis Zb points with camera and thrusters act in -Xb.

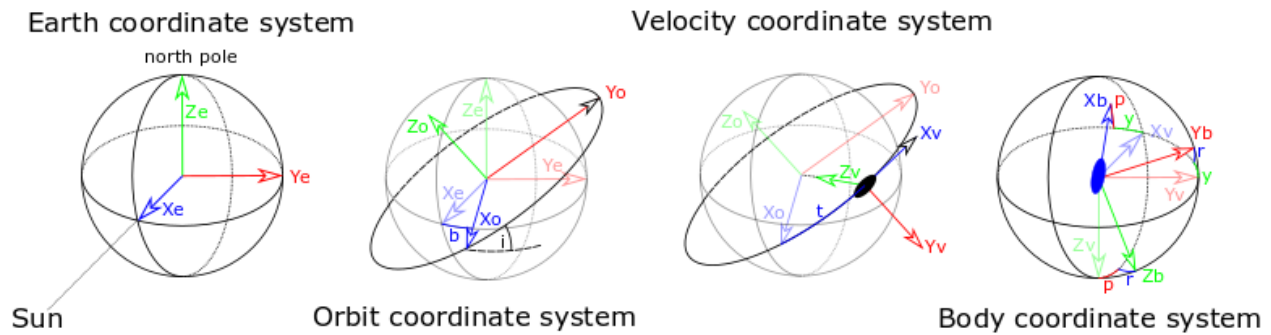


Figure 3.5: Design coordinate systems

3.4 N² chart

Once the functionality of the spacecraft was explicitly defined, the team needed a way to keep track of the interfaces and dependencies between the different subsystems. A useful tool for this is the N² chart. Given in Figure 3.6, the main diagonal of it contains the various departments within the team. Horizontal rows represent outputs, while vertical rows represent inputs. For example, the structures department outputs the general geometry and centre of mass location to the aerodynamics department which then performs calculations using these as input and outputs magnitude of aerodynamic torques to ADCS. The N² chart was used throughout the project to keep track of the different design variables that each subsystem requires from others. Moreover, in case of iteration with no initial estimates it helped choose the starting point. A good example is the final orbit parameters. The orbit & constellation department needed to provide orbital parameters for nearly all departments, but it simultaneously required input from most of them. Visualising this in the chart helped manage the problem and better evaluate which of the parameters are less susceptible to change and freezing them, and iterating between the subsystems to finally arrive at the final orbit parameters in order to be able to continue with the design.

↕	ADCS		Power	Heat capacity, temperature range	Mass, position				
↕	Aerodynamic torques	Aerodynamics				Cd			Telemetry information Cd
↕			Electrical power	Heat capacity, absorbtivity, emissivity, temperature range	Mass, position				Telemetry information
↕			Power	Thermal control	Mass, position				Telemetry information
↕	Moments of inertia, centroid location	Geometry, CoM		Heat capacity, absorbtivity, emissivity, temperature range	Structure	Mass, Geometry, CoM			Mass
↕	Thrust torque		Power	Heat capacity, temperature range	Mass, position	Propulsion			Telemetry information DeltaV
↕	Slew rate, required attitude	Required off-axis orientation, slew rate	Power	Heat capacity, temperature range	Mass, position		Communication		Storage volume, number of data writes in lifetime, telemetry information Data speed
↕	image sharpness criteria, integration time		Power	Heat capacity, absorbtivity, emissivity, temperature range	Mass, position	Data size, FoV, Sensor resolution		Payload	Spatial resolution, FoV
↕			Power	Heat capacity, temperature range	Mass, position				C&DH
↕	Altitude, inclination	Latitude, Longitude, Altitude, Epoch, Attitude	Altitude, inclination, orbit period, argument of the ascending node	Altitude, inclination, orbit period, argument of the ascending node		Orbit period	Altitude, Inclination, longitude of the ascending node	Altitude	Orbit & constellation

3.5 Trade-off

To start off, the trade-off method rationale is introduced in [Subsection 3.5.3](#). The generated concepts and the thought processes leading to them are presented in [Subsection 3.5.1](#), as well as a CAD model for each. [Subsection 3.5.2](#) presents a feasibility study which eliminated certain designs with unacceptable weaknesses. The remaining are considered in a detailed analysis in [Subsection 3.5.4](#), whereby a winner is selected. Lastly, a sensitivity analysis is executed in [Subsection 3.5.5](#) to investigate the robustness of the trade-off to a variation in input and emphasis on different criteria.

Fruitful internal discussions resulted in the generation of seven concepts, each yielding a special attribute. Each concept has been based on the available cameras: the ANT-2A, SEEING 1.8 m and SEEING 7 m, which are presented in [Table 3.1](#)

Name	GSD [m]	FoV [deg]	Swath width [km]	Pixels	Aperture [mm]	Focal length [mm]	Bandwidth [nm]	SNR [dB]	Size [cm]	Mass [kg]	Power [W]
ANT-2A @ 350km	4	2.6	16x16	4000x4000	80x60 (Rect.)	612.5	400-700	88.6 (RGB)	10x10x30	2	2
SEEING 7 @ 600km	7	6.3x4.3	60x40	6000x4000	130	330	475-900	>256 (panchromatic)	16x16 x14	10	30
SEEING 1.8 @ 600km	1.8	1.1x0.7	11x7.5	6000x4000	190	1800	475-900	>128 (panchromatic)	20x20 x20	10	30

1. **CON-3U** is characterised by the ANT-2A camera placed vertically, entailing an extremely compact design.
2. **CON-4U** features an aerodynamic fairing, and a mirror which allows the ANT-2A to be mounted horizontally. This minimises the frontal area and aligns thrust with the velocity vector for efficient burn.
3. **CON-6U-a/b** are two 3x2x1 U concepts differing in camera aperture. A small aperture can be achieved with the ANT-2A camera while for the medium aperture no commercially available camera was found yet. This design is beneficial in terms of ADCS control, as the moments of inertia are similar in all directions.
4. **CON-6U-c** is highly elongated to minimise frontal area and provides freedom to add many solar panels, it also features the ANT-2A camera in the horizontal configuration. To mitigate the high lateral loads occurring in launch, one configuration denoted as **CON-6U-c-H** features a hinge mechanism which unfolds in flight. This will permit launches in 3x2x1 U launch canisters, readily available and cheap.
5. **CON-6U-d** maximises the internal volume by confining the payload mirror on the exterior, additionally maximising the instrument aperture. For this configuration, no commercially available camera was found.
6. **CON-12U-a/b** has symmetric, cuboid shape facilitating ADCS control and housing the larger SEEING cameras. Two configurations are possible: 'a' houses the better Ground Sampling Distance (GSD), narrow FoV SEEING 1.8 m camera, and 'b' houses the worse GSD, wider FoV SEEING 7 m. Both are structurally conventional.

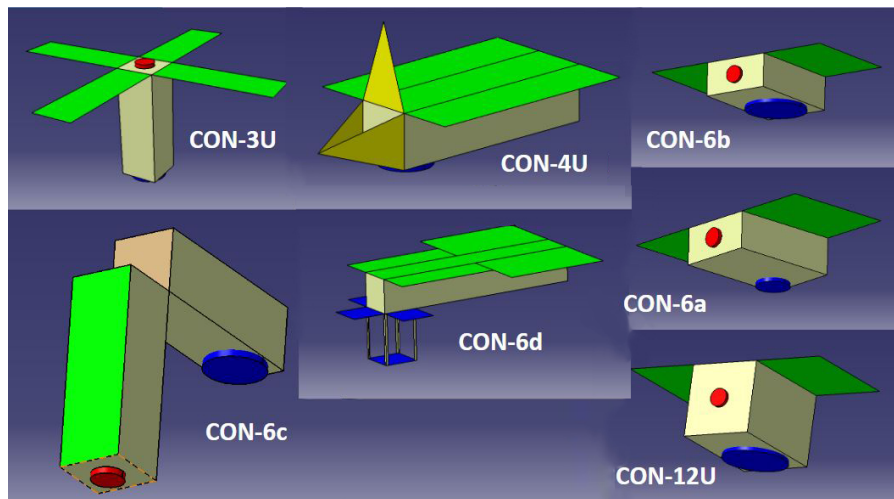


Figure 3.7: CAD models for the generated concepts. Green, red and blue represent solar panels, propulsion system and payload aperture, respectively.

3.5.2 Feasibility study

Feasibility study followed after concept generation to exclude unrealistic designs, presenting the flaws inherent to their layout. The following concepts have been discarded:

- **CON-3U**: The rotation and thrusting approach would drive payload activity to a tight margin. Furthermore, it does not have enough volume to house propulsion.
- **CON-4U**: The ANT-2A camera and mirror configuration would occupy 3U of space, leaving 1U for all other subsystems, which was calculated to not be sufficient. On a positive note, the aerodynamic fairing idea was deemed a possible idea for other concepts as well.
- **CON-6Ua**: The ANT-2A camera and mirror configuration occupy 3U of space, permitting 3U for other systems. While volume-wise this would have been enough for propulsion, any configuration would create either disturbance torques or drag too big to handle.
- **CON-6Ub**: Similar considerations as above, and no commercial camera was found with such dimensions.
- **CON-6Ud**: the external mirror would require incredible precision mounting. These tolerances would incur heavily on the design in terms of weight and cost. Furthermore, atomic oxygen is highly corrosive

at such low orbits². This design inherently adds pitching aerodynamic torques, burdening ADCS design. Notwithstanding such considerations, the surviving concepts present challenges too. These are investigated hereby, to avoid unexpected issues later in the design phase.

CON-6U-c-H sports a folding hinge mechanism. The mechanical feasibility was investigated, with notion to create a mechanism that is as simple as possible to minimise risk. A viable option is to simply include torsional springs with burn-wire release mechanism. Because the disturbances occurring in space are small, the two halves would be held together without any displacement, even when tumbling at a rate of π rad/s. Secondly, the control stability feasibility was investigated. Any object with distinct moment of inertia about its principal axes will be unstable when rotating about one of them. This is known as the intermediate axis theorem³. While the slender shape of this particular concept brought attention to this phenomenon, it applies to many spacecrafts and is not a problem as long the spacecraft's attitude is actively controlled.

3.5.3 Multi-attribute method

The trade-off method provided a framework within which each concept was evaluated. A proper framework scales adequately with the number of concepts and assessors. Other important features are traceability, flexibility with respect to correcting mistakes and fairness.

An important advantage of certain methods consists in dismantling the overall task into easier, smaller questions. This is similar to the famous Fermi estimation, where he estimated the number of piano tuners in Chicago. Rather than guessing their number straight away, it is better to estimate the number of people, households and pianos in Chicago first. This may seem counterproductive at first, because more factors need to be evaluated, but adding sub-estimations can balance out underestimations with overestimations resulting in a better estimate on average.

A multi-attribute utility function has been chosen to compare different concepts due to its compliance with the aforementioned important features. Its only drawback was that the team members had to get acquainted with it first to express their judgement properly. Mathematical expression of multi-attribute utility function can be seen in Equation 3.1.

$$U_{tot} = \sum_x^n k_x U_x(x) \quad (3.1)$$

Total utility U_{tot} is the ultimate composite criterion for judging concepts. Subscript (x) is the criterion, such as cost or innovation and n is the total number of criteria. The weight of criterion x is k_x , which scales from one to five (five meaning vital importance, one being negligible), reflecting the team members' opinions, mission objective and customer needs. This weight represents the emphasis placed on a certain criterion compared to others. Each concept is rated with respect to each criterion using a criterion level x , which also range from one to five. Utility function U_x gives the utility of each criterion level. These functions represent how criterion levels compare to each other and if there exists a requirement on the criterion, a step increase in utility function will reflect it. All these functions had to be defined uniquely for this project and each member had the same weight in the decision. While everyone can vote on each part of the trade-off, the team recognises specific personal expertise in different criteria. For example, only the sustainability officer judged the sustainability criterion based on his analysis. All in all, criterion levels are oriented such that a higher number indicates better performance.

Google sheets is an appropriate platform since it is stored on a cloud - people can access it simultaneously. Additionally, each team members ratings were hidden during the voting phase to minimise cross-member influence that might give rise to a bias in the ratings. Simpler, colour-based methods have been disregarded as they often lack traceability and are seldom automated.

3.5.4 Multi-attribute analysis

Criteria

Composing comprehensive criteria list was a challenge. Criteria had to reflect all customer, design team and market needs, while still being relevant to each concept and preferably independent of each other. Reconciling

²https://www.nasa.gov/topics/technology/features/atomic_oxygen.html [Date accesses: 06-06-2019]

³<https://rotations.berkeley.edu/a-tumbling-t-handle-in-space/> [Date accessed: 04-06-2019]

customer, design team and market needs perfectly has been deemed impossible. To illustrate: A customer requirement is to have a GSD of at least four meters, while market perspective dictates that the criterion should be price per km² of data, which is an unknown function of spatial, spectral, temporal and radiometric resolution. To add to the complexity, design team has a limited available time to make certain decisions. All this had to be evaluated, and in the end, final criteria are a compromise rather than perspective specific. The final list of criteria is presented below:

- **Mission cost** - High-level requirements impose limitations on the development cost of a single satellite unit, however this does not paint the whole picture: from a long-term strategy perspective (ensuring a competitive platform), one should consider both operational and launch costs. The former is impractical to estimate and would not yield a significant difference for the four concepts. The constellation launch cost is based on satellite mass and a viable launcher tariff. The unit cost includes only component costs. Benefiting from economies of scale, the learning curve model quantifies the total constellation cost for the number of units (N) as shown in Equation 3.2 [25] where S is the learning curve factor of 95%.

$$\text{Cost}_{\text{constellation}} = \text{Cost}_{\text{first unit}} \cdot N^{1 - \frac{\ln(100/S)}{\ln(2)}} \quad (3.2)$$

- **Spatial resolution** - directly related to image quality, hence restricting the potential applications. This depends on payload capabilities and orbital altitude.
- **Sustainability** - is directly related to the total constellation mass to be launched, as heavier launchers use more energy and generally have a greater environmental impact.
- **Reliability** - the reliability, robustness of the concept. A measure for safety. Component heritage, technology readiness and single points of failure affect the ranking.
- **Innovation** - the overall novelty of a concept, inherently hard to quantify: personal opinions play role in this. Innovation is inversely correlated with reliability, yet these carry different weights.

Criteria weights

Weights for criteria are in Table 3.2, reflecting what is important for this project and its mission statement. The rankings were based on a scale from totally pointless (1), through average importance (3), to totally vital (5). Mission cost and spatial resolution have the highest weight, as they drive the design from the market and customer perspective respectively. Mission cost is very important, but since it has limited scope, its weight is slightly lower. Sustainability has a high weight as protecting the Earth is of paramount importance. This is ultimately what has to be done so that space missions and human life can continue in the future. The relative weights of innovation and reliability reflect the design team's vision. One of the team's strengths is that it can afford to take risks and explore innovative rather than reliable concepts. Standard deviation is reflecting how do the team members' opinions vary and will be useful later in trade-off sensitivity analyses.

Table 3.2: Criteria weights

	Mission cost	Spatial res.	Sustainability	Reliability	Innovation
Weights	3.44	4.11	3.29	2.44	3.33
Standard deviation	1.01	1.05	0.71	0.73	0.71

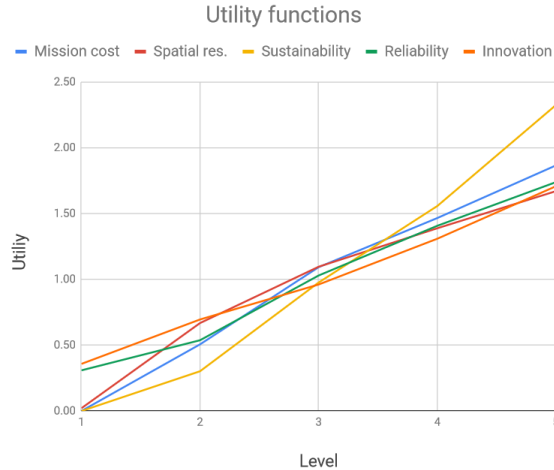
Criteria levels

Where applicable, criteria levels were setup such that 'Satisfactory' means just meeting the customer requirement. Their range was set up such that it encompassed all the concepts.

Table 3.3: Trade-off criteria levels

	criteria levels				
	Unacceptable (1)	Satisfactory (2)	Good (3)	Great (4)	Exceptional (5)
Mission cost	>150 M€	100-150 M€	75-100 M€	50-75 M€	<50 M€
Spatial res.	>4m	4m +/- 0.1m	2.5 - 4m	1-2.5m	<1m
Sustainability	can be launched with the Falcon 9 (8000 kg to SSO)	can be launched with the Soyuz ST-B (4400 kg to SSO)	can be launched with the Vega (1330 to SSO)	can be launched with the Epsilon (590 kg to SSO)	can be launched with the Electron (150 kg to SSO)
Reliability	Nearly all components are design for life with little to no flight heritage	Some components provide redundancy. Most are design for life with flight heritage	Most components employ redundancy; Some design for life components that have flight heritage exist	Concept has no single point of failure; Some parts have flight heritage	Concept has no single point of failure; All parts have flight heritage
Innovation	Concept uses only COTS parts; Similar designs widespread in the market	Concept uses only COTS parts; Similar designs (state of the art) exist	Most of the parts are COTS; Similar designs (state of the art) exist	Many subsystems take advantage of technology currently not available in the market. Similar designs (state of the art) exist	Many subsystems use technology currently not available in the market; Concept does something that hasn't been done yet, but could contribute to the industry

Criteria utility functions



Criteria functions relate individual criteria levels to each other within a criterion. To illustrate this, spatial resolution has a step up in utility on level 2 where it begins to comply with requirements. These functions have been adjusted to have the same average value, so that they are not affecting criteria weights. Utility functions for each criterion are shown in [Figure 3.8](#).

Figure 3.8: Trade-off utility functions

Concept budgets

Technical budgets for the multi-attribute trade-off are presented in [Table 3.4](#). These values were compiled from all relevant subsystems and they decided the concept criteria levels for the mission cost, spatial resolution and sustainability.

The number of satellites per launch was calculated by assuming two orbital planes and one launch for each plane. The amount of satellites in each plane was determined by the altitude and the FoV of the camera. A higher altitude and a wider FoV, means that a single satellite has a higher coverage and thus less satellites are needed in the constellation.

The satellite mass, component cost and energy needed per orbit were acquired by summing the mass, cost and energy needed per orbit of the individual components. From the component cost and constellation size, the mission cost was then derived as explained in [Subsection 3.5.4](#) in Subsubsection 'Criteria'.

Table 3.4: Technical budgets for concepts in trade-off

	CON-6U-c	CON-6U-c-H	CON-12U-a	CON-12U-b
Number of satellites per launch (total)	160 (320)	160 (320)	351 (702)	67 (134)
Satellite mass [kg]	7.16	7.16	17.7	19.3
Total mass per launch [kg]	1190	1190	6371	1229
Component cost [k€/sat.]	183	183	231	315
Mission cost [M€]	83.6	83.6	237.6	60.3
Energy needed [J/orbit]	55480	55480	130400	158400
Lifetime limit [years]	15	15	7	14
Spatial resolution [m]	4	4	0.8	4

The lifetime limit was calculated by evaluating the drag force that acts on a satellite at the altitude required to achieve a spatial resolution of 4 m. It can be seen that the lifetime for the two 6U concepts is very long as they are substantially more aerodynamic. The CON-12U-a flies at similar altitudes as the two 6U concepts and has a shorter lifetime because of its bigger frontal area. CON-12U-b has a longer lifetime because its SEEING 1.8 m camera allows it to fly at higher altitudes.

Trade-off results

The trade-off results are presented in Table 3.5 with colour coding only visualising the numbers. The winning concept is CON-12U-b which is characterised by a satisfactory resolution and wide FoV SEEING camera. Wide FoV is the main positive quality of this concept, as constellation size is dependent on it. Low constellation size improves mission cost and sustainability, ultimately making it the most competitive design. High resolution CON-12U-a has a larger camera inside and can produce higher quality data, however the amount of satellites needed for high temporal resolution proves this mission too costly and unsustainable. Between the CON-6U-c and CON-6U-c-H, the hinged CON-6U-c-H wins as the higher innovation is more important than the lower reliability. This concept, however, still loses to CON-12U-b due to the overall mission cost.

Table 3.5: Multi-attribute analyses results

	Mission cost	Spatial res.	Sustainability	Reliability	Innovation	Total Utility
CON-6U-c	1.13	0.82	0.96	0.82	0.97	4.72
CON-6U-c-H	1.13	0.82	0.96	0.46	1.56	4.94
CON-12U-a	0.00	2.06	0.00	0.89	0.91	3.87
CON-12U-b	1.52	0.82	0.96	0.91	0.91	5.13

3.5.5 Trade-off sensitivity analysis

Parameter values and assumptions of any model are susceptible to change and errors. To investigate this effect, a sensitivity analysis was performed and answered the following questions:

- Is the trade method robust?
- If selection criteria are modified (or removed), will the solution converge differently?
- From a technical perspective, how will concepts differ if a change in performance is required?

Trade method variation

Conceptual trade-offs can be either qualitative, quantitative or a mixture of both. How does one decide which approach is most suitable, and are these methods robust?

As previously mentioned, the team started off with seven concepts to be evaluated qualitatively, as putting definite numbers at an early stage would prove very time consuming and inaccurate. This method is very flexible in itself, as members gathered to point out possible flaws inherent to each design for all subsystems. This eliminated three concepts, deemed unfeasible and/or unprofitable. Afterwards, a more detailed analysis was made for the final trade-off between the concepts. To verify robustness of this method, σ of criteria weights was recorded in Table 3.6, to be used when shifting the weights. In essence, both quantitative and

qualitative approaches were adopted in the trade-off, according to the tolerable level of complexity. As a result, the mechanism incorporated both engineering intuition and numerical evaluation.

Criteria weights variation

In the conceptual design phase, team members have independently ranked five parameters in accordance to the influence these carried on mission success, leading to a preferred design concept as shown in Table 3.5. In the later design phase, however, situations could be faced which might alter the criteria scores. One interesting experiment is to predict such scenarios, modifying the criteria weights accordingly and observe at what point the winning concept is overtaken. This demonstrates the robustness of the performed trade-off to a change in weights. To keep a clear overview of modifications, this operation will follow the one-factor-at-a-time approach, in reality however these factors are intertwined. Consider the following example: the need for a higher altitude will ease the mission cost whilst decreasing spatial resolution at the same time. Table 3.6 quantifies this experiment, reporting the shift required (out of five points) for each criterion to overthrow the winning concept, keeping in mind a positive value indicates a higher emphasis. A larger margin between this and the standard deviation σ indicates a robust trade-off strategy.

Table 3.6: Criteria shift needed to overthrow the winning concept

Criterion	σ	Delta	Emphasis	CON-6U-c	CON-6U-c-H	CON-12U-a	CON-12U-b
Original	/	/	/	4.72	4.94	3.87	5.13
Mission Cost	1.01	1.88	-	4.16	4.39	3.87	4.38
Spatial Resolution	1.05	3.38	+	5.20	5.43	5.56	5.55
Sustainability	0.71	4.67	-	4.98	5.24	3.87	5.23
Reliability	0.73	1.11	-	4.66	5.08	3.73	5.06
Innovation	0.71	1.06	+	4.73	5.12	3.93	5.11

The results are interpreted as follows:

- A negative shift (relaxation) on *cost* favours the hinged 6U concept: this is traced back to a larger constellation size, and thus higher cost. In that case, the hinged concept would then overtake CON-12U-b because of its innovative design. From a business standpoint, the customer might decide to invest more money for a more innovative product.
- If the customers require a sharper *spatial resolution* CON-12U-a would win. It has the best camera, enabling high resolution pictures.
- Concerning *Sustainability*, all concepts have a similar score except the high-resolution SEEING concept, which would require a large constellation to meet the requirement.
- *Reliability* of CON-6U-c-H relates to the introduction of the hinge. This concept has not been used in CubeSats before and thus has more risk. So if less emphasis is put on reliability, CON-6U-c-H wins.
- The hinge adds a score to the *innovation* of CON-6U-c-H, yielding a chance to design something unprecedented in the space environment.

As seen by the difference σ -Delta, the method is fairly robust with regards to a change in criteria. Innovation is the most sensitive aspect, promoting the hinged concept. Despite this, the team is confident that CON-12U-b's 3U of free space bear great potential to improve the concept's innovation as it allows to introduce secondary experimental payloads or subsystems.

4. Orbit analysis and drag compensation

Now that the general mission profile is analysed, a more concrete mission design can be made. This mission design concerns the exact orbit in which the satellite will fly, as well as the design of the constellation which will fulfil the mission. A propulsion system is used to maintain this orbit, compensating the drag evaluated by a sophisticated aerodynamic model.

In this chapter, first, the orbit will be selected, including a launch method, in [Section 4.1](#). Then, the aerodynamic model is presented in [Section 4.2](#), followed by a selection and discussion of propulsion system in [Section 4.3](#). The final altitude at which the spacecraft can sustain the mission duration of five years is derived in [Section 4.4](#), by looking at the capabilities of the propulsion system to counter the drag described by the aerodynamic model. In [Section 4.5](#), mission compliance is ensured by designing a constellation. Finally [Section 4.6](#) combines all mission phases into one ΔV budget.

4.1 Orbit selection

System requirement **SYS-OBJ-PL-4** dictates that the system shall be able to image the 99% of the Earth's surface. This directs the selection of orbits towards polar or Sun-synchronous orbit (SSO). The International Space Station (ISS) orbit is also considered as it has a small satellite orbital deployer, which is dedicated to the deployment of CubeSats¹. Other reasons, such as frequent and regular launches to the ISS, make this a popular orbit for CubeSats. These three potential orbits (polar, SSO and ISS orbit) will be evaluated on coverage, solar input and other orbit specific (dis)advantages.

Polar orbit

A polar orbit is an orbit in which the spacecraft orbits the Earth around the poles, thus having an inclination of 90 deg. It is a popular orbit for Earth observation satellites as it allows for covering the entire Earth daily². So the total coverage is 100%, and thus it would meet requirement **SYS-OBJ-PL-4**.

However, due to the J_2 perturbation, this orbit will rotate around the Earth with respect to the Sun. This means that during every orbit the angle between the orbital plane and the Sun changes, resulting in different input from the Sun on the solar panels. This increases both the complexity of the calculations required for the power input from the Sun and the design for the solar panels. The solar panels should then be designed such that the panels are on multiple sides of the spacecraft or are able to rotate towards the Sun. So, they can still produce enough power as the orbit changes with respect to the Sun.

Sun-synchronous orbit

The J_2 perturbation that causes the polar orbit to rotate with respect to the Sun can also be turned into an advantage. If the inclination is selected carefully for a certain altitude, the rotation of the orbital plane around the Earth will exactly match the rotation of the Earth around the Sun. That way the orbit does not change with respect to the Sun, as illustrated in [Figure 4.1](#), so it processes around the Earth at exactly 360 deg/year³. The change in longitude of ascending node should then be: $\dot{\Omega} = 360 \text{ deg/year} = 2.0 \cdot 10^{-7} \text{ rad/s}$. [Equation 4.1](#) from [29] can then be used to calculate the required inclination for a certain altitude. The unitless perturbation coefficient (J_2) is equal to $1.083 \cdot 10^{-3}$ [29]. Furthermore, the radius of the Earth is denoted by R_{Earth} , the semi-major axis of the orbit by a , the inclination of the orbit by i and the orbital period by T_o . It is calculated that for an orbit at 230 and 380 km the inclination should be 96.4 and 96.6 deg, respectively, to achieve an SSO.

$$\dot{\Omega} = -3\pi J_2 \frac{R_{Earth}^2}{a^2} \cos(i) \frac{1}{T_o} \quad (4.1)$$

This inclination has a disadvantage with respect to the coverage. The highest observable latitudes will be around 83.6 and 83.4 deg for orbits of 230 and 380 km respectively. However, the disadvantage is minimal because the reduction in coverage is minimal. The spacecraft will for example still be able to see the northernmost permanently inhabited place in the world - Alert in Canada⁴, which is approximately 800 km away from the North Pole. On the South Pole the spacecraft would also miss a circle with a radius of approximately 800

¹<https://www.space.com/18091-tiny-satellites-space-station-launch-photos.html> [Date accessed: 15-05-19]

²<https://www-spf.gsfc.nasa.gov/Education/wlopolar.html> [Date accessed: 15-05-19]

³<https://landsat.gsfc.nasa.gov/geometry-of-a-sun-synchronous-orbit/> [Date accessed: 15-05-19]

⁴https://www.dailymail.co.uk/travel/travel_news/article-4207688/Inside-Alert-northerly-settlement-world.html [Date accessed: 15-05-2019]

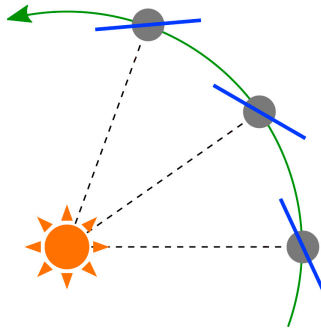


Figure 4.1: Sun-synchronous orbit

km, which is well within Antarctica⁵. So the total coverage of the Earth's surface would still be 99%, which is enough to fulfil requirement **SYS-OBJ-PL-4**.

Due to the fact the orbit does not change with respect to the Sun, the solar power received is the same each orbit. This drastically reduces the complexity of the calculations and the design of the solar panels. Furthermore, a constellation of satellites in an SSO will always observe the same point on Earth at the same local (solar) time⁶. This is beneficial for Earth observation as it ensures the same lighting conditions on the points of interest, which makes the pictures between different days easy to compare.

ISS orbit

Since the inclination of the ISS orbit is only 51.6 deg⁷, the coverage is rather limited. For example, this would mean that it would not be possible to see Delft⁸. So it would also not pass requirement **SYS-OBJ-PL-4**.

For solar input, the ISS orbit would have the same problems as the polar orbit. Thus the complexity of the calculations and the design of the solar panels would increase.

The only advantage of an ISS orbit are the frequent launches to it and its dedicated CubeSat deployer. This might make it a good candidate for the first prototype.

4.1.1 Launch method

The two launch methods that will be considered are a piggyback launch and a dedicated launch, both launch options should be considered according to requirement **SYS-LCH-VEH-1**. Both methods have their own advantages and disadvantages.

Piggyback option

A piggyback has the obvious advantage that it can dramatically reduce launch cost, due to the fact CubeSats can fit in standardised containers that can be put in unused space of launchers.

However, the reduction in cost comes with a price. Because the CubeSat would be launched as secondary payload, they are simply put in the target orbit of the primary payload. If a special orbit is desired, the CubeSat should launch together with a primary payload that has (approximately) the same target orbit. This poses a challenge for this mission. Since there are not a lot of launches to an orbit in VLEO, the CubeSat needs to have a means of transferring from the primary payload orbit to its own target orbit, so each orbit has its own ΔV requirements.

Polar orbit: Satellites in polar orbit are usually in LEO. So, to reach the target orbit of the CubeSat, which is in VLEO an orbit transfer should be performed. To calculate the required ΔV a Hohmann transfer is analysed. In Equation 4.2 [29] the orbital velocity (v) is given as a function of the standard gravitational parameter (μ), which is equal to $3.986 \cdot 10^{14} \text{ m}^3\text{s}^{-2}$ ⁹ and r is the height of the orbit relative to the centre of the orbited body.

⁵https://www.nasa.gov/mission_pages/icebridge/multimedia/fall11/antarctica-US.html [Date accessed: 15-05-2019]

⁶<https://earthobservatory.nasa.gov/features/OrbitsCatalog/page2.php> [Date accessed: 16-05-2019]

⁷<https://spaceflight.nasa.gov/realdata/sightings/SSApplications/Post/JavaSSOP/orbit/ISS/SVPOST.html> [Date accessed: 15-05-2019]

⁸<https://latitudelongitude.org/nl/delft/> [Date accessed: 15-05-2019]

⁹http://maia.usno.navy.mil/NSFA/NSFA_cbe.html#GME2009 [Date accessed: 03-06-2019]

From this equation, the required ΔV to transfer from an initial circular polar orbit at 1000 km to 230 km or 380 km is 417 or 330 m/s depending on the exact altitude.

$$v = \sqrt{\mu \left(\frac{2}{r} - \frac{1}{a} \right)} \quad (4.2)$$

Sun-synchronous orbit: Typical SSO's are at an altitude of 600 to 800 km above the Earth¹⁰. The required inclination at SSO at 600 to 800 km can again be calculated using Equation 4.1. This results in an inclination of 97.8 and 98.6 deg respectively. The ΔV needed to change the inclination from these values, to the required inclination of the target orbit, is about 249 m/s, using Equation 4.3 [29]. The orbit should be lowered after performing this manoeuvre. In the case a Hohmann transfer is used, the orbit will take an additional 219 m/s resulting in a total of 468 m/s. The inclination change, and change to and from Hohmann transfer orbit can be combined in two manoeuvres instead of three. This would then take about 350 m/s.

$$\Delta V^2 = 2v^2 \cdot (1 - \cos(\Delta i)) \quad (4.3)$$

ISS orbit: The ΔV required to bring a satellite down from an ISS orbit at 400 km¹¹ to an orbit between 230 and 380 km would require 98 to 11 m/s using a Hohmann transfer.

Dedicated launch

From the previous section it is clear that piggyback options cannot result in a mission with low ΔV and high coverage. A solution is to use a piggyback launch for a prototype and deploy the final constellation using dedicated launchers. There are a lot of dedicated small satellite launchers in development and quite a few are already in operation [11]. However, note that the drawback is an increase in the cost.

Inspection of the advantages and disadvantages of the three orbits considered yields the SSO as the preferred option. It only minimally compromises on coverage while having a large advantage in power system calculations and design, as well as advantages in lighting conditions for the pictures used in Earth observation.

4.2 Aerodynamic model

In order to more precisely quantify the dynamic behaviour of the satellite, a simulation evaluating aerodynamic torques is developed. The necessity to accurately model these torques stems from their dominant nature at the altitude of interest [30].

4.2.1 Framework selection

For aerodynamic investigation, it is very useful to define the general theoretical framework, and consequently the assumptions, which will be considered in further evaluation and calculations. The Knudsen number (Kn) is taken as a principal indicator to decide whether statistical or continuum mechanics formulation of fluid dynamics should be used [31]. Figure 4.2 fully summarises the relation between the models and the Knudsen number. It can be evaluated through Equation 4.4 where the mean free path (λ_{fp}) is rewritten for a Boltzmann gas to expand the formula. Standard parameters included in the equation are Boltzmann constant (k_B), thermodynamic temperature (T) and total pressure (p).

$$Kn = \frac{\lambda_{fp}}{L} = \frac{k_B T}{\sqrt{2} \pi d_p^2 p L} \quad (4.4)$$

¹⁰https://ipfs.io/ipfs/QmXoypizjW3WknFiJnKLWHCnL72vedxjQkDDP1mXWo6uco/wiki/Sun-synchronous_orbit.html [Date accessed: 15-05-2019]

¹¹https://www.nasa.gov/mission_pages/station/expeditions/expedition26/iss_altitude.html [Date accessed: 15-05-2019]

Using average values of VLEO pressure and temperature [28, 32] and considering molecular oxygen as the main constituent of the thermosphere [33] with a particle hard-shell diameter (d_p) of $1.2 \cdot 10^{-10}$ m, λ_{fp} becomes $8 \cdot 10^4$ m for the lowest possible orbit. Finally, dividing by a possible average reference length (L) of one meter, the Knudsen number is calculated to be in the order of 10^4 , which is comfortably over the limit of ten where pure free molecular flow is considered. Similar conclusion can be found in the reference mission of Δ DSat [34].

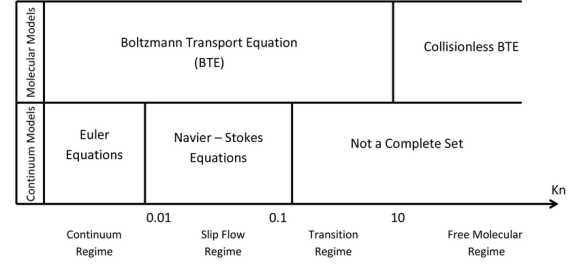


Figure 4.2: Flow characteristic relations [35]

4.2.2 Analytical model

After having identified an appropriate set of the governing equations and models, more specific calculations can be performed. An analytical model can be selected and used to get a first approximation of the forces. The same model will also be used for verification purposes. For this preliminary estimate the only force considered is drag, as lift is at least one order of magnitude smaller [33, 34]. Furthermore, the body of the satellite is assumed to be approximated by a combination of flat plates.

Schamberg's quasi-specular and quasi-diffuse drag coefficients, presented in Equation 4.5 and Equation 4.6, respectively, can be used to give a first order estimate of the drag of a flat plate at an incidence angle (θ_i) [36]. The advantage of this model is that no atmospheric properties (such as specific concentration of single constituents) are needed other than the parameter r which is defined as $r = \sqrt{1 - \alpha_{ac}}$, where α_{ac} is the accommodation coefficient. On the other hand, the equations describe two distinct scenarios without having the capability to capture a possible intermediate situation. Furthermore, no straightforward calculations for α_{ac} exist.

$$C_D = 2(1 - r \cdot \cos(2(\theta_i + \pi/2))) \quad (4.5)$$

$$C_D = 2\left(1 + \frac{2}{3}r \cdot \sin(\theta_i + \pi/2)\right) \quad (4.6)$$

To overcome the two limitations just presented, [36] introduces a number of reasons, such as contamination of the surface material, that can be used to assume that in VLEO the distribution of the molecules is close to the diffuse case and that α_{ac} is close to one, regardless of the surface material. Considering the latter assumptions, Equation 4.6 can be used to calculate the C_D for a flat plate at an arbitrary aerodynamic angle of incidence.

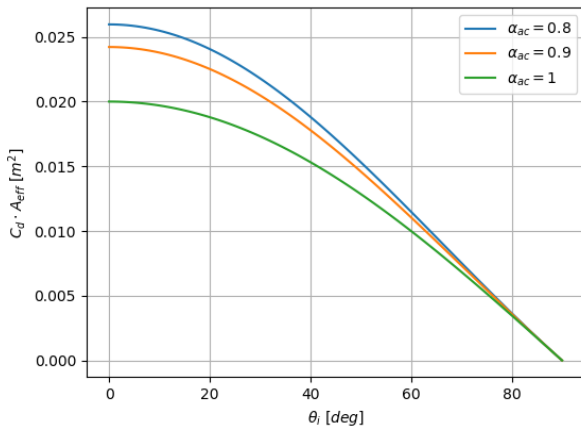


Figure 4.3: Drag dimensional coefficient

Furthermore, a more representative quantity that can later be used efficiently in the drag calculation is the multiplication of the drag coefficient with the effective area - the area of the plate perpendicular to the flow ($C_D \cdot A \cdot \sin(\theta_i)$). Figure 4.3 shows the result for different values of α_{ac} with the area equal to $A = 0.01$ m² (frontal area of 1U); it can be seen that values close to one of α_{ac} lead to overall smaller drag. Then, using the before-mentioned values, a weighted sum considering every unit size surface of the satellite together with speed and density can be fed to the standard drag formula, to get an estimate of the drag force acting on the entire spacecraft [28]. For this analytical model, lift is neglected as it is at least one order of magnitude smaller than the drag [33].

4.2.3 Atmospheric modelization

For further and more precise evaluation of aerodynamic characteristics, a more refined atmospheric model is needed. According to [33], NRLMSISE-00 provides a valid estimate of the density for all constituents of

the atmosphere as well as the thermodynamic temperature, given position, altitude, F10.7 and AP indices of solar and magnetic activities. The forecast for these indices is taken from National Aeronautics and Space Administration (NASA)¹² and then integrated into a Python implementation of the model. The latter can be used to predict the various densities until 2030. Moreover, to better evaluate the drag, the velocity present in the drag equation can be evaluated using a vector addition of the orbital velocity and the wind speed at the given altitude. HWM-14 model can be used to model the wind speed in the thermosphere [37]. A preliminary evaluation of the influence of the wind is performed by performing the mentioned vectorial sum with the possible worst case scenario wind magnitude of 800 m/s in longitudinal direction found in [33] and the orbital speed of 7.7 km/s in direction of the orbit. The relative difference in drag with and without wind consideration can be calculated to be around 0.5%; this percentage is considered negligible in comparison with other uncertainties in the models used, so no wind model will be used for the drag evaluation.

4.2.4 Simulation

After more thorough definition of the environment, the main focus was put on creating a tool capable of simulating the aerodynamics of the satellite with higher precision and more flexibility than the analytical model presented previously could offer.

Chosen model discussion

Ideally, to fully describe the aerodynamic forces acting on the spacecraft, given the very high Knudsen number in VLEO, every individual molecule would have to be simulated through a Monte Carlo simulation. However, given the short amount of time available, a simpler model was chosen based on similar thermodynamic theory of Schamberg's equations, namely a model using Sentman's equations, which offer a better ability to describe situations in between the specular reflection and diffuse re-emission described before in [Subsection 4.2.2](#). They satisfy all the aforementioned needs, even if α_{ac} is still a required input, as, fortunately, the sensitivity of the equation to it is usually quite low [33]. From now onward, given the discretisation used in the chosen model both for surfaces and atmospheric components, subscript j will indicate one atmospheric component while subscript i will refer to a single surface.

Model theory

To begin calculating the required inputs for the particle simulations, other than the relative velocity to the flow (v_r), the thermal velocity (c_{mp}) needs to be known. This can be calculated through [Equation 4.7](#) where molecular mass (m) is used together with other parameters presented in [Subsection 4.2.1](#). From there, the speed ratio (S) is calculated through a simple division given by [Equation 4.8](#); this parameter will be extensively used later [33].

$$c_{mp,j} = \sqrt{2 \frac{k_B}{m_j} T} \quad (4.7)$$

$$S_j = \frac{v_r}{c_{mp,j}} \quad (4.8)$$

Other than the speed ratio previously presented, Sentman's equations take as input also different geometrical parameters. The unit vectors required for the calculation are defined in [Figure 4.4](#). The computations needed for the drag (\hat{u}_D) and the lift (\hat{u}_L) direction vectors are presented in [Equation 4.9](#) and [Equation 4.10](#) [33], respectively; for these, the outward normal direction of the surface (\hat{n}) together with the vector of the relative velocity (\hat{v}_r) is also used.

$$\hat{u}_D = \frac{\hat{v}_r}{\|\hat{v}_r\|} \quad (4.9)$$

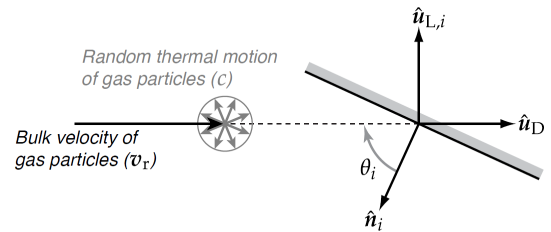


Figure 4.4: Unit vector definition [33]

$$\hat{u}_{L,i} = - \frac{(\hat{u}_D \times \hat{n}_i) \times \hat{u}_D}{\|(\hat{u}_D \times \hat{n}_i) \times \hat{u}_D\|} \quad (4.10)$$

The cosine (γ) of the angle between the inward normal and the drag vector, as well as the cosine (l) of the angle between the inward normal and the lift vector are direct inputs for the model equation and are computed

¹²<https://sail.msfc.nasa.gov/> [Date accessed: 19-05-2019]

though the inner products presented in Equation 4.11 and Equation 4.12, respectively.

$$\gamma_i = \cos(\theta_i) = -\hat{u}_D \times \hat{n}_i^T \quad (4.11) \quad l_i = -\hat{u}_L \times \hat{n}_i^T \quad (4.12)$$

Using a notation similar to the one presented in [38], Sentman's formulas for the drag and lift coefficients can now be shown in Equation 4.9 and Equation 4.10 [33]. The lift vector can have any direction contained within the plane spanned by every vector perpendicular to \hat{u}_D .

$$C_{D,i,j} = \left[\frac{P_{i,j}}{\sqrt{\pi}} + \gamma_i Q_j Z_{i,j} + \frac{\gamma_i}{2} v_{\text{rem}} (\gamma_i \sqrt{\pi} Z_{i,j} + P_{i,j}) \right] \frac{A_i}{A_{\text{ref}}} \quad (4.13)$$

$$C_{L,i,j} = \left[l_i G_j Z_{i,j} + \frac{l_i}{2} v_{\text{rem}} (\gamma_i \sqrt{\pi} Z_{i,j} + P_{i,j}) \right] \frac{A_i}{A_{\text{ref}}} \quad (4.14)$$

For the ease of reading, G, P, Q and Z used above are fully written out separately in Equation 4.15. In the equation for Z , $\text{erf}(x)$ denotes the contraction of the error function¹³.

$$G_j = \frac{1}{2S_j^2}, \quad P_{i,j} = \frac{1}{S_j} \exp(-\gamma_i^2 S_j^2), \quad Q_j = 1 + G_j, \quad Z_{i,j} = 1 + \text{erf}(\gamma_i S_j) \quad (4.15)$$

The only term that is left to be defined is the ratio of the velocities between the re-emitted and the incoming particles (v_{rem}) that appears in the last term of both equations describing the C_D and C_L . The formula needed to calculate is given by Equation 4.16. It uses the satellite temperature (T_{sat}) and the individual gas constant (R), in addition to the parameters previously described.

$$v_{\text{rem}} = \sqrt{\frac{1}{2} \left[1 + \alpha_{ac} \left(\frac{4R_j T_{\text{sat}}}{v_r^2} - 1 \right) \right]} \quad (4.16)$$

As can be seen above from the subscripts, the calculations of C_D and C_L are different for every single surface and atmospheric component considered. Given the non-linear behaviour of the equation pipeline, it is necessary to take a double summation over all the terms including also the relative mass concentration (ρ_j/ρ) as a weight, in order to correctly calculate the force coefficient (C_{tot}) acting on the spacecraft [33].

$$C_{\text{tot}} = \sum_i \sum_j \frac{\rho_j}{\rho} (C_{D,i,j} \hat{u}_D + C_{L,i,j} \hat{u}_{L,i}) \quad (4.17)$$

¹³Also known as Gauss error function, used in statistics and for defining integrals of negative square exponentials

Implementation

To make practical use of the theory explained above a simulation tool written in Python was created. As stated before, the principal aim of this implementation is to provide a very flexible tool based on Sentman's equation, able to easily and correctly simulate every possible geometry encountered during the design process. The complete overview of the code can be seen in [Figure 4.7](#); the corresponding legend for the different types of blocks is presented in [Figure 4.5](#). All the different inputs, processes and outputs are labelled with a unique identifier that will from now on be used to better refer to a particular part of the code. The variables involved in between the processes are indicated on the arrows in plain text. Two abbreviations are used in the diagram: coeff. for coefficient and comp. for component. The top level structure of the program is composed from five main building function groups and is presented in [Figure 4.6](#); these containers are also visualised with the same colour in the complete diagram. Two distinguishable branches are present: one related to the geometry that includes *Mesh initialisation* and *Geometrical evaluation* and the other regarding *Atmospherical calculations*. Both converge into the final chain of functions that evaluate Sentman's equations and output the results.

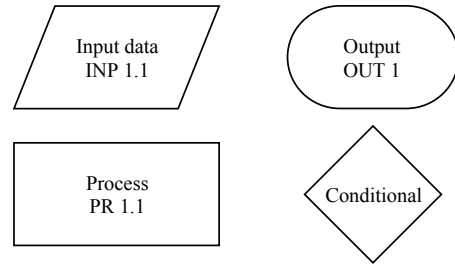


Figure 4.5: Legend of flow chart

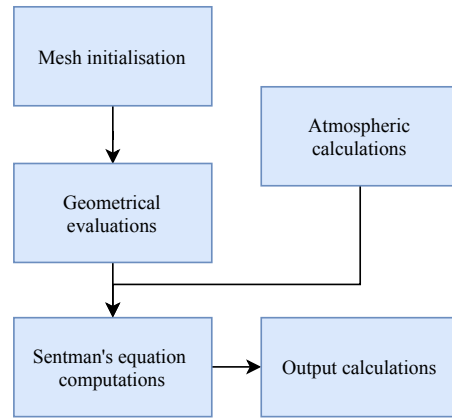


Figure 4.6: Top level [Figure 4.7](#)

In the first group named *Mesh initialisation* the original geometry of the satellite (in .stp format) is imported into SALOME¹⁴ mesh module and a triangular surface mesh is computed and saved in .stl format. Triangular mesh was chosen given its better capability to discretise curved surfaces. The quality of the mesh required depends on the level of geometric detail of the model. For example, curved faces require a lot of triangles in the mesh to represent the geometry correctly enough. The mesh file is now imported into the code through the TRIMESH¹⁵ library. The latter is also used to perform a mesh check and eventually repair (PR 1.1).

Then, in the second group *Geometrical evolution*, the loaded mesh is rotated (PR 1.2) according to the attitude selected (INP 1.1) for the evaluation. Now according to the dimension of the mesh an array of rays is created (PR 4.1) in the same direction as the flow and a ray tracing algorithm included in the TRIMESH module is applied (PR 4.2) to identify the flow facing triangles in the mesh. Once these are identified, all the normal direction vectors are calculated (PR 4.3) and passed on to PR 4.4-4.5 to perform automate calculation of [Equation 4.9- Equation 4.12](#) for each mesh face.

Independently from the processes described above, the functions in the group *Atmospheric calculations* can calculate all the other required inputs for Sentman's equations. First the forecast data for magnetic and solar indices is loaded and processed as splines (PR 2.1) to make them more accessible of future uses. PR 2.2 includes all functions related to the NRLMSISE-00 atmospheric model described above in [Subsection 4.2.3](#). The outputs of the model are further processed (PR 2.3) by running [Equation 4.7](#), [Equation 4.8](#) and [Equation 4.16](#) for each atmospheric component and calculating the relative mass concentrations.

Now, all the quantities calculated are used in *Sentman's equation computations* where [Equation 4.13](#), [Equation 4.14](#) and [Equation 4.15](#) are evaluated for every mesh surface and atmospheric component though 2 concatenated loops. It was chosen to define the reference area as the total area of the faces selected by the ray tracing, allowing to multiply every coefficient just by the area of the face considered and the coefficient just by the dynamic pressure to get the corresponding force or torque. To evaluate the aerodynamic torque coefficient that every face is exerting, the standard formulation is applied, namely the torque vector is equal to the cross product between the distance of the point of application vector and the force coefficient vector ($\hat{\tau} = \hat{r} \times \hat{F}$).

¹⁴<https://www.salome-platform.org/user-section/about/mesh> [Date accessed: 21-06-2019]

¹⁵<https://trimsh.org/trimsh.html> [Date accessed: 21-06-2019]

To present useful results all the coefficients are combined through [Equation 4.17](#) in PR 6. It is possible to choose the output format between a coefficient and dimensional force as can be seen in the *Output calculations*.

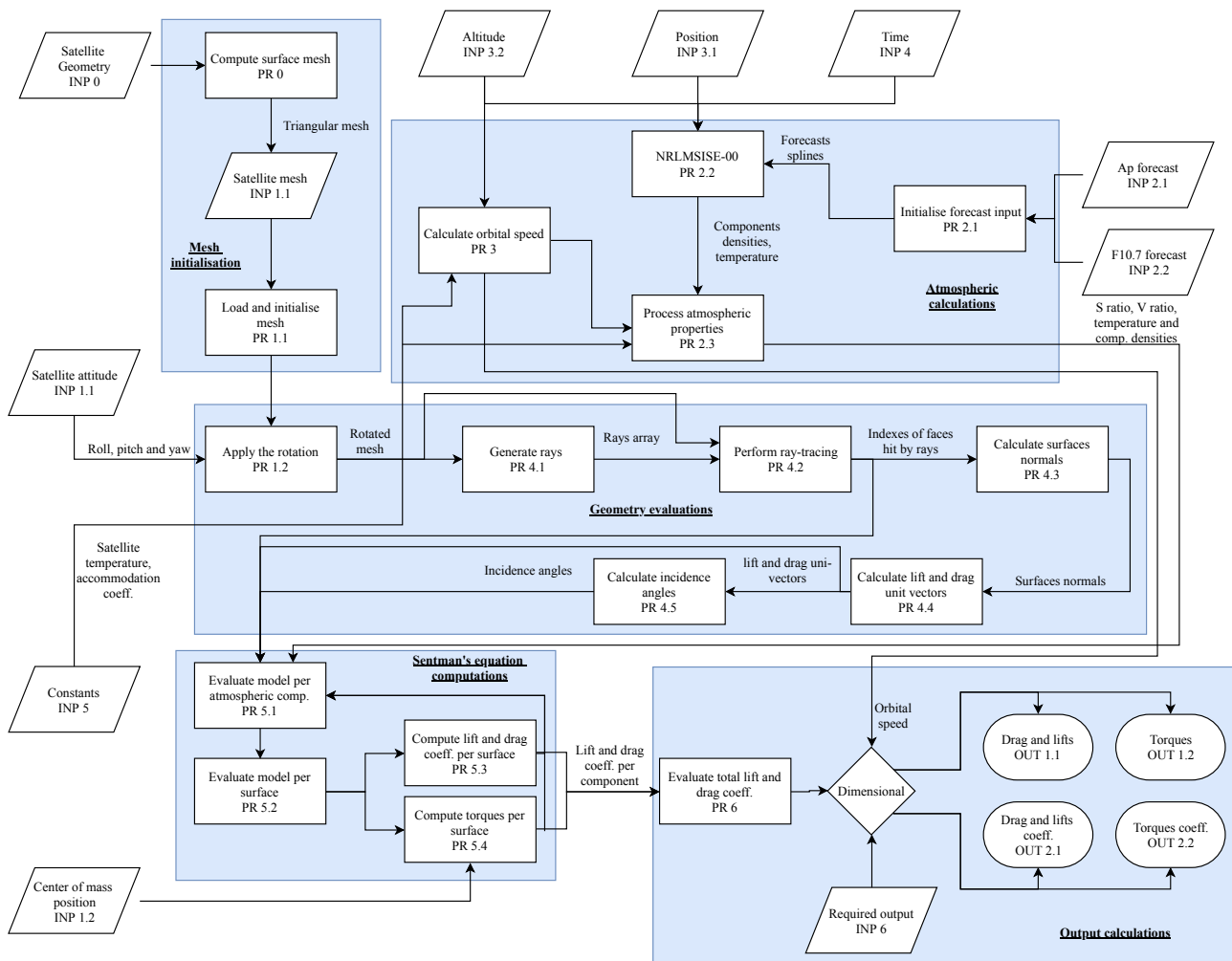


Figure 4.7: Flow chart of the simulation code

The process described above can be iterated many times depending on the different scenarios that are required to be simulated. One-time actions, such as mesh import or spline process, are excluded to reduce computational time. Because of the presence of two distinct pipelines at the start, depending on the needs, simulation time can be reduced if the output of one of them is kept constant. For example, simulating an orbit where the satellite attitude is kept constant will exclude *Geometrical evolution* for each iteration.

4.2.5 Verification and Validation

For the preliminary calculations, analytical method was verified by means of checking single step calculations by hand. It was also validated, with $\alpha_{ac} = 0.95$, by comparing the analytical method with results obtained by the more refined Sentman's set of equations [33]. The atmospheric model verification is provided by the comparison between the code and a NASA online calculator¹⁶ and additionally by comparison with the result presented in [33]. The validation of the atmospherical model is performed and presented in [39], together with the limitations, which were deemed acceptable for level of detailed design carried on in this project.

The verification of simulation code was carried out in different stages. To begin, all the functions and lines of the program were checked through manual calculation. Then all the blocks of the program were checked by inputting in the pipeline specific inputs for which the associated outputs were already known and comparing the result. Lastly, the parts involving the mesh were visually plotted to check for possible mistakes in the evaluation of the surface normals or lift and drag direction vectors.

¹⁶<https://ccmc.gsfc.nasa.gov/modelweb/models/nrlmsise00.php> [Date accessed: 20-05-2019]

Once 100% of the code had been covered with the strategies described previously, a flat plate of 1m^2 of surfaces was input as geometry and two main verification strategies were carried out to verify the correct implementation of the core of the drag coefficient evaluation. The first one uses Figure 4.8 superimposed with the same plot presented in [33]. Given the same inputs as presented in the source, a complete overlay of the plots was observed. The second one employs a comparison between the analytical model presented above in Subsection 4.2.2 and the simulation. The values of the drag coefficient are plotted in Figure 4.9 alongside the kernel density estimate of the absolute error in Figure 4.10. In the latter all the data points are also showed on the x axis to better visualise the distribution.

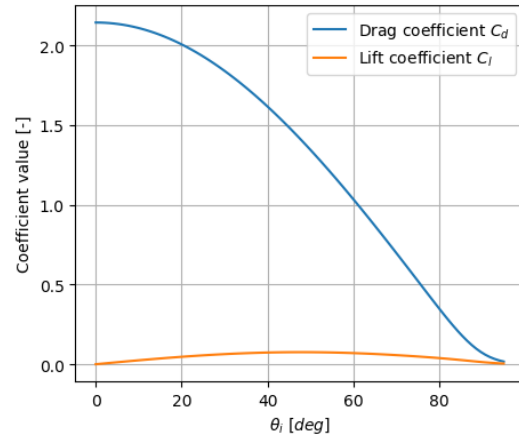


Figure 4.8: Lift and drag of a flat plate

It can be seen, that the analytical model slightly overestimates the drag at low incidence angles and overestimates it at high angles. This is due to the higher influence of the accommodation coefficient on the analytical model described in Subsection 4.2.2, as compared to the one present in the Sentman's equations, as stated in Subsection 4.2.4). From the absolute error distribution, it can be seen that they are equally spread apart in what seems like a uniform distribution (i.e no bias is present) between 0 and 0.1, with a slightly increased density towards 0.08. Figure 4.8 exhibits similarity to a uniform distribution due to the presence of few outliers. As the average error is in the order of 5%, the core of the simulation is considered verified.

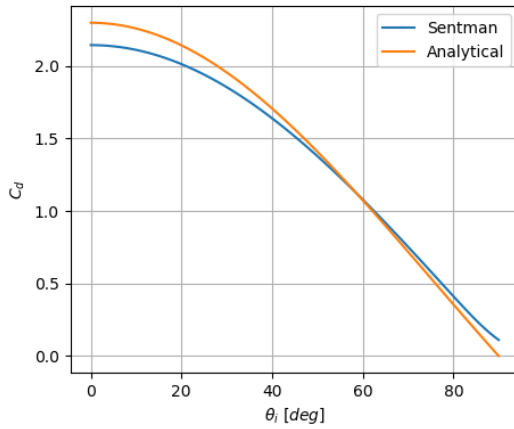


Figure 4.9: Flat plate drag coefficients

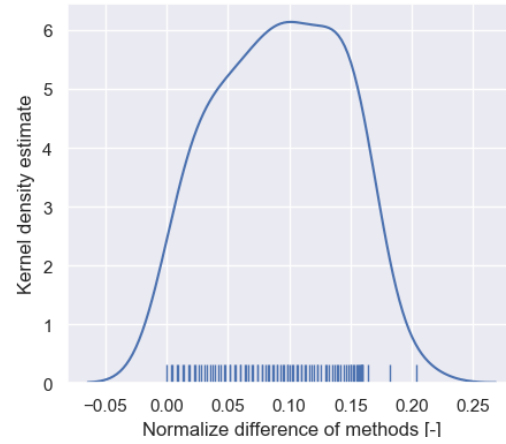


Figure 4.10: Distribution of the absolute error

To verify the whole program the same comparison as the one described above is performed but considering the whole satellite model. It can be seen in Figure 4.11 (where x-axis is now the pitch of the satellite), that there is even a better match as compared to the flat plate comparison. This has to do with the fact that the areas with high and low incidence angles balance themselves out reducing the absolute error. Figure 4.12 shows again the distribution of errors; unfortunately, less points on the polar are available due to computation time, resulting in a not distinctly identifiable distribution. The relative average error is evaluated at 3%, considered low enough to validate the program. Same procedure is performed for the torque and again differences below 5% are found.

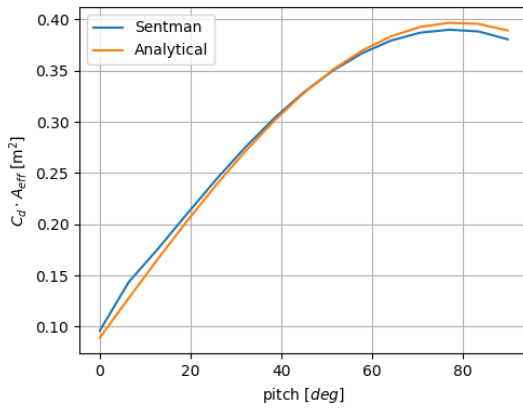


Figure 4.11: Satellite drag coefficients

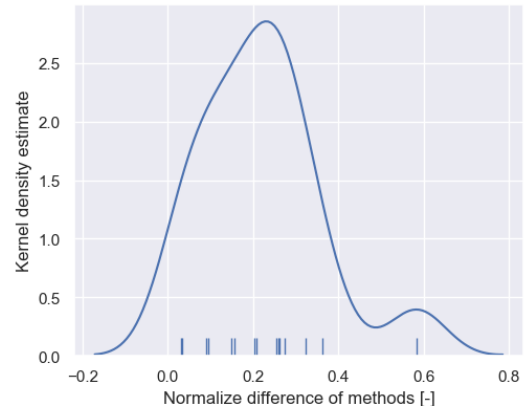


Figure 4.12: Distribution of the absolute error

Mesh convergence problems were not present, as there were no curved surfaces on the satellite. One face of the satellite meshed with two or 1000 surfaces will result in exactly the same drag if the face is completely planar. Values of the drag coefficient are validated through comparison with standard advised drag coefficient for satellites and CubeSats [25], as well as by simulating the SNOE (Student Nitric Oxide Explorer)¹⁷ satellite and comparing the results to the ones presented in a drag research on the satellite [40]. A random variable attitude was considered and the average results were found to match.

Furthermore, validation of this entire model is also presented in [33].

4.2.6 Spacecraft aerodynamic development

It is important to mention that all the simulations ran to get particular values, which are always an average over an orbit position and time or alternatively over different attitudes if fixing the two other parameters just mentioned. This is important in order not to output an outlier value due to, for example, a particularly high solar activity. All of the average results, together with particular required cases, are

Together with all the evaluation needed for other subsystems some studies were performed on optimised aerodynamic shapes. A deployable nosecone was investigated. The distinct gains in minimum drag configuration were compensated by the higher drag at any other attitude resulting in no particular drag reduction over the course on a entire orbit (around 2%). Furthermore, the resulting increase of complexity and mass of the spacecraft would likely outweigh the already insignificant gain.

4.3 Propulsion system

There are two main reasons to have a propulsion system, namely counteracting drag and orbit correction. To perform these actions one can choose from several types of propulsion systems. The three main propulsion types initially considered for the mission are cold gas, chemical and electric. In this section an explanation will be mentioned about each type together with an explanation why it was deemed feasible or not. Furthermore, the chosen propulsion system type together with the chosen thruster will be presented. Moreover, the integration is touched upon together with the risks. The verification procedures will be explained over the section itself, where it is necessary.

4.3.1 Types of propulsion systems

With the current state of the art the following three types of micropropulsion systems were investigated, from which the final integrated propulsion type is chosen. An overview of different characteristics is given in Table 4.1.

Cold gas propulsion systems are the most advanced in terms of design maturity[41]. They operate by accelerating the gas via a nozzle, without any combustion nor heat addition [42]. On a scale of achievable thrust

¹⁷http://lasp.colorado.edu/media/projects/snoe/publications/pdf_docs/AIAAitlop.pdf [Date accessed: 22-06-2019]

magnitudes, they score higher than electric, but lower than chemical systems. However, a disadvantage of this system is that the propellants usually have lower densities and relatively lower I_{sp} . It is important that the mass fraction of the mass of the propulsion system shall be less than 0.4 and that the volume fraction shall be less than 0.3 to make it feasible to integrate the propulsion system [43]. Therefore, for Earth observation in VLEO, aiming for lifetime it becomes an unfeasible design option. This is due to the fact that the propellant on its own requires 30% of the spacecraft volume, excluding the system itself. This will not leave enough space for the other subsystems.

Chemical propulsion systems make use of the propellant's internal energy. Ignition releases energy from the broken molecular bonds, raising the temperature of the propellant. The formed reaction products, when accelerated, create the thrust [42]. There are many chemical propulsion systems in development, diverging from conventional non-sustainable propellants, like hydrazine, to newer systems using green propellants [41]. The disadvantage of this system is that it cannot be launched as a secondary payload, due to the strict regulations it should comply with regarding the pyrotechnics. However, the main reason such a system is not selected, is the lifetime. The propulsion system should at least be able to provide for a lifetime of five years. With the state-of-art systems out there concerning the propellant tank size, the necessary ΔV to maintain the orbit cannot be achieved.

Electric propulsion systems utilise available power on board to generate thrust by heating gas and accelerating it through a supersonic nozzle. Generally, there are three categories in electric propulsion, namely electrothermal, electromagnetic and electrostatic [42]. Despite having very high I_{sp} , it has a noticeably smaller thrust. For these systems a potential bottleneck is the power they require. Despite the power, if it is possible to provide the necessary power, the system is a great fit for orbit maintenance in VLEO.

	I_{sp}	Power	Thrust	ρ_p [kg/m ³]
Cold gas	30-70	< 10 W	10 mN - 10 N	2800-5300
Chemical	190-260	< 20 W	0.1 N - 30.7N	1020-1240
Electric	400-6000	5.5 W-200 W	5 μ N - 50 mN	1600-7310

Table 4.1: Overview of types of propulsion systems [41][42][43]

4.3.2 Field-emission electric propulsion

	I_{sp}	Power	Thrust	TRL
Pulsed plasma and vacuum arc	500-3000	2-4 W	1 - 1300 μ N	5-7
Electrospray	500-5000	1.5-15 W	10-120 μ N	5-7
Resistojet	50-150	15-50	10 mN - 0.45 N	5-9
Ion propulsion	1000-6000	8-60 W	1-10 mN	5-7
Hall effect thrusters	1000-2000	175-200	10 mN - 50 mN	4-8

Table 4.2: Overview of electric propulsion systems [41][42][43]

As electric propulsion is the most suitable propulsion type concerning our mission, a type of electric propulsion needs to be chosen. An overview of different types of electric propulsion is presented in Table 4.2. The first two types that are discarded immediately are Hall effect thrusters and resistojet. The high power required for the Hall effect thrusters will be problematic for the EPS and the resistojet has a low I_{sp} , which requires a large amount of propellant to achieve the lifetime, which cannot be implemented with the state of the art hardware out there. Furthermore, after investigating the pulsed plasma and vacuum arc and electrospray thrusters it is concluded that they cannot provide the total impulse required [43]. So, leaving ion thrusters as the option to go with.

It is decided to go for Field-emission electric propulsion (FEEP) propulsion system for this mission as FEEP has the highest TRL value amongst the ion thrusters and its I_{sp} is relatively high compared to other ion thrusters. Furthermore, it has a high degree of miniaturisation.

FEEP is an electrostatic type of propulsion system. It generates thrust by accelerating ions using electrostatic forces. However, compared to other ion propulsion systems instead of using a gaseous discharge the ions are produced by field emission from a liquid metal supplied the thruster. Moreover, pressurant and valves are not required anymore and relatively high specific impulses can be reached, because of this technique [44].

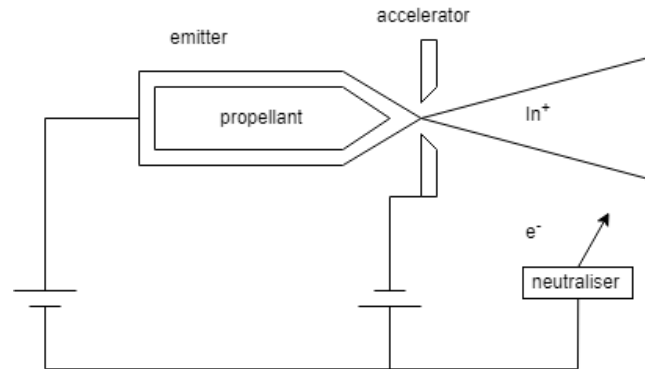


Figure 4.13: Schematic view of a FEEP

A graphical representation of a FEEP system is presented in Figure 4.13. Note that here are multiple configurations for the emitter geometry. For instance, a pin, a needle or a capillary shape. The principle is as follows: as mentioned before a high voltage difference is applied between the emitter and accelerator, which can reach all the way up to 10 000 V [44]. This large voltage difference generates a strong electric field and together with surface tension at high values of the electric field a Taylor cone is created from which ions get extracted. The next step is to accelerate the ions through an opening. As the beam contains positively charged ions, a neutraliser is required to avoid potential failures of the spacecraft, due to potential negatively charging it. So, the neutraliser emits electrons (e^-) into the beam containing positive ions (In^+).

Common types of propellants used in FEEP are caesium (Cs) and indium (In). One of these two propellant types will deem the most feasible for our mission. Comparing the two propellants resulted in indium being the most suitable propellant. This due to the fact that in the case of Cs, reluctance is present regarding its use, due to spacecraft contamination and launch safety issues. This is a problem not arising, when indium is used. Moreover, a Cs thruster brings sever restrictions with respect to the reliability and life expectancy, due to its high susceptibility of arcing. So, all in all making an indium FEEP-thruster more reliable candidate. [45].

As indium is the chosen propellant for our propulsion system, it is important to take the sustainability aspects into account. As the propulsion system is the only subsystem that is actively releasing particles into the atmosphere. Thus, potentially causing harm. This gives rise to the generation of requirement **SYS-SC-SUBSYS-PROP-2**. With the choice of indium this requirement is met, due to the fact that it can be handled in the atmosphere without risk meaning indium as a propellant is non-toxic as presented in [46] and [47].

4.3.3 IFM Nano Thruster

Taking the advantages, disadvantages and the mission lifetime (requirement **SYS-OBJ-LT-1**) into account, a suitable thruster is selected. The most suitable propulsion system for the mission is decided to be the IFM Nano Thruster, which is developed by FOTEC and commercially made available by ENPULSION [47]. It uses indium as propellant, which is carried in solid state and liquified up in space. From the state-of-the-art ion thrusters for small satellites this unit has the highest TRL of 7 [41]. Furthermore, it is the first FEEP thruster that successfully operated in Low Earth Orbit [48]. An overview of the specifications is presented in Table 4.3.

Note that the thruster has an operational range for the thrust as presented in Table 4.3. So, the thrust can be adjusted depending on the amount of power provided to the system as seen in Figure 4.16. This thrust range is controlled through the electrode voltages yielding a low thrust noise. The parameters influencing the thrust and how they relate to each other can be seen in Equation 4.18 [48]. With I_c being the emitter current, V_e being the emitter voltage, f_b being the beam spreading factor and $\frac{m}{q_e}$ being the mass-to-charge ratio of a singly ionised indium ion.

¹⁸<https://www.cubesatshop.com/wp-content/uploads/2017/04/ENP-IFM-Nano-Thruster-Product-Overview.pdf>[Date accessed: 23-06-2019]

Table 4.3: IFM Nano Thruster specifications ¹⁸

Parameter	Value
Thrust range	10 μ N - 0.5 mN
Specific impulse	2000 - 6000 s
Propellant mass	250 g
Total impulse	at least 5000 Ns
Outside dimensions	94 \times 90 \times 78 mm
Wet mass	870 g
Total system power	8 - 40 W
Hot standby power	3.5 W
Command interface	RS422/RS485
Temperature envelope (non-operational)	-50 - 120 $^{\circ}$ C
Temperature envelope (operational)	-20 - 50 $^{\circ}$ C
Supply voltage	12V or 28 V



Figure 4.14: The IFM Nano Thruster [48]

$$F_t = I_c \cdot \sqrt{2 V_e \frac{m}{q_e}} \cdot f_b \quad (4.18)$$

Not only the thrust, but also the I_{sp} has a dynamic range as can be seen in Table 4.3 ranging from 2000-6000 s. This yields that the mission can be planned in the most optimal way containing different types of manoeuvres requiring different values of I_{sp} . When all the electrical parameters are known the corresponding I_{sp} can be determined using Equation 4.19 [48]. With the same variables as mentioned for Equation 4.18 and adding g_0 being the gravitational constant and η being the mass efficiency of the propellant.

$$I_{sp} = \frac{1}{g_0} \cdot \sqrt{2 \cdot V_e \cdot \frac{q_e}{m}} \cdot \eta \cdot f_b \quad (4.19)$$

The dynamic operational range for the thrust relates not only to the power put in, but also to the extractor voltage. This relation plotted for different extractor voltages can also be seen in Figure 4.16. Together with the I_{sp} and the power required, the complete performance envelope can be graphically constructed as presented in Figure 4.15. From this graph the most ideal combination can be chosen regarding the mission needs. Note that this graph is based on the 35 % mass efficiency of the indium as propellant [48] [49]. Moreover, adjusting the thrust levels also influences the beam divergence. Obviously, a small beam divergence is desired to avoid damaging the spacecraft. For instance, the solar panels can be damaged by the exhaust of the thrusters. So, these considerations were taken into account in the design by orienting the panels in a way that they cannot be hit as can be seen in Chapter 9.

The IFM Nano Thruster has three operational modes, which are propellant liquification, hot standby and thrusting. At the start of the mission the indium is still a solid block. This contributes to the thrust completely not having movable part. This positively contributes to the launch safety. However, for FEEP liquid metal propellant is needed. Hence, liquification is required. This can be achieved by using a heater on a constant setting of 8 W power, or be control the heater fully automatic with a 10 W limit. This takes approximately two hours, but it can be more or less depending on the power input. When the liquification is achieved, the controller decreases the heater power to maintain the operational temperature, which is also known as hot standby mode. In this mode it is possible to thrust instantly. This thrusting again can be performed as desired according to operational range [48, 50].

4.3.4 Implementation

In the Sat-ELITE two IFM Nano thrusters will be integrated diagonally as can be seen in Figure 4.17. The reason to have them diagonally for this is that the propulsion system should be oriented in a way minimising disturbance torques created by thrusting. So, unnecessary measures taken by the ADCS are avoided.

¹⁹<https://www.cubesatshop.com/wp-content/uploads/2017/04/ENP-IFM-Nano-Thruster-Product-Overview.pdf>
[Date accessed: 23-06-2019]

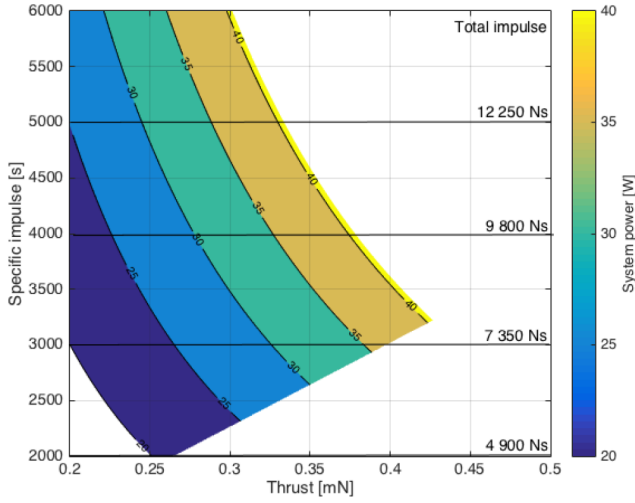


Figure 4.15: Performance of the IFM Nano Thruster [48]

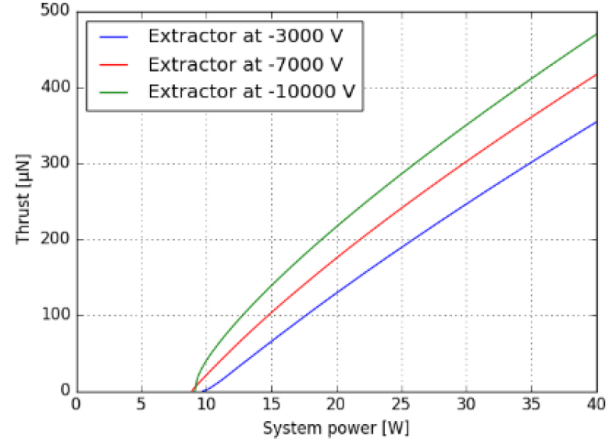


Figure 4.16: Thrust vs system power ¹⁹

The main reason to have two thrusters is, due to the fact that one thruster will barely meet the lifetime **SYS-OBJ-ORB-2** and ΔV **SYS-SC-SUBSYS-PROP-1** requirement. Furthermore, a drawback of having one thruster is it should be integrated in the middle as close to the Center of Mass (CoM). This disrupts the space inside the cube as COTS have defined dimensions. So, one thruster unit with a frontal area of 90×94 mm makes it harder to place subsystems around it. Therefore, inefficiently making use of the space if the other subsystems consist of 1 unit outer dimension.

Furthermore, two thrusters, also shorten the amount of time the spacecraft needs to thrust as two thrusters can provide double the amount of thrust. Moreover, in case of the failure of one thruster, depending on when it happens, theoretically the spacecraft can still maintain altitude even though the operations become way less efficient. This risk will be analysed more thoroughly in the risk subsection [TR-PROP-4].

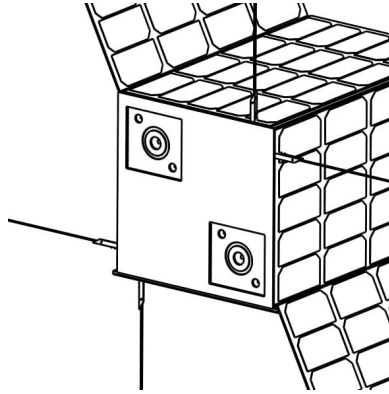


Figure 4.17: Thrusters integrated diagonally

4.3.5 Disturbance torque

By integrating two thrusters into the spacecraft and not having the CoM exactly at the geometric centre, a disturbance torque will be created each time the spacecraft thrusts. The propulsion system thrusts in the negative x-direction creating torques in y and z-direction if the thrusters are perfectly aligned. However, possible misalignments of the thrust vector result in a torque in the x-direction as well. These are torques are defined as M_y , M_z and M_x respectively.

Obviously the torques created shall be smaller than what the ADCS is able to counteract as stated by requirement **SYS-SC-SUBSYS-PROP-3**. Therefore, the magnitude of these torques should be estimated. The approach for this is summing the torques using the right-hand rule to obtain preliminary values. The values for

the lower bound are calculated assuming no misalignments of the thrust vector at all. However possible manufacturing errors, integration errors or unforeseen events may cause a misaligned thrust vector [TR-PROP-3]. The situation is first analysed for the worst case scenario of having both thrusters misaligned contributing to the torque in the same direction to achieve the upper bound for the disturbance torques. As values for the misalignment typical angles range between -5 deg and 5 deg. This range is chosen based on misalignment angles presented in [51] with an extra margin of 1 deg added. Furthermore, the thrust component in the misaligned direction is given by Equation 4.20 and the thrust component counteracting the drag is given by Equation 4.21, with F_t being the magnitude of the thrust vector and ζ being the misalignment angle.

$$F_{t_{misaligned}} = F_t \cdot \sin(\zeta) \quad (4.20) \quad F_{t_{longitudinal}} = F_t \cdot \cos(\zeta) \quad (4.21)$$

The misalignment angles of the thrust vectors are not known beforehand meaning they are non-deterministic as it cannot be determined beforehand what magnitude it will be. To still have realistic estimates a stochastic simulation is necessary. Therefore, the next step is to apply a Monte Carlo simulation to generate the values for misalignment angles, which can be used to simulate the disturbance torques. A Monte Carlo method simulates a process several times each time with a different initial condition, which in this case is the misalignment angle (ζ).

A fitting distribution for ζ is determined to be a normal distribution, with the mean at zero. As a stable thrust vector for an ion thruster is necessary. So, before the installation the real position of the thrust vector can be usually measured reducing the chance of having a manufacturing error resulting in a misaligned thrust vector. However, since only values between -5 deg and 5 deg are considered a bounded normal distribution is created.

The approach of creating the bounded distribution is as follows. From a uniform distribution p numbers are drawn. This procedure is repeated m times, resulting in a $m \times p$ matrix, with each entry containing a random number from a uniform(0,1) distribution. Then the sum will be taken over the columns yielding a $m \times 1$ vector. This vector will be divided by p to normalise the outcomes. The result of this a $m \times 1$ vector named R . The values of ζ are calculated using Equation 4.22. Note that m is equal to the number of iterations performed in the Monte Carlo simulation.

$$\zeta_{vector} = \zeta_{min} + (\zeta_{max} - \zeta_{min}) \cdot R \quad (4.22)$$

This results in how ζ is distributed after 5000 iterations, which is presented in Figure 4.18.

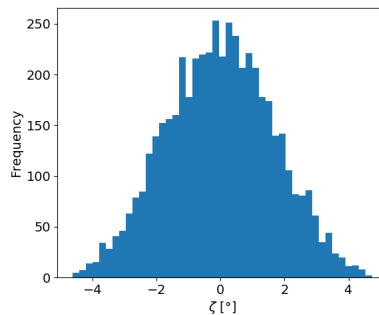


Figure 4.18: Distribution of ζ

The fact that there are two thrust vectors that can be misaligned in two axes means there are four degrees of freedom. This is incorporated in the code by generating four different ζ vectors, which will be the input in the simulation.

The result of these 5000 iterations is presented in Figure 4.19. The simulations yield more precise values for the disturbance torques that can be expected during the mission by taking the sample mean of the results and adding the standard deviation. The values are presented in Table 4.4. Note that these torques are calculated based on having both thrusters at max thrust, due to the fact that this will generate the largest disturbance torques. Furthermore, the simulation shows that the disturbance torques with a large number of simulations tend to go to the lower bound values. Hence, verifying the initial lower bound. Moreover, as the maximum

disturbance torques do not cause a problem for the ADCS. Therefore requirement **SYS-SC-SUBSYS-PROP-3** is still met in case of misalignments.

	M_x [Nm]	M_y [Nm]	M_z [Nm]
Lower bound	0	$-4.20 \cdot 10^{-5}$	$4.20 \cdot 10^{-5}$
Upper bound	$-7.32 \cdot 10^{-6}$	$-5.36 \cdot 10^{-5}$	$3.01 \cdot 10^{-5}$
Average simulation	$1.98 \cdot 10^{-8} \pm 1.23 \cdot 10^{-6}$	$-4.99 \cdot 10^{-6} \pm 2.78 \cdot 10^{-6}$	$1.70 \cdot 10^{-6} \pm 2.79 \cdot 10^{-6}$

Table 4.4: The lower bound, upper bound and expected disturbance torques

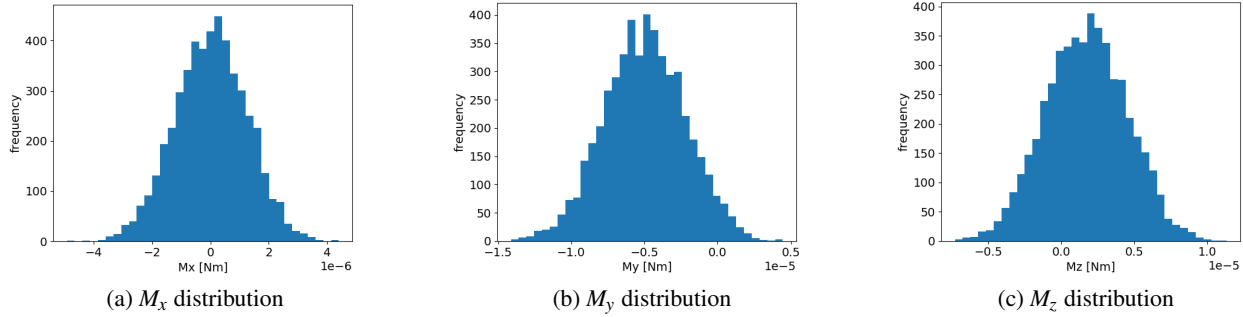


Figure 4.19: Disturbance torques due to 2000 iterations of different misalignment angles

4.3.6 Risks

As briefly mentioned in the Subsection 4.3.2 by expelling positively charged ions, there exists a chance that the spacecraft may become negatively charged [TR-PROP-1]. This is the result of the electrons tunnelling back into the propellant, hence staying in the system. Therefore, it needs to be balanced to avoid failure. This is achieved by using two neutralisers²⁰. The neutralisers are cold-redundant electron sources consisting of a Tantalum disc heated to 2200 K and biased to -200 V [52]. So, releasing the electrons into the ion plume as seen in Figure 4.20. The charge balancing current is measured by the PPU, which can automatically control its heating power. Hence, controlling the electrons emitted. Due to this risk having critical consequences for the mission, the functionality of the neutraliser is verified by the manufacturer by only operating the neutraliser in a test sequence [48]. This checks if the neutraliser is able to operate before the propulsion system is integrated into the spacecraft.

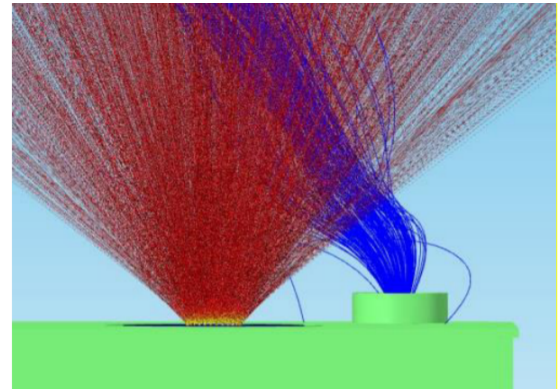


Figure 4.20: Electrons (blue) into ion plume [52]

Furthermore, for an indium liquid-metal ion source it is common to have relatively high currents. This creates instabilities, which lead to microdroplets being emitted in addition to the ion current [49] [TR-PROP-2]. This will consume propellant on a much higher rate. Hence, it is unwanted and if they deposit on the extractor electrode it might be able to close the extractor electrode. Hence, limiting the lifetime of the thruster. This is interlinked together with [TR-PROP-4]. A mitigation approach which is taken, is not using the maximum capabilities of the thruster. Furthermore, a higher voltage difference with a set thrust level will require less current.

²⁰<https://www.cubesatshop.com/wp-content/uploads/2017/04/ENP-IFM-Nano-Thruster-Product-Overview.pdf>[Date accessed: 23-06-2019]

In the case of, one of the thrusters failing, the mission is affected in the sense that larger disturbance torques are created, due to one thruster not being able to compensate anymore. Furthermore, the thrust will be halved yielding a higher thrust time required. This can cause problems for the ADCS to deal with. However, theoretically the one thruster is able to provide enough total impulse to achieve the lifetime. The extreme case scenario should also be taken into account where the spacecraft finds itself in the solar maximum and then the required ΔV should be provided. Staying in this scenario for too long may deem to be problematic.

During the solar maximum where the drag experienced will be the highest, with one thruster inactive, the worst case will be to thrust for 25 % of the orbit time. Theoretically it is possible, however, due to the troubles arising for the ADCS, the mission lifetime will most likely not be reached at that point as the modes during operation will become unreasonable. So, there will not be a need to continue the mission. The troubles for the ADCS rise from the fact a large disturbance torque needs to be countered. To mitigate this risk extensive testing and inspection of the thrusters is required, before it is installed into the spacecraft. Multiple measures by ENPULSION are taken as propulsion systems integrated in a mission are key aspects. Hence, they extensively test the units. For example, every emitter is fired at least two times together and all the mechanical parts of the thruster are examined. Moreover, 100 % traceability of all parts, manufacturing and testing is guaranteed [47]. Furthermore, the performance envelope of the thruster is independently verified by ESA showing its capability to operate at any operational point within the performance envelope as presented in Figure 4.15 [47]. Furthermore, it is verified that the emitter can fire for 13 000 hours without degradation of the performance.²¹ So all in all, this contributes majorly to lowering the risk.

4.4 Mission altitude

According to requirement **SYS-OBJ-ORB-1**, the orbit of the satellite shall be between 230 and 380 km. To refine this range into a final operational range the dependencies on the different subsystems were analysed. From this an upper limit and lower limit were set up. After looking at other considerations, the final operational range was defined.

4.4.1 Upper bound

The upper bound in altitude comes from the payload capabilities and the spatial resolution requirement. A spatial resolution of at least four meters, as specified by requirement **SYS-OBJ-PL-2**, is desired. The SEEING camera has a specified resolution of 7 m at 600 km altitude, since the resolution scales linearly with altitude, the 4 m resolution is achieved at 342 km.

So the upper bound of the altitude is 342 km.

4.4.2 Lower bound

The lower bound on altitude is less straight forward to calculate. The methodology is to look at the total impulse that the propulsion system can provide, and from this derive the maximum average drag that the system can counter over its lifetime, according to **SYS-OBJ-LT-1** the lifetime shall at least be five years. From aerodynamic analysis the altitude at which this maximum average drag will be experienced should be calculated. As a final check, maximum incidental drag moments are analysed to see if the system can handle the worst case drag moments, which occur during a solar maximum.

The total impulse that the propulsion system can provide is 15680 Ns. Taking a 10% margin for unexpected operations, 14112 Ns can be used during the mission. The two other phases of the mission that require the propulsion system are orbit phasing and initial orbit correction as will be explained in Subsection 4.6.3 and Subsection 4.6.2. Subtracting the total impulse needed for orbit phasing and initial orbit corrections, the total impulse that can be used for drag compensation is 13420 Ns. Dividing this by a lifetime of five years (157 788 000 seconds), an average drag of $8.51 \cdot 10^{-5}$ N can be compensated.

To find at which altitude this average drag is experienced, an aerodynamic analysis was performed, with the model described in Section 4.2. The spacecraft is not always in low-drag mode, for example when the spacecraft needs to direct its antenna towards a ground station. Taking this into account, the average angle of

²¹<https://www.cubesatshop.com/wp-content/uploads/2017/04/ENP-IFM-Nano-Thruster-Product-Overview.pdf>[Date accessed:24-06-2019]

attack over the orbit is 20 deg. With this attitude the average drag equal was equal to the average drag that can be compensated at an altitude of 332 km, making this the lower bound.

The highest drag will be experienced during a solar maximum. In that case, the drag will be $1.04 \cdot 10^{-4}$ N at 332 km. Because the maximum thrust is $8.4 \cdot 10^{-3}$ N, the propulsion system should be active for 12.4% of the orbit. This is still deemed feasible and reasonable. The final thrusting times, together with operational times for payload, communication and desaturation are shown in [Section 9.1](#).

4.4.3 Other considerations

Two final considerations were telecommunications and Earth-repeat orbits. The requirements for telecommunications become more demanding as the orbit is lowered since this increases the spatial resolution and thus increases the total amount of data that needs to be transmitted to the ground stations. However, for this small potential range, the difference was so small that it doesn't pose any new restrictions on altitude.

The final consideration is the possibility of an Earth-repeat orbit. This special type of orbit repeats its exact ground track after a certain amount of days. This can be marginally helpful for Earth observation and operations. One advantage is that the same satellite can take the exact same picture of the exact same part of land after a certain amount of days, and the processing of this picture can be automated more easily because it is exactly the same. The options for Earth-repeat orbits with a cycle of less than one week were calculated using [Equation 4.23](#) [29], where j is the number of orbits and k the number of days until the ground track gets repeated. In addition, e is the eccentricity of the orbit, in this case 0, and t_{day} is the duration of one day. By setting a certain a , the required inclination can be found for each altitude. In the range of 332-342 km altitude the options were plotted and compared to the inclination required for an SSO, as shown in [Figure 4.21](#). Unfortunately, at this altitude range, there are no SSO's with an Earth-repeat cycle of less than one week, so this option was discarded based on infeasibility.

$$j \cdot \left| -2\pi \frac{2\pi \sqrt{a^3/\mu}}{t_{day}} - \frac{3\pi J_2 R_{Earth}^2 \cos(i)}{a^2(1-e^2)^2} \right| = k \cdot 2\pi \quad (4.23)$$

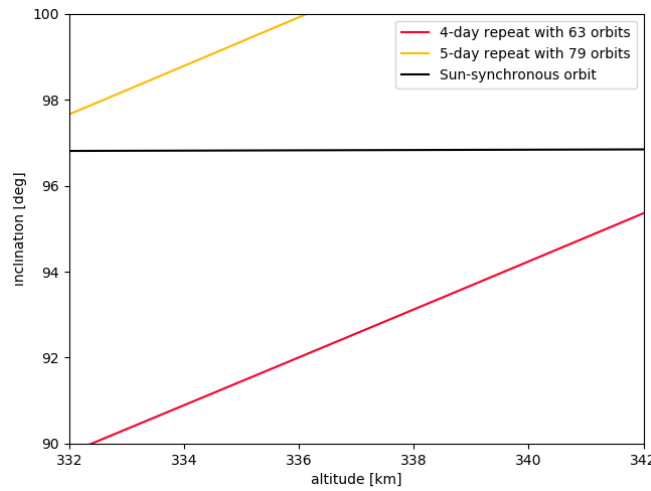


Figure 4.21: Options for Earth-repeat and SSO's

4.4.4 Final operational range

So, it can be concluded that the final operational range of the Sat-ELITE will be between 332 and 342 km. A range is given because during operations it is impossible to remain at exactly one altitude all the time.

4.5 Constellation design

As stated by requirement **SYS-OBJ-PL-3**, a temporal resolution of at least two images per day is required. This will be achieved by designing a constellation of satellites in two Sun-synchronous orbital planes: one

will always see the Earth in the morning and the other in afternoon lighting conditions. This has the added benefit that the shadows are cast in different directions in both pictures, which makes it impossible for objects of interest to hide in the shadows.

The number of satellites needed in each orbital plane should be sufficient to map 99% of the Earth's surface, according to requirement **SYS-OBJ-PL-4**. To find the coverage of one satellite, the swath width needs to be calculated. Assuming that the surface of the picture is flat, the swath width can be easily derived using geometry, shown by Equation 4.24, where h is the altitude of the orbit and FoV is the FoV of the camera. The swath width will be the smallest at the lowest point in the orbit, so that is the critical case for constellation sizing. For an altitude of 332 km, and a FoV of 6.4 deg (as will be explained in Section 5.4), the swath width is 37.1 km.

$$\text{swath width} = 2h \tan(\text{FoV}/2) \quad (4.24)$$

Now that the swath width is known, it can be calculated how much land one satellite cannot see map orbit. As shown in Figure 4.22, the longitude of the ascending node (point in the orbit where the groundtrack crosses the equator from south to north) has shifted to the west after one orbit. This change in ascending node can be calculated by evaluating the rotation of the Earth during one orbital period. The orbital period (T_o) is calculated using Equation 4.25, which can then be substituted in Equation 4.26, to calculate the change in longitude of the ascending node. For an altitude of 332 km, the orbital period is thus 5461.5 seconds (91.0 minutes), and the change in longitude of ascending node is 2530.4 km along the equator.

$$T_o = 2\pi \sqrt{a^3/\mu} \quad (4.25)$$

$$\Delta_{\text{ascending node}} = 2\pi T_o / t_{\text{day}} \cdot R_{\text{Earth}} \quad (4.26)$$

The number of satellites needed for the constellation is then obtained by dividing the change in longitude of the ascending node of one satellite by the swath width of the camera as given by Equation 4.27. This results in a constellation size of 68.2 satellites. Rounding up this gives 69 satellites for each orbital plane, so a total of 138 for the whole constellation.

$$\text{number of satellites per orbital plane} = \frac{\Delta_{\text{ascending node}}}{\text{swath width}} = \frac{2\pi \cdot t_{\text{day}} / T_o \cdot R_{\text{Earth}}}{2h \cdot \tan(\text{FoV}/2)} \quad (4.27)$$

These 69 satellites are all in the same orbit, but spread out evenly. For that a change in true anomaly is required. True anomaly takes a value between 0 deg and 360 deg, so for an even spacing the true anomalies should be: 0 deg, 5.2 deg, 10.4 deg, ..., 354.8 deg. This way of designing the constellation will be verified in Subsection 4.5.4. Further more in Subsection 4.6.3, the method of changing the true anomaly of a satellite will be discussed.

4.5.1 Reliability

The reliability of small satellites is historically quite low, especially for a mission with a lifetime of five years. For the constellation to be operational it is important that there are always enough satellites, so the risk of satellite failure [**TR-OP-4**] should be mitigated.

The minimum constellation size is 138 satellites, and two strategies were investigated to maintain this minimum constellation size during the whole lifetime.

1. Launch all the satellites at the start of the mission. So after five years of operations, still enough satellites would be functioning and no extra launches are required halfway the mission.
2. Initially send a number of redundant satellites to cope with initial failures. But keep monitoring the health of the satellites constantly so that when needed, a new launch can be scheduled to replenish the constellation.

Small satellites with a design lifetime of more than five years, have a reliability of 68% over five years of operation [53]. Meaning that 68% of satellites will still be functional after five years. Using the first strategy, each orbital plane should have 101 satellites, putting the total constellation size at 202 satellites.

However, the second strategy offers a higher flexibility and can assess in real-time if replenishing of the constellation is needed. A launch rate of every two years seems reasonable. So taking the failure rate at the

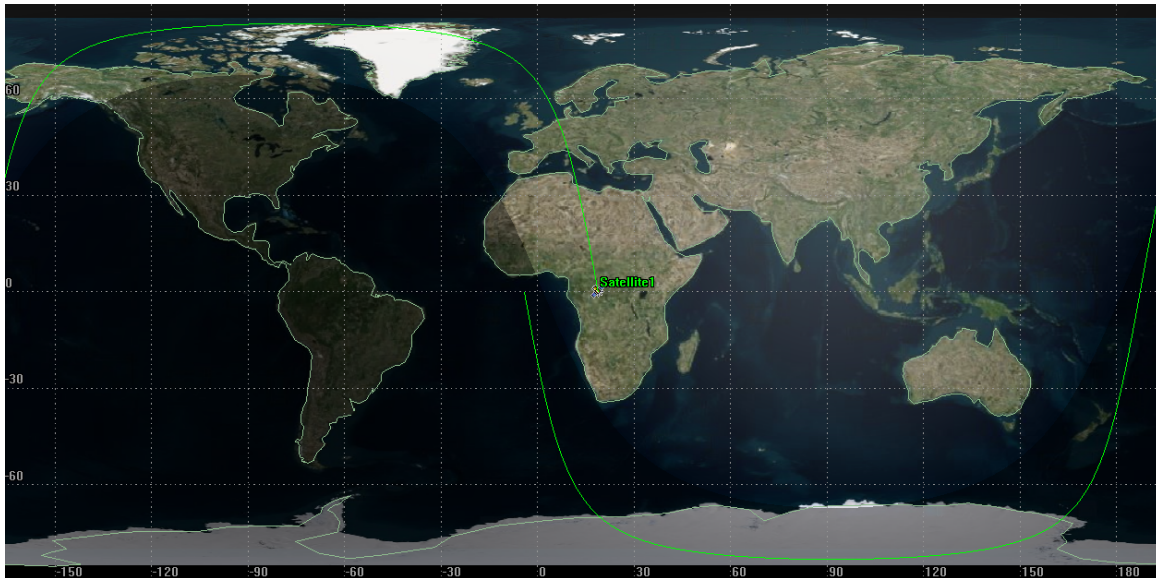


Figure 4.22: SSO ground track (made with the Systems Tool Kit (STK))

end of the second year, which is 79% [53], each orbital plane would need 87 satellites. That makes the total constellation size 174.

Even though the second strategy would require a new launch of satellites every once in a while, its higher flexibility and lower initial amount of satellites that needs to be produced make this the more favourable option. Especially the lower initial size, would make it easier in operation and lower the initial investment required.

The total mass of each satellite is 20.1 kg (which will be derived in Section 9.3). Using a contingency of 10% and multiplying this by the number of satellites in each orbital plane, the total mass per launch is 1923.6 kg. This number will be used for launcher selection in Subsection 4.5.3.

4.5.2 Spacing between orbital planes

The spacing between the two orbital planes is defined as the angle that it has with respect to the sun, since this angle will remain constant over time because the orbit is sun-synchronous. If the right ascension of the ascending node (RAAN) would be defined, this would have to be defined based on a certain Epoch of the orbit, which is overly complicated and not helpful at this point.

The spacing between orbital planes has effects on power received from the Sun, time between the two pictures taken of a certain place each day and lighting conditions. An overview is given in Table 4.5, giving the effects of bigger spacing (large angle A and B in Figure 4.23) and smaller spacing (smaller angle A and B in Figure 4.23).

Table 4.5: Advantages and disadvantages of bigger and smaller spacing

	bigger spacing	smaller spacing
power received	sunlight hits side of spacecraft	sunlight hits top of spacecraft
time between 2 pictures a day	one picture in early morning and one in late afternoon	both pictures around noon
lighting conditions	closer to solar noon	further away from solar noon (longer shadows)

²²<https://medium.com/starts-with-a-bang/5-killer-events-from-space-that-could-wipe-out-human-life-on-earth-53b5aa2b1bb6> [Date accessed: 24-06-2019]

²³<https://theconversation.com/curious-kids-is-there-anything-hotter-than-the-sun-105748> [Date accessed: 24-06-2019]

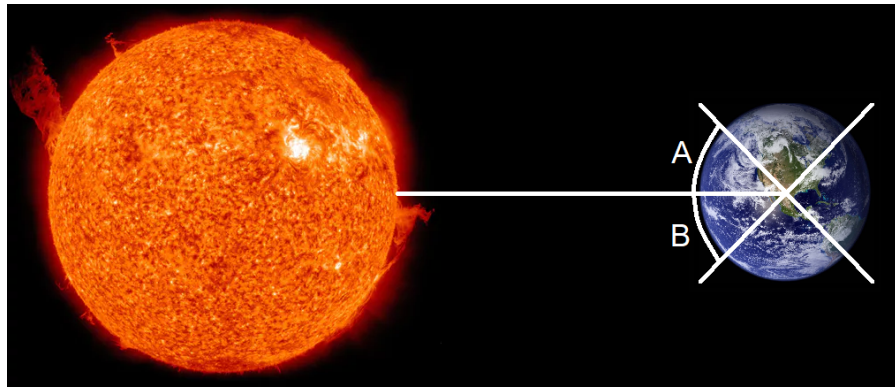


Figure 4.23: Spacing between orbital planes, images from medium (Earth)²² and theconversation (Sun)²³

An angle of ± 45 deg was chosen, for both angle A and B in Figure 4.23. It should be noted that this even spacing might be subject to change because no exact calculations were performed to arrive at this number. It was selected as a compromise between the advantages and disadvantages of bigger and smaller spacing as was shown by Table 4.5. With the selected angle, the time between two observations is always 6 hours, three hours before and three hours after solar noon on the equator.

In the rest of the report the design of the satellite that observes the Earth in the morning will be the main topic. The satellite observing the Earth in the afternoon will be a completely mirrored version, as the sunlight will come from the opposite direction.

4.5.3 Launcher selection

The total mass that one launcher needs to put in SSO is 1923.6 kg. While it is difficult to launch a lot of satellites during one launch, it is not impossible: SpaceX launched 60 Starlink satellites, each weighing 227 kg, on the 24th of May this year²⁴. Maximum payload mass is an important parameter for launcher selection, because this also decides how much mass can be used for a supporting structure, that needs to support the individual satellites while sitting inside the fairing. A 12U canister weights 5.65 kg, as will be explained in Subsection 8.2.1, and it is thus conservatively estimated that a structure that holds all the satellites and connects the individual canisters would weight 7.0 kg per satellite. This would make the total payload mass 2523.6 kg. Besides maximum payload mass, the launchers are assessed on price and sustainability to meet **SYS-LCH-VEH-2**.

In Table 4.6, three different launchers are shown with sufficient capabilities to be used for this mission. The Falcon 9 would be the cheapest option. But even though it is reusable, it is not the most sustainable because it uses the most fuel since it is designed for heavier payloads. The Soyuz ST-B would use the least fuel, but the price would be high. The Vettore Europeo di Generazione Avanzata (Vega) launcher was selected because it is a nice compromise between price and propellant mass needed for launch. In addition, it is advantageous that Vega is developed in Europe as it boosts the European space market, keeps the information within the confines of Europe, and allows for easier communication.

The risk of launch failure [**TR-OP-1**] is mitigated because a high-reliability launcher is chosen. The Vega launcher has a success rate of 100% with 16 successful launches between 2016 and 2019²⁵.

Table 4.6: Launcher options

Launcher	Payload to SSO [kg]	Launches required	Price (total) [\$M]	Propellant mass (total) [ton]
Falcon 9	8000 [54]	2	62 ²⁶ (124)	508 ²⁷ (1 015)
Soyuz ST-B	4400 [55]	2	80 ²⁸ (160)	164 [55] (328)
Vega	1500 [56]	4	37 ²⁹ (148)	123 ³⁰ (492)

²⁴https://www.spacex.com/sites/spacex/files/starlink_press_kit.pdf [Date accessed: 19-06-2019]

²⁵<https://rocketrundown.com/home/rocket-index/avio/vega-avio/> [Date accessed: 20-06-2019]

4.5.4 Verification of constellation design

To verify the constellation design methodology, the final result was put in STK, by AGI³¹. An overview of all parameters that were verified is given in Table 4.7. Since an exact altitude range cannot be put in the software, the lower bound was used. In Figure 4.24 a result from STK is shown, where on the left it can be seen that all the satellites have a different ground track, covering the entire Earth, and on the right that all these satellites are in the same orbit, only with different true anomalies. Thus verifying that the constellation design is correct.

Table 4.7: Orbit and constellation parameters

Parameter	Value
Orbit type	SSO
Altitude	332 km (put in lower bound)
inclination	96.77 deg
Eccentricity	0 [-]
Camera FoV	6.4 deg
Constellation size	69 per orbital plane (+ 18 spare)
true anomaly	0 deg, 5.2 deg, 10.4 deg, ..., 354.8 deg

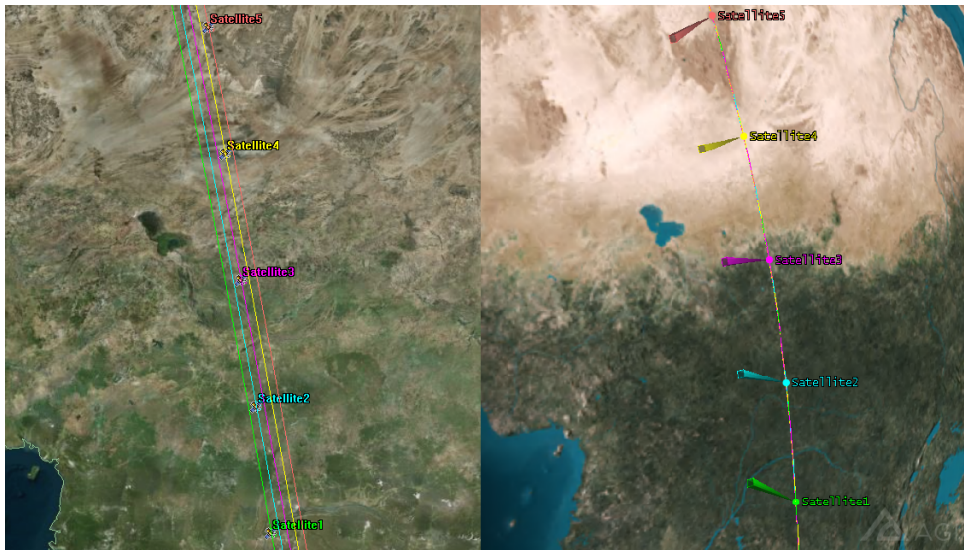


Figure 4.24: Constellation overview (made with STK)

4.6 ΔV budget estimation

The ΔV budget consists of orbit insertion, initial orbit correction, orbit phasing, drag compensation and end of life manoeuvres. A final overview is given at the end of this section in Subsection 4.6.6.

4.6.1 Orbit insertion

Orbit insertion will not require any ΔV because the dedicated launch by the Vega launcher will put the constellation already in the target orbit.

²⁶<https://www.spacex.com/about/capabilities> [Date accessed: 20-06-2019]

²⁷Calculated by subtracting dry mass from total mass

²⁸<https://www.gao.gov/assets/690/686613.pdf> [Date accessed: 20-06-2019]

²⁹<https://www.gao.gov/products/GAO-17-609> [Date accessed: 20-06-2019]

³⁰https://web.archive.org/web/20141101022341/http://www.avio.com/files/catalog/pdf/avum_78.pdf [Date accessed: 20-06-2019]

³¹<http://licensing.agi.com/stk/> [Date accessed: 01-07-2019]

4.6.2 Initial orbit correction

The Vega launcher has an insertion accuracy of ± 15 (3σ) km semi-major axis, ± 0.15 (3σ) deg inclination, ± 0.0012 (3σ) eccentricity, ± 0.2 (3σ) deg RAAN [56]. The latter two are deemed accurate enough, because these parameters don't influence mission success while altitude (variation in drag) and eccentricity (achieving SSO) are vital for this mission. So no ΔV budget is needed to correct eccentricity or RAAN. However, the risk of an offset in semi-major axis and inclination [TR-OP-3] is significant and should be mitigated.

The ΔV required for a semi-major axis correction of ± 15 km to the final phasing orbit of 364.2 km can be calculated using by subtracting the orbital velocities at 349.2 (= 364.2 - 15) km and 364.2 km altitude. Using Equation 4.2, the orbital velocity at 349.2 km altitude is 7701.54 m/s, and at 364.2 km altitude it is 7692.96 m/s. Subtraction yields an ΔV of 8.58 m/s for the semi-major axis correction.

To calculate the ΔV needed for the inclination correction Equation 4.3 was used. Using a Δi of 0.15 deg, and an orbital velocity of 7701.54 m/s, the ΔV for the inclination correction was calculated to be 20.14 m/s.

These two manoeuvres can be combined into a combined manoeuvre where the altitude and inclination are changed simultaneously, reducing the total ΔV for initial orbit correction to about 22.0 m/s.

4.6.3 Orbit phasing

When the launcher inserts the satellites in orbit around Earth, they are all in the same position in that orbit, thus all true anomalies are the same. However, to effectively take pictures of the entire Earth, the satellites need to be spread out evenly over the orbit, and the true anomalies should be 0 deg, 5.2 deg, 10.4 deg, ..., 354.8 deg, as specified in Section 4.5. The difference in true anomaly between two satellites is called the phase angle. The change in phase angle can be achieved by putting the satellites in a phasing orbit, which has a different orbital period than the final target orbit. This phasing orbit is usually higher so that its orbital period is larger than the target orbit, because the orbital period is a function of altitude, as specified by Equation 4.25. The difference in orbital period will cause the satellites to shift with respect to each other. Once the desired phase angle is acquired, all satellites are transitioned into the final orbit and nominal operations can start.

Orbit phasing can be done with propulsion or differential drag control. The latter is a relatively new, innovative method that utilises the difference in drag between low and high drag configuration of the spacecraft. A high drag configuration can be achieved by angling the spacecraft in such a way that the solar panels are perpendicular to the flow, maximising the frontal area. This method has successfully been applied to phase the Flock-2p constellation by Planet [57]. At an altitude of about 510 km, complete phasing took about a year. At an altitude of 332-342 km, because of the denser atmosphere, it could be done quicker. However, at this stage in the project it is impossible to assess how much quicker.

This phasing time can be reduced even further by using the electric propulsion system. In this case the launcher will put the satellites in a circular orbit with a higher altitude than the target orbit, called the phasing orbit. The higher altitude is required to get a difference in orbital period between the phasing and final target orbit, since the orbital period only depends on semi-major axis, as can be seen in Equation 4.25. One-by-one the satellites will activate their two thrusters to decelerate and lower their orbit into the final target orbit. The thrusters should be activated on a certain time interval, expressed as the number of orbits between manoeuvres. There are three parameters at play: the time required between manoeuvres, the transition time between the phasing and the final orbit and the ΔV required to transition between the phasing and the final orbit.

Logically, if there is more time between manoeuvres, the spacecrafts have more time to achieve the right phasing angle. This means that the difference in orbital periods doesn't need to be big and thus that the phasing orbit and final orbit can be relatively close to each other in altitude. Since the orbits are close, not much ΔV is required to transition between them. However, this will lead to a long total phasing time. This can also be seen in Figure 4.25, where the phasing options are shown. It can be seen that for longer times between manoeuvres (red), the total phasing time is longer (x-axis) but less ΔV is required (y-axis).

In the design, both phasing time and ΔV should be minimised, and thus a compromise is taken. In the end, it was decided to take three orbits between manoeuvres. This makes the total phasing time 21.3 days for the whole constellation, and the ΔV required 8.5 m/s per satellite.

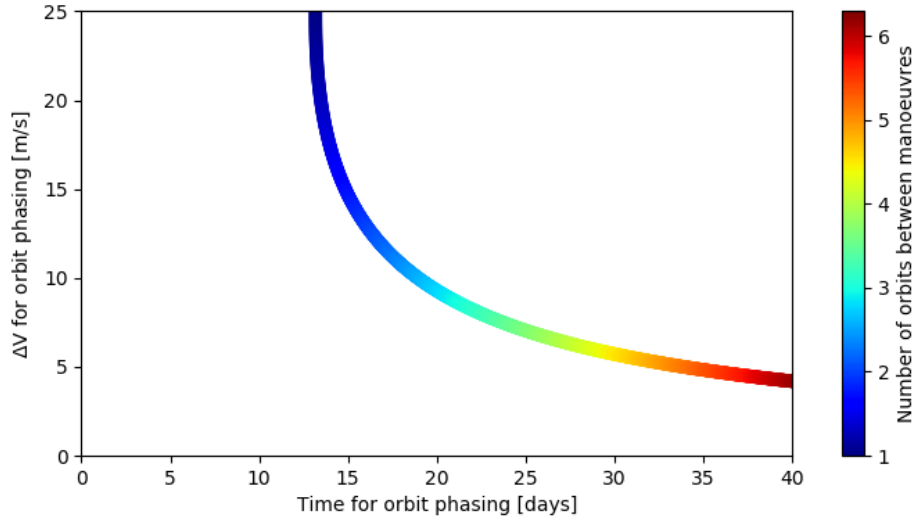


Figure 4.25: Options for orbit phasing

4.6.4 Drag compensation

To achieve the lifetime required for the mission stated in **SYS-OBJ-LT-1** the spacecraft shall be able to provide a sufficient amount of total impulse to achieve this. To calculate this Equation 4.28 is used [43].

$$Total\ impulse = f_d \cdot t \quad (4.28)$$

The total impulse required for the lifetime is checked with the capability of the propulsion system. From this total impulse the required ΔV can be derived using Equation 4.29 to comply with **SYS-SC-SUBSYS-PROP-1**.

$$\Delta V = \frac{Total\ impulse}{M} \quad (4.29)$$

With M being the mass of the satellite. This equation yields the total amount of ΔV required. Furthermore, the average ΔV needed for each orbit can be estimated by dividing the total ΔV by the total amount of orbits over the lifetime. This is obtained by dividing the total lifetime of five years in seconds by the average orbit time resulting in approximately 28858.5 orbits over the mission, resulting in an average ΔV of 0.0169 m/s.

From the average ΔV the average thrust time per orbit can be determined by Equation 4.30. For each thrust level the propulsion can provide, the equivalent thrust time is calculated and an overview is given in Figure 4.26. This information will aid in choosing the most optimal thrust level during operation. Note that the graph is constructed based on the extractor voltage of -7000 V with the power vs thrust relation as seen in Figure 4.16.

$$t = \frac{I_{sp} g_0 m_i}{F_t} \left(1 - e^{\frac{-\Delta V}{I_{sp} g_0}} \right) \quad (4.30)$$

It is desired to thrust for the least amount of time if the power availability allows it, leaving more time to take pictures. So, selecting a thrust level of 0.00084 N, which requires a thrusting time of 408 seconds on average each orbit will be the best option for the mission. This means 0.00042 N per thruster each time the systems thrusts.

There are multiple options to thrust during the orbit. The spacecraft can either thrust continuously the entire time through the complete mission, it can thrust continuously for one orbit and wait a couple of orbits before thrusting again. Furthermore, it can thrust once every orbit or multiple times each orbit.

The drawback of having to thrust continuously throughout the complete mission would give rise to many complications. Especially if the torques are not constant this heavily influence the stability requirement that the ADCS has to provide. Moreover, this option will not be considered at all due to the fact the propulsion system cannot provide a thrust level this low. Therefore, this option is already not feasible.

Thrusting once every orbit and wait several orbits has the drawback of being less efficient in terms of there being an orbit where the spacecraft will not thrust. This, complicates matters by making the operations

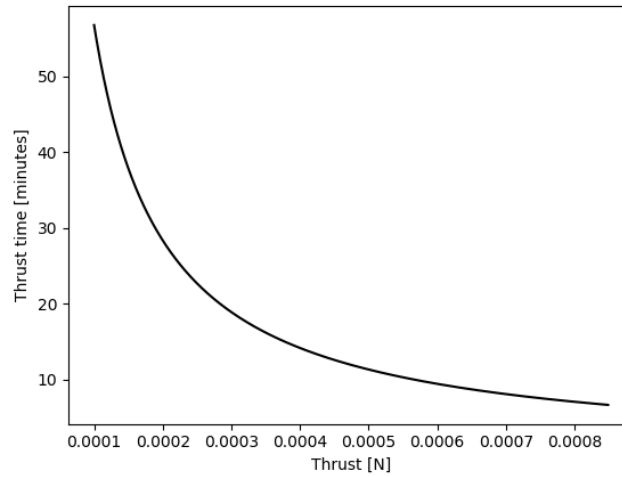


Figure 4.26: Average thrust time for an orbit

dependent on the orbit. So, by minimising the height difference the same operations can be performed each orbit. This means if the height difference is minimised. The spacecraft will experience the same conditions generally. So, the modes will stay approximately the same each orbit.

This can be achieved by thrusting once every orbit or several times in one orbit. The latter one minimises the difference in orbit altitude during the mission. An as high as possible thrust is desired from the propulsion system, as the higher thrust leads to less time as seen in Figure 4.26. In addition, the less time the spacecraft has to thrust the more time it has left to perform other the nominal mode of taking pictures. Therefore, the final thrust mode over the mission will be either thrusting once every or thrust several times in an orbit or a combination of both.

4.6.5 End-of-Life

In order to mitigate space debris generation, there is a guideline to dispose satellites in orbits below 2000 km within 25 years after mission completion³². This has translated into requirement **SYS-SC-EOL-1** and **SYS-SC-EOL-2**, that dictate that after the mission duration of five years, or after a loss of signal, the satellite shall deorbit within 25 years.

To show compliance with these requirements, the DRAMA software by ESA was used³³. Since the satellite will deorbit because of drag, the estimation of drag is important. As discussed in Section 4.2, the solar flux greatly influences the density and thus the drag experienced in VLEO. For this reason, a worst case estimate during solar minimum is assumed when deorbiting starts. The results are displayed in Figure 4.27, it should be noted that the exact dates (x-axis) are not of importance because the solar flux is assumed to be at a constant solar minimum and thus doesn't depend on the time. It can be seen that in this worst case, the spacecraft would deorbit in 1.9 years, which is still well within the requirement of 25 years. This means that no ΔV is required for EOL manoeuvres. Since these manoeuvres are completely passive, the risk of deorbiting failure [TR-OP-5] is negligible.

4.6.6 Overview

The overview of the ΔV budget with all aforementioned phases of the mission is shown in Table 4.8.

As there are two IFM Nano Thrusters that integrated, which combined can provide a ΔV of 766 m/s for a spacecraft of 20 kg³⁴. So, there is enough ΔV for unforeseen events. Hence, meeting the **SYS-SC-SUBSYS-PROP-1** requirement. Furthermore, propulsion wise the spacecraft will meet **SYS-OBJ-LT-1**. However,

³²https://www.esa.int/Our_Activities/Space_Safety/Space_Debris/Mitigating_space_debris_generation [Date accessed: 21-06-2019]

³³<https://sdup.esoc.esa.int/drama/> [Date accessed: 21-06-2019]

³⁴<https://www.cubesatshop.com/wp-content/uploads/2017/04/ENP-IFM-Nano-Thruster-Product-Overview.pdf> [Date accessed: 21-06-2019]

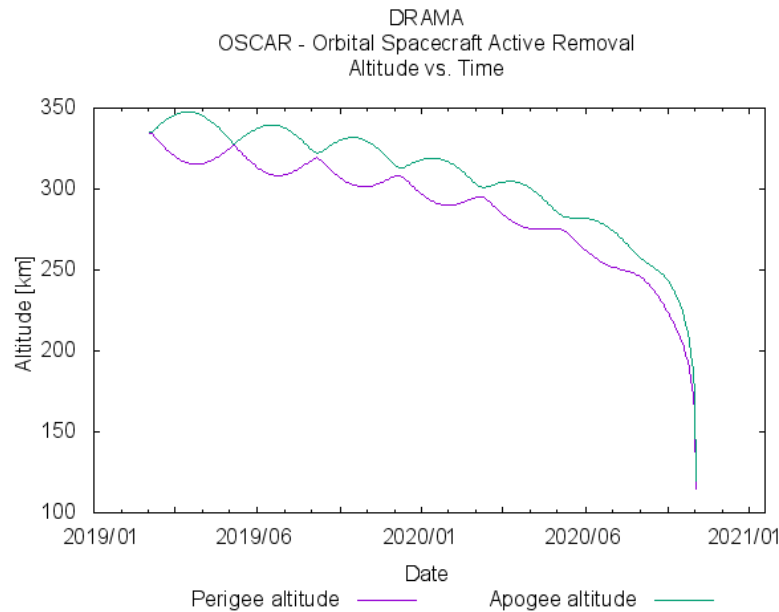


Figure 4.27: EOL manoeuvre

Table 4.8: ΔV budget

	Orbit inser- tion	initial orbit correction	Orbit phas- ing	Orbit main- tenance	End of life	Total
ΔV [m/s]	0	22.0	8.5	489	0	519.5

4.7 Recommendations

During the development and utilisation of the aerodynamic simulation software, some possible improvements were identified. A variable mesh size will be useful to nicely define complex geometric areas while not making it unnecessarily complex for flat surfaces. Moreover, an improved, heavily parallelized, and maybe even implemented for a Graphics Processing Unit (GPU), ray tracing algorithm can be developed to reduce computational time, which is the bottle neck in the simulation. Finally, to have more refined results, especially for complex geometries, a Monte Carlo simulation tool like SPARTA³⁵ should be used [58]. More generally, some more research should be done on active aerodynamic stabilisation as different sources [59, 60] suggest.

Regarding the propulsion system, a better investigation in the quantification of risks may be done, such that according to that, a thrust level can be chosen, since there may be risks that are overlooked. Furthermore, more investigation into the drag simulation may result in the most optimal thrust mode and power distribution, with respect to the modes. Furthermore, actual data can be acquired about thrust misalignments in previous missions and their causes to optimise the expected disturbance torques due to thrusting. Even though chances are small that one propulsion system will completely shut off, as it is an important aspect of the mission a more thorough investigation will be performed with respect to having one engine fail and how it will be mitigated.

To conclude, with an even better aerodynamic model and a more thorough investigation in the thrusting modes, more complete orbital calculations can be performed. These would include also perturbations due to other planets, the moon, the Sun and direct solar flux. This could be done by the tudat software by the Technical University Delft³⁶. Furthermore, this more detailed orbit simulator can include thrusting time such that a better prediction can be made on where in the orbit should thrusting happen.

³⁵<https://sparta.sandia.gov/> [Date accessed: 24-06-2019]

³⁶<http://tudat.tudelft.nl> [Date accessed: 24-06-2019]

5. Payload design

Having determined the orbit and advocated the ability of the design to be able to operate for several years through the use of an innovative propulsion system, the time has come to size instruments. The payload is the combination of hardware and software interacting with the environment to accomplish mission objectives. For this particular mission, the payload is a visible and near-infrared spectrum camera offering a *GSD* of 4 m. At such altitudes, the harsh aerodynamic conditions imply the need for a scrupulous attitude control to counteract disturbances and permit for high-quality image acquisition. Hence, these two systems go hand-in-hand and must cooperate closely.

To refresh the reader's memory on optical systems, a brief overview of optical physics is provided in [Section 5.1](#), where various design choices are considered concerning optical components. Then, physical limitations of the design are considered in [Section 5.2](#) in terms of resolutions. Disturbances affecting optical images are investigated in [Section 5.3](#), along with potential mitigation schemes: namely, the attitude disturbances must be countered with a highly-responsive ADCS. The latter is highly intertwined with the payload, hence effective communication between the two is essential. The selected instrument is presented in [Section 5.4](#), and finally in [Subsection 5.6.1](#) Super-Resolution techniques for image enhancement are examined.

5.1 Physics of electro-optical systems

The architecture of a generic electro-optical system is shown in [Figure 5.1](#):

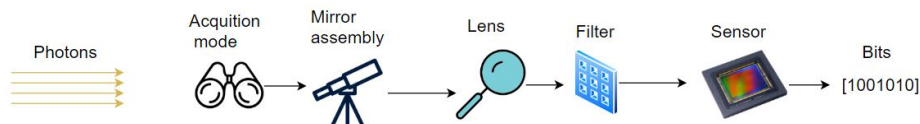


Figure 5.1: Architecture of a generic optical system

Photons are gathered in a scanning or staring fashion, according to three basic image **acquisition modes**, affecting equipment cost and stability requirements. These comprise of:

- *Whiskbroom line Scanners*, recording a small area within their Instantaneous Field of View (IFoV) thus building up a line of recorded signals (pixels) using a moving mirror. In terms of coverage, a large FoV can be achieved without severe distortion at the edges [61]. The main disadvantage is the large sampling frequency needed to cover a continuous wide swath, and a short integration time resulting in lower spatial/spectral resolution.

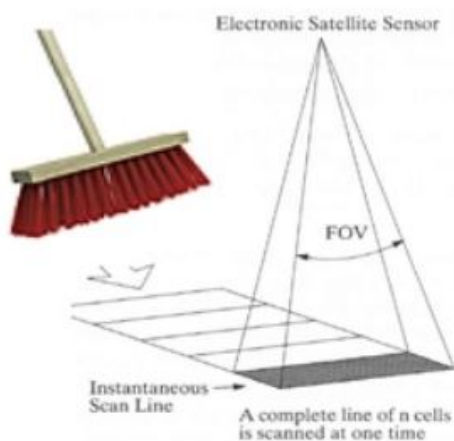


Figure 5.2: Pushbroom Line Scanner ¹

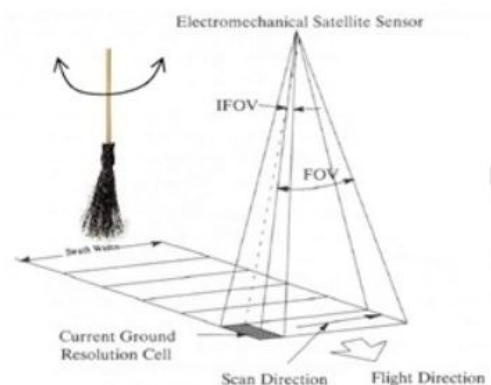


Figure 5.3: Whiskbroom Line Scanner ²

- *Pushbroom line Scanners* use a line of detectors arranged perpendicular to the flight direction of the spacecraft, such that a row of pixels is collected simultaneously during t_i . As it relies on the plat-

²<https://www.harrisgeospatial.com/Support/Self-Help-Tools/Help-Articles/Help-Articles-Detail/ArtMID/10220/ArticleID/16262/Push-Broom-and-Whisk-Broom-Sensors> [Date accessed: 16-05-2019]

form's orbital motion, no moving parts are present limiting wear and yielding high resolution imagery for $FOV < 15^\circ$. Such scanners are vastly employed for the generation of 2-D planetary images, for example Planet's Flock satellites employ this method [62].

- *Matrix or Staring array* can be thought of in terms of a detector staring at the scene to create the image. Two dimensions can be observed simultaneously, admitting measures are taken to correct for the platform's motion: this will pose severe challenges on the ADCS system, having to provide the necessary pointing accuracy not to overlap images. The advantage in sensitivity gained by permitting long dwell time is offset by the high cost [28].

The **mirror assembly** redirects light towards the optical system. As with all space instruments, it shall be lightweight but also stiff to endure launch vibrations. A low Coefficient of Thermal Expansion (CTE) is needed to comply with the operational temperature envelope and minimise the need of active thermal control. Manufacturing aspects should be considered as well; optical systems entail high tolerances and smooth polishing, limiting material selection.

Traditionally, glass is employed for large mirrors operating at room temperatures. It is a convenient choice, as it can be polished to a very smooth surface without a specific grain structure [61]. Manufacturers are able to manipulate the CTE to produce thermally stable optical components, notably the lithium-aluminosilicate glass-ceramic Zerodur[®]³ popular due to its high Young's modulus and excellent polishing qualities. The main drawbacks are high cost and difficult handling. To increase dynamic performance, silvering is performed: this is ideal for observing all wavelengths of light, offering high reflectivity and low emissivity⁴, although tarnishing is very common. This is not the case for aluminium, having the highest reflectivity over a broad spectral band. It is easily machinable, polishable and holds higher specific stiffness than glass, which makes it a viable low-cost alternative⁴. The well-known Hubble Space telescope employs mirrors with aluminium coating⁵.

Lenses are optical components with one or more curved surfaces, forming images according to the refraction principle by bending wave fronts. Bi-convex lenses cause light to concentrate and must be carefully designed to limit aberration effects. The lenses are most often made of crown and flint glass types, depending on the desired refractive index which is usually about 1.5-1.7. Due to the brittleness of these materials, precise alignment is needed to avoid fracture [TR-PL-1] due to launch-incurred vibrations.

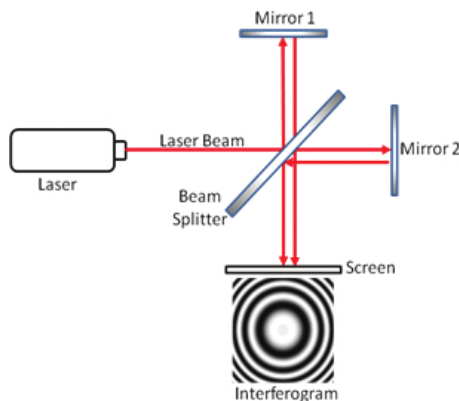


Figure 5.4: A Michelson interferometer. Retrieved from [63]

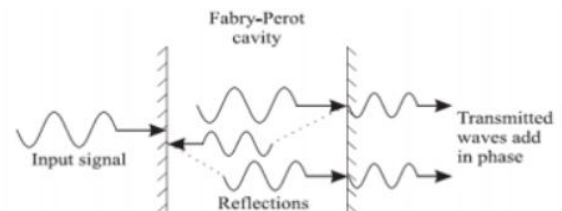


Figure 5.5: A Fabry-Perot interferometer. Courtesy of ⁶

Optical **filters** work by selectively transmitting portions of the spectrum. A special class of filters, known as interferometers, use wave superimposition techniques causing the phenomenon of interference to extract information [64]. Two main types of interferometers exist:

- *Michelson* interferometers, schematically drawn in Figure 5.4. A light input is split into two identical beams by a 45-degree oriented beamsplitter: one path leads to mirror 1 where 50% is reflected back to the beamsplitter, and then 50% reaches the detector focal plane by a 90-degree turn. The reflected beam travels to mirror 2, where the same principle occurs. The two remaining beams interfere to produce

³Registered trademark of Schott AG https://www.schott.com/advanced_optics/english/products/optical-materials/zerodur-extremely-low-expansion-glass-ceramic/zerodur/index.html [Date accessed: 19-06-2019]

⁴<https://www.sharrettsplating.com/blog/silver-aluminium-mirror-coating/> [Date accessed: 16-05-2019]

⁵<https://www.nasa.gov/content/goddard/hubble-space-telescope-optics-system> [Date accessed: 17-05-2019]

⁶<https://www.ques10.com/p/19780/short-note-on-fabry-perot-filters/> [Date accessed: 19-6-2019]

fringes on the detector[61]. Simplicity and availability of equipment is an advantage of this method, as well as the attainable precision: versions of Michelson interferometers have been used to take recordings of the distance to stars and the cosmic microwave background⁷. The continuous splitting however reduces the reliability of measurements. This can be circumvented with cube-corner mirrors in a four-port design, increasing cost and complexity.

- *Fabry-Perot* interferometer as depicted in Figure 5.5: this interferometer makes use of multiple reflections between two closely spaced partially silvered surfaces. Part of the light is transmitted each time, resulting in multiple offset beams[65]. The numerous interferences yield extremely high resolution, similarly to the multiple slits of a diffraction grating. The disadvantage is that in between the peaks, the position is difficult to estimate since the total light throughput is much lower than the peak central transmission⁸.

Sensors capture upwelling radiation and generate an electrical signal depending on its intensity, virtually converting photons to electrons. The light capturing is performed in a limited exposure (or integration) time t_i , determined by the FoV and ground track speed of the satellite. Two types of sensors are possible: Complementary Metal Oxide Semiconductor (CMOS) and CCD (charge coupled device), differing in pixel conversion and image processing scheme.

A CCD sensor has a limited number of nodes to convert each pixel charge to a voltage, then the amplification process and digital conversion happens on an external processor. In CMOS, each pixel has its own charge-to-voltage conversion and imaging functions are performed locally, meaning higher process speeds are possible.

Traditionally, CCD sensors produced crisper images and have less noise as a result of the output data uniformity. They are employed in high-end scientific applications, such as astronomical telescopes. Unfortunately, CCDs consume up to 100 times more power than CMOS sensors with equivalent resolution [66], a significant downside for satellites. They also require special manufacturing, incurring larger costs. This has pushed the advancement of CMOS sensors, which have caught up with their CCD counterparts in terms of sensitivity and dynamic range[67].

A great challenge of satellite optics design is fitting an adequate **focal length** in a constrained space, usually tackled by introducing reflective surfaces. This represents the distance from the lens to the focal point, quantifying how strongly the system converges or diverges light [68]. Larger f leads to higher magnification and a narrower angle of view.

Lastly, the **field stop**: if present, only the light through the centre of the lens can pass through. This is expressed as a focal ratio: a stop whose diameter D is half the focal length f yields $f/2$. Some aberrations, such as Coma and spherical aberration can greatly be reduced this way, as they are caused by differences in light rays in the centre and edges of the frame [69]. As a consequence of less light hitting the sensor, the shutter speed has to be decreased and the Signal-to-Noise Ratio (SNR) is worsened, however the depth of field can be improved. This relates depth of the image where it appears to be sharply focused⁹, however, this does not constitute a great advantage as a circular orbit yields constant distance to the objective.

5.2 Resolution compromise

Performance of a satellite optical system is expressed in terms of spatial, spectral, temporal and radiometric resolutions. These quantify the image sharpness, colour variety, transmission capability and refresh rate. All are considered hereby except for temporal resolution examined in Section 4.5 due to its dependence on orbital parameters.

Spatial resolution of optical systems is limited by aberration or diffraction. Aberration is a property that causes light to be spread out over some region of space rather than focused to a point [70], causing blur or distortion. Generally, this can be overcome by increasing the optical quality—hence cost—of the system, alternatively increasing the field stop. On the other hand, diffraction is primarily determined by the finite aperture of the optical elements. For diffraction limited systems, the *GSD* is dictated by the Rayleigh Criterion:

$$GSD = 1.22 \frac{\lambda H}{D} \quad (5.1)$$

With λ equal to the highest observable wavelength, H the sensor-object distance and D the aperture diame-

⁷<http://w.astro.berkeley.edu/~jrg/ngst/michelson.html> [Date accessed:19-6-2019]

⁸<https://www.sciencedirect.com/topics/engineering/perot-interferometer> Date accessed: 19-06-2019]

⁹<http://hyperphysics.phy-astr.gsu.edu/hbase/geoopt/stop.html#c2> [Date accessed: 15-05-2019]

ter. In conjunction with camera specifications presented in Section 5.4, this represents a physical boundary for the orbit at 342km to meet the *GSD* requirement.

Spectral resolution describes the ability of a sensor to distinguish between wavelength intervals in the electromagnetic spectrum (bands), and is quantified in terms of resolving power:

$$R = \frac{\lambda}{\Delta\lambda} \quad (5.2)$$

where $\Delta\lambda$ is the smallest difference in wavelengths that can be distinguished at a range of λ . Observing all wavelengths together in the visible spectrum results in a panchromatic image. This range can be divided into sub-bands to form a multispectral image, notably the additive red, green, blue (RGB) scheme which allows to rebuild natural colours by composing these channels [71]. What is interesting to note is that special satellite platforms, such as SkySat-1 by Planet, actively interchange *GSD* and *R* to accustom different applications: the same camera can offer panchromatic and multispectral images at 0.72m and 1.0m resolutions¹⁰. High spectral resolution is thus possible with narrow bandwidths which, consequently, decreases the overall signal strength. With the background noise constant, the SNR worsens as a result, limiting the **radiometric resolution** [61]. This relates to the ability to discriminate energy differences in the spectrum [71], effectively quantifying the colour depth, and is expressed in bits. To push this boundary, long integration times and specific filters are applied [72].

The following quantities are closely related: if a high spatial resolution is required, this will limit the FoV for a fixed-size camera. Consequently, this reduces the collectable energy from the ground, leading to a diminished radiometric resolution. To increase the latter without compromising spatial resolution, one should broaden the wavelength range for a particular channel, which in turn affects the sensor's spectral resolution. An effective optical design must compromise spectral, spatial and radiometric resolution to transmit just the right quality of image at an acceptable system cost.

5.3 Disturbances

Imaging data is negatively affected by disturbances, which are classified in two main categories: radiometric and geometric. The former is considered first, followed by various kinds of geometric disturbances.

5.3.1 Radiometric effects

Radiometric disturbances alter the brightness value of the pixels and can occur in two ways. First, the brightness distribution in a given band can be different from the ground scene. Secondly, the relative brightness of a single pixel from band to band can be distorted compared to the spectral reflectance on the region. Both can be caused by atmospheric presence and/or instrumentation effects, although the latter are generally less severe [73].

The most prominent instrumentation error stems from dark current noise, residual current present in the detector when it is not illuminated [69] which is amplified with increasing temperature. This is especially important when using multiple detectors for a single band, and can be corrected by calculating pixel mean brightness and standard deviation using image data from a single detector [73].

Atmospheric errors arise from scattering and absorption, for which compensation is needed to yield high-quality images. Absorption occurs when molecules, such as, oxygen, carbon dioxide, ozone and water, convert energy into heat, attenuating light intensity at the sensor. Temperature and humidity measurements can be used to correct for this [74]. Scattering issues light reaching a pixel that did not originate from the target. In a clear atmosphere only Rayleigh scattering occurs due to the air molecules affecting wavelengths, the reddish appearance of a sunset being a prime example of this phenomenon. Aerosol or Mie scattering, contrarily, results from larger particles, such as, those associated with smoke, haze and fumes [73]. There are two broad ways to mitigate atmospheric disturbances: the first is a detailed correction, requiring atmospheric information that is readily available. Empirical corrections can always be applied, the most common being haze removal. It is based on the principle of estimating and compensating for atmospheric shifts in brightness at different wavelengths, modelling the extent of Mie scattering with $\lambda^{-\alpha}$ (with $0 < \alpha < 4$). Atmospheric effects are more

¹⁰https://www.planet.com/products/satellite-imagery/files/Planet_Combined_Imagery_Product_Specs_December2017.pdf [Date accessed: 19-06-2019]

prominent when the camera is detector-limited and has a wide field of view. As of yet, the investigated cameras are diffraction-limited and survey 15 deg at most.

5.3.2 Earth rotation during acquisition

Sensors recording one line at a time (whiskbroom, staring array) will incur distortion in the images due to the Earth's Eastward rotation. During the capture time, a pixel imaged at the end of the frame would have been further to the west when recording started. The image must hence be calibrated according to this offset [73].

The orbital velocity is $v = 7.7\text{m/s}$. Assuming a typical FoV of 5 deg, this results in a swath height of $s_h = 29.86\text{ km}$ from altitude $H = 342\text{ km}$ (see Section 4.4), meaning the time needed to record a frame is:

$$t_f = \frac{s_h}{v} = 3.88\text{ s} \quad (5.3)$$

The Earth's rotational velocity is $\omega_e = 72.72\mu\text{rad/s}$, yielding a maximal surface velocity of:

$$v_e = \omega_e R_e \cos(\phi) = 463.30\text{ m/s} \quad (5.4) \quad \Delta x = v_e t_f \cos(i - 90) = 1.79\text{ km} \quad (5.5)$$

at the equatorial plane, where the latitude $\phi = 0^\circ$. Accounting a correction for orbital inclination i of 96° , the surface will have moved a total of 1.79 km (Equation 5.5). This is a significant 6% of the 29.86 km frame, hence steps must be taken to correct for this during image processing.

5.3.3 Panoramic distortion

Panoramic distortion occurs when the effective pixel size on the ground is larger at the extremities of the scan than at nadir, shown schematically in Figure 5.7 (to avoid confusion, θ in the figures is FoV/s). Denoting p as the pixel size at nadir, β as the angular resolution and it can be shown trigonometrically that p at the edge of the frame yields:

$$p_{FoV/2} = \beta h \cdot \sec^2(FoV/2) = p \cdot \sec^2(FoV/2) \quad (5.6)$$

Deeming a pixel increment of 5% acceptable, this causes a problem only for cameras with $FoV > 26\text{ deg}$.

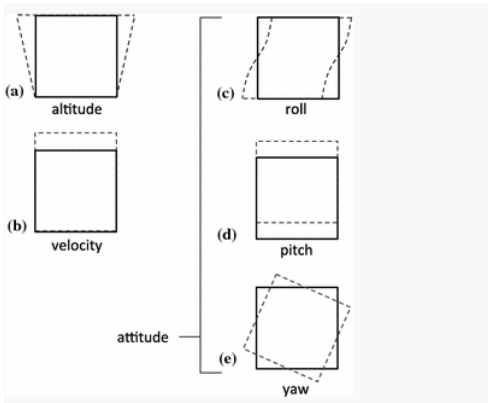


Figure 5.6: Effect of platform position and attitude variations. From [73]

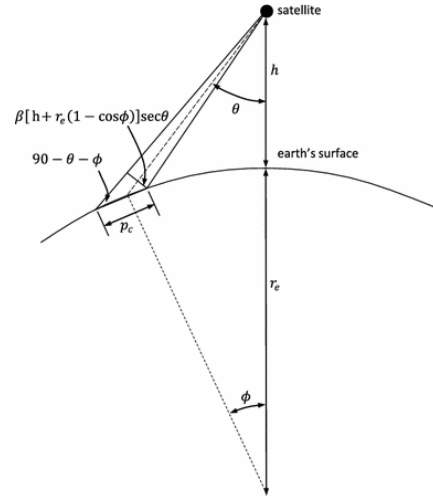


Figure 5.7: Effect of scan angle on pixel size. Courtesy of [73]

5.3.4 Variations in platform altitude, attitude and velocity

A change in elevation or altitude of a remote sensing platform lead to image scaling for a constant FoV: this is illustrated in Figure 5.6(a). This can be corrected straightforwardly, as the altitude is known at all times thanks to the internal GPS as explained in Section 7.2. In a similar fashion, a sudden change in the platform's along-track velocity will shear the image as shown in Figure 5.6(b). This might arise from simultaneous thrusting and image acquisition, which is not the case in the present mission as described in Subsection 3.2.2.

In contrast, platform attitude changes can be resolved into yaw, pitch and roll affecting the results as shown in Figure 5.6(c-e). These effects are obviously undesired, as they will smear the pixels, degrading image quality

[TR-PL-2]. Intuitively, one can deduce that yaw instability is the least severe case, as its effect is not magnified by the orbital altitude.

On the other hand, roll and pitch instabilities are dangerous and shall be countered with a highly responsive attitude control. For this reason, a maximum rotational rate limit requirement is imposed on the pitch and roll axes in Equation 6.2. As the k_{pixel} and t_i parameters are inherent to the instrument, these shall be derived here.

The integration time t_i is readily computed from the orbital velocity and the IFoV:

$$t_i = \frac{x_{IFOV}}{V} = 519\text{ns} \quad (5.7)$$

The image sharpness criterion k_{pixel} is harder to estimate - the Modulation Transfer Function (MTF) must be introduced first. The MTF is an important parameter in measuring the performance of an optical system: it defines the image contrast and thus the image quality at a defined spatial frequency, with a value of 100% being the highest [72]. The MTF can be further decomposed to include effects resulting from jitter, linear and sinusoidal motions of the satellite, however, the method is not trivial and no standard approach has been found, therefore it has been concluded that a detailed analysis in this subject of matter goes beyond the scope of this project. For similar imaging missions, a study has been conducted indicating the values of k_{pixel} ranging from 0.18 to 0.26 of the pixel size are the upper limits, beyond which the MTF dips to an unacceptable extent [75].

5.4 The SEEING camera

Following an extensive overview of commercially available optical systems, the team converged to the SEEING camera developed by Safran Reosc. for ESA's "Φ week"¹¹ during the trade-off. This instrument was chosen over its high resolution counterpart, as the constellation size would have been too large in the latter case, skyrocketing total mission cost. At the time of writing, the instrument is still in experimental phase, however technicalities specified in [76] suggest it shall soon emerge in the market. The most critical parameters are summarised below:

Table 5.1: SEEING specifications

GSD	4 m @342 km	Scanner	Pushbroom
FoV	6.3x4.3 deg	Inferometer	Fabry-Perot
Sensor	FF 35 mm	Bandwidth	475-900 nm
Aperture	130 mm	Operating T	15-25°C
Focal Length	330 mm	Size	14x16x16 cm
In-Orbit MTF	>55%	Mass	10 kg
SNR (panchro)	>256	Power	30 W nominal
N_{ch}	10	Bits per pixel	8

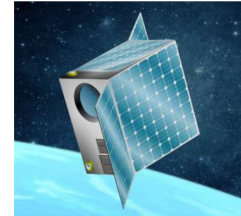


Figure 5.8: Render from [76]

The 4 m resolution requirement is met at 342 km **SYS-OBJ-PL-2**, setting an upper bound on the altitude. Its 35 mm Full-Frame CMOS sensor allows for a moderate FoV, reducing the amount of satellites needed to cover the Earth. Five to ten spectral bands from 475 to 900 nm are available: aside from the visible spectrum **SYS-OBJ-PL-1**, this near-infrared region is of particular importance for biological applications, namely for soil composition and moisture estimation [28]. The high f-stop of F/2.5 is optimised to maximise the SNR whilst allowing for imagery in low light conditions like twilight and polar regions. Image processing software is included in the module **SYS-SC-SUBSYS-CDH-1/3**, reducing the raw data size for C&DH. The mirror involves a lightweight Zerodur[®] design, known for its stable diffusivity facilitating thermal control. With Silicon Carbide constituting the optics, the overall system weighs 10 kg. The ample 130 mm aperture effectively dictates the overall size of the satellite, needing at least eight units for the payload alone. The design MTF is better than 55%, and the SNR is better than 256 in panchromatic mode. The overall cost is estimated at roughly 150 000 € based on instruments with similar capabilities. Magnetic interference is not specified by the manufacturer, and will be investigated during the assembly and testing phase **SYS-SC-CNF-3/4**.

¹¹<https://satelliteobservation.net/2018/12/28/safrans-high-performance-imager-for-cubesats/> [Date accessed: 16-05-2019]

5.5 Signal to noise ratio

For any optical system, a crucial parameter is to achieve a significant SNR in the shortest t_i possible. Over the last decade, the data produced by modern sensors is of increasing quality, as a result of their ability to distinguish similar materials[77]. As the GSD has been shrinking, the SNR have been rising such that values over 100:1 in the visible/near infrared spectrum are common[77]. The signal strength is characterised by the following equation:

$$S_i = L_e \cdot \Omega_s \cdot t_i \cdot N_{TDI} \cdot A_d \cdot \eta \cdot QE \cdot \Delta\lambda \quad (5.8)$$

$$L_e = \frac{2\pi h_p c^2}{\lambda^5} \frac{1}{e^{hc/k_B T} - 1} \quad (5.9) \quad \Omega_s = \pi \left(\tan^{-1} \left(\frac{GSD}{2H} \right) \right)^2 \quad (5.10)$$

Spectral radiance, Equation 5.9 is the radiance of a surface per unit wavelength, it is based on Plank's law[61], with Plank's constant, Boltzmann's constant and speed of sound h_p , k_B and c , respectively. T is Earth's (average) temperature of 287.75 K, whilst the -highest- observed wavelength is 900 nm. The solid angle collected by the instrument is formulated in Equation 5.10, which concludes the orbit-dependent parameters; the rest arise from the detector. N_{TDI} is the number of integrations to record an image, which for a similar 50Mpx sensor of 7920x6004px becomes 6004, as a pushbroom records line-by-line¹². The instrument's aperture is 130mm from Table 5.1. Transmission η shows the electromagnetic throughput despite scattering (increasing with wavelength) and absorption (drop at specific wavelengths due to molecules), shown in Figure 5.9 to be 1 for 0.9 microns.

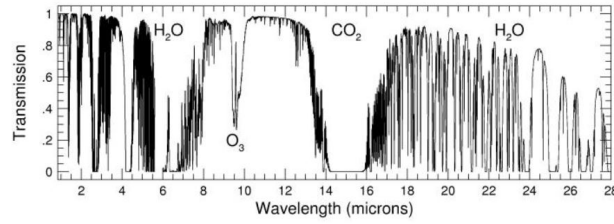


Figure 5.9: Infrared Absorption of the Atmosphere from 1-28 microns. From ¹³

The quantum efficiency QE defines the photon-electron conversion and collection efficiency of the image sensor. Generally, CCD have efficiencies of 70-90%[61]: it is argued that high-quality CMOS outperform CCD in this regard[78], hence a value of 0.85 is chosen. Finally, $\Delta\lambda$ quantifies the selected bandwidth, indicating that in panchromatic mode (900-475nm) the signal strength is highest.

The most prominent noise occurring in shot noise: this results from the randomness of the emission times of the photoelectrons[61], and is modelled with a Poisson distribution. For large numbers, this approaches a normal distribution, hence the standard deviation of shot noise is equal to the square root of the number of counts (photoelectrons):

$$SNR \approx \frac{S_i}{n_{shot}} = \frac{S_i}{\sqrt{S_i}} = \sqrt{S_i} \quad (5.11)$$

A spreadsheet is set up to carry out a SNR multivariate analysis, yielding a final value of 294 in panchromatic mode, which is in general agreement with the manufacturer's claims (Table 5.1). This optimistic value can be defended by the fact that only shot noise was considered, and the CMOS sensor's efficiency is on the high side.

5.6 Super-resolution imagery

Super-resolution imagery refers to techniques enhancing the resolution of an imaging system. In the past decade, this practise has become more common, as it allows for simplifying spacecraft design for high-quality imagery. Example-based and Multiple Image techniques are possible.

¹²<https://www.illunis.com/area-scan-cameras/50-mp-global-shutter-cmos/> [Date accessed:01-07-2019]

¹³<http://www.astronomy.ohio-state.edu/~pogge/Ast161/Unit5/atmos.html> [Date accessed:01-07-2019]

5.6.1 Example-Based super-resolution: PROBA-V approach

This technique uses data interlacing and interpolation of multiple images to achieve resolution enhancements, by the use of Convolutional Neural Networks (CNNs). Deep learning techniques are emerging as a key to face image processing challenges, in particular generative adversarial networks: a generator network produces new data which fits the distribution of the training data. A discriminative model distinguishes classes of data, deciding whether input is coming from the true or fake data set. In other words, the discriminator is guiding the generator to produce realistic data, ultimately improving resolutions. This technique bears great potential in the field of computer vision, however it is not proven in satellite imagery yet, the reason being that the invented details are considered as artefacts.

PROBA-V, a 2013-launched ESA satellite designed to map land cover and vegetation growth across the globe¹⁴ employs this method to enhance its 300m resolution images of the same patch originating from successive revisits over longer periods of time[79]. It must be mentioned, however, that ground truth training data originated from 100m resolution images from a satellite with much lower revisit times. Hence a possible approach for the present mission would be to design a high-orbit satellite, with a large camera, offering high-resolution training data.

5.6.2 Multiple image super-resolution: SkySat-1 case study

Multiple image super-resolution techniques do not employ neural networks, but instead exploit motion vectors to extract pixel information from multiple snaps of the same area. The main advantage of this method is that no data set is required for training. In 2013, Planet Labs launched SkySat-1, the first commercial microsatellite to achieve sub-meter resolution panchromatic as well as 4-band pan-sharpened imagery¹⁵. SkySat-1 is capable of combining data from multiple frames to boost image SNR and decrease the ground sample distance. To get an approximate improvement in resolution factor for the present mission, the optical system of SkySat-1 can be assumed diffraction limited, bounded by physical limitations of Equation 5.1.

Comparing this GSD with the advertised resolution of the platform gives an indication of the achievable enhancement factor. With an aperture of 35cm, observing wavelengths of up to 695nm of from an altitude of 600km[80], this yields a physical boundary of 1.45m, hinting at an improvement factor of 1.5. If the same technique is assumed for the present mission, a significant improvement of 2.67m GSD is possible.

5.7 Future recommendations

A suitable optical system is presented in this section, however the manufacturer is reluctant to disclose information beyond what is offered in [76]. The power consumption of 30 W should be verified through testing, and the instrument should be accurately measured and weighed. Establishing a partnership with Safron Reosc. might result in significant reductions in cost, with 174 instruments to be purchased. With respect to Super-Resolution image processing, two approaches are discussed. Identifying the most suitable method would require an extensive trade-off, keeping in mind the following considerations:

1. Example-based would require the launch of an additional satellite for sharper ground data for training purposes. As post-processing would occur on ground, this would have no direct repercussions on Sat-ELITE's design.
2. Multiple image relies on motion-estimator vector algorithms, which have not been investigated yet. Additionally, the power required for post processing would certainly increase (SkySat uses 120 W per orbit), meaning the design would have to be revamped, possibly with larger solar powers. Highly-capable processing modules would have to be implemented within the Data Handling module, incurring higher costs on the design.

¹⁴<https://kelvins.esa.int/proba-v-super-resolution/problem/> [Date accessed: 20-05-2019]

¹⁵<https://www.satimagingcorp.com/satellite-sensors/skysat-1/> [Date accessed: 18-6-2019]

6. Attitude Determination & Control design

Once the mission profile, target altitude and payload have been selected, work on designing ADCS can begin. The main goal of this subsystem is to ensure control of the spacecraft thus enabling the operational modes described in Table 9.1. Additionally, as explained in Subsection 5.3.4 special attention must be paid not to smear the images during payload operation time by achieving stability.

In this chapter, first ADCS requirements are quantified and analysed in Section 6.1. Next the hardware setup is derived in Section 6.2 and associated risk are identified and mitigation strategies are proposed in Section 6.3. Then external disturbance parameters are quantified in Section 6.4 and Section 6.5 to enable sizing of the ADCS setup in Section 6.6. Finally, his verification and validation is performed in Section 6.7 and final recommendations are then given in Section 6.8.

6.1 Requirements

The requirements related to ADCS are given in Appendix A under SYS-SC-ADCS subcategory. A more thorough analysis of the driving requirements is presented below.

6.1.1 Definition of attitude

Before starting the analysis of the requirements, definition of attitude must be provided. The nominal (i.e. nadir pointing) mode of the satellite corresponds to the "Velocity coordinate frame" shown in Figure 3.5. Since this is the primary operation mode, the attitude is then defined as angular orientation with respect to the "Body reference frame" shown in Figure 3.5.

To be able to track ground station, a rotating coordinate frame is necessary, such that satellite can "lock" itself onto the target. Therefore Ground Station Pointing (GSP) coordinate frame is defined with the origin in the centre of mass of the satellite.

To express direction of the ground station as seen from the satellite, Earth Centered Inertial (ECI) frame must be defined [27], which is done by rotating the "Earth coordinate system" from Figure 3.5 around the z-axis such that the x-axis points towards the Vernal Equinox. Then orientation of the GSP coordinate frame can then expressed with respect to the ECI frame by using yx rotation sequence as shown in Figure 6.1 introduced by Tudreijneveld in [27].

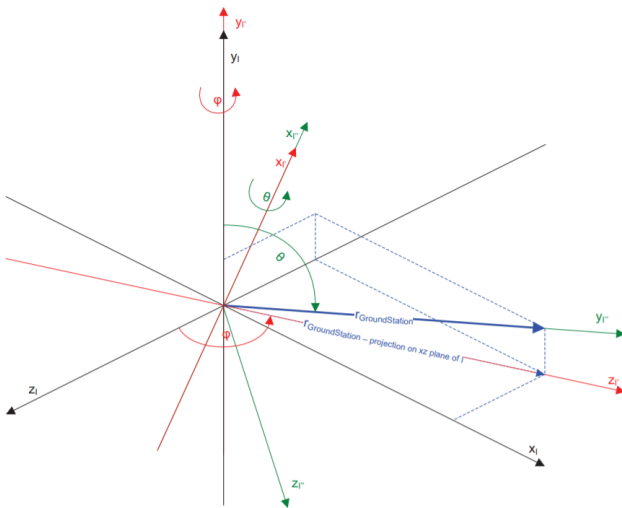


Figure 6.1: Rotations from GSP to ECI coordinate frame

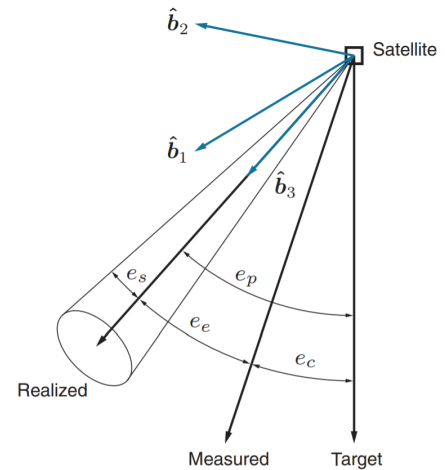


Figure 6.2: Definition of pointing accuracy

In the figure, first, the z-axis of the ECI frame (denoted by the subscript I) is aligned with the projection of the ground station vector in xz plane, thus arriving at I' frame. Then rotating around the x-axis of the I' , $y_{I'}$ is aligned with the ground station vector arriving at I'' or GSP coordinate frame.

$$\mathbf{r}_{G/Sat_I} = \mathbf{r}_{G/I} - \mathbf{r}_{sat/I} \quad (6.1)$$

The direction of the ground station as seen from the Sat-ELITE can then be expressed using Equation 6.1 from [27], where \mathbf{r} denotes the position vector and the ground station and satellite positions have been expressed with respect to the ECI coordinate frame.

6.1.2 Pointing accuracy requirement

Due to its non-singular nature, a more in-depth definition of what constitutes pointing accuracy is needed [26]. A high level approach is shown in Figure 6.2 adapted from a reference mission [26].

In the figure, the e_e is the knowledge error defined as the angle between the measured and realised attitudes and stems from sensor inaccuracies [81], while e_c is the control error defined as the angle between the measured and target attitude. Together they constitute the total pointing accuracy, e_p , corresponding to **SYS-SC-ADCS-2** and **SYS-ADCS-SC-3**. Additionally, jitter (e_s) is present and describes the high frequency attitude motion of the spacecraft¹. The latter is especially important in achieving sharp images and concerns stability as introduced in Subsection 6.1.3.

6.1.3 Stability requirement

The stability requirement flows from the necessity to avoid image smearing, which is governed by the displacement of a single pixel during integration time t_i [75] and is denoted by the unit-less criterion of image sharpness, k_{pixel} , as described in Subsection 5.3.4 of Chapter 5. The associated disturbance is called jitter and is characterised by the angular rate, ω_{max} , which can be calculated using Equation 6.2.

$$\omega_{max} = \frac{k_{pixel} \cdot x_{IFOV}}{h \cdot t_i} \quad (6.2)$$

Using the altitude (h) values provided in Section 4.4 and the field of view, x_{IFOV} , given in Table 5.1 yields ω_{max} in the range of 0.228 deg/s to 0.220 deg/s, corresponding to an altitude of 332 km and 342 km, respectively. The lower bound of this range thus forms **SYS-SC-ADCS-1** requirement.

Root Mean Square (RMS) jitter modelling methods are presented in [82], indicating the stochastic nature of the error. As explained later, this approach will not be adopted. Instead an alternative method will be used and a framework for more accurate, future analysis will be set up.

6.1.4 Slewing requirement

A crucial function of the ADCS is to be able to reorient the spacecraft, subject to slew rate and angular acceleration requirements, which predominately flow from communication needs. Additionally, the spacecraft must always be facing earth for nominal operations and therefore must have a constant rotational speed. Nevertheless, the driving value will come from the former requirement. Using the communication window specifications given in Section 7.2 the peak slew required can be calculated using Equation 6.3.

$$\omega = \frac{v}{r} \quad (6.3)$$

where r is the distance till the pointing object when the satellite is in zenith from the ground station and v is the orbital speed of 7.7 km/s as given in Chapter 4. Using an average altitude of 335 km, the resulting slew rate is calculated to be 1.32 deg/s. It flows that a sufficient angular acceleration shall be provided to reach the slew rate. Altering the equation and expressing r as a function of attitude angle, which can then be expressed as a function time, the required angular acceleration can be calculated to be 0.08 deg/s², defined in **SYS-SC-ADCS-15**.

6.1.5 Detumbling requirement

As described in Subsection 3.2.2 the Sat-ELITE shall have a detumbling mode, subject to **SYS-SC-ADCS-12** and **SYS-SC-ADCS-13** requirements, as set by Subsection 8.2.1 and [27], respectively. NASA's state of the art report indicates the need for a secondary ADCS designed specifically for detumbling, which will also be the approach adopted by the team [41].

¹<http://citeseerx.ist.psu.edu/viewdoc/download?doi=10.1.1.208.3894&rep=rep1&type=pdf> [Date accessed: 17-05-2019]

6.1.6 Desaturation requirement

As will be explained later in the chapter, reaction wheels will constitute the primary system of the ADCS. While providing excellent precision, reaction wheels are subject to momentum build-up and require desaturation [30], thus sparking the need for a desaturation mode subject to **SYS-SC-ADCS-14**.

6.2 Hardware setup

The main driver behind the choices was the current state of the art of precision CubeSat ADCS as provided by NASA in [41]. Additionally, comparison with reference missions was performed, for example, a program developed by NASA named Optical Communications and Sensor Demonstration, which achieved 3-sigma pointing accuracy of 0.024 deg [83].

Distinction between actuators and sensors is made, and the corresponding lists of the employed hardware are presented below. Short reasoning is present for each of the components.

6.2.1 Actuators

Actuators are devices that provide the required torques necessary for attitude control. The chosen actuators are listed below with brief justification of choice.

Reaction wheels: The wheels provide torques by employing Newton's third law and spinning the satellite in the opposite direction of the wheels' spin. They can provide torques over small increments and allow for cheap redundancy implementation (i.e a four wheel setup). Reaction wheels are cheaper than the possible alternative of using Control Moment Gyro (CMG), which are yet to be optimised for miniature applications. Thus, the choice of reaction wheels for the role of the primary actuators is made. A three wheel setup is enough to provide 3-axis control [28]. One limitation is that momentum wheels suffer from momentum buildup [30], which leads to higher power consumption for nominal operations² and needs to be addressed.

Magnetorquers: As explained in Subsection 3.2.2 the Sat-ELITE will need to be detumbled. If reaction wheels were to be used for this purpose it could lead to a potential oversizing of the wheels in order to avoid saturation during the detumbling phase. Furthermore, as already mentioned, the wheels must be desaturated. Altogether, the necessity for a secondary actuator system is made evident and after consulting NASA state of the art report [41] magnetorquers are chosen. As, magnetorquers generate torque by interacting with nearby magnetic field, this choice is further supported by the prominent magnetic field at the operational altitude range of the Sat-ELITE. Three magnetorquers are typically used although in theory two magnetorquers provide the spacecraft with actuation in all three axes.

6.2.2 Sensors

Sensors are tasked with estimating the attitude. Choice of the sensors was once again mainly based on the current precision ADCS state of the art [41], nevertheless certain decisions also flowed from the actuator selection.

Star tracker: The only sensors currently capable of providing knowledge error that allows to meet the required pointing accuracy are star trackers [41]. This stems from the fact that pointing accuracy is built up from several errors, as explained in Subsection 6.1.2 and thus individual error components must be minimised to ensure error propagation is within the required bounds. Star trackers store the entire night-sky and then use pattern recognition to compare the image with the catalogue to determine the attitude of the spacecraft. If more than one star is tracked the sensor determines attitude in all 3 axes [84], thus one star tracker is enough. However, due to the integration time of the sensor, it cannot provide measurements during tumbling as the image gets smeared, therefore other sensors are required [28].

Inertial Measurement Unit (IMU): Gyros provide angular rates necessary to monitor and achieve the required stability. Furthermore, angular rate information can be used for the detumbling. Additionally, Micro-electromechanical Systems (MEMS) gyros will be used to increase attitude update frequency, thus boosting the pointing knowledge between star tracker measurements. Since attitude estimation is performed by integrating the provided angular rate, drift and bias instabilities are a potential drawback, which can be tackled by calibrating the gyros using star-trackers. IMU consists of a 3-axis gyroscope and a 3-axis accelerometer, is considered

²https://cubespace.co.za/ClientDownloads/CubeWheel_Specsheet_V1.3.pdf [Date accessed: 24/06/2019]

due to its widespread use and availability in the market. One such system is enough to provide angular rates and accelerations in 3-axes,

Magnetometers: In order for magnetorquers to be able to achieve the command torque, knowledge of the external magnetic field is necessary. Recent developments outlined in [85] have shown that at significant expense of accuracy magnetorquers themselves can be used to determine the magnetic field. However, this reduced inaccuracy is likely to interfere with desaturation and detumbling requirements, and given the relatively low price the choice is made to include a 3-axis magnetometer. Additionally, using magnetometers provides sufficient magnetic field refresh rate to allow for the usage of the robust B-dot control algorithm for detumbling [86].

Kalman filter: Attitude determination with measurements obtained through noisy sensors is not trivial. Whenever more than a single sensor is used their measurements are not going to conform with each other. In order to be able to control the satellite with high precision, real-time determination is required incorporating the data from the sensors. For this application a Kalman filter is excellent as it uses sensor data with its noise and a prediction of satellite's state to arrive at an estimate of the current state of the satellite. As the problem is non-linear it is necessary to use an Extended Kalman filter that linearises the predictions and estimates around the mean or other variations of the filter that can deal with non-linear systems. These types of filters are the most widely used in navigation and Global Positioning System (GPS) [87].

6.3 Risk assessment

ADCS is crucial for the mission as the payload is rendered effectively useless in case of a complete failure of the ADCS. In the initial designs, redundancy was not taken into account to the extent that is required. One of the reasons for that was that the initially planned mission lifetime was 1.5 years, with it currently being expanded to at least five years. Consequentially, the probability that any part will fail has increased considerably. To assess the risks and consider the mitigation practices it is necessary to go through the different failure modes the system might experience.

Failure of a reaction wheel is catastrophic for the mission, especially as for short-lived missions three reaction wheels are often used. If this is the case, 3-axis precision control is no longer available. In one of the axes, actuation would have to be performed by the magnetorquers, which are less accurate resulting in the satellite pointing requirement not being fulfilled anymore. [TR-ADCS-1]

Star tracker is the most expensive component of the ADCS, therefore, it is often times not viable for a mission to employ more than one. However, in the case of a star tracker failure the satellite would be required to rely on magnetometer readings for attitude determination, which cannot achieve pointing knowledge higher than 1 deg [88]. This would limit the functionality of the camera and also result in the pointing requirement not being fulfilled. [TR-ADCS-2]

Failure of the magnetometer might have a critical negative impact to the ability to detumble and desaturate. Without the ability to desaturate its reaction wheels, the satellite would lose the ability to control its attitude within just a couple of orbits. [TR-ADCS-3]

Gyroscopes are crucial for accurate stability estimates and subsequent stability enforcement. Their failure would force the ADCS to rely on sequential measurements of star trackers in order to estimate the angular rate, which is unlikely to yield the necessary refresh rate. [TR-ADCS-4].

With a clever orientation of magnetorquers it is possible to still have 3-axis control with just two magnetorquers. This is due to the fact that any magnetorquer is able to produce torque in a plane orthogonal to its dipole vector. Accordingly, it is chosen to not introduce additional redundancy on this component. [TR-ADCS-5]

6.3.1 Risk mitigation

Risk mitigation for ADCS is done through the introduction of redundancy within the design. Due to the critical role of ADCS, no single point of failure shall be present in the design, which must also be taken into account when quantifying the ADCS setup. The following section provides analysis on the extent of redundancy necessary for each component.

Primary system

The redundancy of the primary actuator is crucial and ensured by opting for a four wheel setup, as only three wheels would be necessary to achieve 3-axis control [28]. The pyramid configuration will be chosen, due

to the high efficiency of the layout [89].

Ideally a second star tracker must be employed, but being the most expensive component of ADCS it greatly increases the cost and the volume of the ADCS unit. Nevertheless, equipping the entire constellation with a secondary star tracker, and thus eliminating Single Point of Failure (SPF), becomes cheaper than applying a redundancy on the entire constellation itself (i.e. launching extra satellites) as explained in Section 4.5, therefore two star trackers will be chosen.

Finally, the relatively small price tag of gyros and their crucial role makes employing a second IMU an easy choice.

Secondary system

Magnetometers are crucial in enabling the magnetorquers and their failure could therefore render detumbling and desaturation impossible, which would in turn lead to the failure of the mission. Thus, two 3-axis magnetometers shall be used.

As already explained magnetorquers enable detumbling and desaturation. In theory, 3-axis magnetorquer control can be achieved over the entire orbit, however only two axes can be actuated at any given moment as torques are only generated perpendicular to the direction of the magnetic field [85]. Three perpendicularly placed magnetorquers provide the ability to generate a magnetic dipole in any direction, which simplifies desaturation and detumbling, however, it is possible to perform these actions also with only two operational magnetorquers. Therefore, no additional redundancy is added.

6.4 Environmental disturbances

In order to size and ultimately validate, e.g. through simulations, ADCS, the external disturbances and the associated torques must be identified and quantified. When operating in their respective modes, the actuators must be able to deliver torques higher than those introduced by the environment, otherwise control cannot be achieved. Additionally, the resulting momentum buildup must also be quantified in order to proceed with reaction wheel sizing [28], which will further influence the parameters of the secondary ADCS system. This section introduces the relevant disturbances and proposes torque and momentum buildup estimation techniques. As wheel desaturation is planned to be performed every orbit, the contributions to angular momentum budget are considered only through the daytime. Consequently, during night-time mainly the secondary actuation system will be used for satellite control.

6.4.1 Aerodynamic torque

Using methods outlined in Subsection 4.2.4, aerodynamic torques can be determined assuming that the Sat-ELITE will operate in minimum drag configuration throughout all modes but communication. Sat-ELITE is designed such that the minimum drag configuration is achieved during nominal mode. Using Figure 9.5 and Figure 9.4 for the nominal mode, the total torque over the z- and y-axis can be estimated to be $2.4 \cdot 10^{-7}$ Nm. Similarly, the torques present during communication take the worst case peak of $9.6 \cdot 10^{-7}$ Nm.

To estimate momentum buildup, the average torque to be integrated over the mode must be quantified. For nominal modes, this value is still $2.4 \cdot 10^{-7}$ Nm as no intended changes in pitch or yaw angles are required. In communication mode, however, a slew manoeuvre over certain pitch angle range given in Section 7.2 is required. The average can once again be determined from Figure 9.5. Coincidentally, this also results in a total average torque of $2.4 \cdot 10^{-7}$ Nm during communication window.

6.4.2 Gravitational torque

Non uniform gravity field results in gravity gradient torque acting on the spacecraft [27]. Third body influences can be neglected for LEO satellites [90]. The worst case magnitude is then given by Equation 6.4 found in [28].

$$\tau = \frac{3 \cdot \mu}{2 \cdot (R + h)} \cdot |I_2 - I_1| \quad (6.4)$$

The worst case is driven by the maximum possible difference ($|I_2 - I_1|$) of the entries of the diagonal mass moment of inertia matrix of the spacecraft. Using $\mathbf{I}_{pa} = \begin{bmatrix} 0.227 & 0 & 0 \\ 0 & 0.370 & 0 \\ 0 & 0 & 0.405 \end{bmatrix}$ calculated in Subsection 8.2.7,

the worst case for the Sat-ELITE becomes $|I_{xx} - I_{zz}|$ or 0.178 kg m^2 . Using Earth's standard gravitational parameter $\mu = 3.986 \cdot 10^{14} \text{ m}^3 \text{ s}^{-2}$ and radius of Earth, $R = 6378 \text{ km}$ ³, the worst case gravitational torque can be calculated to be $3.53 \cdot 10^{-7} \text{ Nm}$ for the lower bound of the altitude, namely $h = 332 \text{ km}$. Torque due to gravity gradient can be modelled as constant throughout the orbit [28].

6.4.3 Magnetic torque

Due to electronics present on board, the spacecraft will possess a residual dipole moment that will interact with the magnetic field of the Earth, causing disturbance torques [75]. The associated magnetic torque can then be calculated using basic electromagnetic relation shown in Equation 6.5 :

$$\tau = D \times B \quad (6.5)$$

Earth's magnetic field can be estimated using available numerical models, such as SPENVIS proposed by ESA⁴. The model presents that the highest magnetic field magnitude equals $B = 5.6192 \cdot 10^{-5} \text{ T}$ for the year 2020.

In order to quantify the residual dipole moment, D , online testing would be necessary [91], which would have to take place after the satellite has been assembled. This is considered unfeasible for the current phase, so instead an estimate for the residual spacecraft dipole is obtained by scaling the dipole of Delfi-n3Xt, which is estimated to be 0.005 Am^2 per axis [27]. It will be assumed that the residual moment scales linearly with the number of units in use, as seen in reference missions [75]. Since Delfi-n3Xt is a three-unit CubeSat, it is thus estimated that the designed spacecraft will have a dipole moment four times higher, namely $D = [0.02 \ 0.02 \ 0.02]^T$. This yields a worst case torque of $1.12 \cdot 10^{-6} \text{ Nm}$ for the lower bound of the altitude given in Section 4.4.

The torque will exhibit opposite direction during daytime and during the eclipse, due to the flipping direction of the magnetic field over the poles.

6.4.4 Solar torque

Due to the solar pressure centre not coinciding with the centre of mass of the satellite, solar radiation pressure disturbance torque will be present. The worst case takes place when the effective area is the largest and the light is reflected in a specular fashion [30] and can be calculated using Equation 6.6 [28].

$$\tau = (1 + \beta) \frac{I_s \cdot A}{c} \cdot (r_{cp} - r_{CoM}) \quad (6.6)$$

where A is the effective area of the solar panels, I_s is the solar flux, β is the reflectivity coefficient and c is the speed of light. The difference, $r_{cp} - r_{CoM}$, denotes the distance between the centre of mass and centre of solar pressure and acts as the moment arm. The worst case solar pressure torque is calculated using the simulation created for the EPS explained in Section 7.3. The simulation has incorporated different reflectivities for different sections of the surface area. These were calculated by subtracting the corresponding absorptivities found in Table 8.11 from one. A range of $0.1 \leq \beta \leq 0.75$ was therefore used. The maximum solar torque is calculated to be equal to $2.19 \cdot 10^{-7} \text{ Nm}$.

The angle of incidence varies from 0 to π over the daytime part of the orbit. Expressing this change as a function of time allows for the torque to be integrated to arrive at the associated momentum buildup.

6.5 Momentum buildup

As explained before, in order to perform the sizing of the system, momentum buildup must be estimated. The change in angular momentum is defined in Equation 6.7, where h and τ represent angular momentum and torque respectively, as given by Chobotov in [30].

$$\frac{dH}{dt} = \tau \quad (6.7) \quad H = \Sigma \int_t \tau dt \quad (6.8)$$

By re-arranging and integrating both sides with respect to time, the total angular momentum can be expressed in Equation 6.8 as the sum of individual integrals of disturbance torque.

³http://maia.usno.navy.mil/NSFA/NSFA_cbe.html#GME2009 [Date accessed: 20-06-2019]

⁴<https://www.spENVIS.oma.be/models.php> [Date accessed: 20-05-2019]

Thus, the torques described in [Section 6.4](#) are integrated according to their nature of application and summed together to arrive at the total buildup of angular momentum. The integration time is chosen to be within the day time of the orbit, as it is crucial that the primary actuator system that enables payload operations does not become saturated during nominal operation modes. In particular, due to the torque being dependent on the attitude of the satellite the aerodynamic torque is evaluated over the communication window of 7.9 min (as provided in [Section 7.2](#)) and the remainder 37.1 min of the daytime (using the corresponding average torques described in [Subsection 6.4.1](#), similarly as the solar pressure, whilst gravitational and magnetic torques are evaluated over the entire daytime, that is, 45 min. Additionally, the thruster induced torques described in [Subsection 4.3.5](#) are considered, as the Sat-ELITE is expected to thrust for 5.63 minutes at most during daytime as explained in [Section 9.1](#).

Integrating the associated disturbance torques over the corresponding time windows, results in a total momentum buildup of $8.4 \cdot 10^{-3}$ Nms.

6.6 Sizing

This section outlines the numerical data and reasoning behind the sizing of the ADCS setup. The exact components are not introduced during the text, but are instead provided in [Table 6.1](#) at the end of the section.

Once the total momentum buildup is estimated, the reaction wheels can be sized. To eliminate uncertainties the system is sized according to the worst case principle, where one reaction wheel is assumed to accumulate the entire momentum buildup. This results in a total angular momentum buildup of $8.4 \cdot 10^{-3}$ Nms. Additionally, a single wheel must be able provide torque higher than the sum of previously found peak worst case torques, namely $7.72 \cdot 10^{-6}$ Nm. Due to variations in atmosphere density the torque and angular momentum buildup values can increase up to three fold [\[28\]](#), therefore, it was chosen to go for wheels with a maximum torque of 2.3 mNm and maximum angular momentum buildup of 30.61 mNms⁵.

Next, magnetorquers must be sized. Since, the detumbling requirement is not driving due to the high available time, it is decided to size the magnetorquers based on the available desaturation window and then check the ability to detumble.

To maximise the imaging time, desaturation would ideally take place over the night time. The disturbance torques of the day are also present during the night time, thus, if only the momentum built up during the day was dumped, the Sat-ELITE would not exit the night time in the nominal configuration. The total momentum to be dumped is therefore two times the day time build up.

According to [Section 9.1](#) the available time over night time is 27 minutes. Combining [Equation 6.5](#), [Equation 6.7](#) and the lowest average magnetic field of $3.5 \cdot 10^{-56}$ results in a required magnetic dipole of 0.3 Am^2 , assuming one active rod. This, however, would leave no margin of error and thus a bigger dipole is required and a magnetorquer sporting a 1.2 Am^2 dipole is selected based on the market availability. This setup can be estimated to desaturate the system in 6.75 min. A safety margin of two is applied to arrive at the total desaturation time of 13.5 min to be included in operation budgets in [Section 9.1](#).

Using maximum estimated tumbling rates given in **SYS-SC-ADCS-11** to arrive the total angular momentum at the start of tumbling, the setup can be calculated to detumble within 41.5 minutes, assuming perfect control and no additional momentum buildup. This estimate is well within the 1 day requirement of **SYS-SC-ADCS-13**, however it must be verified due to the before-mentioned simplifications.

At last, the ADCS setup is checked to reach the slew rate and angular acceleration requirements. The angular acceleration requirement of 0.08 deg/s^2 is well surpassed with the Sat-ELITE, which is able to achieve an acceleration in excess of 0.32 deg/s^2 .

With all of the requirements discussed and verified, the final setup with the models and relevant parameters is shown in [Table 6.1](#).

6.7 Verification and Validation

This section introduces and executes methods concerning verification and validation of the ADCS requirements.

⁵https://cubespace.co.za/ClientDownloads/CubeWheel_Specsheet_V1.3.pdf [Date accessed 24-06-2019]

⁶<https://www.spennis.oma.be/models.php> [Date accessed: 20-05-2019]

Table 6.1: The finalised setup for the Sat-ELITE attitude determination and control system

Component	Model	Parameters	Number
Magnetorquer	NCTR-M012	Dipole 1.2 Am ²	3
Reaction Wheels	CubeWheel Large	Torque 2.3 mNm Buildup 30.6 mNms	4
Star trackers	KU Leuven	acc. cross-boresight 6 arcsec acc. around boresight 30 arcsec	2
IMU	ADIS16485	Range ± 450 deg Sample rate 9.84 kHz	2
Magnetometers	NSS	Resolution <8 nT	2

6.7.1 Verification

Requirements that can already be considered verified at this stage are **SYS-SC-ADCS-4** and **SYS-SC-ADCS-5** by virtue of the secondary sensor and actuator system, as well as **SYS-SC-ADCS-9** and **SYS-SC-ADCS-10** by means of redundancy explained in [Subsection 6.3.1](#). Additionally, the requirement governing desaturation - **SYS-SC-ADCS-8** - can be considered verified based on the conservative calculations provided in [Section 6.6](#).

For the remainder of the requirements, it was decided to set up numerical simulations, with the help of Dr. Q.P. Chu from Control & Simulation Department of Delft University of Technology. The simulations would additionally serve as means of selecting the control algorithms. Additionally, the compiled simulation was also verified in a later meeting with Dr. Q. P. Chu.

As the starting point, Euler's rotation equation shown in [Equation 6.9](#) was considered.

$$\mathbf{I}\dot{\boldsymbol{\omega}} + \boldsymbol{\omega} \times (\mathbf{I}\boldsymbol{\omega}) = \boldsymbol{\tau} \quad (6.9)$$

where $\boldsymbol{\tau}$ is the total torque vector, \mathbf{I} is the inertia matrix, and $\boldsymbol{\omega}$ and $\dot{\boldsymbol{\omega}}$ refer to angular velocity and angular velocity rate vectors, respectively. The torque can further be expanded into total control and disturbance torques, denoted by $\boldsymbol{\tau}_c$ and $\boldsymbol{\tau}_d$, respectively. Rearranging yields [Equation 6.10](#).

$$\mathbf{I}\dot{\boldsymbol{\omega}} = \boldsymbol{\tau}_c + \boldsymbol{\tau}_d - \boldsymbol{\omega} \times (\mathbf{I}\boldsymbol{\omega}) \quad (6.10)$$

Corresponding change in the attitude is then expressed in [Equation 6.11](#) by employing kinematic differential equations adapted for a spacecraft in a circular orbit in nadir pointing mode as provided by Dr. Q. P. Chu in the Spacecraft Attitude Dynamics and Control course.

$$\begin{bmatrix} \dot{\theta}_1 \\ \dot{\theta}_2 \\ \dot{\theta}_3 \end{bmatrix} = \frac{1}{\cos \theta_2} \begin{bmatrix} \cos \theta_2 & \sin \theta_1 \sin \theta_2 & \cos \theta_1 \sin \theta_2 \\ 0 & \cos \theta_1 \cos \theta_2 & -\sin \theta_1 \cos \theta_2 \\ 0 & \sin \theta_1 & \cos \theta_1 \end{bmatrix} \boldsymbol{\omega} + \frac{n}{\cos \theta_2} \begin{bmatrix} \sin \theta_3 \\ \cos \theta_2 \cos \theta_3 \\ \sin \theta_2 \sin \theta_3 \end{bmatrix} \quad (6.11)$$

where $\theta_{1,2,3}$ represent the attitude, $[\dot{\theta}_1 \dot{\theta}_2 \dot{\theta}_3]^T$ is the change in attitude vector, while n represents the orbital angular rate in deg/s. The term containing the variable n ensures that the satellite will rotate together with the orbit.

A forward Euler method was then applied within the Matlab® environment to propagate the change in attitude and the angular velocity. A single point in orbit was chosen

The simulation includes an implementation of the World Magnetic Model field that is rotated to the body axis to calculate the torques acting on the satellite. This allowed for a realistic implementation of magnetorquer actuation, which was done by projecting the desired torque vector on the plane perpendicular to the magnetic field vector resulting in the closest possible applied torque.

As for the disturbance torques, the current simulations include magnetic disturbance torque due to the residual dipole of the satellite as well as the maximum aerodynamic and solar torques. Thrust torque is omitted as it is not planned to image when thrusters are firing. Due to the simulations being used to verify the control setup and not the saturation of the reaction wheels, the varying nature of the torques was implemented by adding the worst case torques multiplied with a sine function with a frequency of 5 oscillations per orbit, as per suggestion of Dr. Q. P. Chu.

Additionally, to imitate realistic control behaviour, controller refresh rate was set to match the refresh rate of the attitude sensor in use.

Detumbling

Detumbling is the task of the secondary ADCS system. Considering the employed hardware, the designers are presented with two options, detumbling using only the magnetic field readings or making use of the IMU to obtain angular rate feedback. Two control algorithms were therefore considered, namely Bdot and bang bang proportional omega controller, and a comparison was performed. The corresponding control laws can be seen in Equation 6.12 and Equation 6.13, where k_p is the proportional gain, \dot{B} is the derivative of the magnetic field and D is the required control dipole, which can be converted to the control torque using an equivalent of Equation 6.5. The results can be seen in Figure 6.3 presenting the associated reduction in angular rate.

$$D = -k_p \dot{B} \quad (6.12) \quad \tau_c = -k_p \omega \quad (6.13)$$

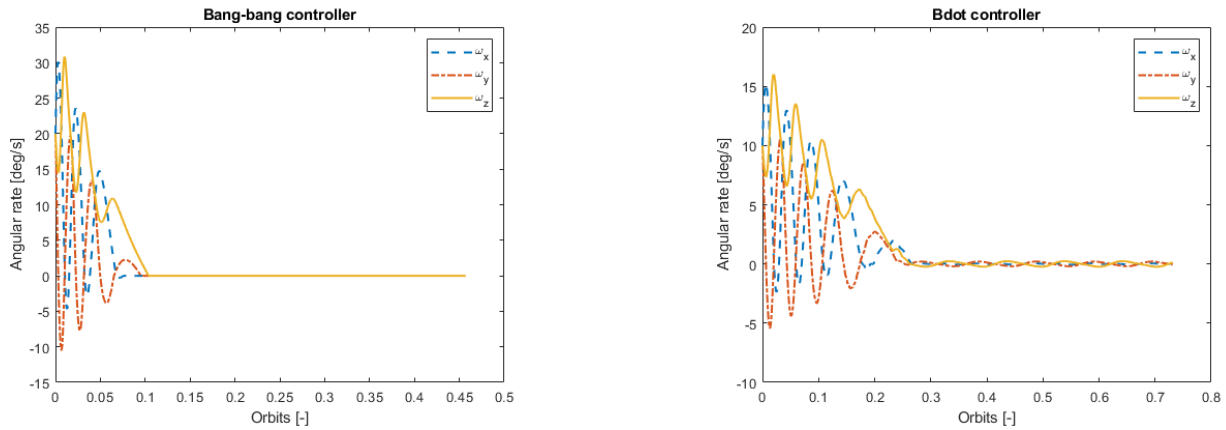


Figure 6.3: Comparison of control laws

It can clearly be seen that, irrespective of the controller, the design is capable of reducing its angular rates to the desired threshold of < 1 deg/s well within the required 1 day. Requirements **SYS-SC-ADCS-12** and **SYS-SC-ADCS-13** can therefore be considered verified.

It is also evident from Figure 6.3 that the so called bang-bang controller detumbles considerably faster. However, as mentioned previously this method relies on data provided by IMU on board, which was selected to be a MEMS gyro that is susceptible to drift. While the associated inaccuracy can be considered negligible given the small detumbling time and gyro can be calibrated using launcher data just before satellite deployment, this would not be the case during detumbling operations performed after exit from the safe mode. This has to do with the fact that safe mode can in theory last indefinitely and thus it is highly probable that the gyro will have drifted a significant amount. Furthermore, as all the non-critical devices are switched off, it is likely that calibrating the gyro would not be possible. The decision was therefore made to employ the Bdot algorithm.

Pointing

Pointing the satellite is necessary to be able to utilise the payload and obtain sharp pictures of the desired locations. This is the most critical mission aspect as without it the satellite is rendered practically useless. Both Proportional Integral Derivative (PID) and Proportional Derivative (PD) controllers were considered but it was determined that PD control is enough to attain the required accuracy through simulations. Both of these are closed loop feedback mechanisms that constantly calculate the error between a setpoint and a measured process variable. The associated control law is shown in Equation 6.14, where additional derivative gain k_d has been introduced when compared with a P controller. A huge advantage of the PD control algorithm is that it is inherently stable, whereas the PID control gains have to be tuned carefully to ensure that the satellite does not lose control. At the same time PD controllers are susceptible to steady state error. A common method to deal with this is to use variable gain depending on the pointing error. Even a simple system of just two gain levels - coarse pointing and fine pointing gain - is enough to bring down the steady state error to a value lower than 0.25 deg as can be seen in Figure 6.4. The tuning of the gains was done numerically, taking into account the maximum torque of the reaction wheels and the pointing accuracy margins.

$$\tau_c = -k_p\theta - k_d\omega \quad (6.14)$$

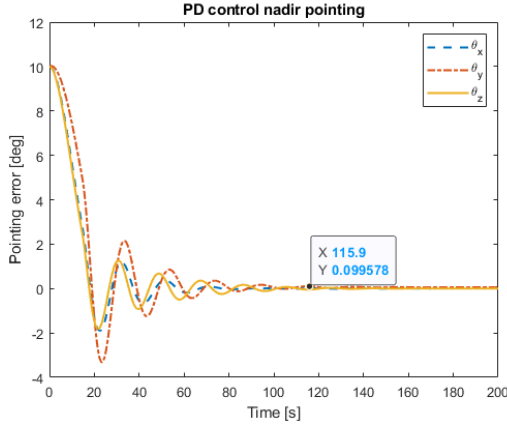


Figure 6.4: Pointing performance from non zero initial pointing error

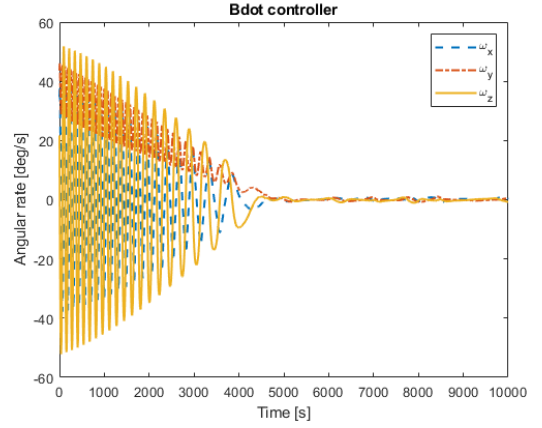


Figure 6.5: Detumbling simulation. Parameters from the paper by Dr. Mirko Leomanni [92]

Figure 6.4 clearly shows that the driving accuracy requirement **SYS-SC-ADCS-3** has been met and can be verified. $k_p = 0.0023$ and $k_d = 0.02$ in coarse pointing mode. In fine pointing mode k_p is 10 times larger, while k_d stays the same. Furthermore, the total pointing accuracy is also estimated using the star tracker accuracy. It is estimated to be approximately 10 times the 3- σ accuracy of the star tracker around boresight resulting in a pointing accuracy of 0.08 deg.

To observe the stability of the control system, it was chosen to take the sum of worst case torques and multiply it with a sine function that completes four full periods during one orbit as per suggestion by Dr. Q. P. Chu. The simplification had to be performed due to the fact that the model did not include any orbit propagation. It was observed that the control algorithm is not influenced by gradual changes in torques and exhibits the same stability as when constant torques are used. Nevertheless, the proposed model is deemed unable to verify stability requirements, due to a number of limitations, most importantly, the decision to model the satellite as a rigid body. Verification of the stability requirement is instead addressed in Section 6.8.

Model validation

To validate the simulations, it was chosen to replicate the results of a paper published by Dr. Mirko Leomanni [92], thus validating the underlying control and dynamic implementations. The simulation was set up with the same parameters that were used in the study and then the detumbling settling time compared for the Bdot control algorithm. The implementations do slightly differ, namely, in the paper discussed a control sampling rate of 10 Hz and orbit propagation was used. Nevertheless, the results suggest that the model is indeed valid. As seen in Figure 6.5, the initially high angular velocities of the satellite get reduced to under 1 deg/s within 4500 s. This is in close agreement with the findings of the discussed paper.

6.7.2 Validation

To validate that the design can fulfil its designed function it is necessary to create a prototype and launch it using a piggyback launch option. Unfortunately, it is not possible to validate the system by any other means as the environment experienced by the satellite is hard to reproduce on the Earth.

6.8 Future framework

The team recognises the limitations of the simulation presented above, namely the simplified dynamic and disturbance torque implementations. Therefore, a framework is established for future simulations, that could be used to achieve verification of pointing and stability requirements with a higher degree of confidence.

6.8.1 Nominal, detumbling & desaturation operations

The recently developed Aerospace Blockset CubeSat Simulation Library developed by MathWorks® for Simulink®, is recommended for further verification of pointing and detumbling requirements. Whilst being in its early stages, it provides the ability to set up 6 degrees of freedom dynamics of CubeSat systems and can be used to develop a simulation that incorporates orbit propagation. This would allow for significantly more accurate magnetic and gravitational torque simulations, which would now be based on the factual position within the orbit. This implementation could be further supplemented by aerodynamic torque calculation methods presented in [Subsection 4.2.4](#). A tool was successfully developed by the team to port the Python implementation of aerodynamic calculations to Matlab® environment and is ready for future applications. Unfortunately, the tested runtimes were too high to simulate an entire orbit, therefore optimisation of the code and parallelization or cluster employment is recommended. With the addition of sensor noise, the team is confident that such a simulation would be capable of verifying the Sat-ELITE's pointing, detumbling and desaturation requirements to a high degree of confidence.

6.8.2 Attitude stability

As indicated by ESA's Pointing Engineering Handbook [81], jitter estimates require probabilistic approach. The handbook recommends the use of ESA's Pointing Error Engineering Tool (PEET), a Matlab® based software designed for implementing the pointing error methodology used by ESA.

The team was able to acquire PEET software and was granted a user licence. However, deeper analysis of the tool showed that a more complete and thorough knowledge of the satellite's system than currently available is required, especially concerning non-rigid dynamics. The tool's manual states that no universal guidelines are available and expertise in the field is necessary [93]. The decision was made not to invest time into implementing the methodology, but rather to establish a framework for future developments.

After consulting the pointing error handbook [81], the pointing error sources likely to be present in the system were identified and are presented in [Table 6.2](#) alongside their respective classification within the PEET framework.

Table 6.2: Pointing error sources

Error source	Type	Signal class
Environmental Disturbance Torque Noise	Time-random	random
Actuator noise	Time-random	random
Reaction Wheel Imbalances	Time-random	periodic
Attitude Sensor Noise	Time-random	varying bias + random
Inertial Sensor Noise	Time-random	random
Guidance Sensor Noise (e.g GPS)	Time-random	random
System dynamics induced errors (e.g. sloshing, flexible modes)	Time-random	transient
Structure Thermal/Mechanical (due to orbiting)	Time-random	periodic
Misalignment (payload - sensor)	Time-constant	bias
Calibration uncertainty (e.g IMU calibration)	Time-constant	bias

The future designer is then encouraged to develop and implement the corresponding higher level inter-error relations as per the methods suggested in the PEET manual [93], to arrive at a final stability estimation and verify the relevant requirements. The tool is considered especially capable of stability verification due to its ability to simulate non-rigid connections within the satellite.

7. Data Handling, Telecommunication and Electronics

Sat-ELITE now has two specified orbits with propulsion, payload, and has an ADCS sized to ensure nominal payload operation. This chapter will first follow the flow of data from payload. Command and data handling in [Section 7.1](#) is essentially a brain of the whole satellite and the first step in processing image data. Command and data handling decides when to communicate, while the communication itself is done by Telecommunication system designed in [Section 7.2](#). To finish electricity consuming systems, EPS will be designed in [Section 7.3](#) to meet the most demanding cases for electricity consumption. In the end, general failure modes for electrical subsystems will be discussed in [Section 7.4](#).

7.1 Command and data handling

The function of a command and data handling subsystem is to perform on-board operations and internal communication, analogously to a brain and nervous system in a human body. Several actions fall under its expertise:

- Receiving, decoding, validating and distributing ground station commands to other subsystems. These originate from ground station operators or from internal modules housing the software needed for autonomous operation.
- Provide data storage until connection with a ground station is available
- Prepare payload and housekeeping data for downlink, in the form of processing and encoding
- Monitoring and responding to a wide range of on-board problems that might occur
- Keeping track of time-required for synchronisation and the time stamping of information [94]

7.1.1 Telemetry points, on-board hardware and software

C&DH complexity scales proportionally to the telemetry points to be administered, and the payload data processing rates. Subsystems chiefs must thus determine the amount of data to be transmitted on ground for housekeeping. Certain parameters must be monitored frequently, such as attitude measurements processed several times per second. Others, like the operational temperatures, can be more sporadic. This data can be either digital, bi-level or analogue. If this is the case, a conversion process must take place in the equipment interface modules as illustrated in [Figure 7.1](#).

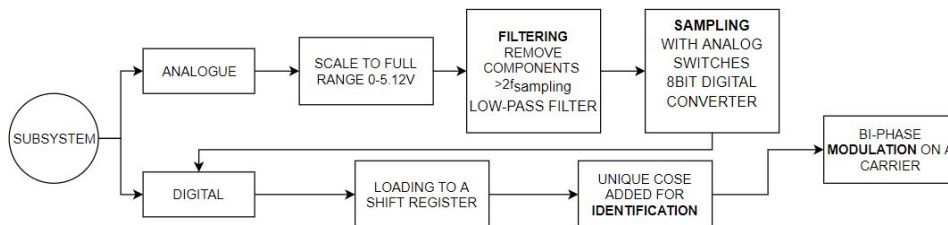


Figure 7.1: Analog, Digital/Bi-level data flow

The moment the satellite launches, there is no way to manually retrieve relevant data from its subsystems. This will be all performed by on-board software, managing the data stemming from telemetry points of each subsystem. The software packages to be implemented have been compiled in [Table 7.1](#), next to the necessary Software Lines Of Code (SLOC) estimated for a generic spacecraft from [25]. These do not define the exact software size, but merely serve as an indication of software cost and amount of testing required for code validation.

Table 7.1: On board software

Software	Justification	SLOC
ATTITUDE DETERMINATION AND CONTROL		
Kinematic integrator	Estimates current attitude by integrating sensed body rates	2000
Precession control	Determines torque needed to achieve desired attitude	3500
Kalman filter	Enhances attitude determination precision of sensors	6000
ATTITUDE ACTUATOR PROCESSING		
Momentum management	Monitors reaction wheels for saturation then unloads it using magnetorquers	3000
COMMUNICATION		
Telemetry processing	Packs information in a telemetry stream	1000
Compression algorithms	Reduces raw data size (especially from the payload)	3500
PAYLOAD		
Payload management	Monitoring payload status, assuring support from other subsystems (pointing), collecting data, pre-compression	2000
UTILITIES		
Run-time kernel	Support higher-order languages. Represent, order, store and pack data across mixed-language interfaces	
Matrix mathematics	-	2000
Time management and conversion	-	700
Coordinate transformation	-	2000
Built-in test	Testing and diagnostics for software	2400
POWER		
Power management	Controls battery (dis)charge and monitor power bus	1200
FAULT DETECTION		
Monitor	Identifies failures or adverse conditions in onboard equipment and downlink them for on-ground diagnosing	4000
Fault detection and correction	Processing for corrective actions	7500

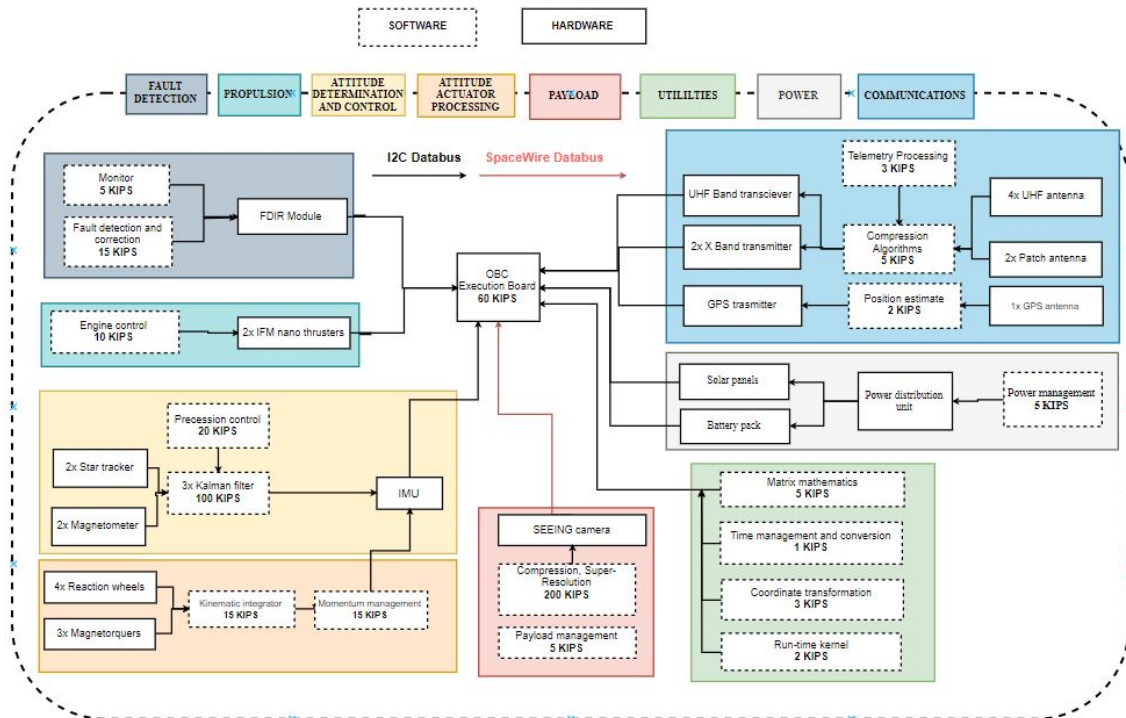


Figure 7.2: Hardware and software block diagram

In conjunction with the selected hardware components (see Table 9.3), the combined hardware and software

block diagram for Sat-ELITE is drawn in Figure 7.2. Handling speed is defined in terms of thousands instruction per second (KIPS), which have been estimated for on-board functions from [28] and [25] for a similar-sized satellite. Eight different colours are implemented to differentiate between subsystem modules, with hardware-software interactions outlined by means of arrows.

7.1.2 Sizing process

Command and data handling systems are generally conservative, evolutionary designs due to their mission-critical nature [28]. Incorporating a high degree of reliability is key to make sure the correct data is downlinked, and the right commands are distributed. For the case of a smaller spacecraft, these objectives are complicated by the use of highly integrated systems and the need for power and mass efficiency¹. The advent of the smartphone and its ever-increasing processing power has triggered the appearance of certain smartphone components on satellite busses. STRaND-1, developed at the Surrey Space Centre, will be the first to demonstrate the feasibility of using cheap smartphone electronics to control a spacecraft².

The heart of the system is the On-Board Computer (OBC), running the software responsible for managing all on-board operations. A key part of the OBC software is Failure Detection, Isolation and Recovery (FDIR). This functionality is implemented throughout several levels, with a top-level FDIR module acting as health monitor and recovery action controller to the system [95]. On lower levels, equipment handlers overlook proper data communication between OBC and S/C equipment, warning the FDIR module in case of anomalies (equipment failed to respond, equipment mode transition failed...). In the event of occurrence, the FDIR module might decide to:

- Switch off equipment. C&DH is closely tied with the EPS through a low-speed data link: by continuously monitoring the available power, the OBC can decide to turn off non-critical subsystem to prevent system shutdown [96]
- Trigger a reconfiguration to the redundancy of a failed equipment [95]
- Bring the spacecraft to another operational mode (Safe Mode)

A suitable candidate for this purpose is the OBC by ISIS Delft³, at a price of 4400 € see Table 7.2 and Figure 7.3. Equipped with a processor speed of 400 MHz, it can easily process the 471 KIPS estimated from Figure 7.2. The operating temperature must be kept within -25 to 65°C, possibly through mounting of thermistors onto the OBC boards [95]. This instrument has been tested for radiation hardening and has flight heritage since 2014: this contributes to the reliability of the design. To circumvent potential mission failure due to an OBC malfunction [TR-CDH-1], two of these are selected. This will also allow for increased computational speed by running in parallel. An internal watchdog unit is provided to determine eventual computer failures independent of the processor itself. In case the OBC does not refresh a countdown timer, the watchdog undertakes a predefined recovery action, including a hard reset which is maintained until cleared by a ground command.

Table 7.2: ISIS OBC specifications

Processor	400 MHz ARM
RAM	64 MB
Storage	2x Redundant 8 GB high reliability SD
Clock	2x Redundant RTC
Power	average 400 mW max 550 W at 3.3 V
Operating Temperature	-25 to 65°C
Size	96x90x12.4 mm
Mass	94 g



Figure 7.3: The actual OBC from ISIS

The main databus interface is I^2C , which focuses on low power consumption and simplicity: typical consump-

¹<https://sst-soa.arc.nasa.gov/08-command-and-data-handling> [Date accessed: 13-06-2019]

²<https://amsat-uk.org/satellites/tlm/strand-1/> [Date accessed: 21-06-2019]

³<https://www.isispace.nl/product/on-board-computer/> [Date accessed: 21-06-2019]

tion is 10mW, independent from the number of nodes [97]. I^2C is very reliable, and only needs two wires for the whole databus. This connection has been employed on-board the Delfi-C³ and Delfi-n3Xt. Most I^2C devices support speeds up to 400 kbps, which is not enough to handle the payload data. Hence, a separate SpaceWire connection is established between the payload and the OBC. SpaceWire⁴ is specifically designed for space applications by ESA to accommodate data rates up to 400 Mb/s and verifies the requirement **SYS-SC-CDH-2**. It is a full duplex bus, meaning that there are dedicated outgoing lines for data transmission, as well as incoming lines for reception, which can be operated simultaneously. Furthermore, it can automatically reroute the data in case of single link failures. SpaceWire cabling is provided by Axon, permitting high data transfer speeds and radiation resistant for up to 300 Mrad⁵. The selected "28AWG SpaceWire cable" has a diameter of 1 mm, comprises of silver plated copper and weighs 85 g/m⁶. The overall cabling harness mass will be estimated from Delfi-n3xt, which houses 120 g in total for a comparable 3U platform.

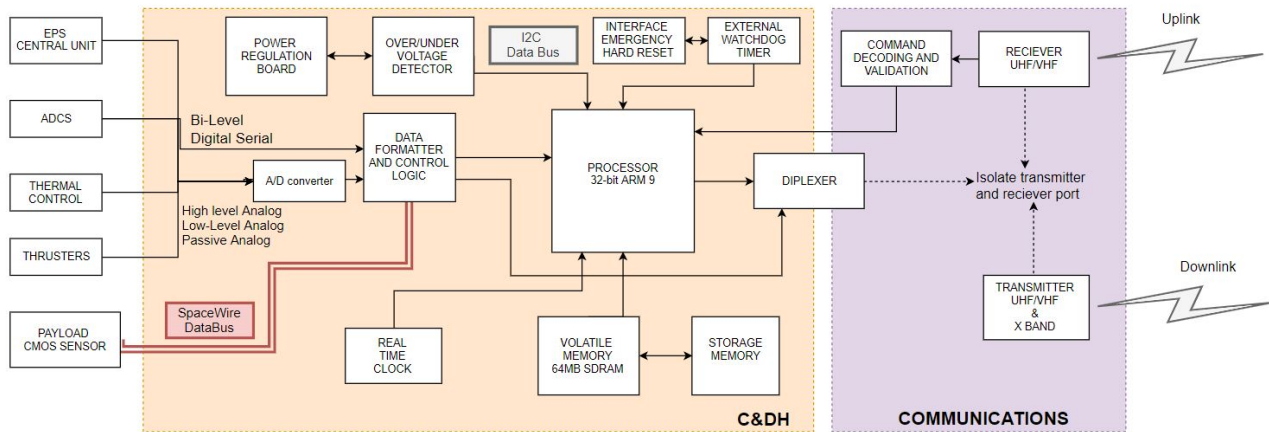


Figure 7.4: C&DH block diagram

Memory storage must be incorporated to accommodate internal data, mainly stemming from the payload. As found in [Subsection 7.2.7](#), this amounts to roughly 339 GB, a conservative estimate in case of unavailable ground stations. Flash memory is preferred over SSD in CubeSat applications, the reasons being twofold. Firstly, it offers extremely fast read and writing speeds, an advantage in such demanding situations. Most importantly, this non-volatile memory can cope with eventual power shortages without losing data. Flash devices trap electrons to store information; therefore, they are susceptible to data corruption from radiation[**TR-CDH-2**].⁷ Fortunately, space equipment manufacturers guarantee radiation tolerances on their equipment. DDC, an experienced supplier in the field, offers the "Rad Hard NAND Flash Memory 69F256G16" with a product sheet available on [8](#). This component is RAD-PAK certified, capable of withstanding doses of 100 krad. Specifications guarantee an endurance of 60 000 cycles, which marginally exceeds our requirement of 58 000 estimated in [Subsection 7.2.7](#). Two units are selected, capable of 256 and 128 GB at 75 € and 63 € respectively; these occupy $2.54 \times 0.65 \times 3.96 \text{ cm}^3$ of space, weighing only 19 g.

7.2 Telecommunication

In the beginning of this section the main functions and requirements of this subsystem are laid out. Afterwards, a brief summary of the literature study phase is presented to familiarise the reader with available design options. Lastly, certain design option is chosen and is analysed in more detail.

⁴<http://spacewire.esa.int/content/Home/HomeIntro.php> [Date accessed: 13-6-19]

⁵http://www.axon-cable.com/en/03_assemblies/02_high-data-rate/03/index.aspx [Date accessed: 21-06-2019]

⁶Data sheet <http://www.axon-cable.com/publications/HIGH-SPEED-LINKS.pdf> [Date accessed: 21-06-2019]

⁷https://www.nasa.gov/pdf/716078main_Staehle_2011_PhI_CubeSat.pdf [Date accessed: 20-06-2019]

⁸<https://www.ddc-web.com/en/space-1> [Date accessed: 20-06-2019]

7.2.1 Design logic

Within the outline of the mission, telecommunications subsystem plays a supportive role. In other words, it does not directly contribute to meeting the mission objective. The main function of this subsystem is to provide a reliable communication link between the spacecraft and ground, such that all payload data can be retrieved, and the status of the spacecraft can be monitored.

Both the mission orbit and camera characteristics serve as inputs for the subsystem's design and are extensively used throughout this section. These elements have been discussed in [Chapter 4](#) and [Chapter 5](#) and it is assumed that the reader is familiar with them. The overall design flow is shown in [Figure 7.5](#). It shows sequentially the key design parameters, Input/Output (I/O), as well as iterations. Detailed description of I/O is also displayed in the N² chart in [Section 3.4](#). The requirements related to this subsystem are given in [Table A.1](#) in [Appendix A](#) under **SYS-SC-COM** and **SYS-GND** subcategories.

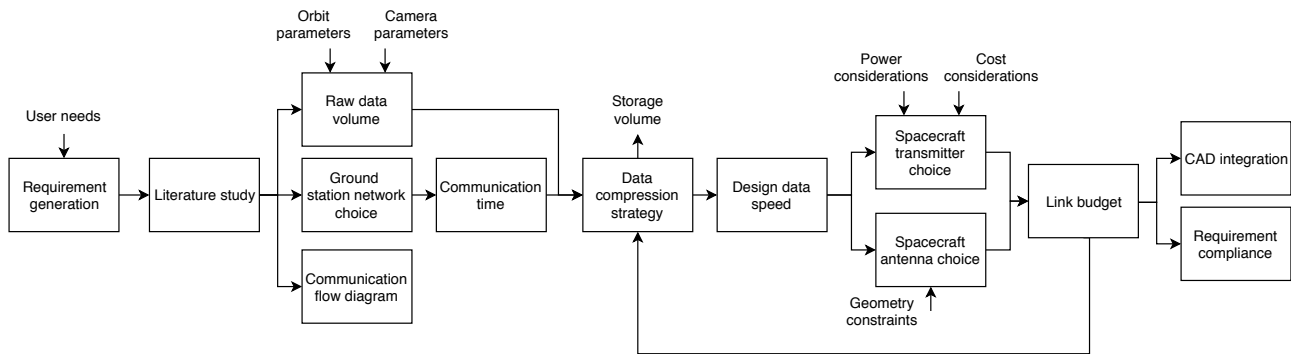


Figure 7.5: Telecommunication subsystem's design flow diagram

7.2.2 Design options

In the beginning of the project a literature study was performed to investigate state-of-the-art communication strategies for small satellites. This subsection presents its main findings and design conclusions.

Communication bands

According to the Nanosatellite database ⁹, the majority of nanosats employ communication across two distinct radio bands ranging from VHF to Ka band, as defined by Institute of Electrical and Electronics Engineers (IEEE). [Figure 7.6](#) shows which bands correspond to which frequencies and how IEEE band definition compares to other standards. Lower frequency bands such as VHF or UHF use little power but also provide typical data speeds up to 9600 bps¹⁰. Its main application is telemetry uplink and downlink. For this mission UHF downlink/VHF uplink was chosen to guarantee communication during tumbling and avoid a SPF as governed by requirement **SYS-SC-DES-2**. X-band was chosen for high data rate communication. Although Ku through Ka bands provide wider bandwidth for communication, these bands suffer more losses due to atmospheric attenuation and have less COTS components for small satellites.

⁹<https://airtable.com/shrafcwXODMMKeRgU/tbldJoOBP5w1N0JQY?blocks=hide> [Date accessed: 20-06-19]

¹⁰<https://www.isispace.nl/product/isis-uhf-downlink-vhf-uplink-full-duplex-transceiver/> [Date accessed: 20-06-19]

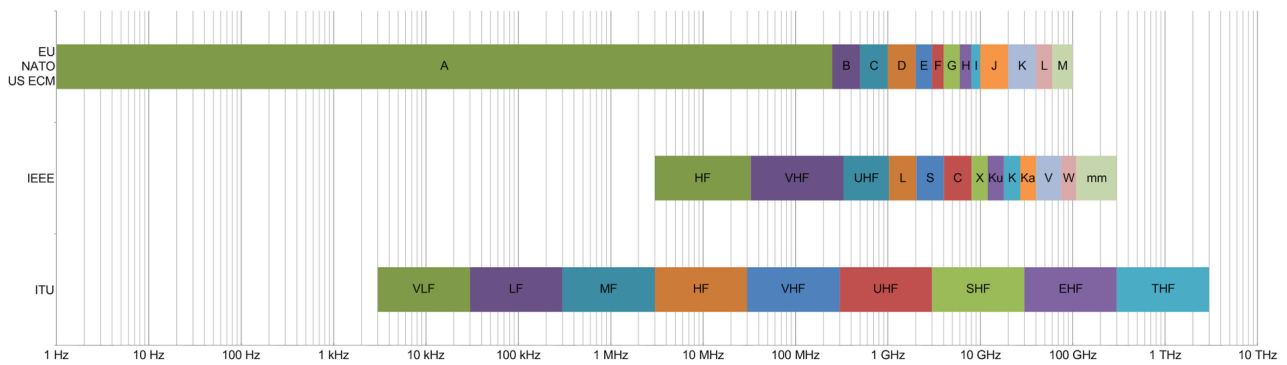


Figure 7.6: IEEE radio band spectrum ¹¹

Relay versus ground communication

Using a relay satellite has the potential to provide a permanent communication link, however further investigation into this did not yield any strong advantages compared to directly communicating with ground. For Geostationary Earth Orbit (GEO) relay satellites the space loss is extremely large compared to a direct link with ground while existing LEO networks such as Globalstar cannot provide communication speeds high enough.

Orbit position determination

Two options were considered to track the spacecraft's position in orbit. One is using the so called Two Line Element (TLE) radar data provided by North American Aerospace Defense Command (NORAD) while the other is using an on-board GPS receiver. The former is publicly available completely for free but is updated only daily. On the other hand, GPS is practically continuously updated and also provides accurate time estimates. Considering that it is unrealistic to develop a ground station network with the given development budget, accurate position estimates are key to optimise ground station operation expenses ¹², thus it was decided to include a GPS receiver. A suitable receiver was chosen from NanoAvionics, who provided the specifications sheet in an e-mail conversation. Summary of this component is given in Figure 9.6.

Future possibilities

With the increasing interest in smaller satellite platforms, both governmental space agencies and private companies are accelerating the development of miniaturised laser communication systems. In late 2017 NASA launched a 1.5U CubeSat technology demonstrator dubbed OCSD, which had a body-fixed laser and has achieved communication speeds up to 200 Mbps. It is also mentioned that with relatively simple upgrade the technology could achieve speeds up to 2.5 Gbps ¹³. Additionally, a German company TESAT, along with industry partner DLR, is developing a commercial laser communication platform for CubeSats, which could enable communication speeds up to 10 Gbps. In collaboration with Gomspace and Kongsberg Satellite Services (KSAT), a technology demonstrator mission PIXL (OSIRIS4CubeSat) is planned for launch in 2019 ¹⁴. These developments highlight that laser communication is a technology to be reckoned with in future small satellite missions. However, for this project it was deemed too risky due to lack of publicly available design parameters and lower TRL compared to the mature radio communication solutions.

7.2.3 Communication flow diagram

Once the general structure of the communication procedure is set, it can be summarised in a communication flow diagram. This tool was used to keep track of progress of the different design aspects of the telecommunications subsystem and also allowed to more easily communicate the team's design approach with internal experts. The final communication flow diagram is presented in Figure 7.7. Since it is the final iteration, the exact ground station network is already mentioned although officially it is discussed only later in Subsection 7.2.5.

¹²Spacecraft position contingency would require to book larger ground station time slots to guarantee communication.

¹³https://www.nasa.gov/directorates/spacetech/small_spacecraft/ocsd_project.html [Date accessed: 20-06-19]

¹⁴<https://www.tesat.de/en/media-center/press/813-nanosatellite-sees-the-light> [Date accessed: 20-06-19]

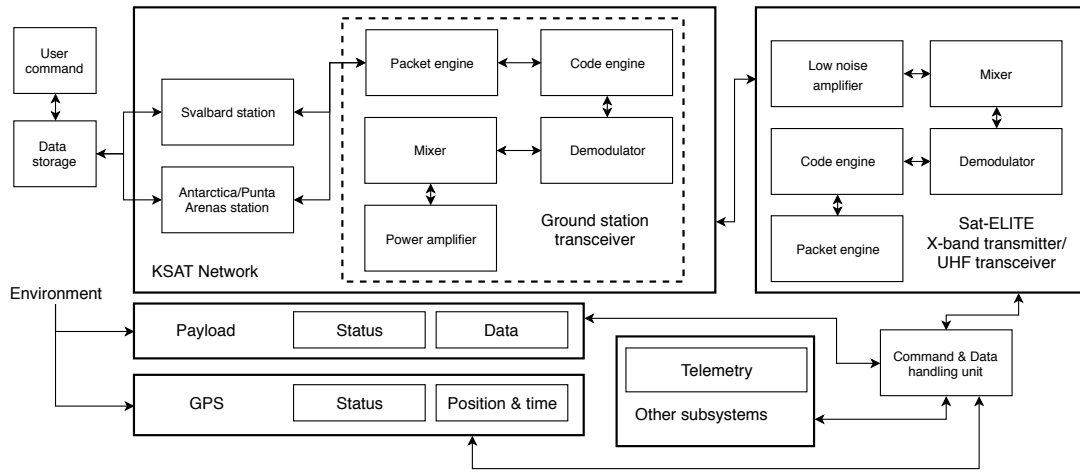


Figure 7.7: Communication flow diagram

7.2.4 Raw data volume

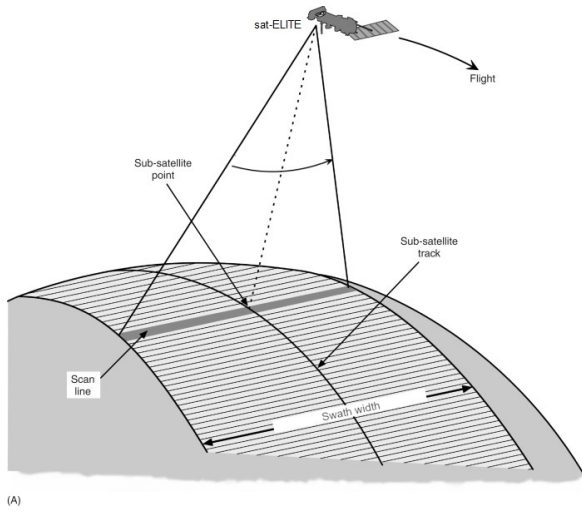


Figure 7.8: Visualisation of the sub-satellite ground track. Figure adapted from ¹⁵

Ideally, raw data volume should be estimated using the sensor resolution, exposure time, and bits per pixel. However, the exposure time is not known, so the volume was estimated by multiplying the number of pixels in one scan line with the number of scan lines that fit in the ground track of the satellite. Figure 7.8 helps visualise the approach. The Earth was assumed to be round and the ground track was simply taken as the circumference of the Earth using the volumetric mean radius of 6371 km. Based on relevant parameters summarised in Table 7.2 and using Equation 7.1, the raw data volume is calculated to be 6445.1 Gbit. Bear in mind that this is the maximum data volume estimate and does not consider the different operational modes or optimisation strategies, which is discussed later in Subsection 7.2.7.

$$DATA = PIX_{swath} \cdot PIX_{length} \cdot BPP = PIX_{swath} \cdot \frac{2\pi R_{Earth}}{GSD} \cdot N_{CH} \cdot BPC \quad (7.1)$$

7.2.5 Ground station network description

Because the satellite shall fly in a sun-synchronous orbit, ground stations at high latitudes are beneficial as the spacecraft will pass over these more often than over ground stations near the equator due to rotation of the Earth. Compared to other competitors like Planet, this project does not have the resources to invest in the development of our own ground station network, so existing solutions need to be considered. Many commercial networks exist on the market, such as the ones from Swedish Space Corporation (SSC), BridgeSAT, Amazon's AWS, SatNOGS, KSAT or StellarStation. Although it is possible to operate across multiple networks, logistically it is easier to choose one. Considering available stations, the potential market missed at station locations, and small satellite services, the soundest choice is the KSAT network. Of all the mentioned ones, KSAT has the most northern ground station, leading to increased communication time. Besides that, Svalbard is a small

¹⁵<https://www.sciencedirect.com/topics/earth-and-planetary-sciences/satellite-instrument> [Date accessed: 18-06-19]

island in the Arctic ocean so less land area is missed compared to, for example, SSC's stations in Alaska, USA. As illustrated in Figure 2.1, maritime applications make up only 4% of the EO market making land coverage a priority. On top of that, KSAT advertise small satellite tailored solutions and reduced prices compared to conventional satellite operation ¹⁶.

Unfortunately, any ground station specifications (including cost) are not available on KSAT's website and representatives of the company did not reply to our inquiries. However, the relevant parameters to complete the link budget (Subsection 7.2.9) were found in a report by SpaceX ¹⁷. Table 2 of this document displays parameters of various KSAT operated ground stations. Judging by latitude and longitude, SG25, SG42 are antennas in Svalbard and TR3, TR4 are antennas in Antarctica. It is not clear which antenna of the two would be used so values for the smallest one (SG42, TR4 lower gain antennas) shall be used in the link budget. Concerning the ground station requirements, **SYS-GND-3** to **SYS-GND-5** can be verified with information available at KSAT's website. **SYS-GND-1** and **SYS-GND-1** are not possible to verify at this point, as further discussion with the operator would be necessary.

7.2.6 Communication time

According to Figure 7.5, after choosing the ground station network, the next step is calculating the communication time. The approach was based on theory from Chapter 9 in "Mission Geometry: Orbit and Constellation Design and Management" by James R. Wertz [98]. It gives an easy-to-follow cookbook style approach to estimating ground pass time for a single orbit and also evaluates examples, which were used to verify our calculations. The approach itself is purely based on geometry and simple orbital mechanics so it is considered valid. Interested reader is advised to consult the mentioned book to review the formulas. The ground pass time was calculated for a full day, considering the shift in longitude of the ascending node over the orbital period as input for the next calculation. The per-orbit results are presented in Figure 7.9. The range of the values is 3.49-13.02 min with an average communication time of 7.9 min.

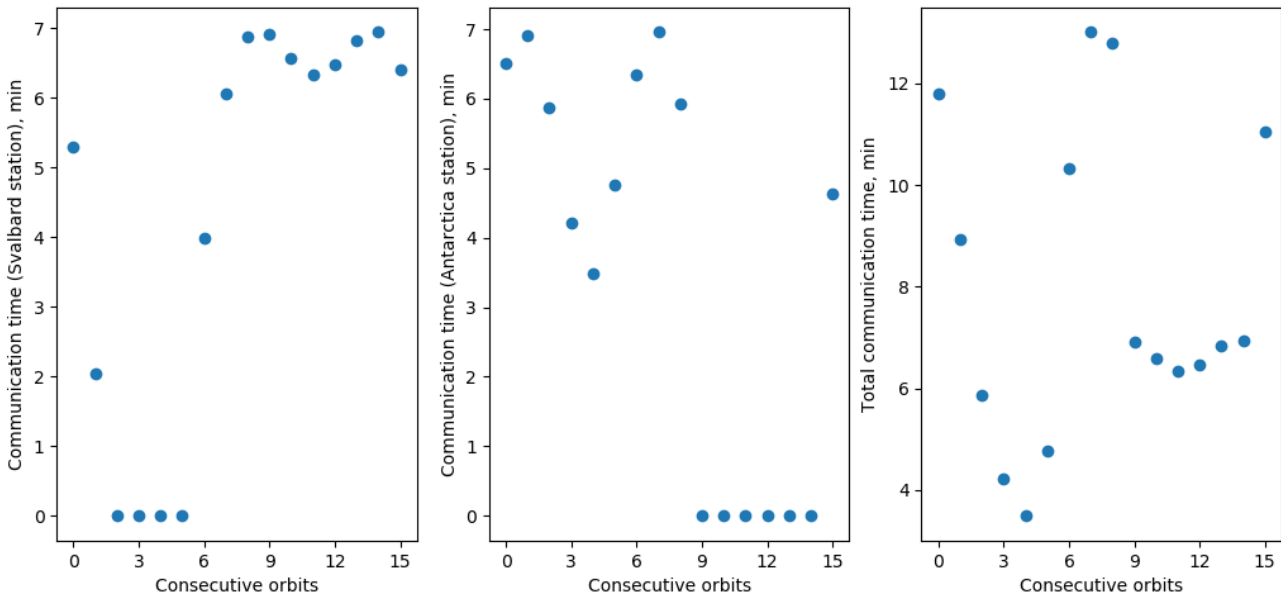


Figure 7.9: Communication time over a day with KSAT stations in Svalbard and Antarctica

7.2.7 Data compression strategy & data speed

From previous sections it was estimated that the upper data volume bound generated by the payload is 6445.1 Gbit and the communication time (t_C) is in the range 3.49-13.02 min with an average of 7.9 min. Considering that half of the pictures would be taken in eclipse (t_E) and that the satellite does not take pictures while it communicates, this number can be reduced. Furthermore, a great reference mission for more detailed on-board

¹⁶<https://www.kongsberg.com/ksat/services/ksatlite/> [Date accessed: 21-06-19]

¹⁷<https://apps.fcc.gov/els/GetAtt.html?id=197812&x=.> [Date accessed: 18-06-19]

data processing is the Hyperscout nanosatellite, which uses a 50 band hyperspectral camera¹⁸. After initial data cube stacking and geomapping, the on-board software is capable of reducing the size of an 8.4 GB image to roughly 19 MB using change detection, image segmentation, and spectral region splitting [99]. Data cube stacking is simply the process of taking the data streams from all individual bands and stacking them into images. Geomapping uses on-board raster maps to align and fit these images with existing ones. These two operations only prepare the data for optimisation. Geomapping is particularly useful for change detection, which looks at the previous image and identifies if any changes have occurred. If no changes are observed, the data is discarded. Otherwise the image is segmented to only transmit the pixels that have changed with respect to previous image. Lastly, spectral region splitting averages the data value across adjacent bands to effectively reduce the total number of bands. It is not specified in the paper how much data is lost through this process, but it is mentioned that many bands contain redundant information and the data loss is minimal. These methods have been validated using imagery from other satellites [99]. Since it is not clear how often changes would be observed, change detection and segmentation is avoided for this mission. Avoiding this also negates the need of geomapping, which actually increases the total data volume. Spectral region splitting however can be incorporated and judging by information in the paper, the procedure reduces data volume by a factor of four ($CR_{SRS} = 4$). Furthermore, within a single image, adjacent pixels can have identical values. Instead of sending all the values, the image can be compressed by, for example, specifying one value and number of pixels after it with the same value. Such compression can either be lossless or lossy. For this mission lossless format is preferred and a typical ratio is three ($CR_{LL} = 3$) [100]. Further improvement carried out by other missions is image classification [101]. Particularly interesting for this mission is classification of cloud or ocean covered images. Roughly 70% of Earth's surface is covered by ocean ($F_O = 0.7$)¹⁹. Moreover, at any moment only 45% of land ($F_{Lcloud} = 0.45$) and 28% of ocean surface ($F_{Ocloud} = 0.28$) is cloud free [102]. Lastly, since the maritime market share is so small, the design will be limited to transmitting only 10% of cloud-free ocean images ($F_{OOI} = 0.1$). This value and strategy in general were chosen after several design iterations considering available transmitters, antenna gains etc. All points covered in this subsection are summarised in Equation 7.2. It equates to 40.6 Gbits and requires 85.8 Mbit/s using the average communication time. The presented approach verifies **SYS-SC-CDH-1**.

$$DATA_{optimised} = DATA \cdot \frac{\left(1 - \frac{t_E + t_C}{T_o}\right) \cdot ([1 - F_O] \cdot F_{Lclouds} + F_O \cdot F_{OOI} \cdot F_{Oclouds})}{CR_{SRS} \cdot CR_{LL}} \quad (7.2)$$

Storage considerations

For a full orbit 6445.1 Gbit of raw data is generated, which means that the raw data speed equals 1.18 Gbit/s. Considering eclipse time (0.5P), average communication time (7.9 min) and average thrusting time ($0.5 \cdot 408s$), where data is not generated, actual raw data equates volume equates to $6445.1 \cdot (0.5P - 7.9 \cdot 60 - 0.5 \cdot 408)/P = 2422.84$ Gbit. According to **SYS-SC-CDH3** and **SYS-OBJ-PL-3**, data needs to be stored for 12 h, which is about 8 orbits. Given the high data generation speed, the data will likely be processed during the night. This means that the limiting storage case is 7 orbits of compressed data and one orbit of raw data. This leads to $(7 \cdot 40.6 + 2422.84)/8 = 338.38$ GB of storage to meet the requirement. Considering that data is written twice per orbit (raw and compressed) and that during 5 years time (1 leap year) there are about $(4 \cdot 365 + 364) \cdot 24 \cdot 60/P = 28842$ orbits, during the spacecraft's lifetime approximately 58 thousand (rounded up) write operations shall be performed.

7.2.8 Spacecraft transmitter & antenna considerations

To better understand how to choose a transmitter, it is important to understand the Shannon–Hartley equation given in Equation 7.3.

$$C = B \log_2(1 + SNR) \quad (7.3)$$

In the equation, C is the channel capacity in bits per second, B is the available bandwidth and SNR is the signal to noise ratio. For any application bandwidth is fixed and determined by regulatory entities. This means

¹⁸<https://hyperscout.nl/wp-content/uploads/2016/07/product-leaflets-2016-hyperscout-web.pdf> [Date accessed: 21-06-19]

¹⁹<https://hypertextbook.com/facts/1997/EricCheng.shtml> [Date accessed: 22-06-19]

that the only way to increase channel capacity is by increasing the SNR. Since the orbit altitude and ground station choice has been fixed, SNR can only be increased on the spacecraft's side. Moreover, it can be done by increasing the transmitter power or antenna gain (Equation 7.6). After considering X-band transmitters from several companies (Tethers Unlimited, IQ Spacecom, Makesat, IMT, Space Micro, Syrlinks, Clyde Space, and Endurosat), the only transmitter that is not too big and can provide data speeds higher than 85.8 Mbit/s is EWC27 from Syrlinks²⁰. This fixes the transmitter power and leaves only the antenna gain as a design variable, and this depends on the shape of the antenna. Many were considered for the project - horn, helical, patch antennas, deployable, gimbal steered, placed inside or outside the spacecraft. In the end, all but the patch antenna were discarded due to either drag penalty, lack of space or increased complexity. To be more precise, the 2x2 patch array antenna from Endurosat was chosen²¹.

For the secondary link, a communication bundle from Innovative Solutions in Space (ISIS) was chosen, as it offers a good price and the company is located in Delft²².

7.2.9 Link budget

Link budget is an essential tool for any telecommunication link which keeps track of all the gains and losses and is used to calculate the link's SNR. As dictated by **SYS-SC-COM4**, the communication link margin for this mission shall be larger than 3dB. The budget template is based on "Satellite Communication Systems" lecture by Stefano Speretta. Values used are presented in Table 7.3 and margin calculation is done using Equation 7.6. The terms are grouped in square brackets and are labelled with Tx, S (space), Rx, and O (other) to more easily identify the source of each term.

$$D = 0.5 \left(-2R_{Earth} \sin \epsilon + \sqrt{4R_{Earth}^2 \sin^2 \epsilon - 4(R_{Earth}^2 - (R_{Earth} + h)^2)} \right) \quad (7.4)$$

$$L_S = 20 \log_{10} \left(4\pi \frac{D}{0.3/f} \right) \quad (7.5)$$

$$M = [P_{RF} - L_{Tx} + G_{Tx}]_{Tx} - [A_{air} - L_S - L_a]_{space} - [L_p - L_{Rx} + G/T]_{Rx} - [10 \log_{10} B - L_i]_O \quad (7.6)$$

Table 7.3: Primary and secondary link margin

Parameters	Symbol [Unit]	Primary link	Secondary link
Constants			
Altitude	h [km]		332
Temperature	T [°C]		-50
Pressure	p [hPa]		1013
Water vapour	ρ [g/m ³]		7.5
Atmospheric variance	L_a [dB]		1
Transmitter loss	L_{Tx} [dB]		1.2
Polarisation loss	L_p [dB]		0
Receiver loss	L_{RX} [dB]		2
Variables			
Frequency	f [GHz]	8.2	0.435
Transmitter gain	G_{Tx} [dBi]	12	0
RF power	P_{RF} [dBW]	3	3
Figure of merit	G/T [dBK]	25	25
Bitrate	B [Bit/s]	$80 \cdot 10^{-6}$	9600
Air attenuation	A_{air} [dB]	1.1	0.24
Results			
SNR Margin	M [dB]	8.3	62

²⁰<https://www.syrlinks.com/en/space/nano-satellite/x-band-transmitter-ewc27> [Date accessed: 24-06-19]

²¹<https://www.endurosat.com/products/cubesat-x-band-2x2-patch-array/> [Date accessed: 24-06-19]

²²<https://www.isispace.nl/product/cubesat-communication-bundle/> [Date accessed: 24-06-19]

Space loss calculation is done using [Equation 7.5](#) and [Equation 7.4](#), where D is the spacecraft to ground distance and ϵ is the worst case spacecraft elevation above the horizon. As per requirement **SYS-SC-COM-5**, this value is set to 5 deg. The air attenuation is calculated by an extensive model provided by S. Speretta. It is a function of T , ρ , and p and are valid for frequencies up to 350 GHz. Worst case estimates (low temperature, low pressure, and high water vapour density) were used for these atmospheric parameters but since no precise sources were found, a loss parameter was added to account for variance in the atmospheric properties. Transmitter gain, RF power, and figure of merit were acquired from specification sheets of the chosen components discussed earlier. Bitrate was also calculated in a previous section. Implementation loss, receiver/transmitter loss, and polarisation loss are values recommended by S. Speretta. As shown in [Table 7.3](#), the **SYS-SC-COM4** requirement is met. Based on the discussion of this chapter, all other **SYS-SC** requirements are met as well.

7.2.10 Risks

Every subsystem design comes with risks and telecommunications is no exception. The ones identified are:

- **[TR-TC-1]** X-band transmitter failure. In such an event, payload data can no longer be downlinked, meaning it is a single point of failure. Redundant transmitter was added for mitigation.
- **[TR-TC-2]** UHF-band transmitter failure would greatly complicate communication while tumbling. The likelihood of these two events occurring together is small.
- **[TR-TC-3]** GPS failure would require using NORAD TLE's for orbit position estimates. This method is less accurate and would increase operational costs.
- **[TR-TC-4]** Delays related to compression software development can have a financial impact on the project.
- **[TR-OP-9]** Ground station failure is beyond the control of the team. The likelihood of such an event is low but in case it does happen, the operator is expected to provide alternative communication links within the network.

7.2.11 Recommendations

Lessons learned during the design of this subsystem could potentially help future DSE teams progress faster. The main recommendations are:

- During feasibility studies do not automatically assume radio communication as laser communication will be a realistic option for CubeSat platforms in the near future.
- Consult internal experts for parameter estimations as companies are reluctant to share information and experts generally have a good overview of the industry.
- Read NASA's yearly-published "State of the Art Small Spacecraft Technology" to familiarise with currently available technology and save time on research in the beginning of the project.

7.3 Electrical power

Power needed for each subsystem's operation is in form of electrical power. Electrical energy is necessary continuously from satellite's deployment, throughout the whole mission and until the satellite starts burning in the atmosphere during deorbiting manoeuvre. Since all subsystems have to be used continuously or regularly, reliability is crucial for any EPS. Requirements, risks, verification and validation methods will not have a separate subsection, but will be spread throughout the section, where they contextually fit.

7.3.1 Electrical power subsystem structure

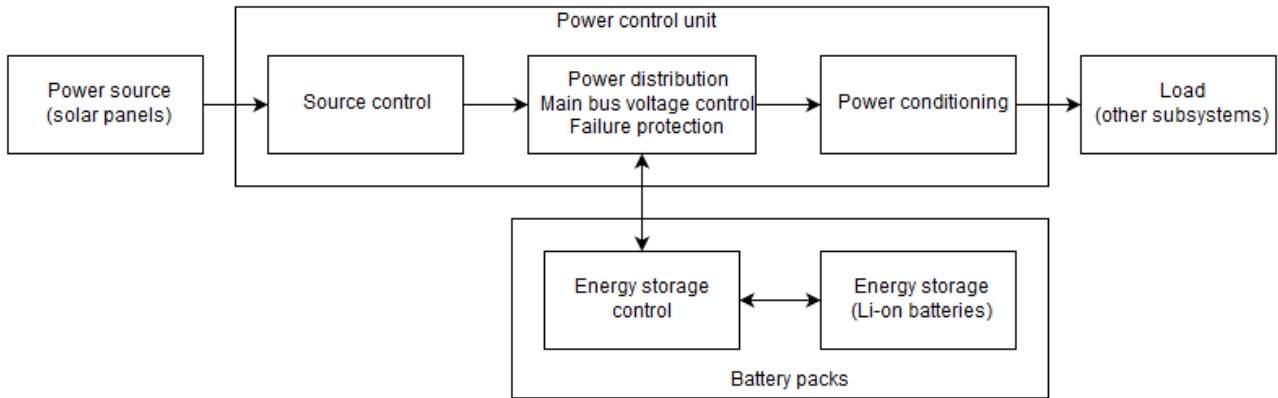


Figure 7.10: EPS structure overview

The high level EPS structure is presented in Figure 7.10. Power sources capture solar energy and transform it into an electron flow. To get the highest efficiency from solar panels, source control keeps voltage and current at optimal levels. Power distribution block serves as a fork which directs power either to subsystems or to energy storage. If the power goes to batteries for storage, it goes first through energy storage control which ensures that batteries are charging in correct conditions and not overcharging. If the power goes to subsystems, it goes through power conditioning which ensures that it has the specified voltage and current necessary for subsystems. This structure makes the EPS fully automatic, validating requirement **SYS-SC-POW-5**. Overall, this diagram helped identify risky points in EPS and components, for which efficiencies have to be quantified.

7.3.2 Power sinks and sources

Power sink is defined not as everything that consumes electrical power, but as something that consumes power for specific and required purpose. This distinguishes sinks, described in Section 9.1, from other lossy components such as cables or transformers.

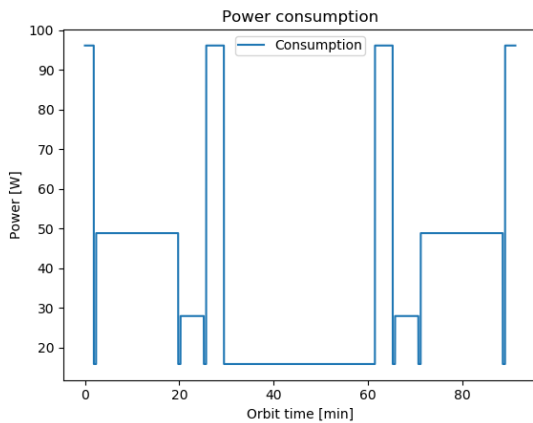


Figure 7.11: Power consumption over one orbit

The overall power consumption over an orbit is given by Figure 7.11. In the figure, and also for all subsequent figures in this section, orbital time starts when the satellite is in ascending node. Case presented for power consumption estimates is the most demanding average case multiplied with a safety margin of 1.1, so that requirement **SYS-SC-POW-3** can be validated. Risk mitigated by this is the risk of insufficient power production **TR-EPS-1** which can arise due to reasons such as unexpectedly quick component degradation. There are three (one is split in two halves) high peaks for thrusting, which are scaled for solar maximum when the drag is the highest. Power consumption of around 50 W is required for imaging, 28 W is for communication and the rest is for reaction wheel desaturation and mode switching.

Solar panels have been chosen as a power source due to a multitude of reasons. They can reliably provide long-term power, and as such, they are the go-to choice for almost all earth orbiting small satellites. Their technology is flight proven and widely available, subject to only a minor efficiency (η_{sc}) upgrade from time to time. Solar panels have just two main drawbacks as a standalone power source, namely the power is not generated in Earth's shade and it is inefficient to design them to cover peak power consumption. Both of the drawbacks can however be solved by combining solar panels with batteries for energy storage.

To produce electrical power (P_{gen}), solar cells have to be experiencing photon flux. In space, this is usually in the form of direct solar flux (I_s) or solar flux reflected from other celestial bodies (albedo). Total power generated is proportional to effective solar cell area, or total cell area (A_{sc}) and the incidence angle (θ_i) of the incoming solar flux. For purposes of this mission, albedo is disregarded in power production as there are no solar panels facing the Earth's surface.

$$P_{gen} = I_s \cdot A_{sc} \cdot \cos(\theta_i) \cdot \eta_{sc} \quad (7.7)$$

To get incidences over the orbit, the orbit positions have to be specified. For EPS design software, simplification of an actual orbit specified in [Subsection 4.5.2](#) is sufficient. Orbit is 3D but assumes smooth ball-like Earth and circular orbit. SSO simplifies calculations for sun incidence vector, as this vector is constant with respect to orbital plane. Coordinate systems from [Figure 3.5](#) are used throughout the simulation and when figures present faces of the satellite (+X -X +Y..) they mean +Xb -Xb +Yb... Sun vector transformation is further simplified by the fact that satellite has camera nadir pointing mode to take pictures and to minimise drag during the whole orbit (roll(r), pitch(p) and yaw(y) are 0). To get a good representation of illumination, one more thing needs to be added and that is Earth's shade. Satellite is in shade if it meets two conditions - centre of satellite is behind Earth's centre with respect to the Sun and component of Earth-satellite vector perpendicular to Sun-Earth vector is smaller than Earth's radius. As shade is extremely important to power generation, even smaller effects were considered. These are effects due to penumbra, Earth's flattening and Sun motion. Earth's flattening has the longest effect on shade - 22 s - but this has been neglected as it only takes away from shade in SSO [\[103\]](#). To validate this part of the simulation, simple orbits are presented in [Figure 7.12](#), where their correctness is evident. Angle b is the argument of ascending node with respect to sun and i is inclination.

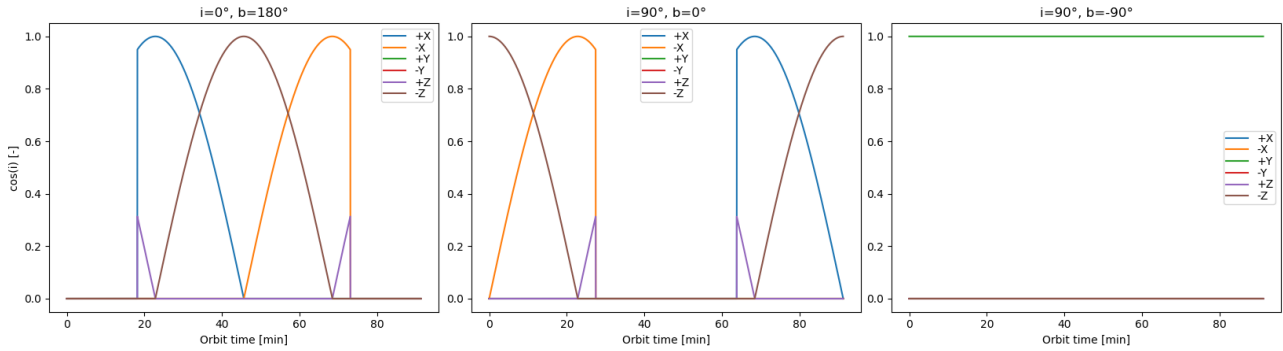


Figure 7.12: Simple test orbits

Another thing needed to scale power producing solar panels is their position on satellite. First requirement here is that they are not creating unnecessary drag. Their surface vector has to be perpendicular to satellite's velocity vector, which means that panels with effective area in +Xb and -Xb direction can be only covering satellite's body. Second requirement is imposed by structural loads. Solar panels should avoid complicated structural designs and so only body-mounted, single and double folding solar panels are taken into account. Third requirement comes from the stability requirement; solar panels should be positioned symmetrically to avoid continuous disturbance torques and moving the c.g. away from the geometrical centre. Lastly, to increase power generated per orbit, fraction of total incidence per body face has to be evaluated. Left graph in [Figure 7.13](#) presents these values for a morning orbital plane. +Y and -Z faces are the most effective and therefore solar panel will be placed such that they face these directions. These requirements helped narrow down solar panel positioning to what is presented in [Appendix E](#). Their angle is further determined with the help of a simulation, which varied the angle of solar panels with respect to Z axis. Most optimal angle is found to be 26.5 deg as is presented in second graph of [Figure 7.13](#).

To do the final solar panel area determination, two more things need to be included, and that is the EPS efficiency and the yearly solar cell degradation. It is however more convenient to introduce EPS efficiency in the following subsections regarding EPS distribution, conditioning and storage units. Therefore, only solar cell EOL efficiency (η_{scEOL}) is discussed here. It is equal to yearly efficiency degradation for Gallium-Arsenide (GaAs) solar cells ($\eta_d = 0.9725$ [\[25\]](#)) to the power of satellite lifetime duration in years ($l_y = 5y$). This satisfies the requirement **SYS-SC-POW-2**, which states that the EPS should be designed with degradation due to

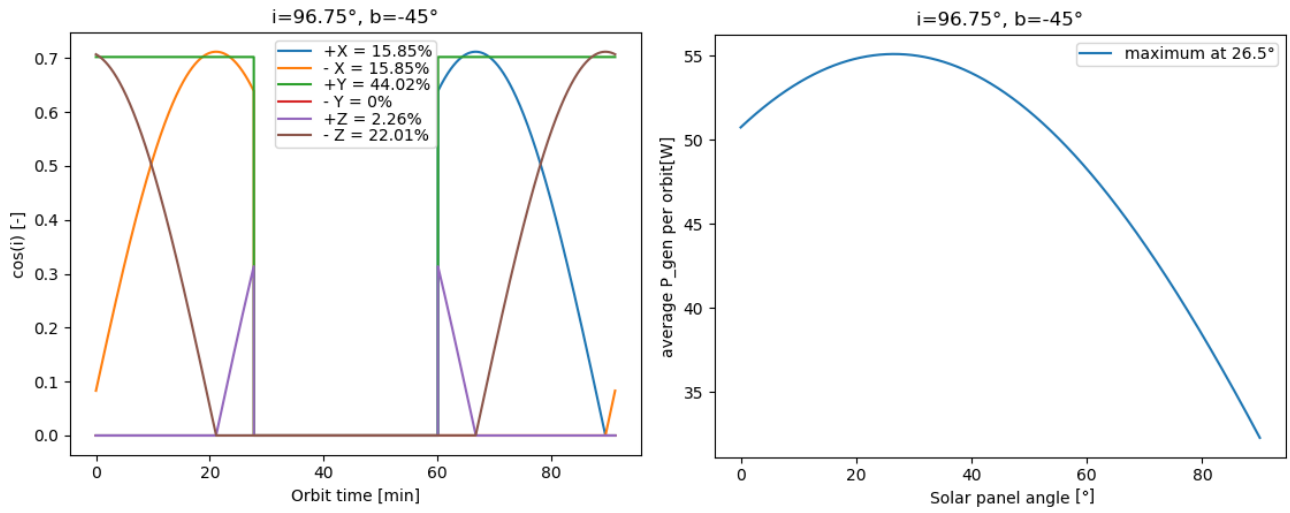


Figure 7.13: Graphs comparing efficiency of different body faces and inclination of solar panels

environmental conditions in mind.

$$\eta_{EOL} = \eta_d^{(l_y)} \quad (7.8)$$

Final values for satellite power production and consumption are presented in Figure 7.14. These are achieved by having 6 (21.3 cm x 36.6 cm) solar panels with 20 solar cells (4 cm x 8 cm) each. 2 panels are body mounted and the other 2 pairs are custom deployable panels on spring loaded hinges. All panels have glass composite backbone panel 1.6 mm thick and are estimated to cost 43200 € based on similar commercially available panels. With the EPS power sources designed to meet the worst conditions at EOL, requirements **SYS-SC-POW-1** and **SYS-SC-POW-3** are now validated.

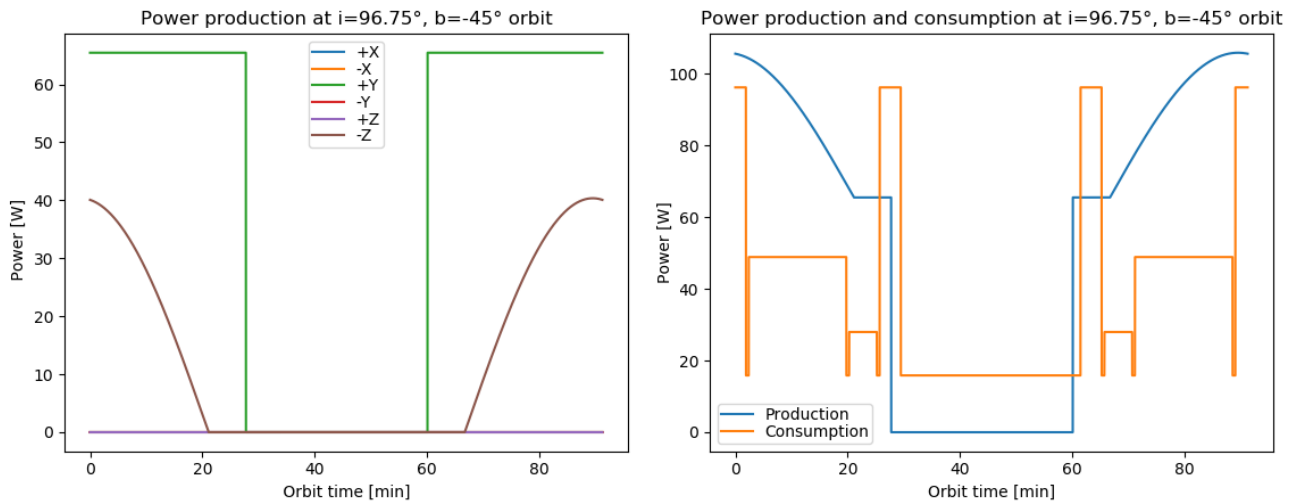


Figure 7.14: Graphs comparing efficiency of different body faces and inclination of solar panels

7.3.3 Power distribution and conditioning

Power control (distribution and conditioning) is a linking component between solar cells, battery packs and power sinks. It's structure is shown in Figure 7.15 where solid lines are electrical connections and dashed lines are for telemetry measurements. While single connecting line would be a SPF, in reality these are doubled and contain fuses to mitigate risk of electrically shorted circuit (**TR-EPS-2**). Electrical short can have devastating consequences as it can destroy sensitive electronics. This is omitted in the diagram, so that it is not overcrowded. Three maximum power point trackers (MPPTs) are acting in parallel to get the most out of the three solar panel orientations. MPPTs employ an algorithm which adjusts voltage and current such that power is the highest. Their efficiency is dependent on P_{gen} variability and can vary from 68% to 98% [104]. For our purposes an

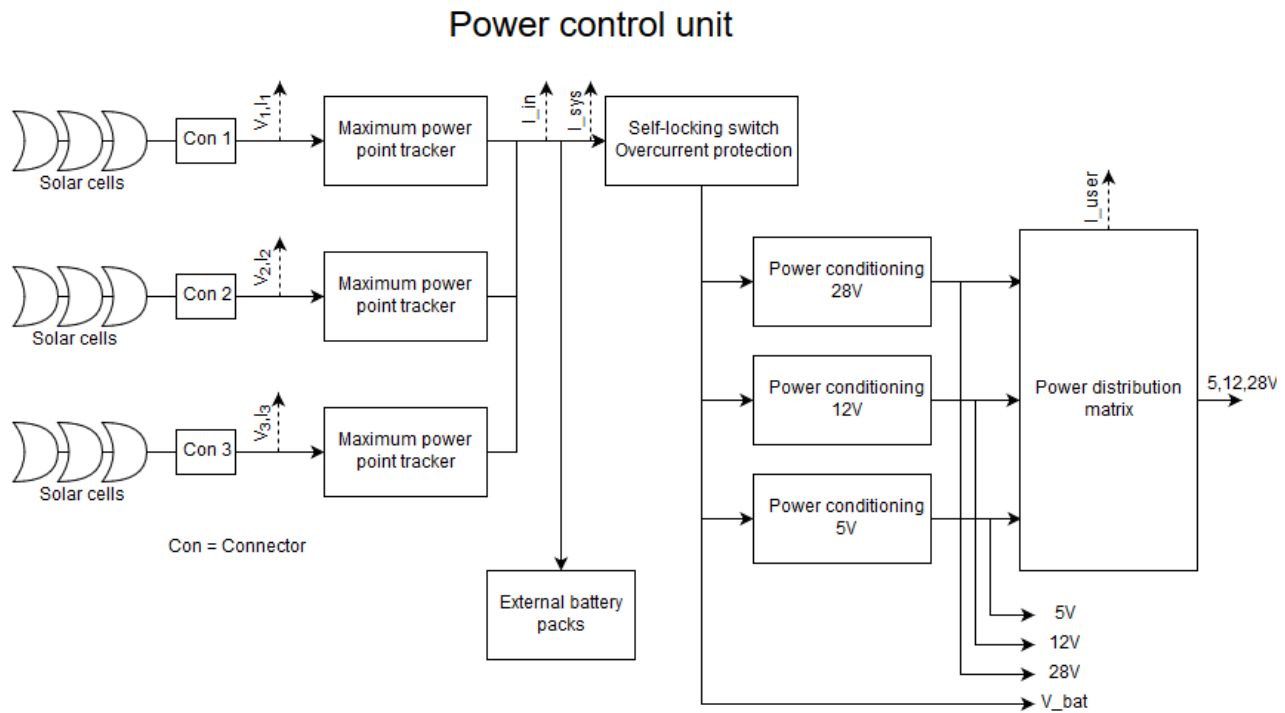


Figure 7.15: Power distribution and conditioning unit overview

estimate of 90% has been taken as the Y+ face has constant solar flux. Self-locking switch block contains main safety features, can initiate safe mode and is responsible for connection to the launcher. Power conditioning transforms power to voltages required by other subsystems, this step has 98% efficiency [104]. Power control units are essential for all satellites, however they are highly specific to the mission needs. As power needs of this satellite are higher than for most other CubeSats, custom circuit board will be needed. Commercial CubeSat part retailers usually provide EPS systems only up to 30-40 W. Diagram presented for power control unit is however heavily inspired by reliable and tested commercial units, just scaled for higher power transfer.

7.3.4 Electrical power storage

Batteries are an essential part of EPS and as such, they are put to work each orbit. Lithium-ion batteries are one of the best when it comes to energy density, reaching up to 153 Wh/kg [41]. In this regard, from commercially used batteries only lithium polymer ones can top them, but these are less resistant to space conditions such as vacuum. With price and reliability in mind, Gomspace battery packs²³ have been chosen for Sat-ELITE. Batteries have to last for 5+ years which is 28000+ charging cycles. To prevent extensive degradation, depth of discharge must be kept below 17% in one orbit Figure 7.16.

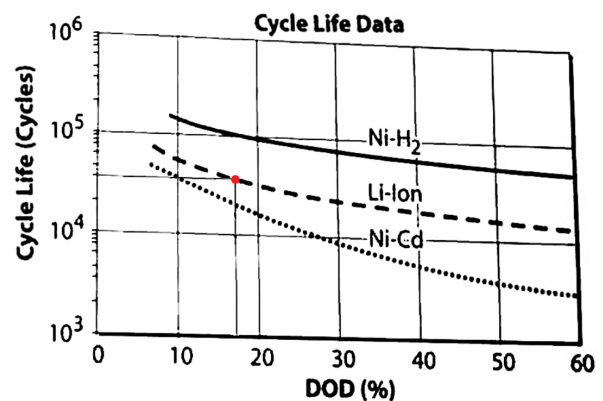


Figure 7.16: Diagram showing battery degradation [25]

Depth of discharge has to cover all energy needs during the night, and even some energy peaks have to be covered during the day. To keep the batteries operating at optimal temperatures, small 4 W resistor heaters are included between the cells to keep them from discharging at freezing temperatures. In total, 2 battery

²²<https://gomspace.com/shop/subsystems/power/nanopower-p31u.aspx> [Date accessed: 02-07-2019]

²³<https://gomspace.com/shop/subsystems/power/nanopower-bpx.aspx> [Date accessed: 23-06-2019]

packs (each for 7500€) with total capacity of 554400 J will be sufficient. Even in worst case presented in Figure 7.17, only 12% depth of discharge is reached, satisfying the requirement **SYS-SC-POW-4** of having 10% redundancy at EOL. In this plot, the total stored battery charge is presented on the right graph, while on the left graph, power is plotted. The blue curve shows difference between power generated measured before maximum power point trackers, and actual power consumed by power sinks. The orange curve shows power charging or discharging the batteries, which is lower than the blue curve due to efficiencies when charging (above zero). When discharging (below zero), it can be seen that more power is leaving the batteries than is required by sinks, due to discharging efficiencies.

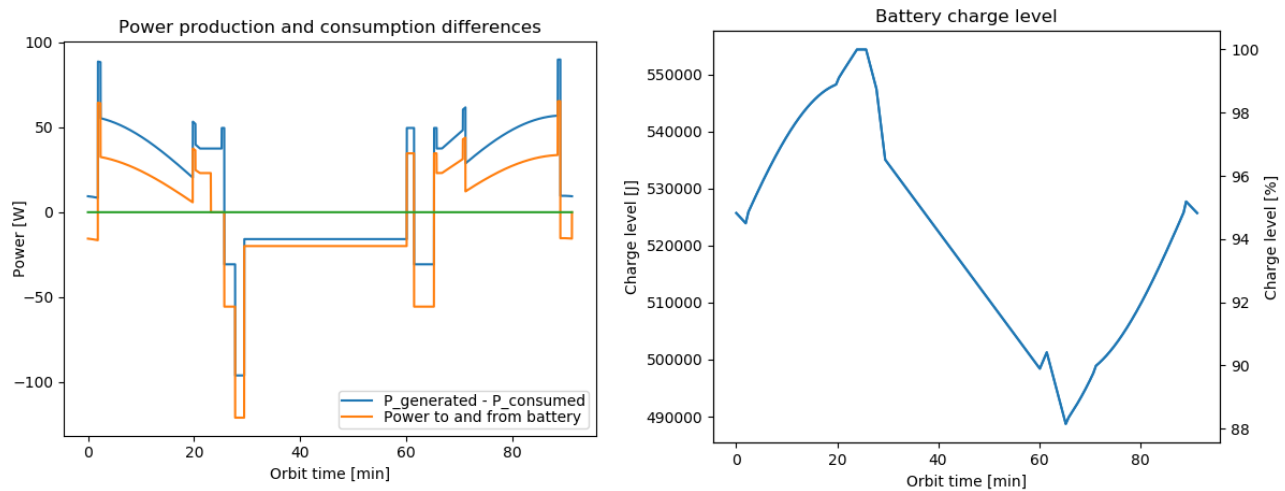


Figure 7.17: Graphs showing battery charging and discharging

Battery pack electrical block diagram is presented in Figure 7.18, the power flows from power control unit primarily straight to batteries, which is moderated by battery charge control (96% efficiency [104]). Battery charge control together with temperature sensor activate heater through heater control block. Even with active temperature control, conventional batteries have efficiency of about 91% [104]. Battery charge control failure is important also from risk mitigation perspective. **TR-EPS-3** - Energy storage failure is minimised when batteries operate in nominal environment.

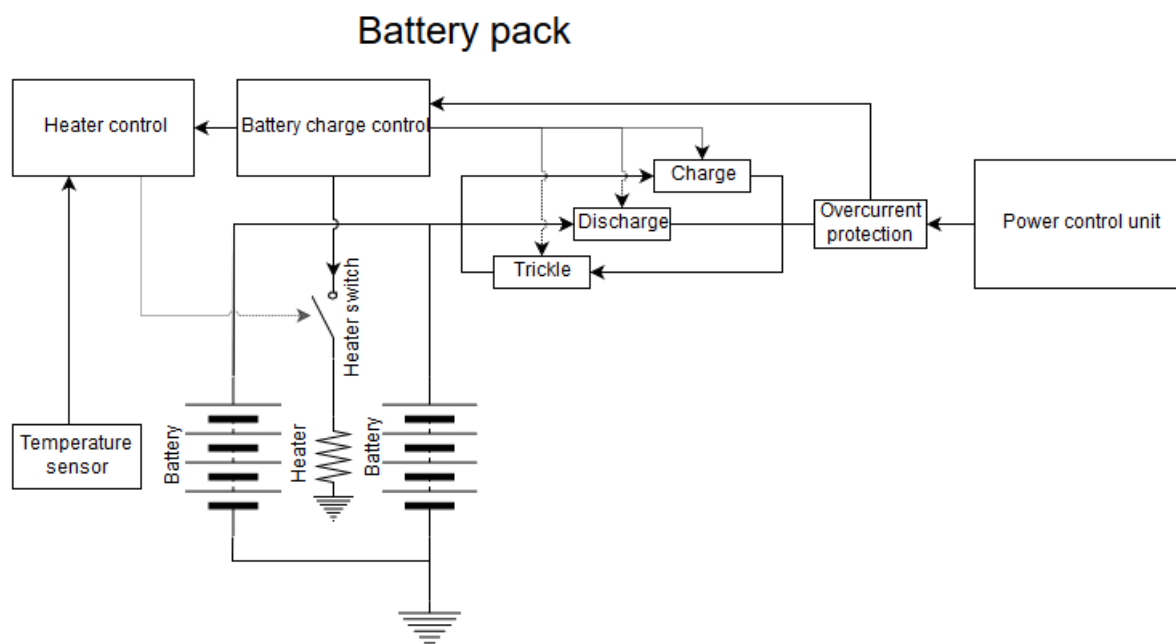


Figure 7.18: Battery pack electrical block diagram

²³<https://gomspace.com/shop/subsystems/power/nanopower-bpx.aspx> [Date accessed: July 2, 2019]

7.4 Possible failure modes

Unless 100M€ are available to send a repair team into space, electrical and software failures are critical in that the flow of downlink data is interrupted, or the data is erroneous. In this section, different types of failures inherent to electrical systems are investigated.

7.4.1 Human Errors

Software bugs [TR-CDH-3] are a common failure cause in spacecraft: NASA's Mariner 1 crashed due to a code error, ultimately costing a massive 18.2 M\$ in 1962. These can be circumvented through code checking and unit tests. Electrical design flaws, component manufacturing and assembly errors should be minimised through accurate inspection and testing. A badly soldered joint can lead to a corruption of information on the OBC.

7.4.2 Radiation-induced failures

Radiation in electrical components can undertake three forms: charging, ionisation and single event upsets.

Plasma interactions, charged particles, solar radiation and magnetic fields are the major contributors to surface charging of a spacecraft. Internal charging is due to energetic electrons penetrating into dielectric materials inside the spacecraft [105]. This creates a voltage potential difference which can lead to biasing of transistors, degradation of sensors and solar cell panels [TR-EN-1]. A proper grounding of the body and the solar panels can prevent most charging issues [96], even though these are not very present in a VLEO environment.

As a result of impact with a radiation particle, atoms or molecules are ionised over time, which can have two effects: bit-flips or leakage currents. Even a relatively low energy cosmic ray will produce about $3 \cdot 10^6$ electrons, which can cause a state change from "zero" to a "one" [106]. To circumvent this, error detection and correction for FLASH is incorporated in the OBC.

Single Event Upset (SEU) is the corruption of information stored in a memory element [107] occurring immediately after a radiation particle impact. CMOS circuits can "latch up" into a state where excessively high current is drawn, effectively destroying itself. Built-in protection is characteristic of modern CMOS devices intended for use in high radiation environments [106], usually surrounded with an insulating oxide layer.

7.4.3 Mitigation techniques

Aside from aluminium shielding (see Subsection 8.4.1), which protects the structure at a system level, there are several ways to mitigate failures in electrical components. Many errors can be avoided through forms of *redundancy* [107]:

- Hardware redundancy is the addition of extra hardware, for example a secondary OBC to mitigate risk of failure and increase computational power
- Software redundancy is the inclusion of extra software, aimed at detecting and tolerating faults
- Information redundancy is the addition of extra information beyond what is required for a function, like an error detection code
- Time redundancy uses supplementary time to perform certain functions such that fault detection tolerance can be achieved.

Proper *component selection* can prevent a large number of failure types: a common approach is selecting those with flight heritage. *Conformal coating* is a thin polymeric film which is applied over a fully assembled electronic board, preventing moisture insertion and adding structural rigidity. Finally, *testing* is conducted, however it can only be performed on final stage before delivery, often falling victim to time and budget mismanagements [96].

8. Structural and Environmental Hazards

All the subsystems present on the spacecraft need to be supported and protected from the hazards of the space environment throughout the whole Sat-ELITE's lifetime. Material choice and structures design to achieve the aforementioned objective are discussed in [Section 8.1](#) and [Section 8.2](#) respectively. Furthermore, the Sat-ELITE will experience drastic temperature ranges for which a Thermal Control System (TCS) is needed and designed in [Section 8.3](#). Other hazards are explored in [Section 8.4](#).

8.1 Material selection

When designing a structure, the material it is made of plays an important role and is often the first to be selected. In this case, there are three main criteria considered when selecting the material: stiffness, thermal expansion and impact resistance, for which the reasons are given below.

8.1.1 Stiffness optimisation

It is important that the material has high stiffness such that it maintains integrity under violent vibrations during launch. In [Figure 8.1](#) the stiffness (E) is plotted against the density (ρ). The material in consideration should have high stiffness and low density, which means that the top left of the diagram is where we want the material to be located. This means that technical ceramics and metals are most fit in this regard. However, technical ceramics are brittle, which means that they would have difficulty sustaining the launch loads, and thus are not the best option.

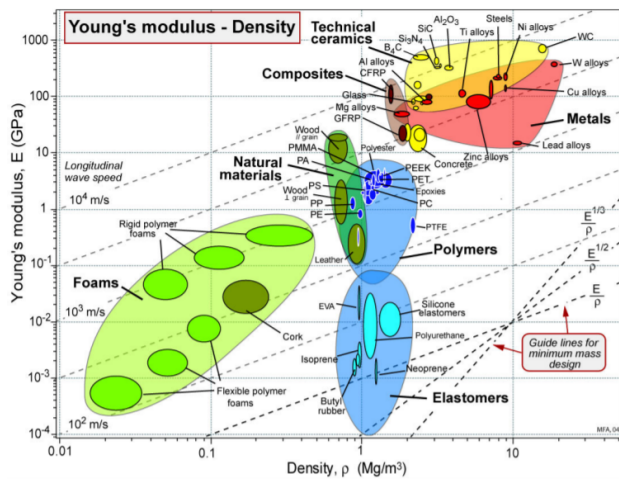


Figure 8.1: Young's modulus, E , against density, ρ [108]

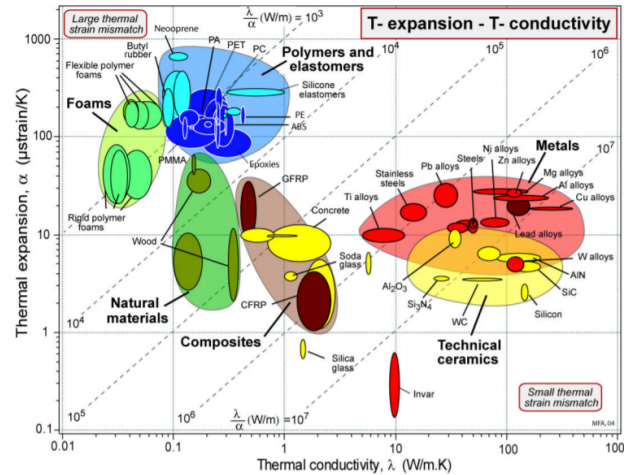


Figure 8.2: Thermal expansion coefficient, α , against thermal conductivity, λ [108]

8.1.2 Thermal expansion

Another important aspect to consider is the variety of temperatures that the structure will endure during the orbit. These variations should not misalign the structure to an extent that mission performance is impaired. This means that λ/α should stay as low as possible, which in turn means that we want the material to be in the bottom right of the diagram in [Figure 8.2](#). Here one can see that Invar, a material specifically designed to have low thermal expansion, could be a useful material. The problem with Invar is that it cannot offer as much stiffness compared to metals.

8.1.3 Debris

Debris impact poses a serious threat to the satellite, hence a tough material is desired. Toughness is characterised as a material's ability to absorb energy before failure. Fortunately, as discussed in [Subsection 8.4.2](#), the presence of debris in VLEO is minimal. A decision was made to neglect impact design for material selection, as it would be too costly in terms of weight and money.

8.1.4 Chosen material

All factors considered, metals are best suited for the mission. Looking into more detail, aluminium alloys show the most potential as they provide a good mix of stiffness, strength and thermal coefficients. This can also be observed in the CubeSat market, as most structures are made of aluminium 7075-T6 and aluminium 6061-T6 [41]. Aluminium 7075 constitutes the better option, as it provides higher stiffness, which will be the main driver for the structural design. The properties of this material are given in Table 8.1. In terms of sustainability, aluminium is easily recyclable ¹, so any material waste gathered during production can be recycled.

Table 8.1: Material properties of Aluminium 7075-T6 ²

Property	Value	Property	Value
Density, ρ	2.81 g/cm ³	Fatigue strength, σ_f	159 MPa
Ultimate tensile stress, σ_u	572 MPa	Shear modulus, G	26.9 GPa
Tensile yield strength, σ_y	503 MPa	Shear strength, τ_u	331 MPa
Modulus of elasticity, E	71.7 GPa	Thermal expansion coefficient, α	25.2 $\mu\text{m/mK}$
Poisson's ratio, ν	0.33	Thermal conductivity, λ_t	130 W/mK

8.2 Structural design

The structure holds the Sat-ELITE together. That is why it should be able to properly handle all loads induced during its lifetime. This includes loads during launch, deployment and orbit. The models used to calculate these loads are mentioned throughout this section, together with the ways these models were validated.

8.2.1 Launch canister

For the launch, the Canisterised Satellite Dispenser (CSD) from Planetary Systems Corporation shall be used [109]. The CSD has several advantages over other canisters available. First of all, the CSD is fully documented, with available mechanical and electrical interfaces, making the design process considerably easier. This documentation also comes with a full CAD model of the canister, as can be seen in Figure 8.3. Secondly, it secures the payload using pre-loaded tabs, allowing for more accurate load calculations. Moreover, the system is flight validated, gaining a TRL of 9 in 2013 [109]. Finally, the CSD has multiple secure systems to ensure deployment, leading to high probability of success, as shown in Table 8.2. These reliabilities are based on data from more than 3000 deployments. During these there have not been failures in neither laboratory nor real-life environments, which results in the mentioned values [110]. This means that the risk of deployment failure is very small [TR-OP-2]. According to the specification, the canister has a mass of 5.65 kg and the rotational rates after deployment shall be less than 10 deg/s about each axis. This will be taken as the critical case for detumbling, as mentioned in Subsection 6.1.5.

Table 8.2: Minimum reliability and confidence level of the CSD [109]

Probability of success	Confidence level [%]
>0.999	60
>0.998	85
>0.997	95
>0.996	97.5

8.2.2 Proposed structural configuration

To start of the structural design, a basic load bearing structure was assumed. In Figure 8.4 the basic geometry of this structure can be seen. The load-bearing beams have a width of ten millimetres and thickness of two

¹<https://www.aluminum.org/aluminum-sustainability> [Date accessed: 23-6-2019]

²<http://asm.matweb.com/search/SpecificMaterial.asp?bassnum=MA7075T6> [Date accessed: 21-05-2019]



Figure 8.3: The Canisterised Satellite Dispenser by Planetary Systems Corporation [109]

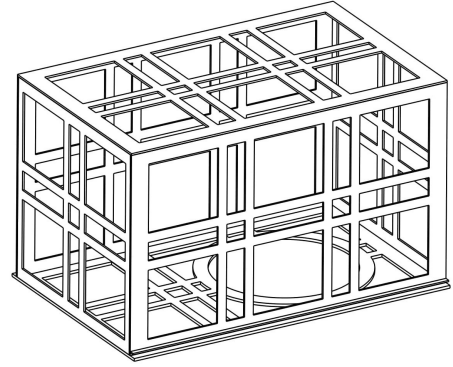


Figure 8.4: Technical drawing of the proposed structure

millimetres. This proposed structure is based on standard CubeSat structures like the ones being sold by commercial companies^{3,4}. The outer dimensions have been determined such that the structure fits the requirement of the CSD, as stated in the manual [111]. Furthermore, the bottom of the structure is missing some members, as the camera requires an opening of 16x16 cm.

8.2.3 Static launch loads

The main structural loads that the Sat-ELITE will need to withstand are the launch loads, which are composed of static and vibrational loads, of which the former will be addressed first. The launcher used is the Vega, as described in Subsection 4.5.3, and its load diagram is given in Figure 8.5. It can be seen that the strongest force will be acting in longitudinal direction. This force has a value of 7 g and is acting in compression. The Sat-ELITE will have a mass of 20.092 kg, and multiplying this with 7 g will yield a force of 1379 N. For the lateral direction, the same method can be applied, yielding a lateral force of 117 N.

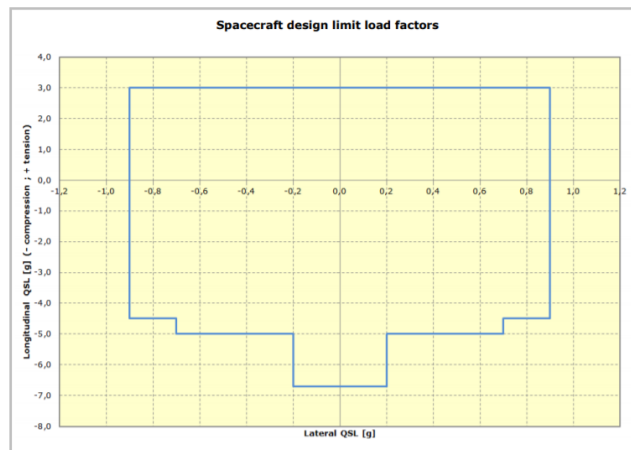


Figure 8.5: Vega static limit loads [56]

These static loads will need to be withstood by the structure. This means that the structure should be made in such a way that it will not buckle under this load. For this model, the structural elements are expressed as beams with cross sections of 2 by 10 mm and lengths of 10 cm, as this is the part which would buckle under a load. For the effective length of a beam the higher value of 2.0 is taken to be safe [112], since the proper clamping

³<https://www.isispace.nl/products/cubesat-structures/> [date accessed: 19-06-2019]

⁴<https://endurosat.com/products/#all-cubesat-structures> [date accessed: 19-06-2019]

method is difficult to determine for a more complex structure. Since this geometry satisfies Equation 8.1, the Euler column buckling formula, given in Equation 8.2 can be used to calculate the critical load on a single member [112]. This analytical method has been validated before [113]. Plugging in the values yields a critical force on one member of 117.9 N. Since there are 20 members in the longitudinal direction, the total force that the structure can withstand without critical buckling is 2358 N. This is well above the force of 1379 N acting in that direction. For the lateral loads, the limiting direction will have 14 members (x direction, camera removes 2), resulting is a critical buckling force of 1650.6 N, which is also way higher than the experienced load of 117 N, which means that the structure can handle the static launch loads and satisfies requirements **SYS-LCH-FL-1** and **SYS-LCH-FL-2**.

$$S_{eff} > \sqrt{2\pi^2 E / \sigma_y} \quad (8.1)$$

with S_{eff} the effective slenderness ratio which is determined with Equation 8.3 [112], E the Young's modulus (71.7 GPa for Al-7075), and σ_y the yield strength (503 MPa for Al-7075).

$$P_{cr} = \frac{\pi^2 EI}{L^2 C^2} \quad (8.2)$$

with E the Young's modulus (71.7 GPa for Al-7075), I the moment of Inertia, L the length of the beam, and C the effective length of the beam.

$$S_{eff} = \frac{LC}{\sqrt{I/A}} \quad (8.3)$$

with L the length of the beam, C the effective length of the beam, I the moment of Inertia, and A the cross sectional area.

8.2.4 Launch vibrations

Besides the static launch loads, the launch also imposes vibrational loads in the structure. This results in requirements for mode frequencies, and these are stated in Table 8.3 [56]. These are the values that set the frequency requirement of the Sat-ELITE.

Table 8.3: Vega mode frequency requirements

	Lateral	Longitudinal
Mode frequency	$f \geq 15 \text{ Hz}$	$20 \text{ Hz} < f < 45 \text{ Hz}$ or $f > 60 \text{ Hz}$

To determine the frequency of the Sat-ELITE, it will be modelled as a spring-mass system [114]. The two propulsion units, ADCS, C&DH, telecommunications unit, EPS and payload will all be modelled as masses. This will create a seven Degree of freedom (DOF) system. In Figure 8.6 one can see the six views of the spacecraft and the springs connecting the masses. These springs represent the beams of the structure connecting certain subsystems. The body coordinate system is used, such that x is in flight direction and z is pointing downward to Earth. This means that in the launcher the longitudinal direction is in z, and the lateral directions are in x and y.

The main equation that spring-mass system needs to satisfy is given in Equation 8.4 [114]. Note that this equation is given in the x direction, but the same would apply for the other two directions. In this equation \mathbf{x} is the position vector, and $\ddot{\mathbf{x}}$ is the acceleration vector. The mass matrix \mathbf{M} is given in Equation 8.5, and it is a diagonal matrix, with the masses of the subsystems given on the diagonal.

$$\mathbf{M}\ddot{\mathbf{x}} + \mathbf{K}\mathbf{x} = \mathbf{0} \quad (8.4) \quad \mathbf{M} = \begin{bmatrix} m_1 & 0 & 0 & \dots & 0 \\ 0 & m_2 & 0 & \dots & 0 \\ 0 & 0 & m_3 & \dots & 0 \\ \vdots & \vdots & \vdots & \ddots & \vdots \\ 0 & 0 & 0 & \dots & m_7 \end{bmatrix} \quad (8.5)$$

The most intricate element of the spring-mass system is the stiffness matrix \mathbf{K} , which is given in Equation 8.6. The off-diagonal terms consist of single spring stiffness. For example, k_{13} would be the spring

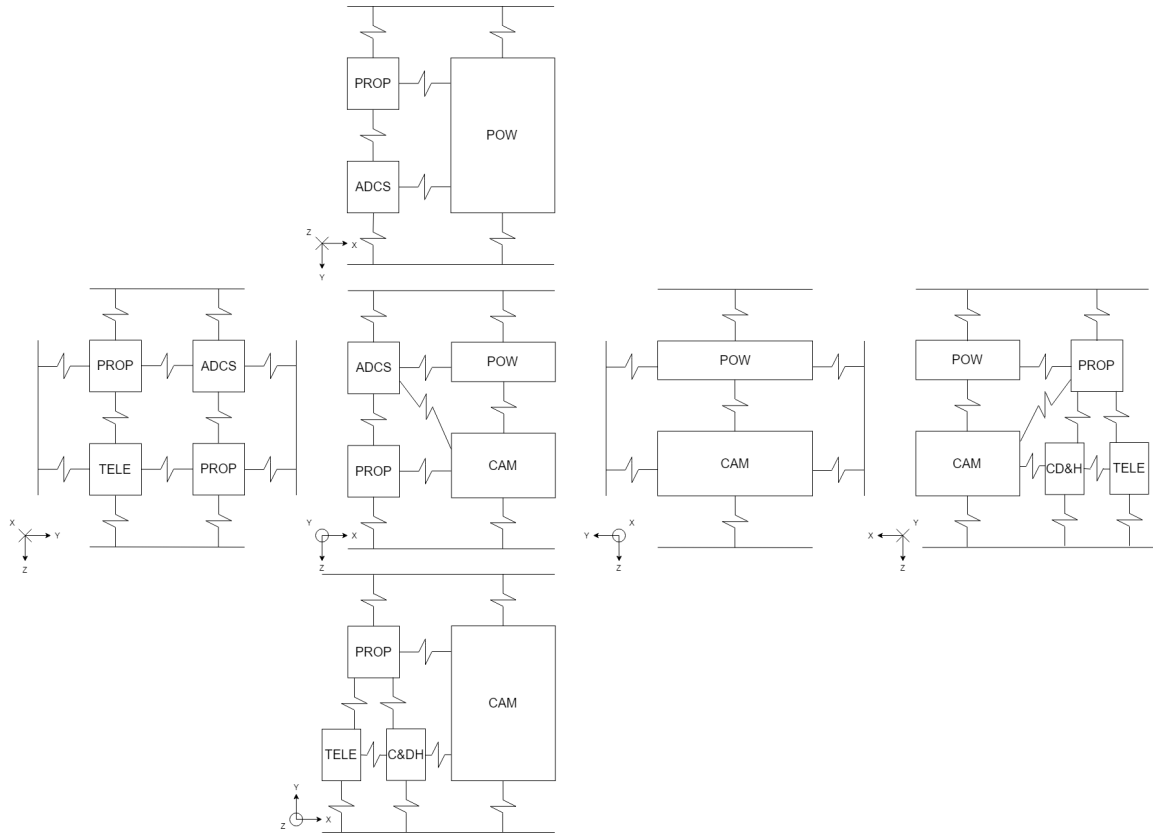


Figure 8.6: Spring-mass system modelling the Sat-ELITE

stiffness between mass 1 and mass 3. Take note that these off-diagonal terms have a negative magnitude. The diagonal terms are more extensive. They consist of the sum of multiple spring stiffnesses, as shown in Equation 8.7 for k_1 . The first k_{01} represents the interaction mass 1 has with the outer walls of the structure, since these will be fixed in place by the launch canister. It is assumed that these walls only constrain the structure in the y and z directions, as this is where the Sat-ELITE is constrained by the CSD. The other stiffnesses making up the diagonal terms have the same definition as the off-diagonal terms but are positive in magnitude.

$$\mathbf{K} = \begin{bmatrix} k_1 & -k_{12} & -k_{13} & \dots & -k_{17} \\ -k_{12} & k_2 & -k_{23} & \dots & -k_{27} \\ -k_{13} & -k_{23} & k_3 & \dots & -k_{37} \\ \vdots & \vdots & \vdots & \ddots & \vdots \\ -k_{17} & -k_{27} & -k_{37} & \dots & k_7 \end{bmatrix} \quad (8.6)$$

$$k_1 = k_{01} + k_{12} + k_{13} + k_{14} + k_{15} + k_{16} + k_{17} \quad (8.7)$$

To actually determine the relevant spring stiffnesses between the masses, Equation 8.8 and Equation 8.9 are used. Great care should be taken in whether the longitudinal or lateral formula should be used. For example, if two masses are arranged next to each other in x direction, Equation 8.8 should be used when calculation the stiffness for x direction, but Equation 8.9 should be used for the y and z directions. Furthermore, when multiple beams are connecting masses, their stiffnesses can be added together, since springs in parallel have an equivalent stiffness of the individual stiffnesses added together.

$$k_{long} = \frac{AE}{L} \quad (8.8) \quad k_{lat} = \frac{12EI}{L^3} \quad (8.9)$$

Now that the matrices have been defined, one can finally start to determine the mode frequencies. First of all, the stiffness matrix \mathbf{K} needs to be converted to the mass normalised stiffness matrix $\tilde{\mathbf{K}}$ as is shown in Equation 8.10 [114]. The eigenvalues of this matrix are equal to ω_n^2 . This value is than quite easily converted to the natural frequency f_{nat} in Hz by the use of Equation 8.11. This will yield a multitude of different natural

frequencies, but there is mostly interest in only the lowest one of these, as that frequency is the mode frequency, which will dictate whether or not the requirements are met.

$$\tilde{\mathbf{K}} = \mathbf{M}^{-1/2} \mathbf{K} \mathbf{M}^{-1/2} \quad (8.10)$$

$$f_{nat} = \frac{\sqrt{\omega_n^2}}{2\pi} \quad (8.11)$$

The resulting mode frequencies are given in [Table 8.4](#) and comparing with [Table 8.3](#), the requirements are met. The margins are quite large, so the design is rather safe. The closest margin is in x direction, and this is equal to 50.72 Hz, which is 3.3 times the value of the requirement. This model should be properly verified, since it is quite intricate. If the values turn out to be largely overestimated it could put the Sat-ELITE in the resonant range.

Table 8.4: Calculated mode frequencies

Direction	Calculated value [Hz]	Requirement [Hz] [56]
x	65.72	$f \geq 15$
y	483.66	$f \geq 15$
z	421.87	$20 < f < 45$ or $f > 60$

To validate the approach taken, it is implemented on the ANUSAT-II [115] for which the frequencies are known. This CubeSat was modelled in the same way as the Sat-ELITE and then the values were compared to the values given by the numerical methods in the report. The results of this are in [Table 8.5](#). As can be seen, our own model underestimates the frequency by 13.6%, which is likely due to incorrect assumptions. As the frequency requirements state a lower bound, an underestimation is better than an overestimation. Furthermore, this shows how the spring-mass model gives an answer in the right order of magnitude, and thus indicates that requirements **SYS-LCH-FL-3** and **SYS-LCH-FL-4** can be met.

Table 8.5: Validation of the spring-mass system model

	Validation model [Hz] [115]	Own model [Hz]	Difference
lowest frequency	718.04	620.67	-13.6%

8.2.5 Launcher change

To investigate how a launcher change would influence the structure, a small sensitivity analysis is done. The Vega launcher is compared to the Soyuz and Falcon 9, as those were option discussed in [Subsection 4.5.3](#). For the longitudinal case the requirements go down, as the loads are lower, but for the lateral case they go up to 1.8 g for the Soyuz launcher, and 2.0 g for the Falcon 9. Since the critical load in lateral direction is 1886.4 N, and the mass is 20.092 kg, the critical lateral g's would be 9.6, and that is far below the loads experienced in any of the launchers. The mode frequency requirements are also less strict for these other launchers, resulting in the fact that the structure is able to withstand the loads of any of these launchers.

Table 8.6: Structural parameters of different launchers

	Vega [56]	Soyuz [55]	Falcon 9 [54]
Longitudinal static load	+3.0 g, -7.0 g	+1.8 g, -5.0 g	+2.0 g, -6.0 g
Lateral static load	± 0.9 g	± 1.8 g	± 2.0 g
Longitudinal mode frequency	20 Hz to 45 Hz or > 60 Hz	≥ 35 Hz	≥ 25 Hz
Lateral mode frequency	≥ 15 Hz	≥ 15 Hz	≥ 10 Hz

8.2.6 Deployment & orbit loads

The loads experienced during launch are the highest loads the structure will experience, but this does not mean that the structure does not experience loads after this. In this section the other loads experienced will be quantified to check whether or not the structure can indeed withstand these loads.

- **Force deployment spring** The spring which will deploy the Sat-ELITE from the CSD has a constant applied force of 11.6 N per spring. Since the CSD will have a maximum of four springs the maximum total force is 46.4 N [109]. This force is only 2.5% of the critical load of 1886.4 N as calculated in Subsection 8.2.3, and thus will be no problem to the structure.
- **Bending of the solar panels** The worst case scenario load on the solar panels will be around $5 \cdot 10^{-4}$ N. This small load will slightly bend the solar panel. Using the formula for bending of a cantilever beam [116] one can determine the tip displacement of the solar panel, which turns out to be approximately 0.5 nm. This does not take into account the hinges, however, since the force and displacement are so small, it was determined that this bending definitely would not be critical.
- **Static loads** There are also static loads acting upon the main body of the Sat-ELITE which the structure has to withstand. The magnitude of these loads, which are mainly aerodynamic, are less than 1 N, and as shown in Subsection 8.2.3 the structure is able to withstand much more than this, meaning the in-orbit loads are negligible.

8.2.7 Moments of inertia determination

Besides the calculations of loads and strength, other important values that come out of the structural design are the centroid position and the mass moments of inertia, which will be primarily used by ADCS, as can be seen in Chapter 6. For the calculations, most subsystems will be modelled as cuboids, the camera will be modelled as a cylinder, and the structure itself will be modelled as beams. To calculate the centroid position, Equation 8.12 is used, where M_i are the component masses, and x_i , y_i and z_i are the positions of the centroid of the components [112].

$$\bar{x} = \frac{\sum M_i x_i}{\sum M_i} \quad \bar{y} = \frac{\sum M_i y_i}{\sum M_i} \quad \bar{z} = \frac{\sum M_i z_i}{\sum M_i} \quad (8.12)$$

Table 8.7: Calculated centroid position

	Calculated value [mm]	Requirement [mm] [111]
Δx	+2.6	± 50
Δy	+4.0	± 40
Δz	+6.0	± 35

In Table 8.7 the found values for the centroid are given. These values denote the difference between the geometric centre and the centre of gravity. Next to the calculated values are the requirements that the CSD sets upon the design. As can be seen, the centroid is really close to the geometric centre, and well within the bounds [111]⁵. The centroid position will be used throughout the design, for example to calculate thrust misalignment in Subsection 4.3.5. Furthermore this will also be the point around which the mass moment of inertia will be calculated. In Equation 8.13 the full matrix and all its terms are given. To calculate these terms, Equation 8.14 and Equation 8.15 can be used. Here, for example, $I_{xx,i}$ is the moment of inertia of the idealised component itself, and the rest is the Steiner term, to get the moment of Inertia around the centroid [112].

$$\mathbf{I} = \begin{bmatrix} I_{xx} & I_{xy} & I_{xz} \\ I_{xy} & I_{yy} & I_{yz} \\ I_{xz} & I_{yz} & I_{zz} \end{bmatrix} \quad (8.13)$$

$$\begin{aligned} I_{xx} &= \sum (I_{xx,i} + M_i((y_i - \bar{y})^2 + (z_i - \bar{z})^2)) \\ I_{yy} &= \sum (I_{yy,i} + M_i((x_i - \bar{x})^2 + (z_i - \bar{z})^2)) \\ I_{zz} &= \sum (I_{zz,i} + M_i((x_i - \bar{x})^2 + (y_i - \bar{y})^2)) \end{aligned} \quad (8.14)$$

$$I_{xy} = -\sum M_i(x_i - \bar{x})(y_i - \bar{y}) \quad I_{xz} = -\sum M_i(x_i - \bar{x})(z_i - \bar{z}) \quad I_{yz} = -\sum M_i(y_i - \bar{y})(z_i - \bar{z}) \quad (8.15)$$

Applying these equations results in the inertia matrix $\mathbf{I} = \begin{bmatrix} 0.372 & 0.003 & -0.015 \\ 0.003 & 0.356 & -0.076 \\ -0.015 & -0.076 & 0.273 \end{bmatrix}$. This matrix is

⁵The centroid was also calculated with the solar panels not deployed, and this did not make a significant change in the centroid position.

also diagonalised [112], this is the matrix around the principle axis $\mathbf{I}_{pa} = \begin{bmatrix} 0.227 & 0 & 0 \\ 0 & 0.370 & 0 \\ 0 & 0 & 0.405 \end{bmatrix}$.

These are the values which are used for the ADCS calculations which can be found in Chapter 6.

To verify this inertia model, multiple unit tests were executed. The idealised moments of the components were double checked on paper, and the configuration was slightly modified to check whether the changed result made sense. As the model was written, it was constantly being checked for bugs and errors, as well as sanity checks on the achieved results. As it is difficult to actually measure the mass moment of inertia of in orbit satellites, the model was verified by comparing it to the analysis of a 3U CubeSat [117]. The results of this comparison are stated in Table 8.8. As can be seen, the values in the x and y direction are really close, but the z direction is off. However, the actual difference in magnitude is only 0.0009 m^4 , which is not that high. This means that the model does not that good with really tiny values. Since the values for the Sat-ELITE, are of the same order of magnitude as the ones in x and y direction of the validation model, one can thus assume that the model is working as intended.

Table 8.8: Validation of the mass moment of Inertia model

	Validation model [m^4] [117]	Own model [m^4]	Difference
I_x	0.2273	0.2333	+2.6%
I_y	0.2273	0.2287	+0.6%
I_z	0.0040	0.0049	+22.5%

8.2.8 Structural risks

The structure, like any other subsystem, brings some risks with it. These risks will be assessed and checked whether or not any of them prove critical.

- It is analysed what will happen if a structural member were to break, for whatever reason [TR-STR-1]. If the structure were to have one less member, it still would be able to withstand all the loads, since it was decided to be over designed.
- If the structure would yield, it could misalign subsystems [TR-STR-2]. To prevent this from happening, the structure has been designed for yield stresses opposed to ultimate stresses. Furthermore, thermal expansion was taken into account when selecting the material, which also reduces the chance of mis-alignments. All of this makes sure that the structure is able to satisfy requirement **SYS-SC-STR-2**
- When components are not properly mounted it could prove detrimental to the mission [TR-STR-3]. Although the mounting structures have not been designed yet, it can be said that they will be based on existing mounting structures. This means that the TRL of the mounting structures will be quite high, reducing the risk of detachment.

8.2.9 Final structural assessment

Finally, it is important to check whether the structure is on track to meet all its requirements. Requirement **SYS-SC-DES-2** from structures point of view is satisfied because a single member failing does not cause failure, as stated in Subsection 8.2.8, and the requirements **SYS-LCH-FL** are all satisfied as shown in Subsection 8.2.3 and Subsection 8.2.4. This in response verifies requirement **SYS-SC-STR-4**, and as shown in Subsection 8.2.6 requirement **SYS-SC-STR-5** is also met. Proper alignment is achieved since Aluminium-7075 has a low thermal expansion, and with the temperature ranges experienced, misalignments will not occur, which means that requirement **SYS-SC-STR-2** is also met.

The mounting structure will be designed post DSE, this means that requirement **SYS-SC-STR-1** sadly is not met at this stage, but when designing the mounting structures this will be the main priority. Furthermore, there is one other structural requirement that has not been verified: **SYS-SC-STR-3**. This is because the ground operations have not been clearly defined yet. These loads will probably be lower than the launch loads and not prove critical, but they will need proper analysis once ground operations are defined. This also extends to requirements **SYS-LCH-PRE**, as they also depend on the ground operations.

8.2.10 Recommendations

Some of the models used to calculate the structural parameters could be made more flexible, some flexibility was built in, but it is hard to change parameters. Furthermore the models could be integrated into one big structural model, as now they are all separate. Lastly, there could be looked more into the boundary conditions for the spring-mass model, as now they are all defined very analytically, and not necessarily 100% true to life.

8.3 Thermal control

The TCS ensures that all subsystems stay within their operational temperatures and thus function correctly. If operational temperatures are not satisfied [TR-TCS-1], components are forced into safe mode, if applicable, and might degrade faster. This risk is just a minor nuisance, unless it happens regularly. Not satisfying survival temperatures carries a much bigger risk [TR-TCS-2]. Once beyond survival temperature range, a component can become inoperable indefinitely, causing a mission failure. Requirements, risks, verification and validation methods will not have a separate subsection, but will be spread throughout the section, where they fit contextually.

8.3.1 Thermal balance in space

There are 4 components to thermal balance in space. Namely: heat input (Q_{in} [W]), storage ($M c_h \frac{\Delta T}{\Delta t}$), distribution ($Q_{conduction}$) and output (Q_{out}):⁶

$$Q_{in} - Q_{out} + Q_{conduction} = M c_h \frac{\Delta T}{\Delta t} \quad (8.16)$$

In space, heat inputs for CubeSat include direct solar flux (I_s), solar flux reflected from Earth ($I_s k_{alb}$), Earth's infrared radiation (I_E), space background radiation ($k_B T_{space}^4$) and internal heat creation ($P_{internal}$). All of these, except $P_{internal}$, are multiplied with Satellite areas on which they act (A_s, A_E, A_{sat}) and absorbtivity coefficients specific to the incoming spectrum.

$$Q_{in} = I_s A_s \alpha_{sun} + I_E A_E \epsilon_{IR} + I_s k_{alb} A_E \alpha_{sun} + A_{sat} k_B \epsilon_{IR} T_{space}^4 + P_{internal} \quad (8.17)$$

Heat storage depends on specific heat capacitance (c_h) multiplied with mass (M) of all components and their potential phase change. Phase change will likely happen only in propellant or phase change-thermal mass components.

Heat distribution relies mostly on components' thermal conductivity, but it can also be facilitated by internal radiation and absorption. Since there is no air inside the structure, convection is not present. For this design stage, temperature in the satellite has been assumed uniform. This is a big assumption which simplifies further simulation extensively, but will need to be revisited in further design stages. It isn't however completely unfounded, the whole structure and most faces are from aluminium, which has excellent heat conductivity of 130 W/m/K⁷, and should distribute heat quickly and evenly.

Radiation in the infrared part of the spectrum ($k_B T_{sat}^4$) is the main form of heat output for CubeSats, yet satellite can also lose some heat (P_{out}) through communication's radio frequency output (2 W) and also through propulsion expelling hot propellant (34x2 W).

$$Q_{out} = P_{out} + A_{sat} k_B \epsilon_{IR} T_{sat}^4 \quad (8.18)$$

Absorbtivity (α_{sun}) and emissivity (ϵ_{IR}) are essentially the same thing. They reflect how much incoming energy is absorbed or emitted. As the satellites emit in infrared part of spectrum and the Sun emits radiation in ultraviolet part, those coefficients are set up in presented method by convention.

Last thing that needs to be mentioned, is a viewing factor. Viewing factor of surface A and B describes the ratio of energy which left surface A and landed on B, to the total energy which left surface A. These are partially included in effective areas, but will be missing for energy radiated away by the satellite. Even though this viewing factor would be close to one, there are some concave surfaces reducing it, due to deployable solar panels. Concave surfaces affect it, because energy leaving a concave surface, can be absorbed by the same surface, while going in a straight line.

⁶<https://ocw.mit.edu/courses/aeronautics-and-astronautics/16-851-satellite-engineering-fall-2003/lecture-notes/123thermalcontro.pdf> [Date accessed: 24-06-2019]

⁷<http://asm.matweb.com/search/SpecificMaterial.asp?bassnum=MA7075T6> [Date accessed: 24-06-2019]

8.3.2 Design options

Design options for TCS are broadly separated into two camps - active and passive temperature control. Active options are to be avoided due to their complexity and lower reliability. However, there are some simple active options, such as resistor heater which are implemented in battery packs. Passive options have no energy consumption and in general are also cheaper. Some passive options are a must due to their simplicity and effectiveness. These are radiators, reflective coating and heat conducting or heat insulating structural connections. Since TCS is overall just a supportive subsystem, simplicity, reliability and low energy consumption are highly valued. This creates another level of options which could be used, but have to be necessitated by a different subsystem. Options such as extra thermal mass, phase change thermal mass, conductive filler, FEATS (flexible and enhanced active thermal straps) and miniaturised louvres [41]. Options, which are simply unfeasible for CubeSats are heat ablation, cryogenic system, chemical heater and mechanical coolers [28].

Mentioned above are the design options for controlling temperature, but there is another option, that is to just choose thermally resistant components. This is often the trend for supporting subsystems, for example, batteries have increased their thermal performance significantly over the decades (SMAD [28] versus new release of SMAD [25]). On the other hand, imaging payloads are way more performance oriented and the trend is reversed in this regard. Most critical operational and survival temperature ranges for Sat-ELITE are presented in Table 8.9.

Table 8.9: Most critical operational and survival temperatures per subsystem

	operational range [°C]		survival range [°C]	
ADCS	-10	60	-30	90
Propulsion	-20	50	-50	120
Payload	15	25	-30	60
EPS	-10	60	-35	80
TCS	-180	350	-180	350
TT	-20	45	-40	78
CDH	-25	60	-40	80
Structures	-40	80	-200	400

8.3.3 Worst case scenarios

For TCS design, the worst case maximum and minimum heat inputs have to be established to meet first condition of **SYS-SC-TC-1**. In this regard, flying in an SSO simplifies things since the Sun exposure does not change throughout the mission. The worst cases therefore boil down to a combination of Earth's albedo, solar flux and Earth's infrared radiation which create the highest and the lowest heat input. All can be estimated from historical data and can be seen in Table 8.10. T_{earth} and albedo presented are the maximum and minimum effective average value over SSO LEO⁸.

Table 8.10: Hot and cold case variance

	Hot case	Cold case
T_{earth} [K]	256	246
Albedo (k_{alb}) [-]	0.4	0.24
I_s [W/m ²]	1368 [118]	1363 [118]

8.3.4 Material properties

Multiple material properties are vital for modelling thermal behaviour. These are specific heat capacity [J/kg/K], absorbtivity [-] and emissivity [-]. Specific heat capacity is heavily dependent on material composition, and it

⁸<https://exchange.esa.int/download/thermal-workshop/workshop2015/parts/OrbEnv.pdf> [Date accessed: 20-06-2019]

Table 8.11: Thermal material properties

	c_h [J/kg/K]		absorbivity [-]	emissivity [-]
aluminium 7000	920	aluminium 7000	0.15	0.05
PCB (FR-4)	1200	PCB (FR-4)	0.75	0.89
copper	390	solar cells	0.9	0.85
Lion batteries	830			
silicon carbide	750			
zerodur	820			
indium	240			

can be a function of temperature. Absorbivity and emissivity are both even harder to establish. They are not only dependent on material, but also on surface roughness, microscopic oxide layers, relevant spectrum, surface temperature and it can also be an interplay between multiple layers of material. Overall, material properties can be readily found in scientific literature, but as the conditions are seldom fully specified, these values vary significantly. This can be seen on a rather extreme example of specific heat for GaAs solar panels. First source [119] provides 1600 J/Kg/K, while second source provides a value of 350 J/Kg/K [120]. This problem cannot really be solved by a sufficient analysis on each property within a time frame available for this design phase. To minimise the damage, values used will be tracked in Table 8.11, so that possible inconsistencies can be easily spotted in the future.

8.3.5 Thermal simulation

A simulation was created to estimate satellite temperature fluctuations. Part describing the orbit is the same as in Subsection 7.3.2, with all the coordinate systems. Sun incidence is the same as for EPS, however areas for each face are now only satellite body faces. The simulation assumes that no heat flows from deployable solar panels to the body. This assumption reduces temperature fluctuations and is reasonable as the solar panels are connected to the satellite through only 4 hinges, which can contain heat non-conductive parts. Another incidence has been added, and that is Earth incidence. Albedo and Earth's radiation act in this direction. Over the orbit, only +Z face is directly exposed to the Earth as can be seen in Figure 8.7. There are multiple

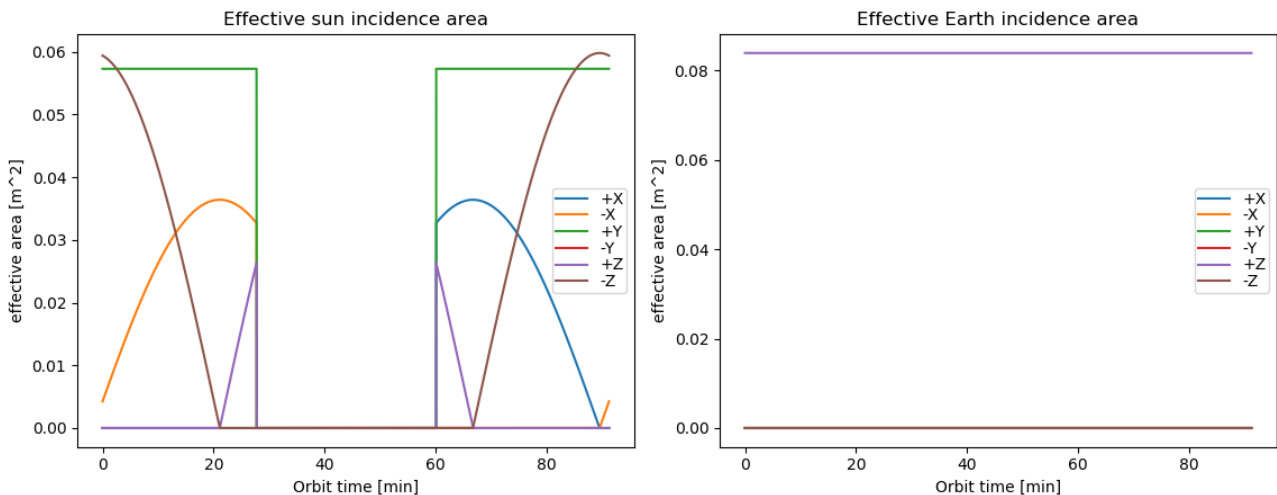


Figure 8.7: Graphs showing TCS relevant effective incidence areas

approaches on how to implement the fact that solar flux is transformed into electricity in solar cells. In our approach, solar cell efficiency is ignored, and solar cells absorb all energy as heat. To balance this out, power transfer to batteries is subtracted and power discharge from batteries is added to the heat balance (Figure 8.8). This assumes that all electrical energy is eventually transformed into heat, with the exception of energy leaving through propulsion and communication units. Another form of power output - radiation - is also shown in Figure 8.8 on the second graph.

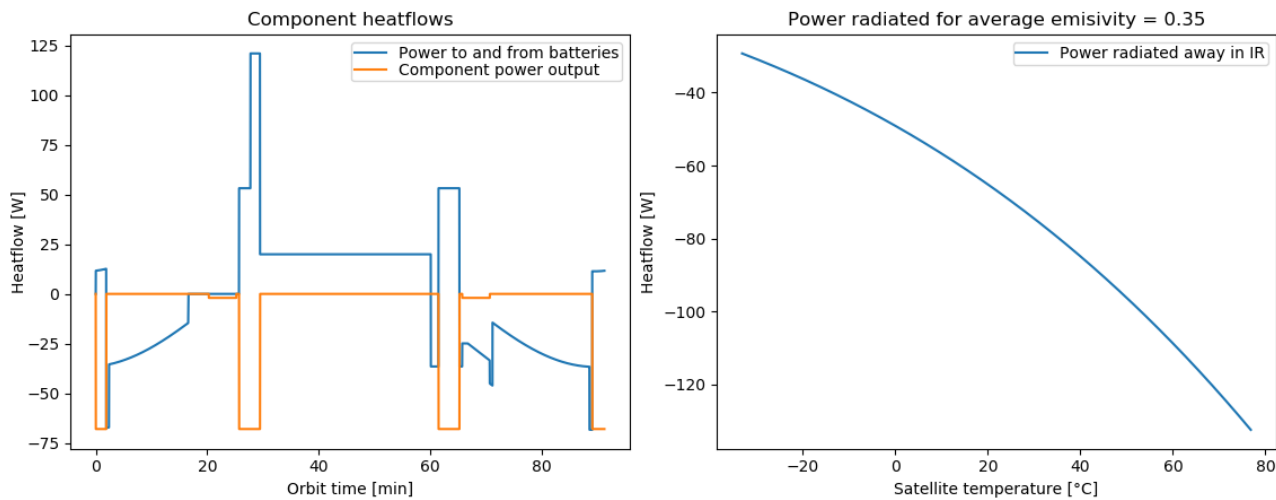


Figure 8.8: Graphs showing heat flow outputs

With all the heat flows prepared, the simulation can be run with some arbitrary starting temperature. This is always done over multiple orbits, until the satellite temperature levels off at some temperature range. Surfaces aren't painted over and therefore they consist of aluminium, FR-4, solar cells and aluminium coated primary mirror. Results for this case are presented in Figure 8.9, first graph shows all heat flows for cold case, then second and third graphs show cold and hot case respectively. This case will then be used to decide which thermal control coatings to use.

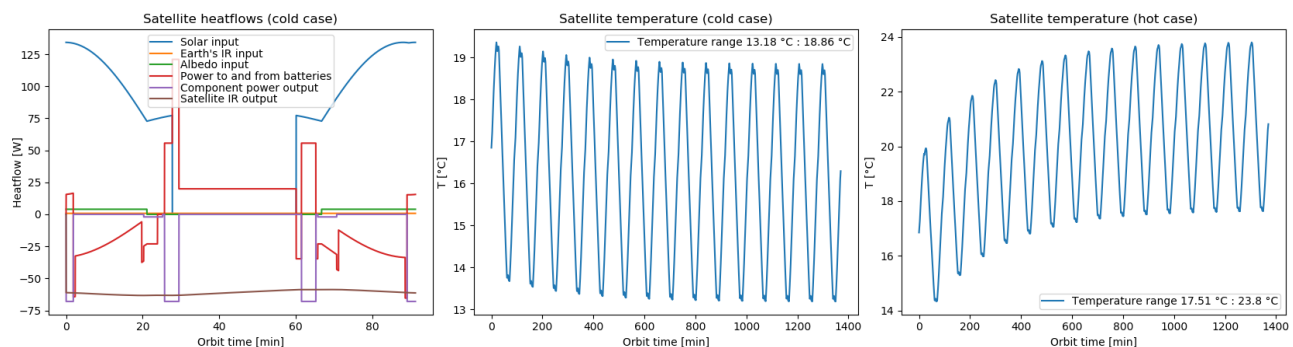


Figure 8.9: Graphs initial heat flows and temperature range

Surprisingly, temperatures for most extreme hot case, are within the operational temperature range of even the most thermally sensitive subsystem - payload camera (15 °C - 25 °C). The cold case temperatures dip below allowed 15 °C rendering payload inoperable for picturing most southern parts of the Earth. But this isn't too bad due to two reasons. Firstly, there is enough space around the camera for extra thermal insulation. This thermal insulation would reduce the temperature range around the average, which is 16 °C. Aerogels are suitable for this application, they are extremely light (80 kg/m³) and have extremely small heat conductivity, only 12 mW/m/K⁹. In Sat-ELITE, there is plenty of space around cylindrical SEEING camera to place insulating blanket from silica aerogel. Secondly, surfaces in LEO degrade due to radiation and atomic oxygen, this degradation usually pushes satellite temperatures up over time [25]. To sum up, requirements **SYS-SC-TC-1** to **SYS-SC-TC-5** can't be fully marked as verified yet. Adding paints to the design would push it to meet the cold case scenario, but the temperature increase would cause problems in the hot case. However, this is a failure of the thermal simulation rather than the design itself. Requirements **SYS-SC-TC-6** and **SYS-SC-TC-7** are met, as the design uses fully passive means of thermal control and temperature sensors have been included in C&DH design. Also, with implementation of silica aerogel insulation, there is a risk of it coming loose during launch - [TR-TCS-3], but this is easily mitigated with simple fastening. Regarding the fact that there is only single thermal control component, the first two risks of not providing operational [TR-TCS-1] and survival [TR-TCS-2] temperatures

⁹<http://www.esa-tec.eu/space-technologies/from-space/silica-based-aerogel/> [Date accessed: 20-06-2019]

are very unlikely. Especially once the prototype mission is deemed successful.

8.3.6 Recommendations

There is much to be refined after this thermal analysis. One point of improvement could be to remove assumptions, such as no heat coming from solar panels, which were made because of time constraint. Another one could be to include all viewing factors, between all concave surfaces and also all surface protrusions to improve the estimate for energy radiated away. Next, it is also important to refine and establish consistent material properties. This part is rather difficult during conceptual design, but once components have been bought, simple testing equipment could get precise values. Lastly, simulation should be split up into more nodes, with temperature calculated for each. This would necessitate also adding thermal conductivity radiation coefficients for all materials. This may seem like a daunting task, but there is industry grade thermal modelling software like ESATAN developed by ESA specifically for these purposes. There are reasons why this software was not used for this design phase. Experts at TU Delft have recommended to avoid using such software, as it is better to have a simple model with known shortcomings, than to use software without understanding it properly.

8.4 Environmental protection

Various sources of radiation are present in the hostile space environment. The presence of atomic oxygen and space debris also threaten the integrity of the structure. These effects will be investigated in the following section.

8.4.1 Radiation shielding: Dose-depth analysis using SHIELDOSE-2 model

Particle radiation is capable of penetrating and damaging vital components of the system, namely the optical sensor and electronics as discussed in [Subsection 7.4.2](#); degradation of paints, coatings, and various polymeric materials is also common. To circumvent this issue, shielding is applied to the satellite structure. For small satellites such as CubeSats, shielding is provided by the supporting aluminium structure itself. It is however important to note that shielding in close proximity to the actual electronics can lead to a larger flux of Bremsstrahlung [96]. This induced radiation occurs when an electron impacts the shielding, which as a consequence of energy equivalence releases a photon: for high-energy particles this will be in the X-ray spectrum, inducing degradation. In order to approximate the extent of shielding needed, the "weakest link" in the satellite must be identified. Inspection has shown that the most sensitive component of the design with regards to radiation is the CMOS optical sensor. Tests conducted by the Jet Propulsion Laboratory [121] on similar CMOS sensors estimate that a dose of 10 krad would be fatal. To quantify the upwelling radiation dosage on the sensor as a function of aluminium shielding, SHIELDOSE-2, within the SPENVIS toolbox¹⁰ is employed. The tool models' electrons and trapped electrons present in the atmosphere as a result of Earth's magnetic field, as well as the influence of Bremsstrahlung. For an accurate analysis, however, this program requires a specific geometrical input, namely the isotropic shielding distribution [in % of 4π solid angle/ g/cm^2] around the sensor. Essentially, one must determine the amount of material surrounding the component by means of ray tracing. Hindered by time constraints, a crude approximation is made, by assuming the reference point to coincide with the centre of a single-layer aluminium sphere, which represents the satellite's outer shell. This is actually a conservative approximation, as the sensor is not only protected by the outer structure, but also by the multiple components surrounding it. Inputting the orbital parameters and the launch period (relevant for solar cycle activity) in SHIELDOSE-2 yields the plot shown in [Figure 8.10](#).

¹⁰<https://www.spennis.oma.be/>[Date accessed: 21-06-2019]

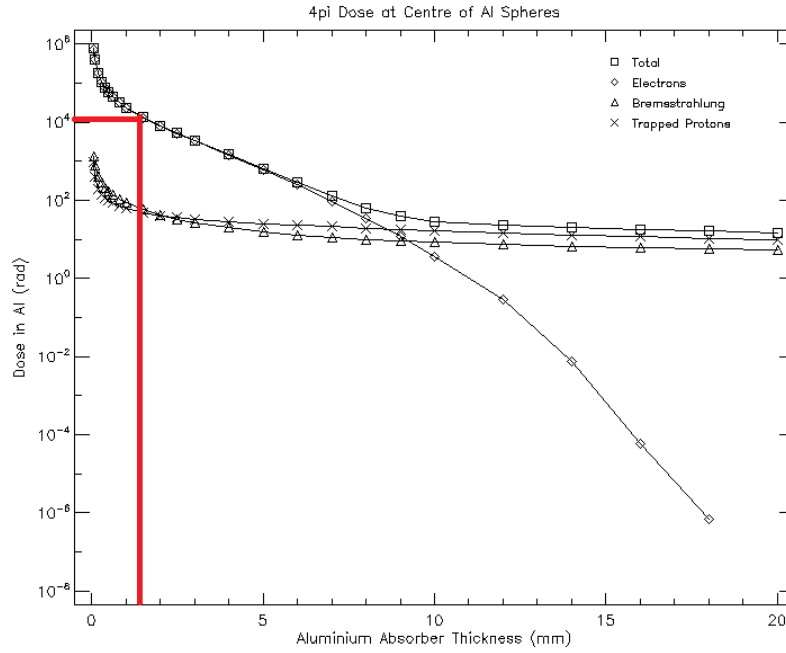


Figure 8.10: SHIELDOSE-2 simulation: radiation dose on the centre of an aluminium shell

From the figure, it can be extrapolated that a thickness of 1.2 mm is needed to shield the sensor from harmful radiation. In reality, the structure offers multiple layers of protection as opposed to a single-layer shell, as discussed previously. Hence, the shielding is deemed satisfactory in that it shall not pose threats to the integrity of the mission.

8.4.2 Space debris: a NASA 90 model simulation

Debris is any non-operational object orbiting the Earth, which can be natural (e.g. micrometeoroids, asteroid particles) or human-generated, resulting from mission launches [28]. Aside from large, trackable objects such as fairings and interstage adapters, undetectable (<10 cm in VLEO) debris poses a threat to modern satellites due to the high orbital velocities of several km per second. For instance, the deliberate explosion of Fengyun-1C by the Chinese in 2007 and the accidental collision between an American and a Russian spacecraft in 2009 have increased the large orbital debris population in LEO by approximately 70%¹¹. As statistical approach will be used to estimate the risk of critical collision at the established altitude of 342km[TR-EN-3].

For single-sheet protection, penetration and perforation threshold equations have been developed by [122]. Equation 8.19 relates the penetration depth of debris into a target of semi-infinite depth, which is not the case, so the second equation corrects for that. The plate thickness to prevent perforation and detached detached spall is found as:

$$P_{\infty} = 5.24 \cdot d^{19/18} \cdot H^{-0.25} \cdot \left(\frac{\rho_p}{\rho_t} \right)^{0.5} \cdot \left(\frac{V_n}{C} \right)^{2/3} \quad (8.19)$$

$$t = 2.2P_{\infty} \quad (8.20)$$

with $C=0.8\text{km/s}$ the speed of sound in target [123], $\rho_p = \rho_t = 2.81\text{g/cm}^3$ the density of aluminium, V_n the normal component of projectile velocity, H the Brinell hardness of target and P_{∞} the penetration depth into a semi-infinite block of target material. Assuming a frontal hit on the 1.2mm aluminium wall (Brinell Hardness $H=150$ ¹²), the critical projectile diameter results as $d=0.01\text{cm}$.

By extrapolating the SPENVIS Nasa 90 tool for 2020 at a Sun-Synchronous orbit of 342km as done in Figure 8.11, one can find that the probability of impact is around $0.7\text{m}^{-2}\text{yr}^{-1}$.

¹¹<https://www.hq.nasa.gov/office/hqlibrary/pathfinders/debris.htm> [Date accessed 17-6-19]

¹²<http://asm.matweb.com/search/SpecificMaterial.asp?bassnum=MA7075T6> [Date accessed: 17-06-2019]

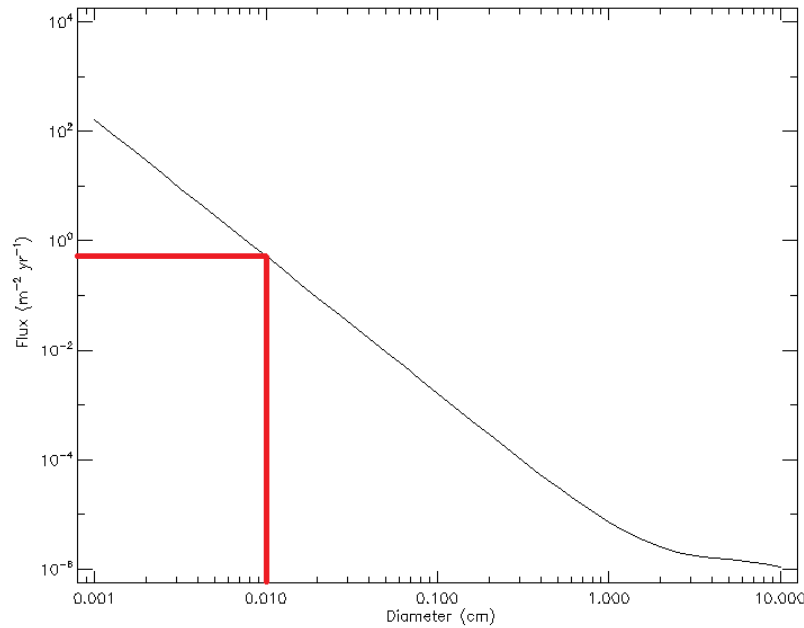


Figure 8.11: SPENVIS: NASA 90 model for space debris characterisation ¹³

For a frontal area of $0.045m^2$ and a mission lifetime of 5 years, the chance of critical impact becomes 0.157%, which is clearly a tolerable risk. This is justified by dominant atmospheric presence at low orbits, disintegrating debris through friction. Additionally, the majority of debris is concentrated around the equatorial plane, a rare encounter for the considered inclination.

In the unlikely event of collision, the structural vulnerability to atomic oxygen will increase, leading to a faster rate of corrosion. As previously discussed, aluminium is quite insensitive to oxygen corrosion. Despite this, the thermal stability of instruments will be compromised, threatening the mission.

Space debris is a global challenge menacing the safeguard of the space environment needed for future missions. Sat-ELITE will not contribute to this threat by ensuring correct end-of life manoeuvres as outlined in [Subsection 4.6.5](#).

8.4.3 Atomic oxygen

In direct contrast to radiation levels, atomic oxygen is more present at lower altitudes. This extremely vigorous oxidizer severely corrodes materials [TR-EN-2], dictating the use of non-oxidizing surface coverings for extended missions [106]. The degree of surface degradation is directly proportional to atomic oxygen fluence, which varies with altitude, orientation, orbital inclination, mission duration and solar activity variation [124]. Using the SPENVIS¹⁴ ATOMOX tool, atomic oxygen fluence was estimated at $10^{19}atoms/cm^2$ for the selected orbit. For Kapton, a material frequently employed for coating, this corresponds to an erosion depth of less than a mm. As aluminium is less than three times as erosion sensitive as Kapton [124], no significant damage will be induced on the structure. In general, metal oxides have negligible erosion rates since they are completely oxidised already [125].

¹⁴<http://www.spennis.oma.be/> [Date accessed: 20-19-2019]

9. The Sat-ELITE

In this chapter a complete overview of the Sat-ELITE is given. Firstly, the operational modes are described in [Section 9.1](#) followed by a design sustainability assessment in [Section 9.2](#). Secondly, a summary of the technical budgets is given in [Section 9.3](#). Thirdly, the cost breakdown is discussed in more detail in [Section 9.4](#). Lastly, a summary of the spacecraft's technical performance is presented in [Section 9.5](#).

9.1 Description of operational modes

In [Subsection 3.2.2](#), an operational overview of the modes was given. In this section a more technical overview is shown. The communication, thrusting and desaturation modes require a certain minimum time each orbit, while the nominal mode ¹ needs to be active for as long as possible in each orbit to take as many pictures as possible. For thrusting mode, this minimum time changes depending on the solar flux, as this influences the density of the atmosphere, and thus the drag that needs to be compensated. Two cases were analysed, the average case (average solar activity) and worst case (solar maximum). Both are shown in [Table 9.1](#), together with the power consumption of each mode which is simply a sum of the individual active subsystems.

The time distribution of the different modes over the orbit is shown in [Figure 9.1](#), where the top of the figure is the North pole and the right side is towards the Sun. It can be reasoned that thrusting three times each orbit is most efficient. That way the time where you need to thrust during daytime is minimised. From the figure it makes sense that the increase in thrusting time (as displayed in [Table 9.1](#) for a solar maximum) takes away only 33% of this time from payload time and 67% from waiting time. In addition, waiting mode is activated for half a minute between each mode to ensure a smooth transition between modes and can account for any unforeseen delays.

It should be noted that the exact time distribution of the modes will heavily depend on the position in the orbit where thrusting needs to happen. At this point of the project it is unfortunately impossible to make accurate estimates for this.

Table 9.1: Detailed modes overview

Mode	Time - solar average [min]	Time - solar maximum [min]	Average Power [W]
Nominal	38.3	36.8	44.4
Communication	9.9	9.9	25.4
Thrusting	6.8	11.3	87.4
Desaturation	13.5	13.5	14.4
Safe	0	0	14.4
Waiting	22.5	19.5	14.4

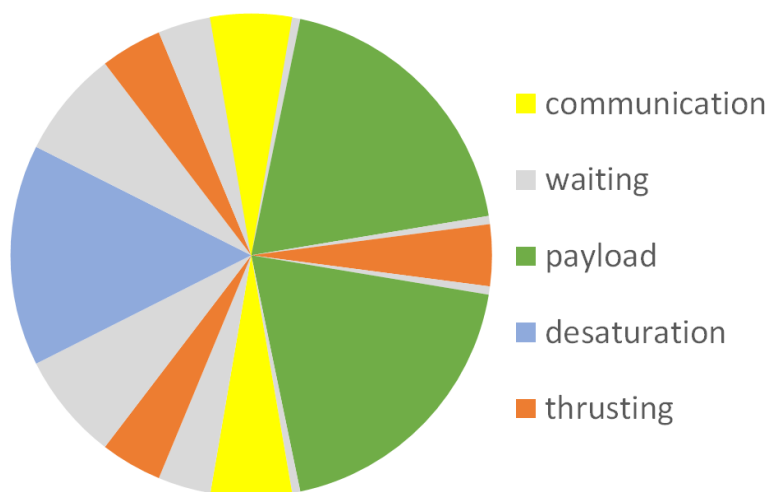


Figure 9.1: Time distribution of modes

¹Nominal mode is when the spacecraft's payload is active and taking pictures

9.2 Sustainability assessment

It was not possible to quantitatively assess sustainability with the tools available to the team. Irregardless, a qualitative assessment is put forth in this section. As suggested in Figure 2.8, the design and the different design phases are evaluated with respect to the non-energy resources used, energy used and emissions to different environmental media.

The design was guided with mission life time in mind, with the final design having a life time of over five years. This is considerably longer than other missions in VLEO, making sure that the emissions and energy used in production of the satellites is not wasted in a quickly disposable machinery but remains operational in orbit for as long as possible.

9.2.1 Non-energy and energy resource usage

Most notable materials used for the design are: copper for electronics, lithium for batteries, gallium and arsenic for photo-voltaic cells and rare metals used in circuit boards. Of these the most critical ones are lithium, gallium and arsenic. With the onset of solar power and electrical cars, the production rates of these materials have increased but still, especially lithium, is not managed sustainably [126]. Indium is obtained as a byproduct during the extraction of zinc, therefore, its supply flow is steady. Gallium is extracted with low efficiency but this is likely to change due to the planned increase in demand with the rise of solar power [127]. The structure is made out of aluminium and constitutes a large part of the total mass of the satellite. Luckily, this material is one of the most abundant in the Earth's crust and its extraction and manufacturing is not energy intensive with respect to alternative materials, such as carbon fibre reinforced composites. Aluminium also allows for the reuse of all waste material as it can be just remelted. Unfortunately, as the satellite disintegrates during re-entry, none of the materials can be reused and are thus lost.

Energy expenditure within the means of influence of the project mostly lays within the logistics and production cycles. For estimates of the energy expenditure during extraction processes more research has to be performed. With regards to logistics, minimising the distance between different manufacturing sites or having all of the production done in a single site would be the best with respect to logistics.

9.2.2 Emissions and waste

The largest emissions come from the launch of the satellites, thus special attention has been directed towards the choice of the launcher to ensure that one with the least emissions is chosen. For the launch Vega launcher was chosen due to its lower environmental footprint. Unfortunately, due to reliability more satellites are launched than are required at the start-of-life for operation, which pushes the weight to the extent that 2 launches are required for each orbital plane, which significantly increased the contribution in this sector of the design. In a perfect world a more tailored launcher could be used.

The GHG emissions are fairly well known for lithium ion battery manufacturing but toxicity aspects are often overlooked [126]. Regrettably, no other more sustainable alternatives are available that would reach similar power density and durability.

9.3 Technical budgets

Certain budgets have shifted during the evolution of the design through different stages. The mass limitation was first taken from CubeSat guidelines mentioning 1.33 kg/U, however, the true limitations are set by launch canisters, which usually allow up to 2 kg/U. As the understanding of the mission developed, it became clear that launching a full constellation as secondary payloads is not feasible. Dedicated launches will be necessary for which the Sat-ELITEs will be a primary payload. Despite of this, the possibility of canister launch concept was not thrown away, as it is great for prototyping and allows the whole mission to work on an existing architecture. For the final canister chosen in Section 8.2, the maximum available satellite mass is 24 kg. The dry mass of one Sat-ELITE is 20.55 kg and the propellant mass is an additional 0.5 kg totalling 21.05 kg.

Volume restraint has changed more significantly. Originally, it was assumed that one unit is exactly 10x10x10 cm. In reality, this is again heavily dependent on launch canisters, but generally it is a bit more in each direction. Instead of dimensions 20x20x30 cm resulting in 12 dm³, the outer dimensions are constrained to 22.9x22.3x36.6 cm, totalling 18.7 dm³. Not all of this space is available for use, as the structure

Table 9.2: Spacecraft technical budgets

	ADCS	Propulsion	Payload	EPS	TCS	Telecom	C&DH	Structures	Total
Mass [%]	9.45	8.47	48.69	20.04	0.97	4.60	1.10	9.11	20.537 kg
Volume [%]	23.28	12.16	27.24	15.07	9.50	6.16	1.68	4.87	13.2 dm ³
Power [%]	-18.99	-44.84	-31.49	100	0	-3.58	-1.10	0	55 W
Cost [%]	24.48	12.98	27.82	12.28	0.37	17.60	1.73	2.78	539,000€

contain elements such as rails on which it slides out. Electrical power budget of 55 W on average was not a hard limit from the start as it is always possible to add more panels. This does however increase the mechanism complexity and deployment risk. For this mission double folded solar panels are used. The configuration was deemed feasible based on other reference missions; anything larger than a double folded solar panel is rarely seen on CubeSats. Cost breakdown is explain in more detail in [Section 9.4](#).

9.4 Cost

The target cost as specified by the customer shall be below 500,000 €. This includes the cost for design, development, test model and its production. The design was done during the DSE and is performed by voluntarily working engineers, thus completed for free. It is assumed that further development could also be done within a university project and can thus be completed at no cost as well. The cost estimation will thus only come from recurring and non-recurring costs per each unit built.

CubeSat projects throughout time have had a large variation in total costs. A satellite by Planet, with comparable mission requirements to Sat-ELITE only costs a few tens of thousands of euros to produce ². They have a benefit in scaling; making a large series of satellites is cheaper per unit than making one large satellite. Thus it is estimated that producing one imaging satellite with similar capabilities would cost around 100,000 € to 200,000 € ³. Sat-ELITE will benefit from this as well, since the constellation size is 174 satellites. There is a potential for production of more constellations if the design is successful, but for now only one is planned due to how quickly technology progresses. There is a relationship between average unit cost, first unit cost, and number of unit made, which can be seen in [Subsection 3.5.4](#) [25]. This will be used once a complete first unit cost is set up.

9.4.1 Recurring costs

Recurring costs are those, that need to be covered for each produced unit. Within the scope of the project these costs include the retail component, production and assembly costs. All components are either commercially available or have a production cost estimated based on similar commercially available products. Component costs can be seen in [Table 9.3](#). Assembly costs are estimated by estimating hourly worker wage and number of hours needed for assembly. Assembly also includes some testing to verify whether each component meets its specifications. The average early-career aerospace engineer salary is 41,000 €. There are approximately 172 working hours per month, so an hourly wage is approximately 20 €. Assembly with testing for a single CubeSat may take a crew of 10 about two weeks, resulting in an assembly cost of 16,000 €.

9.4.2 Non-recurring costs

Non-recurring cost are those that need to be covered only once. These may include the cost of building a clean room, testing equipment or tooling price. It would also be research and development cost, but it has been established that this is done by volunteers. Clean room, testing equipment and tooling prices can vary tenfold, depending on specificity and precision required. These cost are estimated at a conservative estimate of 2,000,000 €.

²<https://www.forbes.com/sites/jonmarkman/2018/05/28/this-maker-of-tiny-satellites-is-disrupting-the-space-industrial-complex/> [Date accessed: 21-06-2019]

³<https://space.stackexchange.com/questions/33740/cost-of-an-earth-observation-cubesat-satellite-like-planet-s-doves> [Date accessed: 21-06-2019]

Table 9.3: Subsystem component budgets

	Name	Number [units]	Mass [kg]	Volume [cm ³]	Heat capacity [J/K]	First unit Cost [€]
ADCS	Reaction wheels	4	0.900	409.4	360	6,500
	Magnetorquer	3	0.150	55.0	57	2,000
	Magnetometer	2	0.170	144.7	204	15,000
	Star tracker	2	0.500	427.5	600	30,000
	IMU	2	0.220	57.9	264	5,000
PROPULSION	IFM nano thruster	2	1.740	1600.0	937	70,000
PAYLOAD	SEEING	1	10.000	3584.0	7500	150,000
EPS	Solar panels 6U	6	2.100	673.0	3360	43,200
	Battery packs	2	1.000	873.3	853	15,000
	Cable harness	1	0.616	500.0	493	1,000
	Distribution + conditioning	1	0.400	324.0	372	7,000
TCS	Aerogel camera blanket	1	0.200	1250.0	400	2,000
TELECOM	X Transmitter	2	0.450	449.3	405	75,000
	X Patch array	2	0.300	229.0	270	4,500
	ISIS communication bundle	1	0.175	129.6	158	9,900
	GPS receiver and antenna	1	0.020	2.4	18	5,500
C&DH	FLASH memory	2	0.038	13.1	21	276
	ISIS OBC	2	0.188	214.3	188	8,800
STRUCTURE	Aluminium structure	1	1.87	641	1795.2	15,000

9.4.3 Other costs

There are other costs relevant to the mission as a whole but not to the budget analysis required by the customer. Certification, transportation, storage, launch, ground stations, mission control, data analyses and marketing are all aspects of this mission, which need to be financed. In general, the mission is designed to be competitive with respect to other Earth imaging platforms, and as such should pay for itself with the valuable data it produces.

9.4.4 Total unit cost

To verify requirement **SYS-OBJ-COST-1**, recurring costs are summed to 549,176€, which is reduced to 371,000€ after a learning curve with a low learning coefficient of 0.95 is applied. Non-recurring costs equal 9,900€ per satellite. Altogether, average cost per one satellite including cost components required by the customer equals 380,900€. The different costs are also summarised in Figure 9.2, where values in the brackets denote the cost after the learning curve is applied.

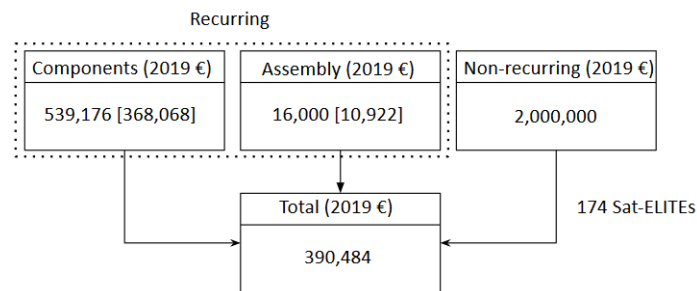


Figure 9.2: Adjusted cost of one satellite unit

9.5 Performance and general characteristics

9.5.1 System configuration

Internal and external configurations are displayed in Appendix E. When referencing the orientation of the satellite the system of reference considered is the one presented in Figure 3.5. The satellite is shown in operational configuration with its panels extended. The bottom-front (2x2x1.6 U) of the spacecraft is occupied by the camera together with the two star sensors mounted on the left side. The power subsystem is placed in the remaining volume of the frontal part. The rear section (1x2x2 U) is distributed between the two parts of

the propulsion system, which are arranged diagonally taking two 0.8 U blocks, and the remaining subsystems. These include ADCS in the top right corner and C&DH together with telecommunication in the bottom left. Double folded solar panels are hinged in radially symmetric positions to optimise the effective area for solar power generation in SSO. VHF/UHF antennas are placed on the rear of the spacecraft diagonally in the units left free from propulsion while both X-band patch antennas are placed on the bottom side. Not every component in the assembly is shown to keep the drawing understandable. The dimensions showed in the drawing are still affected by the contingencies of this phase of the design.

9.5.2 Aerodynamic performance overview

Aerodynamic characteristics of the Sat-ELITE are evaluated with the tools described in [Section 4.2](#). All the result are presented as dimensional forces calculated at the average atmospherical condition and altitude. [Figure 9.3](#) visualise the drag force for all possible pitch and yaw angles. These are defined as standard flight dynamics angle from the system of reference presented in [Figure 3.5](#). It can be seen as the minimum drag occurs for zero pitch and yaw as the solar panels are completely aligned with the flow. On the other hand, the maximum drag is achieved when the solar panel are completely exposed to the flow (26 deg of yaw). Torques around y-axis and z-axis, considering the same coordinate system mentioned above, are showed in [Figure 9.5](#) and [Figure 9.4](#) respectively. It can be seen that the small offset in the centre of mass with respect to the geometric centre cause asymmetries in the graphs.

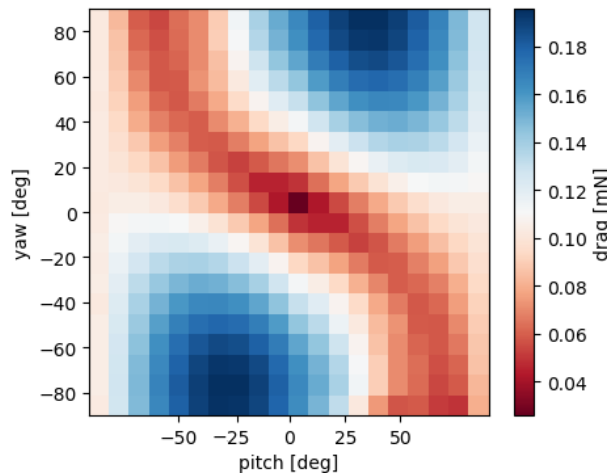


Figure 9.3: Drag force values for different pitch and yaw

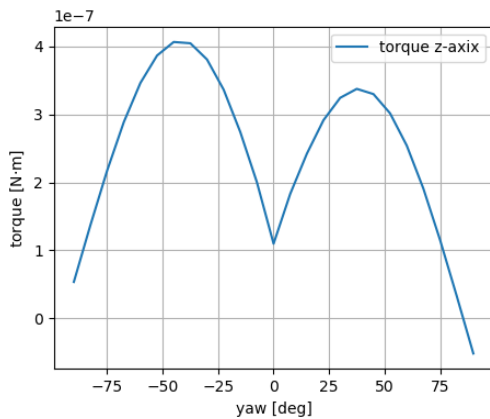


Figure 9.4: Torque around body z-axis

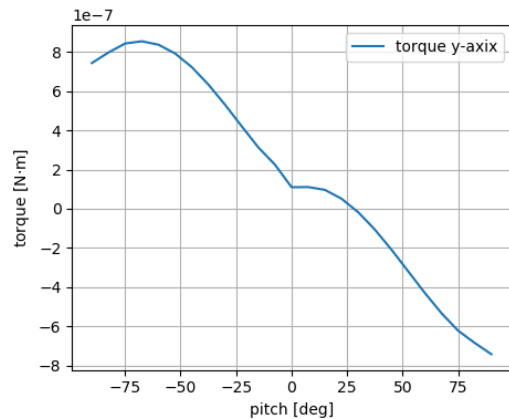


Figure 9.5: Torque around body y-axis

9.5.3 Orbit and subsystem performance overview

Figure 9.6: Subsystem performance characteristics and orbit/constellation parameters

Orbit & Constellation	
Orbit type	SSO
Altitude	332-342 km
Inclination	96.8 deg
Orbital period	91 min
Eccentricity	0
Constellation size	101 per plane
Orbital planes	2
Plane spacing	+/- 45 w.r.t the Sun
Launcher	Vega
Launch method	Piggyback & dedicated

TELECOMMUNICATIONS	
Primary	
Data rate	100 Mbps
Modulation	Filtered OQPSK
SNR margin	8.3 dB
Secondary	
Data rate	9600 bps
Modulation	BPSK/GMSK
SNR margin	62 dB
GPS	
Data rate	9600 bps
Position accuracy	2.5 m
Velocity accuracy	0.1 m/s
Timing accuracy	10 ns

Structure	
Material	Aluminium 7075-T6
Long. frequency	422 Hz
Lat. frequency	66 Hz

EPS	
Average power	55 W
Peak power	110 W
Bus voltages	5/12/28 V
Mass	4.11 kg
Battery capacity	554,400 J
Battery cycles	30,000

Propulsion	
Thruster	2x IFM Nano
Propellant mass	500 g
Thrust level	0.84 mN
Total impulse	14112 Ns
Hot standby	7 W
Liquefaction	16 W
Thrusting mode	80 W

Payload	
GSD	4 m
FoV	6.3x4.3 deg
SNR (panchro)	>256
Bandwidth	475-900 nm

ADCS	
Primary	
Reaction wheels	4x
Star trackers	2x
IMU	2x
Max torque	2.3 mNm
Pointing accuracy	0.08 deg (3 sigma)
Secondary	
Magnetorquers	3x
Magnetometers	2x
Max torque	2.3 mNm
Pointing accuracy	0.08 deg (3 sigma)
Detumbling time	0.35 orbits

C&DH	
Processor speed	400 MHz
RAM	64 MB
Flash memory	384 GB
Databus	I ² C, SpaceWire

TCS	
Hot case	17.5 - 23.8 °C
Cold case	13.2 - 18.9 °C
Payload insulation	1 cm silica aerogel

10. Design assessment

Now that the entire satellite configuration is defined, a reflection on the system's performance is needed. This assessment will begin with a sensitivity analysis in [Section 10.1](#), where the impact of sudden changes in key system parameters on the design is investigated. Secondly, verification and validation procedures are analysed in [Section 10.2](#). A final system-based risk assessment is performed in [Section 10.3](#), with all aforementioned risks assembled on a risk map.

10.1 Sensitivity analysis

Unforeseen events may lead to higher key system parameters (e.g. mass, power) than expected. Therefore, a sensitivity analysis is performed to investigate the robustness of the design to changes in major system parameters. If these major system parameters happened to differ from the expectations, what would be the influence on the complete system? Would the design still meet the requirements or would the result be critical? The result of this analysis is a degree in feasibility of the final design.

10.1.1 Methodology

Mass, power, volume, drag and cost were chosen to be varied in the sensitivity analysis. As theoretically it is possible to force any design to change by using arbitrary changes in parameters, it is instead decided to vary the parameters by a specific magnitude. The magnitude of the change was based on the contingencies presented in [\[128\]](#), as these were the margins taken into account during calculations. Thus, it is a reasonable margin to take as an extra change.

In order to capture the propagation of changes through-out the system (i.e. how changes in subsystem affect one another), a spreadsheet was set up. An excerpt can be seen in [Table 10.1](#). The spreadsheet was organised based on the subsystem hierarchy provided in the N^2 chart seen in [Section 3.4](#). Each subsystem engineer was then asked to evaluate the effect of the given change (i.e. whether it increased, decreased or remained the same) on the design parameters of their subsystem and specify the affected requirements. The extent to which the requirements were affected was also asked to be conveyed by means of a colour grading also explained in [Table 10.1](#). Due to the N^2 hierarchy, the provided changes in subsystem parameters could be used by each subsequent subsystem to quantify the changes in their parameters.

It should be noted, that no non-linear relationships between the subsystems (e.g. the snowball effect) will be investigated, due to the limited time resource available at the current stage of the project.

Table 10.1: Excerpt from the sensitivity analysis spreadsheet

	Mass (+8%)		
	Parameter	Change	Requirements affected
Structures			
	Mass	+	SYS-LCH-FL-1 SYS-LCH-FL-2 SYS-LCH-FL-3 SYS-LCH-FL-4
	Power	0	SYS-SC-STR-4
	Volume	+	
	Cost	+	

	requirement not met
	requirement negatively affected but met

Mass

An increase of the total mass of 8% was considered, while mass distribution and volume parameters remained fixed. The number was based on an up-scaled value of current phase mass contingencies found in [\[128\]](#), as explained in [Subsection 10.1.1](#). Such an increase could be a result of not using COTS (e.g. as in the

case of power and thermal subsystems) or could arise from the fact that the structure is not yet designed for the exact alignment of components ([TR-STR-2],[TR-STR-3]) as shown in [Table 10.3](#).

Based on the spreadsheet, the subsystems to be most affected by a change in mass were found to be ADCS, power and structures. For ADCS it was concluded that the size of the primary actuators was unlikely to change. This has to do with the fact that no significant increase in momentum buildup caused by gravity is expected due to the preserved mass distribution. Furthermore, the existing design already provides slew and pointing accuracy well within the requirements, indicating no need for bigger actuators. Similarly, the Sat-ELITE is expected to still be able to successfully detumble, albeit at a longer time. Alternatively, torque rods equipped with higher magnetic dipole could be used. This extended detumbling time would comply with the detumbling requirements, but would also require more power storage. As detumbling is powered by the batteries, their amount would need to increase, however, as explained in [Subsection 7.3.4](#), the current design is able to provide significantly higher power storage than necessary for detumbling. The total increase in mass can then be accounted for by an increase in the thickness of the structure, without the necessity to change the configuration. The biggest concern arises when considering the maximum mass per unit requirement imposed by the launch canister. The current margin of error is 20%, so an increase in 8% when considering the snowball effect could potentially invalidate the requirement and force to employ a 16 U canister, resulting in extra increase of 2 kg¹ per Sat-ELITE. This could potentially invalidate the total launch mass requirement set by the launcher, as well lead to a different load introduction into the Sat-ELITE during the launch. The margin set in [Subsection 4.5.3](#) shows the ability to accommodate a potential change in launch mass, but the launch load requirements would still remain affected.

Power

A 10% increase of the required total power was considered. Possible causes could be wrong estimate of nominal and peak power cycles of components.

The suggested increase would result in the EPS requiring more solar cells and batteries. This invalidates **SYS-SC-POW-1** and **SYS-SC-POW-3**. So, changes to the design should be considered. With regards to space, fitting batteries is not a problem. However, if the length of the solar panels exceeds its current length it will become problematic, due to an extra hinge adding another 2×3 unit of solar panels to the extending one. This makes the spacecraft harder to control. The solution for this is to add another unfoldable panel to the design or solar cells at the front face of the spacecraft. The option regarding unfolding to the back can be immediately discarded due to the placement of the propulsion system. The relatively large ion plume divergence may cause the added panel to be damaged during thrusting. Furthermore, unfolding to the front increases the drag, hence, the aerodynamic torque is increased. Additionally, the panel will most likely fluctuate, which will pose significant difficulties for the ADCS, negatively affecting the stability requirements. Hence, the changes in the design will induce other subsystems to be affected.

Volume

If all other parameters remain fixed, a 10% increase in volume of the subsystems is likely to only have an effect on the structural and launch requirements, since the current design can accommodate 20% more volume than currently allocated stated in [Section 9.3](#). Possible causes include the already mentioned neglected exact alignment of components.

Drag

For the drag a contingency of 5% was taken into account, which could stem from discrepancies in the atmospheric model considered for drag estimates carried out in [Section 4.2](#).

If this parameter is higher than expected, it will directly influence the requirements corresponding to the lifetime. So, the subsystem affected is the propulsion system. However, due to already using the maximum capabilities of the thrusters, it means that that the thrusting mode will take more time as there is more drag. Hence, more ΔV is required on average for the orbit maintenance and higher aerodynamic torques will be the case. Nonetheless, based on the ADCS and the propulsion system this is not something the spacecraft cannot deal with. Crucially stability of the system is governed by the nature of the disturbances which will not have changed, rather than their magnitude. Hence, this not something that cannot be met, due to having extra ΔV left in case of unforeseen events, which should be more than enough to account for a change of drag of 5 %.

¹<https://www.isispace.nl/wp-content/uploads/2016/02/CubeSat-deployers-Brochure-web-compressed.pdf>
[Date accessed: 23-06-2019]

Cost

Even though contingencies of approximately 10% are accounted for in the cost estimations, the effect of having the unit price increased by another 10%, due to unforeseen costs, which was not accounted for results in a unit price of €586740. However, after applying the learning curve as explained in Equation 3.2. As this yields the constellation cost and from there the unit cost can be established. The change in this parameter will affect [SYS-OBJ-COST-1]. After applying the learning curve the unit cost equals approximately €40000. Hence, the requirement is still met without any implications and compromises.

10.1.2 Conclusion

The requirements affected by the changes are presented in Table 10.2.

As can be seen, changes in power have revealed a certain sensitivity of the design, namely a 10% increase in power is likely to lead to invalidation of two subsystem requirements. Furthermore, it can be seen that despite not proving critical, mass and drag parameters have a negative effect on a large number of requirements. This could suggest a potential degree of sensitivity on these parameters, as the chances of a requirement becoming invalidated in case of a more severe change are higher than for other parameters.

Nevertheless, the design can be considered robust to changes in all but power parameters. Special care and extra tight contingencies on power are therefore recommended for the next phase when considering the EPS subsystem. Additionally, it is recommended to keep tighter than usual contingencies on mass and drag parameters, based on the large number of requirements affected.

Table 10.2: Requirements affected

Mass ↑8%	Power ↑10%	Volume ↑10%	Drag ↑5%	Cost ↑10%
SYS-LCH-FL-1	SYS-SC-POW-1	SYS-SC-POW-1	SYS-SC-SUBSYS-PROP-1	SYS-OBJ-COST-1
SYS-LCH-FL-2	SYS-SC-POW-3	SYS-SC-POW-3	SYS-SC-SUBSYS-PROP-3	
SYS-LCH-FL-3		SYS-SC-ADCS-1	SYS-OBJ-LT-1	
SYS-LCH-FL-4			SYS-OBJ-ORB-2	
SYS-LCH-FL-4				
SYS-LCH-VEH-2				

10.2 Verification and Validation procedures

This section clarifies the V&V procedures performed for all the design choices so far and also identifies future procedures to-be-performed post DSE. Methodology and definitions taken from [129].

10.2.1 Introduction

Different project stages require different V&V procedures and due to the short length of DSE, not all are applicable for the stages covered during this project. Figure 10.1 illustrates this point by displaying all project phases and approximate time stamps of DSE deliverables. It also marks the location where System level requirements should be finalised.

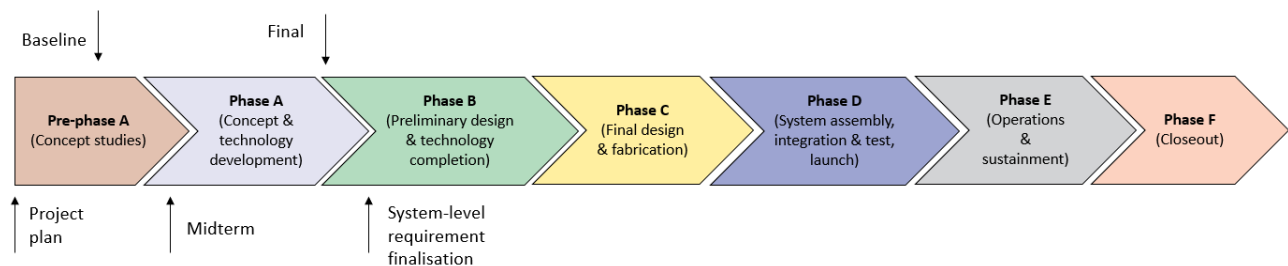


Figure 10.1: Project life cycle phases

Judging by [Figure 10.1](#), the team cannot truly verify the requirements, or validate the product as the project has not reached a state where the requirements should even be finalised. It is possible though to indicate whether the team is on track to meet them given the current level of detail and also discuss requirement definition validity and mathematical model verification, possibly validation. This is done in [Subsection 10.2.2](#). A future outlook with V&V procedures performed by the team at later phases of the project is discussed in [Subsection 10.2.3](#).

10.2.2 Current progress

Throughout the project, the systems engineers have closely collaborated with department chiefs to define and update system and subsystem requirements. These are presented in [Appendix A](#), where requirements that are well on track to be met are marked in green, ones that require further analysis are marked in yellow, and requirements that the team has identified to be impossible to meet would be marked in red. Effectively, red requirements would kill the project. Fortunately, no requirement has been identified to be red.

Before beginning work on various simulations, team members estimated the approximate time required to finish and verify them and discussed with the risk officer whether it is feasible to achieve the intended goal. Taking these aspects into account, the team avoided Finite Element Analysis (FEA) software as there simply was no time to verify the approach and acquire meaningful results. The model verification approach for each method is described in its corresponding chapter or section throughout the report to maintain the flow of the text.

10.2.3 Future plan

From the very beginning of the project, the team took the verifiability and validity of the particular analysis approaches into account. However, the project only spans ten weeks, which limits what is realistically achievable. In many cases this led to pursuing more simplistic models that cannot fully meet the requirements, however can be properly justified and analysed. More sophisticated models that would be pursued in the future are:

- **Structures** would perform vibration & frequency analysis using FEA software to validate launcher requirements. Many FEA software packages exist and such a model can be validated either by papers discussing similar approaches or by performing a vibration test.
- **ADCS** intends to use PEET by ESA and Aerospace Blockset CubeSat Simulation Library by MathWorks to develop a full day-in-the-life simulation that simulates the spacecraft's operation in orbit and monitor the ADCS's performance.
- **Aerodynamics** department has already created a powerful tool based on ray-tracing, however due to the stochastic nature of the particles motion a Monte Carlo simulations would be performed. The results would be compared to the existing tool, which has been validated. However, note that the final validation requires prototype flight measurements.
- **TCS** has identified a tool by ESA called ESATAN-TMS, which is used for full scale thermal modelling and requirement verification. However, a problem identified so far for thermal modelling is the lack of information about input parameters. This highlights the need to perform tests to actually validate the system.
- **Orbit management & propulsion** plan to model orbital mechanics including as many disturbances as possible to verify the mission lifetime requirement. Possible tool to do this is tudat developed at TU Delft.

Furthermore, the tests that shall be performed to verify the subsystem and system requirements are discussed in [Section 11.3](#). Once the performance of the system is verified, a prototype Sat-ELITE shall be launched to validate compliance with stakeholder needs and the MNS.

10.3 Final risk assessment

Lastly, there has to be a proper reflection on the risks. Throughout this report, a multitude of subsystem based risks have been discussed. This however leaves the system risks unaddressed, which is why there will now follow a discussion of these risks.

- **[TR-OP-7]** Production mistakes could have a large impact on the mission, depending on the severity of the mistake. This is why quality assurance and testing have to be properly managed during production. This is taken into account when designing the Project Design & Development Logic (PDDL), as can be seen in [Section 11.1](#).
- **[TR-OP-8]** During transport to the launch site, incorrect transport handling could cause damage to the Sat-ELITE. This is why proper care should be taken in the transport, however also pre-flight checks should be done to check whether the Sat-ELITE is damaged. So, the damage can be repaired.
- **[TR-OP-10]** A wrong control command could be given, either due to a software bug, or human erroneous input. The impact of this could be marginal if it results in some wasted mission time, however catastrophic if it results in an unwanted deorbit. This is why double authorisation will be implemented, which will also protect the system against malicious activities.

With this all the risks have been defined. An overview of the complete list is presented in [Appendix D](#)

The next step is to insert the risks into a risk map, where likelihood is plotted against impact, to get a feel of the overall severity of the risks. This risk map can be seen in [Table 10.3](#). These risks are displayed with the severity after mitigation processes have been applied as explained throughout the report. Note that the TR-prefixes are removed, since they would clutter up the graph. As can be seen, there is one major risk remaining: **[TR-STR-3]**, Improper subsystem mounting. This high risk might seem like a problem, but this is because the mounting structures have not been designed yet. This means that care has to be taken to mitigate this risk when designing these structures. This will be done by making sure proper safety factors are taken into account in the models and multiple attachment points need to be introduced to eliminate SPF. These mitigation processes will probably move this risk down to the bottom right of the risk map, but this has not been shown yet, since the processes have not been actually implemented. However, this would leave no significant risks that would kill the design.

Table 10.3: Risk map showing final risks

Highly likely	OP-3, OP-4			red
Likely				
Possible	TC-4			STR-3
Unlikely	STR-1	PROP-3, CDH-3, TC-3, EPS-1, EPS-3, TCS-1, OP-6	PROP-4, TC-2, STR-2, OP-7, OP-8	
Highly unlikely	OP-5, OP-9 <i>green</i>	ADCS-4, CDH-2, TCS-2, EN-2	PROP-1, PROP-2, PL-2, ADCS-3, EPS-2, OP-10	PL-1, ADCS-1, ADCS-2, ADCS-5, CDH-1, TC-1, TCS-2, EN-1, EN-3, OP-1, OP-3
Mitigated	Negligible	Marginal	Critical	Catastrophic

Table 10.4: Legend for the risk maps

Highly likely	Concepts are feasible in theory.
Likely	Concepts are based on working laboratory models.
Possible	Concepts are based on existing non-flight engineering.
Unlikely	Concepts are extrapolated from existing flight designs.
Highly unlikely	Concepts are based proven flight designs.
Negligible	Risk is only an inconvenience to the mission.
Marginal	Risk causes degradation in secondary mission or small reduction in technical performance.
Critical	Risk causes big reduction in technical performance where mission success is questionable.
Catastrophic	Risk causes complete mission failure resulting in a non-achievement of the objective.

11. Post-DSE developments

The span of the DSE is 10 weeks but it does imply that the project is done. In this chapter the team outlines the initial post-DSE plan in the form of a PDDL, project Gantt chart. Furthermore, a production and testing plan is sketched out for the later stages of development.

11.1 Project Design & Development Logic

To organise the future phases and activities of this project the PDDL is created, and can be seen in [Figure F.1](#) presented in [Appendix F](#). The diagram is divided into six main consecutive phases identified by the different blocks visible in the legend in [Figure 11.1](#). The different phases are connected sequentially with standard arrows to define the order of steps. On the right margin, all the managerial tasks are presented and these need to be carried out along the whole development of the spacecraft.

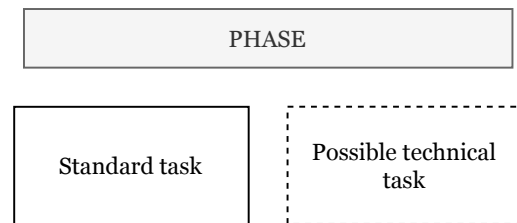


Figure 11.1: Legend for the PDDL

The first phase block includes all the activities necessary to perform the detail design of the Sat-ELITE. It is important to note that at this stage it is impossible to exactly know the necessary technical tasks as the team awaits feedback from the final review. It is even possible that the concept chosen could be changed. For this reason, some specific technical tasks that at the present stage are considered fundamental are planned as probable and indicated with a dashed contour line, as can be seen in [Figure 11.1](#). Also, possible iteration loops are considered at every key stage of the design in case the requirements are not met.

Once the design is complete, the production of the prototype and the test phase can begin. The in-house production organisation and prototyping can take place in parallel to the ordering of COTS components. The plan is to start testing the subsystem separately to avoid continuing the assembly with defective components.

The next phase includes the design and building of the assembly line as well as testing of the complete satellite. Some of these tests are outlined in [Section 11.3](#). Now that the prototype satellite is ready to be launched, all the related organisational tasks are performed to allow the satellite to piggyback on a launcher. Once launched, all possible lifetime scenarios are simulated and data about them is collected. After the nominal capabilities are verified, stress tests are performed to test the limits of the spacecraft.

The conclusions from the obtained data could be implemented in the design if needed and the system could be validated. The last step needed to start production is the design of the production line. This includes the organisation of tools, crew and check-up on the quality of the products delivered. This ends the main phase of project development, although small improvements such as software updates can be done throughout the whole mission duration.

11.2 Project Gantt chart

To get a better overview of how the project will be executed post DSE, the PDDL diagram serves as a baseline for the definition of the project Gantt chart. According to NASA's CubeSat guide [\[130\]](#), a reasonable time frame till the end of production is about two years, which was used as an estimate for this project. The final project Gantt chart is shown in [Appendix G](#). Note that the managerial tasks have been collapsed, as they would overflow the page and their place in the Gantt chart is not that important as they are continuous tasks that happen for the entire project.

11.3 Production and testing plan

The previous two sections defined a high level timeline of tasks that need to be done to finish the project after the initial ten weeks. A major fraction of these tasks is related to the production of testing both the prototype and constellation. These aspects in particular are considered in more detail in this section.

11.3.1 Prototype

Besides validating the system, the prototype spacecraft will be extremely useful to establish integration and assembly procedures for future production of the constellation. All tests will also be performed on the prototype to decrease the total production time. Testing wise, since everything besides the structure of the satellite are COTS components, many components or even subsystem tests are performed by the manufacturers. However, the quality assurance policy and quality standards that they meet depends per company. It is difficult to estimate what tests would be required on a component/subsystem level before any formal contact with the manufacturers is established. However, the team has designed a test decision making flow diagram that could help deal with this in the future. It is given in [Figure 11.2](#).

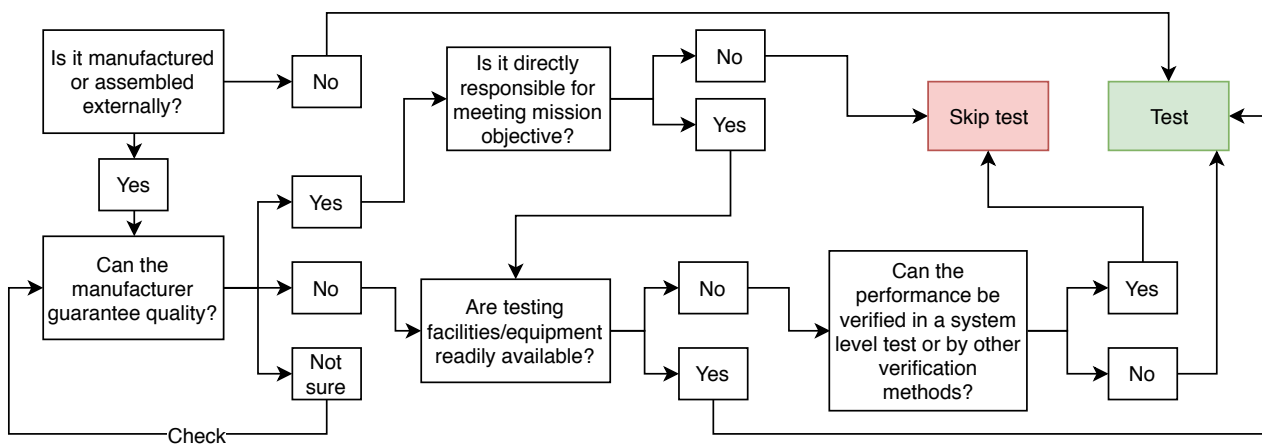


Figure 11.2: Testing decision making flow diagram

On a system level, eight tests were identified that would be required to meet the requirements and ensure robust integration strategy for the production phase.

SYS-TEST-1: Flat sat integration test A satellite contains many electrical components that are linked to each other by wires. For this correct integration is crucial as otherwise signals might be fed to wrong locations or could even short-circuit components. The idea of a flat sat integration test is to lay out all the components on a flat surface and deal only with integration of electrical connections without impeding visibility or accessibility. In this way the assembly procedures can be extensively checked and updated.

SYS-TEST-2: Full assembly test Once electrical component integration procedures are finished, the team can proceed with testing the assembly of the full satellite. The purpose of this test is to verify that the assembly procedures are complete, that everything fits and aligns as expected and that visual inspection or accessibility of components is possible when required.

SYS-TEST-3: Simulated communications test By communicating with a ground station from a substantial distance, the whole telecommunications subsystem can be verified. The data sent can be arbitrary, however a good idea is to send on-board sensor data thus verifying their performance as well.

SYS-TEST-4: Complete charge cycle In this test the spacecraft should demonstrate the ability to charge and discharge batteries. In best case, the charging should be performed with the spacecraft's solar panels. Besides this, also the ability to stop charging once the batteries are full as well as the ability to enter safe mode once the batteries reach Depth of Discharge (DoD) should be demonstrated.

SYS-TEST-5: Command execution test The intention of this test is to perform every command that can be done by the spacecraft. Besides fully testing the command & data handling unit, this allows to verify that any of the commands do not cause any sort of damage to the spacecraft.

SYS-TEST-6: Thermal vacuum test This test should verify the thermal management system by showing that the spacecraft is able to operate in a space-like environment.

SYS-TEST-7: Vibration test During launch a spacecraft experiences violent vibrations. In order to make sure that the performance of the spacecraft is not hindered, a dedicated vibration test should be performed that simulates the launch conditions of the chosen launch vehicle.

SYS-TEST-8: Thrust test Using two thrusters aligned off the centre of mass will introduce a disturbance torque due to misalignments. Besides verifying manufacturer properties, a thrust test is performed to measure

the magnitude of the thrust disturbance torque.

11.3.2 Constellation

If the development up to the launch of the prototype is successful, the performance of the system shall be validated and assembly procedures shall be clearly defined. The next challenge after that is assembling tens of satellites as efficiently as possible. Given the product series, the most applicable assembly approach is line production. The idea is that the work is divided in equally time constrained work packages and assigned to different stations. Each work package is executed by capable teams of technicians. The product moves along from station to station while the teams stay at the same place and the work packages per team do not vary. This approach allows to establish habits and improve the efficiency of each station over time. Quality assurance procedures are integrated after each station to assure the performance of each satellite. The line assembly approach is summarised in [Figure 11.3](#).

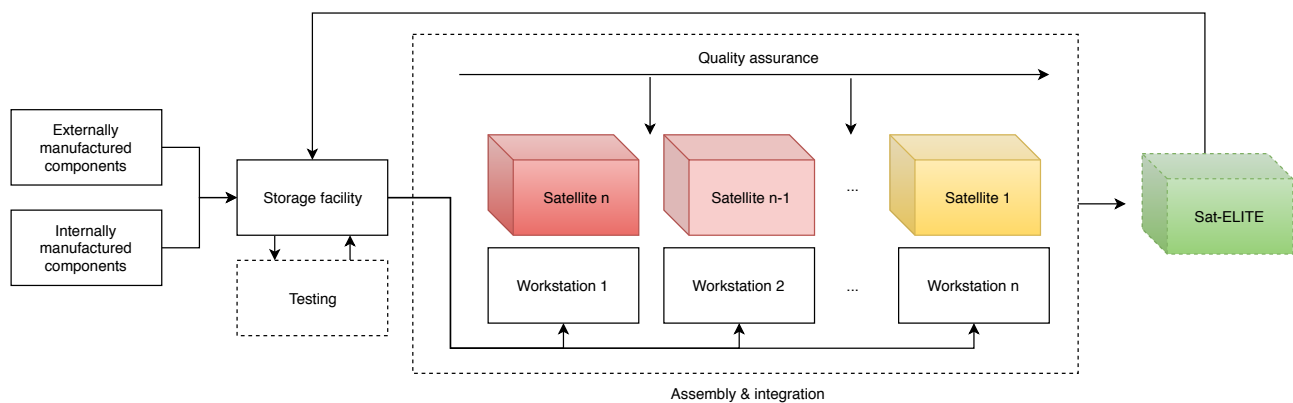


Figure 11.3: Constellation assembly block diagram

12. Conclusion & Recommendations

This project was spearheaded by the mission to challenge existing Earth observation platforms, utilising the VLEO concept. To achieve that, extensive market analysis was performed, which identified a design direction that could lead to an edge over the current competitors, namely maximising the lifetime.

This resulted in the definition of the main objective for the project - to design a Very Low Earth Orbit CubeSat for Earth observation with a spatial resolution of less than four meters, a pointing accuracy of less than 0.25 deg and a lifetime of more than five years. It was identified that micro-propulsion, and attitude determination and control capabilities of the spacecraft were critical to fulfilling this objective and required special focus.

With the goal in mind, different design concepts were established and traded off during the conceptual phase of the project. Special care was taken not to discard potentially winning concepts due to parameter inconsistencies, so extensive sensitivity analysis was performed. As a result, the Extended Lifetime Innovative Technology Satellite - or briefly, the Sat-ELITE - was conceived. The 12U 3x2x2 concept sports the versatile **SEEING 7m** camera, which provides an excellent compromise between achieving the spatial resolution and spanning the largest field of view. The latter is especially beneficial for a decreased constellation size, which allowed the Sat-ELITE design to outperform its rivals in sustainability and cost evaluations.

The next design phase was then entered, and the concept was developed in detail. Sun-synchronous orbit was chosen to provide consistent power, such that imaging phase can be maximised. This, combined with innovative data management methods, allowed to achieve an Earth coverage of more than 99% at a temporal resolution of 12 hours. The attitude determination and control setup was based on the current state-of-the-art of precision CubeSat systems, which have shown the ability to comply with the stringent pointing accuracy and stability requirements. The Sat-ELITE was further supplemented by the novel Field-emission electric propulsion system, which pushed the design over the five year lifetime goal.

This report therefore concludes that an innovative and competitive design, capable of challenging the current Earth observation platforms, has been presented in the form of the Sat-ELITE. A constellation of 202 Sat-ELITEs would provide Earth coverage of more than 99 % at a spatial and temporal resolutions of four meters and twelve hours, respectively. The life time of individual satellites would be no less than five years and the total cost per unit will converge to less than 390 000 € after the effects of large scale production have been quantified.

Whilst the team is confident in the potential of the design, a number of recommendations can be proposed. The report already features technical suggestions aimed at the improvement of the Sat-ELITE, categorised per subsystem. Additionally, the team recommends a full-blown integrated simulation, combining inputs from all the subsystems to achieve automated iteration and complete verification of the system. Furthermore, logistic and external regulation aspects were neglected at the current stage of the project. It is therefore recommended to attempt to quantify the costs associated with logistics in order to arrive at more precise mission cost estimates. Additionally, compliance with external regulations must be checked to ensure the validity of the entire mission.

The team also recommends pushing innovation in payload, propulsion and telecommunication subsystems. The imaging instruments are actively being miniaturised and together with developments in super resolution could allow for an increase in spatial resolution at a reduced size and power consumption. Alternatively, the orbit could be brought higher, resulting in an increase in lifetime. Similarly, the emerging field of electric micro propulsion offers possibilities of flying even longer and with more optimised power consumption could allow to image during thrusting phase. At the same time, exploring novel telecommunication possibilities, such as laser communication, can allow for less data loss when transmitting.

Overall, the team is confident that the Sat-ELITE concept can remain competitive in future markets if a close eye is kept on the fields of miniature earth imaging and propulsion technology. Equipped with the new components the Sat-ELITE will still provide greater lifetime than its potential competitors, whilst reaping the explained innovation benefits.

Bibliography

- [1] Unknown, “Cubesat market by application, end user, size, subsystem, and region - global forecast to 2023,” tech. rep., Markets and Research, December 2018.
- [2] M. Safyan, “Overview of the planet labs constellation of earth imaging satellites.” Planet Labs, March 2015.
- [3] A. van Boeijen, J. Daalhuizen, Y. Zijlstra, and R. van der Schoor, *Delft Design Guide*. BIS Publisher, 2014.
- [4] “Satellite-based Earth observation: Market prospects to 2025,” tech. rep., Euroconsult, 2016.
- [5] C. Brekke and A. Solberg, “Oil spill detection by satellite remote sensing,” *Remote Sensing of Environment*, 2005.
- [6] H. Greidanus, “Satellite imaging for maritime surveillance of the european seas,” *Remote Sensing of the European Seas*, 2008.
- [7] Unknown, “Cubesat market size, share, report, analysis, trends & forecast to 2026,” tech. rep., Market-Watch, January 2019. Full report is paid, only used abstract.
- [8] Unknown, “Cubesat market by application, end user, size, subsystem, and region - global forecast to 2023,” tech. rep., Markets and Markets, December 2018. Full report is paid, only used abstract.
- [9] B. Lal, E. de la Rosa Blanco, J. R. Behrens, B. A. Corbin, E. K. Green, A. J. Picard, and A. Balakrishnan, “Global trends in small satellites,” tech. rep., Science & Technology Policy Institute, July 2017.
- [10] G. Denisa, A. Claveriea, X. Pascob, J.-P. Darnisc, B. de Maupeoua, M. Lafayed, and E. Morela, “Towards disruptions in Earth observation? new Earth observation systems and markets evolution: Possible scenarios and impacts,” tech. rep., Acta Astronautica, 2017.
- [11] C. Niederstrasser, “Small launch vehicles – a 2018 state of the industry survey,” tech. rep., MNorthrop Grumman Corporation, 2018.
- [12] P. Mani, “Computational imaging for earth surveillance,” tech. rep., TU Delft, 2017.
- [13] D. H. Meadows, D. H. Meadows, J. Randers, and W. W. Behrens III, “The limits to growth: a report to the club of Rome (1972),” *Google Scholar*, 1972.
- [14] G. H. Brundtland, M. Khalid, S. Agnelli, and S. Al-Athel, “Our common future,” *New York*, 1987.
- [15] United Nations, “Transforming our world: The 2030 agenda for sustainable development,” *Resolution adopted by the General Assembly*, 2015.
- [16] S. Madry, P. Martinez, and R. Laufer, *Innovative Design, Manufacturing and Testing of Small Satellites*. Springer, 2018.
- [17] N. Jean, M. Burke, M. Xie, W. M. Davis, D. B. Lobell, and S. Ermon, “Combining satellite imagery and machine learning to predict poverty,” *Science*, vol. 353, no. 6301, pp. 790–794, 2016.
- [18] J. Huesing, “Introducing eco-design to ESA – an overview of the activities towards a coherent eco-design approach,” *5th CEAS Air & Space Conference*, pp. 1–11, 2015.
- [19] ISO14044:2006, “Environmental management – Life cycle assessment – Requirements and guidelines,” tech. rep., ISO, 2006.
- [20] A. J. Dababneh, N. Swanson, and R. L. Shell, “Impact of added rest breaks on the productivity and well being of workers,” *Ergonomics*, vol. 44, no. 2, pp. 164–174, 2001.
- [21] M. Ross and J. Vedda, “The policy and science of rocket emissions,” April 2018.
- [22] K. Mohanakumar, *Stratosphere troposphere interactions: an introduction*. Springer Science & Business Media, 2008.
- [23] S. A. Whitmore, D. P. Merkley, M. I. Judson, and S. D. Eilers, “Development and testing of a green monopropellant ignition system,” in *49th AIAA/ASME/SAE/ASEE Joint Propulsion Conference*, p. 3967, 2013.
- [24] W. Deininger, C. Gilmore, M. Hale, C. McLean, V. Moler, R. Osborne, B. Porter, A. Brown, M. Marlow, D. Rand, *et al.*, “Description of the green propellant infusion mission (gpim) mission system,” in *2014 IEEE Aerospace Conference*, pp. 1–13, IEEE, 2014.
- [25] J. R. Wertz, D. F. Everett, and J. J. Puschell, *Space Mission Engineering: The New SMAD*. Space

Technology Library, 2015.

- [26] D. O. de Morais Alves Rondão, “Modeling and Simulation of the ECOSat-III Attitude Determination and Control System,” Master’s thesis, Instituto Superior Técnico, Lisbon, Portugal, 2016.
- [27] P. Reijneveld, “Design of the Attitude Determination and Control Algorithms for the Delfi-n3Xt,” Master’s thesis, Delft University of Technology, Delft, Netherlands, 2012.
- [28] W. J. Larson and J. R. Wertz, *Space Mission Analysis and Design (second Edition)*. Dordrecht/Boston/London: Kluwer Academic Publishers, 1996.
- [29] R. Noomen, “Lecture notes in Orbital Mechanics,” 2019.
- [30] V. A. Chobotov, *Spacecraft Attitude Dynamics and Control*. Malabar, Florida: Krieger Publishing Company, 1991.
- [31] N. Laurendeau, *Statistical Thermodynamics: Fundamentals and Applications*. Cambridge University Press, 2005.
- [32] NASA, Washington, DC 20546-0001, *Low Earth Orbit Spacecraft Charging Design*, 2007.
- [33] E. N. Doornbos, “Thermospheric density and wind determination from satellite dynamics,” Master’s thesis, Delft University of Technology, 2011.
- [34] J. Virgili, P. C. Roberts, S. Hobbs, and J. Kingston, “Aerostability for low altitude flying cubesats,” *IAA-CU*, 2013.
- [35] S. Celik, *Analysis of single phase fluid flow and heat transfer in slip flow regime by parallel implementation of lattice boltzmann method on GPUs*. PhD thesis, 09 2012.
- [36] D. M. Prieto, B. P. Graziano, and P. C. Roberts, “Spacecraft drag modelling,” *Progress in Aerospace Sciences*, vol. 64, pp. 56–65, 2014.
- [37] D. P. Drob, J. T. Emmert, J. W. Meriwether, J. J. Makela, E. Doornbos, M. Conde, G. Hernandez, J. Noto, K. A. Zawdie, S. E. McDonald, *et al.*, “An update to the horizontal wind model (hwm): The quiet time thermosphere,” *Earth and Space Science*, vol. 2, no. 7, pp. 301–319, 2015.
- [38] E. K. Sutton, “Normalized force coefficients for satellites with elongated shapes,” *Journal of Spacecraft and Rockets*, vol. 46, 2009.
- [39] J. M. Picone, A. E. Hedin, and D. P. Drob, “Nrlmsise-00 empirical model of the atmosphere: Statistical comparisons and scientific issues,” *Journal of Geophysical Research*, vol. 107, 2002.
- [40] C. Pardini, L. Anselmo, K. Moe, and M. Moe, “Drag and energy accommodation coefficients during sunspot maximum,” *Advances in Space Research*, vol. 45, p. 638–650, 2010.
- [41] NASA/TP—2018–220027, “Small spacecraft technology state of the art,” tech. rep., NASA, 2018.
- [42] K. Lemmer, “Propulsion for CubeSats,” *Acta Astronautica*, vol. 134, pp. 231 – 243, 2017.
- [43] M. Leomanni, A. Garulli, A. Giannitrapani, F. Scortecchi, “Propulsion options for very low earth orbit microsattellites,” *Acta Astronautica*, vol. 133, pp. 444 – 454, 2017.
- [44] A. D. Ketsdever and M. M. Micci, *Micropropulsion for small spacecraft*. American Institute of Aeronautics and Astronautics, 2000.
- [45] J. Mitterauer, “Indium - an alternative propellant for feep-thrusters,” July 2001.
- [46] M. Tajmar and C. A. Scharlemann, “Development of electric and chemical microthrusters,” *International Journal of Aerospace Engineering*, vol. 2011, May 2011.
- [47] T. Schönher, D. Krejci, A. Reissner, and B. Seifert, “Flight data of the ifm nano thruster on recent satellite applications,” May 2019.
- [48] D. Krejci, A. Reissner, B. Seifert, D. Jelem, T. Hörbe, P. Friedhoff, and S. Lai, “Demonstration of the ifm nano feep thruster in low earth orbit,” May 2018.
- [49] M. Tajmar and A. Genovese, “Experimental validation of a mass- efficiency model for an indium liquid-metal ion source,” *Applied Physics A*, vol. 76, pp. 1003–1006, April 2003.
- [50] B. Seifert, N. Buldrini, T. Hörbe, and F. Plesescu, “In-orbit demonstration of the indium-feep ifm nano thruster,” May 2018.
- [51] M. Tartz, E. Hartmann, R. Deltschew, and H. Neumann, “Thrust-vector tilting caused by grid misalignment,” *International Electric Propulsion Conference*, October 2001.

- [52] B. Seifert, A. Reissner, D. Jelem, and T. Hörbe, “Development of a low cost ppu for feep electric propulsion using cots components,” *E3S Web of Conferences*, vol. 16, p. 15003, January 2017.
- [53] J. Guo, L. Monas, and E. Gill, “Statistical analysis and modelling of small satellite reliability,” *Acta Astronautica*, vol. 98, pp. 97–110, [May-June] 2014.
- [54] *Falcon 9 Launch Vehicle Payload User’s Guide*, scm 2008 [U+2010]010 rev. 1 ed., 2009.
- [55] E. Perez, *Soyuz User’s Manual*, issue 2, revision 0 ed., March 2012.
- [56] ESSB-HB-E-003 Working Group, *Vega User’s Manual*, issue 4, revision 0 ed., April 2014.
- [57] C. Foster, J. Masony, V. Vittaldevz, L. Leungx, V. Beukelaers, L. Stepank, and R. Zimmerman, “Differential drag control scheme for large constellation of planet satellites and on-orbit results,” tech. rep., Planet, 2018.
- [58] J. Bullard, “Satellite drag analysis using direct simulation monte carlo (dsmc),” Master’s thesis, University of Hertfordshire, 2018.
- [59] S. A. Rawashdeh and J. James E. Lumpp, “Aerodynamic Stability for CubeSats at ISS Orbit,” *Journal of Small Satellites*, vol. 2, no. 1, pp. 85–104, 2013.
- [60] J. Auret, “Design of an aerodynamic attitude control system for a cubesat,” Master’s thesis, Stellenbosch University, 2012.
- [61] A. Kamp, *AE4-880 Space Instrumentation Engineering*. TU Delft, 2007.
- [62] Planet Labs, “Planet imagery product specifications,” August 2018.
- [63] J. M. Maciel, F. Rodríguez, J. Casillas, G. M. Mora, F. G. P. Lecona, and V. M. D. Ramírez, *Optical Interferometry: Digital Processing Techniques for Fringe Analysis*. Houghton Mifflin Harcourt, 2009.
- [64] A. Bunch, Bryan H; Hellemans, *The History of Science and Technology*. Houghton Mifflin Harcourt, 2004.
- [65] K. Nair, *Atomic Spectroscopy*. MJP Publisher, 2019.
- [66] J. Fraden, *Handbook of Modern Sensors*. Springer, 1993.
- [67] D. Litwiller, “CCD vs. CMOS: Facts and Fiction.” *Photonics Spectra*, 2001.
- [68] J. Greivenkamp, *Field Guide to Geometrical Optics*. SPIE Press, 2004.
- [69] DSE Group 9, “Advanced nano telescope a cornerstone solution for earth observation,” tech. rep., TU Delft, 2011.
- [70] G. W. L. Kirkpartick, *Physics: A World View (2nd ed.)*. Harcourt Brace College Publishers, 1992.
- [71] F. Tupin, J. Inglada, and J. Nicolas, *Remote Sensing Imagery*. Digital signal and image processing series, Wiley, 2014.
- [72] H. J. Kramer, *Observation of the Earth and Its Environment: Survey of Missions and Sensors*. Springer, 1994.
- [73] J. Richards, *Remote sensing digital image analysis*. Springer, 1986.
- [74] Y. J. Kaufman, “Atmospheric effects on remote sensing of surface reflectance,” tech. rep., University of Maryland and Goddard Laboratory for Atmospheric Sciences, 1984.
- [75] D. Ju, “Attitude Control Subsystem Design of the Stable and Highly Accurate Pointing Earth-imager,” Master’s thesis, Delft University of Technology, Delft, Netherlands, 2017.
- [76] R. R. Geyl, J. Rodolfo, and J. Girault, “High performance optical payload for microsatellite,” tech. rep., Safran Electronique & Defence, 2011.
- [77] C.-I. CHANG, *Hyperspectral Data Exploitation: THEORY AND APPLICATIONS*. JOHN WILEY SONS, 2007.
- [78] U. Jain, “Characterization of cmos image sensor,” Master’s thesis, Delft University of Technology, Delft, Netherlands, August 2016.
- [79] M. Martens, “Super-resolution of proba-v images using convolutional neural networks,” tech. rep., European Space Agency, 2018.
- [80] K. Murthy, M. Shearn, B. D. Smiley, A. H. Chau, and J. Levine, “Skysat-1: very high-resolution imagery from a small satellite,” tech. rep., SPIE Remote Sensing, 2014.

- [81] ESSB-HB-E-003 Working Group, *ESA pointing error engineering handbook*. ESA, July 2011.
- [82] D. S. Bayard, "State-space approach to computing spacecraft pointing jitter," *Journal of Guidance, Control, and Dynamics*, vol. 27, no. 3, pp. 426–433, 2004.
- [83] T. Rose, D. Rowen, S. LaLumondiere, N. Werner, R. Linares, A. Faler, J. Wicker, C. Coffman, G. Maul, D. Chien, A. Utter, R. Welle, and S. Janson, "Optical Communications Downlink from a 1.5U CubeSat: OCSD Program." Aerospace Corporation, August 2018.
- [84] C. C. Liebe, "Star trackers for attitude determination," *IEEE Aerospace and Electronic Systems Magazine*, vol. 10, no. 6, pp. 10–16, 1995.
- [85] Ping Wang and Y. B. Shtessel, "Satellite attitude control using only magnetorquers," in *Proceedings of the 1998 American Control Conference*, vol. 1, pp. 222–226 vol.1, June 1998.
- [86] M. Lovera, "Magnetic satellite detumbling: The b-dot algorithm revisited," in *2015 American Control Conference*, pp. 1867–1872, July 2015.
- [87] E. Wan, "Sigma-point filters: An overview with applications to integrated navigation and vision assisted control," in *2006 IEEE Nonlinear Statistical Signal Processing Workshop*, pp. 201–202, Sep. 2006.
- [88] T. E. Humphreys, M. L. Psiaki, E. M. Klatt, S. P. Powell, and P. M. Kintner, "Magnetometer-based attitude and rate estimation for spacecraft with wire booms," *Journal of Guidance, Control, and Dynamics*, vol. 28, no. 4, pp. 584–593, 2005.
- [89] H. Kurokawa, "A geometric study of single gimbal control moment gyros," *Report of Mechanical Engineering Laboratory*, vol. 175, pp. 135–138, 1998.
- [90] I. Gavrilovich, *Development of a robotic system for CubeSat Attitude Determination and Control System ground tests*. PhD thesis, Université Montpellier, 2016.
- [91] C. Jéger, "Determination and compensation of magnetic dipole moment in application for a scientific nanosatellite mission," Master's thesis, KTH Royal Institute of Technology, Stockholm, Sweden, 2017.
- [92] M. Leomanni, "Comparison of control laws for magnetic detumbling," October 2012.
- [93] Astos Solutions, *Pointing Error Engineering Software Framework*. ESA, March 2017.
- [94] P. Fortescue and J. Stark, *Spacecraft systems engineering*. Chichester: Wiley, 1995.
- [95] J. Eickhoff, *Onboard Computers, Onboard Software and Satellite Operations*. Springer, 2011.
- [96] J. Bouwmeester, "AE3534-Spacecraft Technology: Command and Data Handling Lecture notes." TU Delft.
- [97] J. B. S. de Jong, G.T. Aalbers, "Improved command and data handling system for the delfi-n3xt nanosatellite," tech. rep., TU Delft, 2008.
- [98] J. R. Wertz, *Mission Geometry: Orbit and Constellation Design and Management*. Microcosm Press and Springer, second ed., 2009.
- [99] M. Soukup, J. Gailis, D. Fantin, A. Jochemsen, C. Aas, P. Baeck, I. Benhadj, S. Livens, B. Delauré, M. Menenti, *et al.*, "Hyperscout: Onboard processing of hyperspectral imaging data on a nanosatellite," in *Proceedings of the Small Satellites, System & Services Symposium (4S) Conference, Valletta, Malta*, vol. 30, 2016.
- [100] S. Qian, *Optical satellite data compression and implementation*. 2013.
- [101] G. Yu, T. Vladimirova, and M. Sweeting, "Image compression systems on board satellites," *Acta Astronautica*, vol. 64, no. 9-10, pp. 988–1005, 2009.
- [102] M. D. King, S. Platnick, W. P. Menzel, S. A. Ackerman, and P. A. Hubanks, "Spatial and temporal distribution of clouds observed by modis onboard the terra and aqua satellites," *IEEE Transactions on Geoscience and remote sensing*, vol. 51, no. 7, pp. 3826–3852, 2013.
- [103] R. Noomen, "AE2230-Flight and orbital mechanics notes." TU Delft, 2018.
- [104] N. Mousavi, "The design and construction of a high efficiency satellite electrical power supply system," *Journal of Power Electronics*, vol. 16, pp. 666–674, March 2016.
- [105] T. Mikaelian, "Spacecraft charging and hazards to electronics in space," tech. rep., York University, 2001.
- [106] M. D. Griffin, *Space Vehicle Design*. American Institute of Aeronautics and Astronautics, second ed.,

2000.

- [107] A. Menicucci, “AE4S15: Space embedded systems.” Delft University of Technology, 2018.
- [108] G. Design, *The CES EduPack Resource Booklet 2: Material and Process Selection Charts*. Cambridge University, 2009.
- [109] P. S. Cooperation, “Canisterized satellite dispenser (csd) data sheet,” August 2018.
- [110] P. L. Conley, *Space Vehicle Mechanisms: Elements of Successful Design*. John Wiley & Sons, Inc., 1998.
- [111] P. S. Cooperation, “Payload specification for 3u, 6u, 12u and 27u,” August 2016.
- [112] R. Budynas and K. Nisbett, *Sighley’s Mechanical Engineering Desisn, 10th edition*. McGraw-Hill, 2014.
- [113] T. Kleefstra, “Buckling validation according to eurocode3,” tech. rep., TU Delft, 2014.
- [114] D. J. Inman, *Engineering Vibrations, TU Delft edition*. Pearson, 2000.
- [115] H. Chiranjeeve, K. Kalaichelvan, and A. Rajadurai, “Design and vibration analysis of a 2u-cubesat structure using aa-6061 for anusat – ii,” tech. rep., Karpaga Vinayaga College Of Engineering & Technology, 2014.
- [116] T. Megson, *Aircraft Structures for Engineering Students*. Elsevier Science & Technology.
- [117] E. Bender, “An analysis of stabilizing 3u cubesats using gravity gradient techniques and a low power reaction wheel,” tech. rep., California Polytechnic State University, San Luis Obispo, 2011.
- [118] S. Yeo, Krivova, “Solar cycle variation in solar irradiance,” *Springer Science*, p. 139, July 2014.
- [119] D. Claricoats, “Design of power, propulsion, and thermal sub-systems for a 3u cubesat measuring earth’s radiation imbalance,” *MDPI*, June 2018.
- [120] H.-U. O. Soo-Jin Kang, “On-orbit thermal design and validation of 1 u standardized cubesat of step cube lab,” *International Journal of Aerospace Engineering*, 2016.
- [121] H. Becker, M. Dolphin, D. Thorbourn, and J. Alexander, “Commercial sensor survey fiscal year 2008 compendium radiation test report,” tech. rep., Jet Propulsion Laboratory, 2008.
- [122] E. L. Christiansen, “Design and performance equations for advanced meteoroid and debris shields,” tech. rep., NASA Johnson Space Center, 2001.
- [123] V. G. Kirtskhalia, “Speed of sound in atmosphere of the earth,” tech. rep., Ilia Vekua Sukhumi Institute of Physics and Technology, 2012.
- [124] S. Samwel, “Low earth orbital atomic oxygen erosion effect on spacecraft materials,” *Space Research Journal*, p. 30, 7: 1-13. 2014.
- [125] S. Packirisamy, D. Schwam, and M. H. Litt, “Atomic oxygen resistant coatings for low earth orbit space structures,” *JOURNAL OF MATERIALS SCIENCE*, p. 30, July 1995.
- [126] D. B. Agusdinata, W. Liu, H. Eakin, and H. Romero, “Socio-environmental impacts of lithium mineral extraction: towards a research agenda,” *Environmental Research Letters*, vol. 13, no. 12, p. 123001, 2018.
- [127] C. Licht, L. T. Peiró, and G. Villalba, “Global substance flow analysis of gallium, germanium, and indium: Quantification of extraction, uses, and dissipative losses within their anthropogenic cycles,” *Journal of Industrial Ecology*, vol. 19, no. 5, pp. 890–903, 2015.
- [128] L. Guerra, “Margins and contingency module.” NASA’s Exploration Systems Mission, 2008.
- [129] S. R. Hirshorn, L. D. Voss, and L. K. Bromley, *Nasa systems engineering handbook*. 2017.
- [130] NASA CubeSat Launch Initiative, *CubeSat101: Basic Concepts and Processes for First-Time CubeSat Developers*, October 2017.

A. Technical requirement compliance matrix

This appendix gives the complete list of system and subsystem requirements. It also displays if each requirement has been validated or not.

How to use the table

In [Table A.1](#) the grey rows define the different requirement category, so that it is clear what each identifier represents. The darker grey denotes highest level category while lighter grey denotes a subcategory of requirements. Moreover, these rows also contain the sections of the report where verification of each set of subcategory requirements is justified and its current progress is colour coded. For the actual requirements, the verification column can be either red, yellow or green. Red identifies killer requirements. Fortunately, no such requirements are present but the label is included in the legend as such an option was considered. Yellow means that the requirement shall be verified at a later project stage since the team lacked information to do so now. Reasons for this can be, for example, missing documentation, unknown variables or lack of detail in current analysis tools. Green means that the requirement is currently met. The colours used are labelled below. Finally, driving requirements are highlighted in bold while key requirements in italic.




Red	Yellow	Green
		

Table A.1: System and subsystem level requirements.








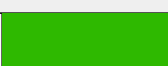

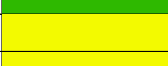



Identifier	Category/Requirement	Verification
SYS-OBJ	Mission objective	
SYS-OBJ-ORB	Orbit/constellation requirements (Chapter 4)	
SYS-OBJ-ORB-1	<i>The spacecraft shall orbit in the altitude range 230-380km</i>	
SYS-OBJ-ORB-2	The spacecraft shall have the capability to maintain its orbit during nominal mission lifetime by means of propulsion	
SYS-OBJ-PL	Payload/Observation requirements (Chapter 4 , Chapter 5)	
SYS-OBJ-PL-1	<i>The spacecraft shall provide visible spectrum imaging capability</i>	
SYS-OBJ-PL-2	<i>The spacecraft shall provide images with a spatial resolution better than 4m</i>	
SYS-OBJ-PL-3	<i>The spacecraft shall provide images with a temporal resolution of at least 2 image/day</i>	
SYS-OBJ-PL-4	<i>The spacecraft shall provide imaging capabilities of at least 99% of Earth's surface area</i>	
SYS-OBJ-LT	Lifetime requirements (Subsection 4.6.4)	
SYS-OBJ-LT-1	The spacecraft shall be designed to have a mission lifetime of 5 years or more	
SYS-OBJ-COST	Cost requirements (Section 9.4)	
SYS-OBJ-COST-1	<i>The unit price of the spacecraft (design, development, test model, and production) shall be less than 500k Euros</i>	
SYS-SC	Spacecraft requirements	
SYS-SC-DES	Design requirements (Various sections)	
SYS-SC-DES-2	Excluding the payload the spacecraft shall not have a single point of failure	
SYS-SC-DES-3	The spacecraft shall have a reliability higher than 60%	
SYS-SC-DES-4	It shall be possible to update all spacecraft software developed by the team	
SYS-SC-DES-5	The spacecraft shall not produce any debris under normal operational circumstances	
SYS-SC-CNF	Configuration requirements (Various sections)	
SYS-SC-CNF-1	The spacecraft shall adhere to the CubeSat architecture standard	

Table A.1 continued from previous page

Identifier	Category/Requirement	Verification
SYS-SC-CNF-2	Units on-board the spacecraft responsible for imaging and communication shall have an unobstructed view towards Earth	
SYS-SC-CNF-3	The spacecraft configuration shall not electromagnetically interfere with the payload to an extent that mission objective requirements can no longer be met	
SYS-SC-CNF-6	The complete payload shall fit inside the spacecraft	
SYS-SC-OP	Operation requirements (Section 7.1 , Section 7.3)	
SYS-SC-OP-1	The spacecraft shall have the capability to determine internal temperature for mission critical parts	
SYS-SC-OP-3	The spacecraft shall be able to operate autonomously between communication sessions	
SYS-SC-OP-4	Earth's magnetic field shall not influence the operation of the spacecraft	
SYS-SC-OP-5	The spacecraft shall be able to downlink data while in eclipse	
SYS-SC-OP-7	The spacecraft shall be able to power all electrical units over its mission lifetime	
SYS-SC-ADCS	ADCS requirements (Chapter 6)	
SYS-SC-ADCS-1	The spacecraft shall have a pointing stability along all 3-axis better than 0.22 deg/s (3σ)	
SYS-SC-ADCS-2	The spacecraft shall have a target pointing knowledge better than 0.025 deg (3σ)	
SYS-SC-ADCS-3	The spacecraft shall have a Nadir pointing accuracy better than 0.25 deg (3σ)	
SYS-SC-ADCS-4	The ADCS shall be able to perform jitter control	
SYS-SC-ADCS-5	The ADCS shall be able to perform drift control	
SYS-SC-ADCS-6	The ADCS shall be able to perform attitude determination and control during day time	
SYS-SC-ADCS-7	The ADCS shall be able to perform attitude determination and control during eclipse time	
SYS-SC-ADCS-8	The ADCS shall meet payload positioning requirements during day time	
SYS-SC-ADCS-9	Attitude determination capabilities shall be made redundant	
SYS-SC-ADCS-10	Attitude control capabilities shall be made redundant	
SYS-SC-ADCS-11	The ADCS shall include a Safe Mode of operation	
SYS-SC-ADCS-12	The ADCS shall be able detumble the spacecraft from 10 deg/s around all axes to less than 1 deg/s around all axes	
SYS-SC-ADCS-13	The ADCS shall be able to perform detumbling within 1 day	
SYS-SC-ADCS-14	The ADCS shall be able to desaturate fully saturated reaction wheels during eclipse	
SYS-SC-ADCS-15	The ADCS shall provide angular acceleration for the required link margin	
SYS-SC-PROP	Propulsion requirements (Section 4.3)	
SYS-SC-PROP-1	The propulsion subsystem shall provide enough ΔV to meet the mission lifetime requirement	
SYS-SC-PROP-2	The propulsion system shall avoid fuels with serious environmental hazard risks	
SYS-SC-PROP-3	Disturbance torque created by the propulsion unit shall be smaller than what the ADCS can counteract	
SYS-SC-STR	Structural requirements (Section 8.2)	

Table A.1 continued from previous page

Identifier	Category/Requirement	Verification
SYS-SC-STR-1	The structure shall provide support and attachment for all subsystems	
SYS-SC-STR-2	The structure shall support alignment for payload and sensors	
SYS-SC-STR-3	The structure shall withstand the static and dynamic loads induced by ground handling operations	
SYS-SC-STR-4	The structure shall withstand the static and dynamic loads induced by the launch vehicle	
SYS-SC-STR-5	The structure shall withstand the static and dynamic loads induced by in-orbit operations	
SYS-SC-POW	Power requirements (Section 7.3)	
SYS-SC-POW-1	The electrical power subsystem shall (EPS) provide the spacecraft with the required electrical power load during all mission phases and all operational modes	
SYS-SC-POW-2	Degradation of EPS components shall be included in the design to account for the change of performance due to exposure to space environment, thermal and load cycling	
SYS-SC-POW-3	The worst case power margin at end-of-life shall not be less than 10%	
SYS-SC-POW-4	The energy storage unit shall have a 10% capacity safety margin at EOL, at the expected number of load cycles, temperature loading and DoD.	
SYS-SC-POW-5	The subsystem shall be fully automatic including switching between operational modes and battery charging and discharging	
SYS-SC-TC	Thermal requirements (Section 8.3)	
SYS-SC-TC-1	The TCS design shall be compatible with the expected orbital environment for which worst hot and cold cases shall be identified and analysed	
SYS-SC-TC-2	The TCS design shall accommodate the expected degradation of surface properties during the mission lifetime	
SYS-SC-TC-3	The TCS shall be designed to provide 10% safety margins in the predicted worst hot and cold cases for the required subsystem thermal environment	
SYS-SC-TC-4	The spacecraft shall be able to maintain temperature in the range defined by component operating temperatures	
SYS-SC-TC-5	The TCS shall provide the necessary thermal environment to the subsystem components so that the alignment for payload is maintained and the stability of the alignment is ensured	
SYS-SC-TC-6	The thermal control shall be achieved by passive means preferentially over active means	
SYS-SC-TC-7	The TCS shall include sufficient number of sensors to allow temperature monitoring and control	
SYS-SC-COM	Telecommunication requirements (Section 7.2)	
SYS-SC-COM-1	The spacecraft shall be able to communicate using two different communication bands	
SYS-SC-COM-2	The subsystem shall support tracking operations	
SYS-SC-COM-3	The total data rate shall not exceed those that can be provided by COTS components	
SYS-SC-COM-4	The communication link margin shall be larger than 3 dB	
SYS-SC-COM-5	The spacecraft shall be able to communicate with ground from at least 5 deg above the horizon	

Table A.1 continued from previous page

Identifier	Category/Requirement	Verification
SYS-SC-CDH	C&DH requirements (Section 7.1 , Section 7.2)	
SYS-SC-CDH-1	The C&DH unit shall be able to perform on-board image processing tasks	
SYS-SC-CDH-2	The C&DH subsystem shall be able to handle the payload data rate	
SYS-SC-CDH-3	The C&DH subsystem shall provide data storage for the amount of data generated during the time equal to the temporal resolution	
SYS-SC-EOL	End-of-Life requirements (Subsection 4.6.5)	
SYS-SC-EOL-1	The spacecraft shall de-orbit within 25 years after end of mission lifetime	
SYS-SC-EOL-2	The spacecraft shall de-orbit within 25 years in case of loss of contact	
SYS-LCH	Launch requirements	
SYS-LCH-PRE	Pre-launch operational requirements (Section 8.2)	
SYS-LCH-PRE-1	The spacecraft structure shall not be visibly damaged during ground operations	
SYS-LCH-PRE-2	The spacecraft electronics shall pass extensive pre-flight check procedures	
SYS-LCH-PRE-3	While on ground, the spacecraft shall be stored in a dust and moisture free environment	
SYS-LCH-PRE-4	Mechanical loads experienced during procedural ground operations shall not exceed those experienced during flight	
SYS-LCH-VEH	Launch vehicle requirements (Chapter 4)	
SYS-LCH-VEH-1	The spacecraft shall consider both dedicated and shared launch options	
SYS-LCH-VEH-2	The spacecraft shall choose a launcher with the smallest environmental impact of the ones considered for the mission	
SYS-LCH-FL	Flight requirements (Section 8.2)	
SYS-LCH-FL-1	The spacecraft shall be able to sustain longitudinal accelerations of RMS 7 g	
SYS-LCH-FL-2	The spacecraft shall be able to sustain lateral accelerations of RMS 0.9 g	
SYS-LCH-FL-3	The spacecraft shall have a lateral mode frequency higher than 15 Hz	
SYS-LCH-FL-4	The spacecraft shall have a longitudinal mode frequency in the range 31-45 Hz or higher than 60 Hz	
SYS-GND	Ground segment requirements (Section 7.2)	
SYS-GND-1	The ground segment shall be available at all times when communication is possible	
SYS-GND-2	The ground segment shall be able to download one orbit's worth of data over the average communication time	
SYS-GND-3	The ground segment shall be able to send commands and software updates to the spacecraft	
SYS-GND-4	The ground segment shall provide backup data storage	
SYS-GND-5	Communication links shall adhere to standards set by regulatory entities	

B. Functional flow diagram

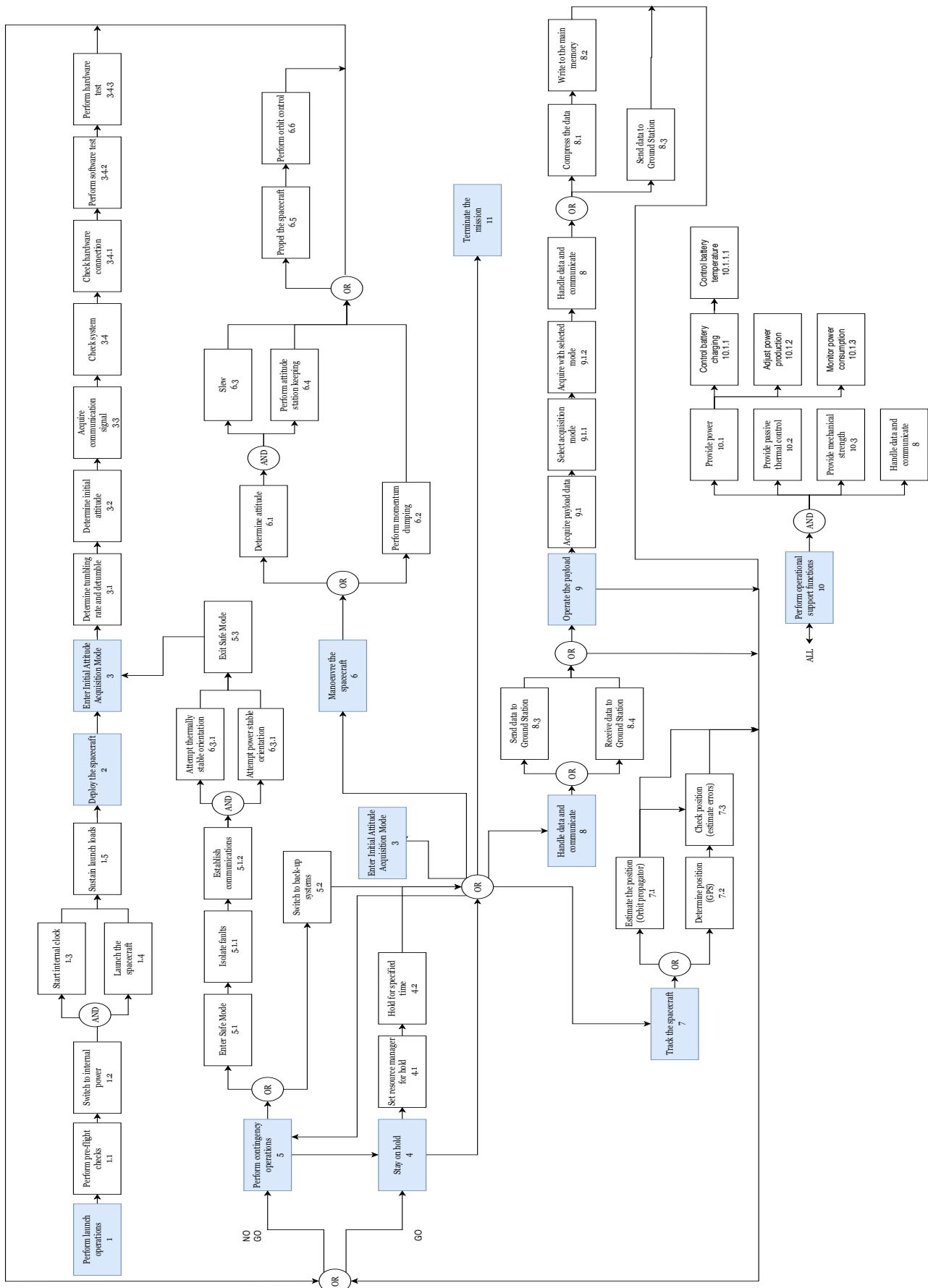


Figure B.1: Functional Flow Diagram

C. Functional breakdown structure

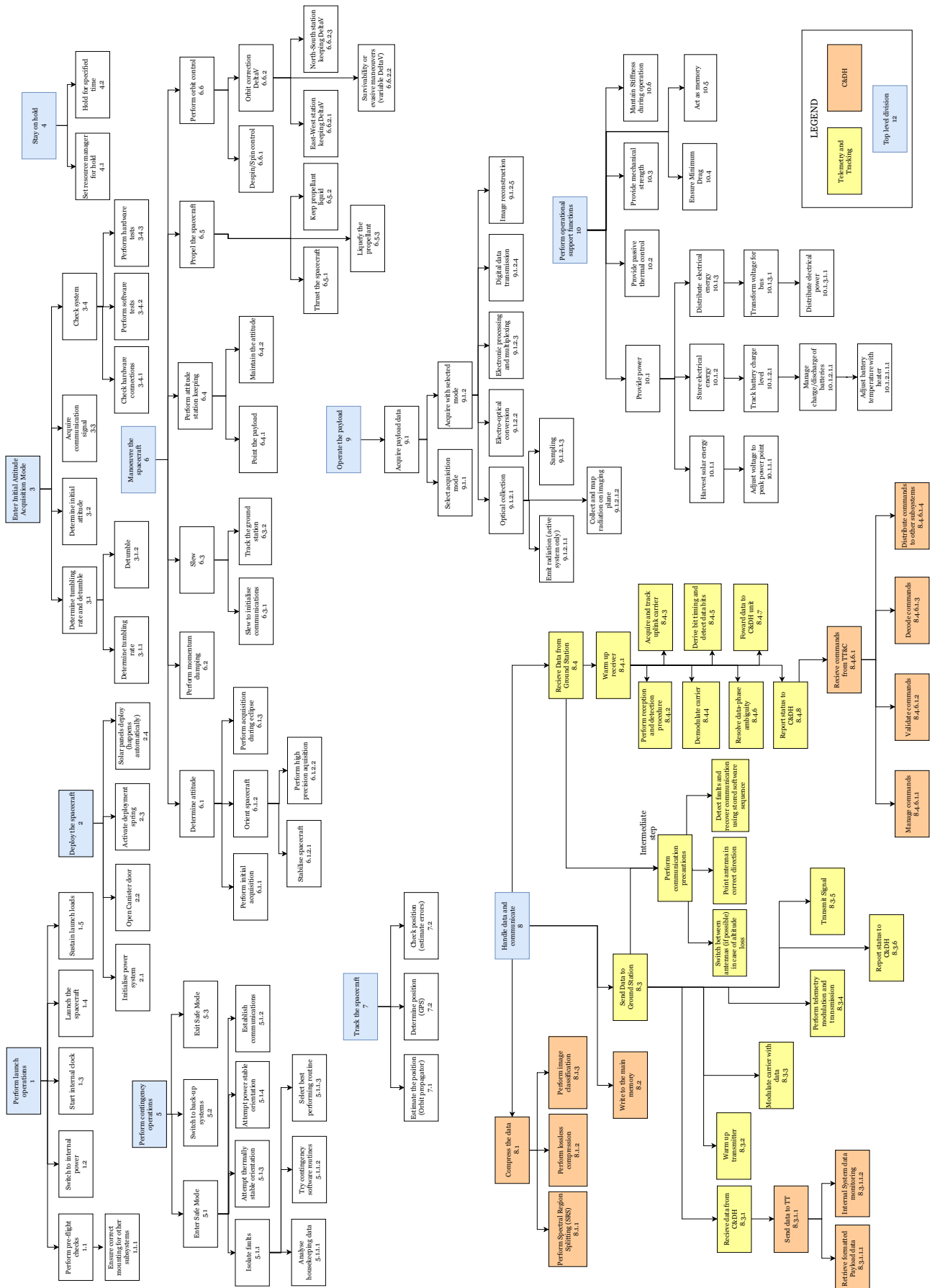


Figure C.1: Functional Breakdown Structure

D. List of technical risks

[TR-PROP-1]: Electrostatic charging of the satellite	Subsection 4.3.6
[TR-PROP-2]: Microdroplets in the extractor	Subsection 4.3.6
[TR-PROP-3]: Thrust misalignment	Subsection 4.3.5
[TR-PROP-4]: Propulsion unit completely fails	Subsection 4.3.6
[TR-PL-1]: Broken optical lenses	Section 5.1
[TR-PL-2]: Smeared image pixels	Subsection 5.3.4
[TR-ADCS-1]: Reaction wheel failure	Section 6.3
[TR-ADCS-2]: Star tracker failure	Section 6.3
[TR-ADCS-3]: Magnetometer failure	Section 6.3
[TR-ADCS-4]: Gyroscope failure	Section 6.3
[TR-ADCS-5]: Magnetorquer failure	Section 6.3
[TR-CDH-1]: OBC malfunction	Subsection 7.1.2
[TR-CDH-2]: Data corruption	Subsection 7.1.2
[TR-TC-1]: X-band transmitter failure	Subsection 7.2.10
[TR-TC-2]: UHF-band transmitter failure	Subsection 7.2.10
[TR-TC-3]: GPS failure	Subsection 7.2.10
[TR-TC-4]: Software development delays	Subsection 7.2.10
[TR-EPS-1]: Insufficient power generation	Section 7.3
[TR-EPS-2]: Electrical short	Section 7.3
[TR-EPS-3]: Energy storage failure	Section 7.3
[TR-STR-1]: Structural member fails	Subsection 8.2.8
[TR-STR-2]: Misalignment of subsystems	Subsection 8.2.8
[TR-STR-3]: Improper subsystem mounting	Subsection 8.2.8
[TR-TCS-1]: Exceeding operational temperature	Section 8.3
[TR-TCS-2]: Exceeding survival temperature	Section 8.3
[TR-TCS-3]: Thermal insulation failure	Section 8.3
[TR-EN-1]: Radiation damage	Subsection 7.4.2
[TR-EN-2]: Corrosion due to atomic oxygen	Section 8.4
[TR-EN-3]: Collision with space debris	Section 8.4
[TR-OP-1]: Launch failure	Table 4.6
[TR-OP-2]: Deployment failure	Subsection 8.2.1
[TR-OP-3]: Inaccurate orbit insertion	Subsection 4.6.2
[TR-OP-4]: CubeSat in constellation fails	Section 4.5
[TR-OP-5]: Deorbit failure	Subsection 4.6.5
[TR-OP-6]: Design oversight	Subsection 2.4.2
[TR-OP-7]: Production mistakes	Section 10.3
[TR-OP-8]: Incorrect transport handling	Section 10.3
[TR-OP-9]: Ground station failure	Subsection 7.2.10
[TR-OP-10]: Wrong control command	Section 10.3

E. Technical drawings

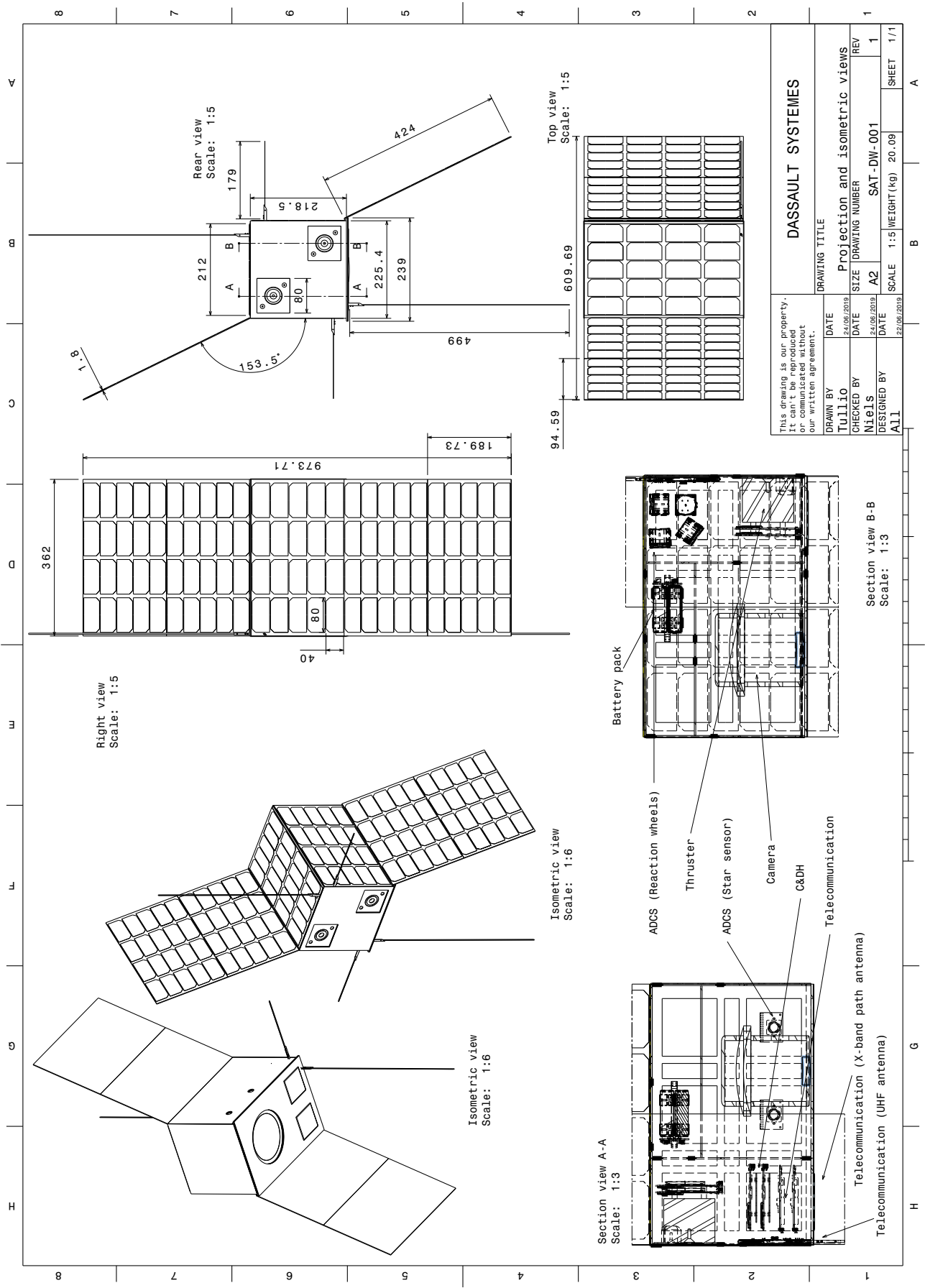


Figure E.1: Projection and isometric views

F. Project design & development logic

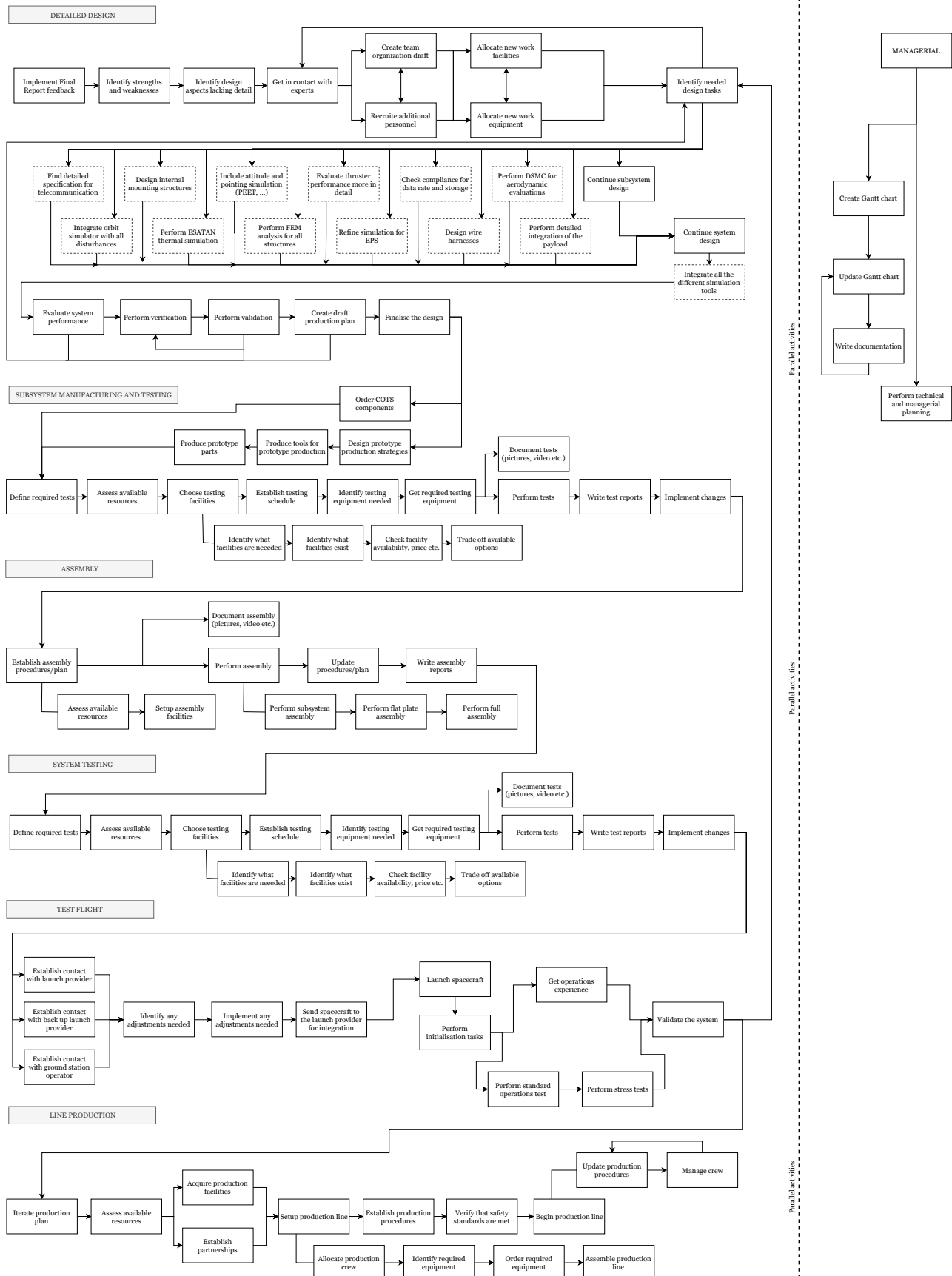


Figure F.1: Project design & development logic

G. Project Gantt chart

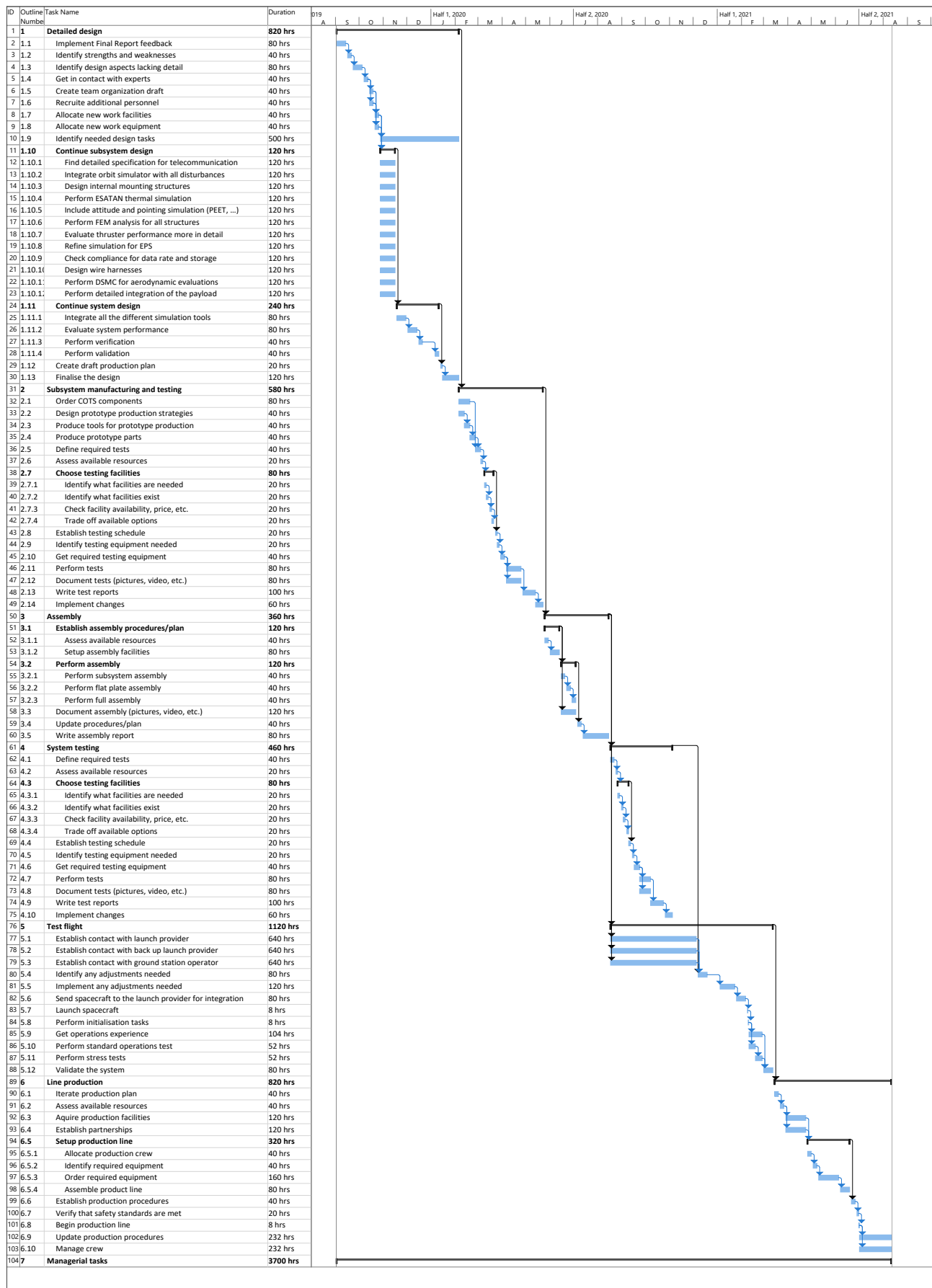


Figure G.1: Project Gantt chart